Universidade de Santiago de Compostela

Centro Singular de Investigación en Química Biológica y Materiales Moleculares (CIQUS)

Departamento de Química Física

PhD Dissertation

Beyond the harmonic approximation in the theoretical study of flexible molecules. Application to chemical reactions and tunneling splittings.

Luis Simón Carballido

Santiago de Compostela

USC
UNIVERSIDADE
DE SANTIAGO
DE COMPOSTELA

D. Antonio Fernández Ramos, Investigador Principal del Centro Singular de Investigación en Química Biológica y Materiales Moleculares (CiQUS) y Profesor Titular del Departamento de Química Física de la Universidade de Santiago de Compostela,

CERTIFICA:

Que autoriza la presentación de la tesis doctoral titulada "**Beyond the harmonic approximation in the theoretical study of flexible molecules. Application to chemical reactions and tunneling splittings.**" realizada bajo su dirección por D. Luis Simón Carballido.

Y para que conste a todos los efectos, firma el presente certificado en Santiago de Compostela, a 1 de marzo de 2017,

Dr. Antonio Fernández Ramos

USC
UNIVERSIDADE
DE SANTIAGO
DE COMPOSTELA

Contents

Agradecimientos

Me gustaría expresar mi más sincero agradecimiento a todas aquellas personas con las que he compartido todos estos años desde el primer día en el que pisé la facultad de Química hasta la finalización de esta tesis doctoral. Durante todos estos años he tenido la oportunidad de encontrarme con grandes compañeros y profesores, y en menor medida, con algunos francamente malos. Sin embargo, debo agradecer a ambos bandos ya que todos ellos en su conjunto me han enseñado lecciones valiosas, no sólo en el ámbito científico, sino en la vida en general.

De forma especial, agradezco toda la ayuda e interés a mi director de tesis durante los últimos cinco años, el Dr. Antonio Fernández Ramos. No se trata de ninguna exageración el manifestar que esta tesis no hubiese sido posible sin su trabajo, conocimiento y esfuerzo. Creo que tanto a nivel personal como profesional he aprendido mucho de él durante este tiempo, y si bien, su rigurosidad y perfeccionismo me han supuesto algún que otro dolor de cabeza, son dos de las virtudes que recordaré siempre de él.

También agradecer al resto de profesores del grupo Emilio Martínez Núñez, Saulo Vázquez Rodríguez y Jesús Rodríguez Otero por las conversaciones compartidas.

Desde un punto de vista técnico, agradecer al CESGA por ofrecernos sus ordenadores y asistencia durante estos años. Y al CIQUS y a su personal, por aportarnos unas instalaciones magníficas para el desempeño del trabajo.

Por supuesto, me gustaría agradecer fervientemente a todos los magníficos compañeros que han pasado por el despacho durante estos años. De forma especial, a Juanjo, Rubén, Marcos y Hubert por acogerme con tanta amabilidad y ayudarme en esos pasos iniciales que suelen ser los más complicados. Y de igual manera, a los compañeros que me han acompañado durante la parte final de la tesis, a Iván, Martín, Tiago y David, por toda su ayuda, que ha sido mucha, y por permitirme ganar a las cartas en contadas ocasiones.

Por último, agradecer todo el apoyo y cariño a mi familia, novia y amigos, que a pesar de no tener muy claro a qué me dedicaba exactamente, siempre han estado ahí para ofrecerme todo el ánimo y ayuda posible.

USC
UNIVERSIDADE
DE SANTIAGO
DE COMPOSTELA

Resumen

La Termodinámica Estadística es la teoría responsable de unificar la Termodinámica Clásica y la Mecánica Cuántica. Surge en los inicios del siglo XX como resultado de los estudios de Bolztmann y Gibbs fundamentalmente, pudiendo considerarse coetánea con la Mecánica Cuántica. Uno de los conceptos matemáticos más relevantes introducidos por dicha teoría es la función de partición, generalmente representada por la letra Q. Podemos interpretar la función de partición como una medida del número de estados termodinámicamente accesibles a una temperatura dada. Por definición, la función de partición se expresa mediante la siguiente ecuación:

$$Q = \sum_i e^{-\beta E_i}$$

siendo $\beta = 1/kT$, donde k es la constante de Boltzmann, i el nivel energético considerado y E la energía correspondiente. La importancia del cálculo preciso de funciones de partición estriba en las funciones termodinámicas que pueden determinarse a partir de ella. Por ejemplo, la energía interna puede obtenerse resolviendo la siguiente derivada:

$$U = U(0) - \left(\frac{\partial ln Q}{\partial \beta}\right)_{\mathrm{V}}$$

donde $U(0)$ se corresponde con la energía interna cuando $T \to 0$ y V hace referencia al volumen. Una función termodinámica como la entropía se obtiene como:

$$S = \frac{U - U(0)}{T} + k\ lnQ$$

La energía de una molécula puede expresarse de forma aproximada como:

$$E_i = E_{\mathrm{t},i} + E_{\mathrm{r},i} + E_{\mathrm{v},i} + E_{\mathrm{e},i}$$

donde E_{t} se refiere a la contribución energética debida al movimiento de traslación, y de forma análoga, E_{r} a la rotación externa, E_{v} a la vibración y E_{e} a la contribución electrónica. Esto implica que si la energía puede ser obtenida como una suma, la función de partición puede calcularse como un producto, dado que:

$$Q = \sum_i e^{-\beta E_{\mathrm{t},i} - \beta E_{\mathrm{v},i} - \beta E_{\mathrm{r},i} - \beta E_{\mathrm{e},i}} = Q_{\mathrm{t}} Q_{\mathrm{v}} Q_{\mathrm{r}} Q_{\mathrm{e}}$$

Si consideramos una molécula (no lineal) de N átomos, la vibración vendrá definida en base a $3N - 6$ coordenadas (o grados de libertad). El análisis más común es el de los modos normales, el cual permite asociar a cada uno de los grados de libertad un movimiento de una serie de átomos mientras el centro de masas permanece fijo. La función de partición vibracional resultante dentro de ciertas aproximaciones puede expresarse como el productorio de las funciones de partición individuales asociadas a cada uno de los grados de libertad, de forma análoga a lo expuesto previamente.

Durante varios capítulos de esta tesis nos centramos en uno de estos movimientos de vibración: la torsión o rotación interna. Un tipo de movimiento generalmente asociado a frecuencias bajas, que a diferencia de la rotación, donde todos los átomos de la molécula giran de forma conjunta, nos encontramos con que en este caso solo un grupo de átomos gira alrededor de un eje interno de la propia molécula.

Existen una serie de conceptos clave para comprender la metodología empleada durante esta tesis, cuya explicación se incorpora en un apéndice. En este apéndice se describen con cierto detalle conceptos clásicos como el *momento de inercia*, clave para comprender desde un punto de vista energético la rotación, el *momento de inercia reducido*, necesario para describir las rotaciones internas dentro de una molécula, el cual suele dividirse en tres categorías:

1. Rotores simétricos o equilibrados: para aquellos cuyo centro de gravedad coincide con el eje de rotación. El grupo -CH_3 se encuentra dentro de esta categoría.

2. Rotores con pequeños factores de desequilibrio: incluye aquellas situaciones donde la rotación interna tiene poco efecto sobre el momento de inercia reducido. Típico en grupos como -OH, -NH_2 o -CH_2D.

3. Rotores con grandes factores de desequilibrio: generalmente asociados a rotores con átomos no situados sobre el eje de rotación y de masas muy diferentes, como pueden ser los grupos -CH_2Cl o -CHO.

De igual forma, se introducen conceptos físicos como la *matriz S* y la *matriz D*, fundamentales para poder obtener las funciones termodinámicas del sistema. Se incluye el desarrollo matemático necesario para llegar a la expresión de la función de partición según el método de Pitzer & Gwinn y, también, la expresión clásica exacta de la función de partición para lo cual se emplea el teorema de Edinoff & Aston. Esta función de partición clásica proporciona resultados precisos a temperaturas elevadas. A temperaturas bajas es importante tener en cuenta los efectos cuánticos por lo que hay que cuantizar la expresión de Pitzer & Gwinn. Dicha cuantización se puede llevar a cabo mediante la ecuación de Schrödinger e incluyendo acoplamientos entre los rotores tanto en la energía cinética como en la energía potencial. Por conveniencia, la superficie de energía potencial de torsión que se genera a partir de cálculos de la estructura electrónica se ajusta a series de Fourier; esto permite la resolución de la ecuación de Schrödinger aplicando el teorema variacional y utilizando como funciones de onda de prueba aquellas que son solución de la ecuación de Schrödinger para la partícula en un anillo. Hasta el momento este procedimiento nos ha permitido calcular funciones de partición cuánticas para dos rotores acoplados, por lo que el método se denomina de dos dimensiones no separables o 2D-NS (del inglés *Two-Dimensional Non-Separable*).

La parte teórica incluida en el apéndice concluye con el procedimiento matemático para la obtención de las funciones termodinámicas a partir de las funciones de partición.

Esta serie de conceptos se repiten a lo largo de este trabajo, si bien, cada capítulo incorpora nuevos elementos teóricos y modificaciones para el cálculo de funciones de partición.

A continuación, realizamos un pequeño resumen de cada uno de los capítulos centrándonos en los objectivos así como las conclusiones más relevantes de cada uno de ellos. Las figuras o tablas así como la metodología matemática no se incluirán en estos resúmenes y estarán incluidas en los capítulos correspondientes o en el apéndice.

Capítulo 1

En este primer capítulo se incluye un supuesto práctico donde utilizamos el método 2D-NS para el cálculo de funciones de partición torsionales en dos moléculas con dos rotores impedidos como son el 2-propenol y el 3-fluoro-2-propenol. Tanto en este capítulo como en los restantes que contengan supuestos prácticos se incluyen todos los mínimos conformacionales para cada una de las moléculas, así como otros datos de interés como son: el método y base empleados para su obtención, la simetría de los rotores o el software empleado durante las distintas etapas del cálculo de las funciones de partición.

La primera de estas moléculas puede considerarse como un ejemplo de dos rotores débilmente acoplados mientras la segunda presenta un acoplamiento mucho mayor. La función de partición $Q_{\mathrm{tor}}^{\mathrm{2D-NS}}$ se obtiene como el sumatorio de los valores propios $E_{\mathrm{tor},j}$ resultantes de la resolución de la ecuación de Schrödinger correspondiente:

$$Q_{\mathrm{tor}}^{\mathrm{2D-NS}} = \frac{1}{\sigma_{\mathrm{tor}}} \sum_j e^{-\beta E_{\mathrm{tor},j}}$$

donde σ_{tor} es el número de simetría de la rotación interna.

A continuación, el capítulo incluye una breve descripción de los métodos matemáticos empleados para calcular el resto de funciones de partición con las cuales vamos a comparar nuestros resultados.

La comparación entre los diversos métodos demuestra la validez del método 2D-NS para representar adecuadamente ambas situaciones (acoplamiento débil y acoplamiento fuerte entre torsiones). Los métodos monodimensionales ofrecen resultados pobres cuando el acoplamiento es fuerte, ya que, dicho método parte de la premisa de que ambas rotaciones internas pueden ser tratadas independientemente.

Cabe señalar, que la función de partición clásica no es idéntica a la cuántica hasta alcanzar temperaturas superiores a la temperatura ambiente, con lo cual, es importante tener en cuenta los efectos cuánticos hasta temperaturas en torno a los 500 K.

Otro detalle interesante es el hecho de que las frecuencias obtenidas mediante el análisis de modos normales son relativamente similares a las frecuencias torsionales obtenidas. Esto pone de manifiesto que los modos normales se corresponden fundamentalmente con el movimiento de rotación interna considerado.

El ratio entre la función de partición $Q_{\text{tor}}^{\text{2D-NS}}$ y la obtenida mediante la aproximación del oscilador armónico $Q_{\text{tor}}^{\text{MC-HO}}$, ya sea esta última obtenida empleando las frecuencias de los modos normales o con las frecuencias torsionales, presenta la misma tendencia. A temperaturas bajas el ratio $Q_{\text{tor}}^{\text{2D-NS}}/Q_{\text{tor}}^{\text{MC-HO}}$ es ligeramente mayor que la unidad, mientras que a temperaturas altas se produce un cambio de tendencia y pasa a ser ligeramente menor que la unidad. Esto es debido a que el oscilador armónico sobreestima la densidad de estados a temperaturas altas. Además, dicha inversión se produce a temperaturas más bajas para el 2-propenol que para el 3-fluoro-2-propenol, ya que las barreras energéticas entre pozos son menores para el primero. También se concluye que la incorporación del acoplamiento entre torsiones en la energía cinética tiene poco efecto en las funciones de partición.

Capítulo 2

El capítulo 2 ahonda en las posibilidades que nos brinda el método 2D-NS. En este caso, estudiamos tres sistemas donde se produce un desdoblamiento del nivel fundamental de vibración mediante efecto túnel (tunneling splitting) debido a las rotaciones impedidas. El efecto túnel es un efecto cuántico que puede producir el desdoblamiento de un nivel de energía debido al solapamiento de las funciones de onda asociadas a dos pozos idénticos en una región clásicamente prohibida.

A temperaturas bajas, el efecto túnel es el único mecanismo que permite explicar el tránsito de la molécula entre los dos mínimos. Hay dos factores clave a la hora de considerar la posibilidad de que se produzca dicho tránsito:

1. Masa de la partícula: cuanto menor sea la masa de la partícula que debe atravesar la barrera mayor será la posibilidad de que se produzca el efecto túnel. De ahí que, en el caso de los átomos, el hidrógeno sea el mejor candidato.

2. Ancho de la barrera del potencial: el aumento en la anchura de la barrera a atravesar, disminuye la incidencia del efecto túnel.

Si bien, existen multitud de estudios que analizan el desdoblamiento que surge como consecuencia del efecto túnel para reacciones de transferencia de hidrógeno, en nuestro caso, este desdoblamiento es debido a la rotación interna. Atendiendo a su magnitud, en el primer caso suele ser del orden de cm^{-1} mientras que, en el segundo caso los valores suelen ser mucho más bajos, del orden de MHz.

Para interpretar este fenómeno, necesitamos obtener la función de onda del estado fundamental y de los primeros estados excitados para poder así entender entre qué pozos del potencial se origina el desdoblamiento. No se trata únicamente de un análisis cualitativo del fenómeno, dado que, también, tratamos de calcular la magnitud de dichos desdoblamientos y compararlos con los valores obtenidos experimentalmente existentes en la literatura científica.

Las moléculas estudiadas son el benzylalcohol (BA), el 3-fluorobenzyl alcohol (3FBA) y el 4-fluorobenzyl alcohol (4FBA) que, según los datos experimentales, presentan unos desdoblamientos de 492.82 MHz, 0.82 MHz y 337.10 MHz, respectivamente. Las tres moléculas son aparentemente muy similares, sin embargo, debido a la posición del átomo de flúor en el

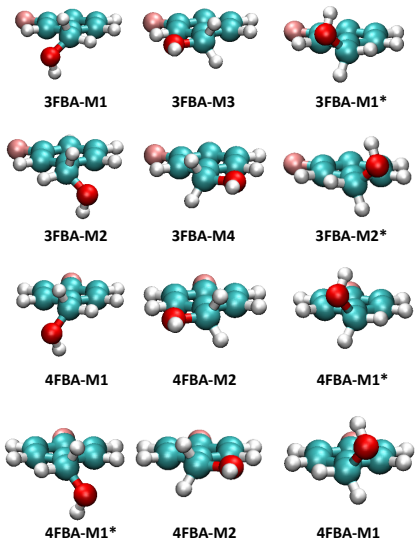

Figura 1: Representación de las geometrías de equilibrio para el 3FBA y 4FBA. Las geometrías para el BA son análogas a las obtenidas para el 4FBA, y por ello no se incluyen. Gris claro, rojo, marrón y cian representan hidrógeno, oxígeno, flúor y carbono, respectivamente.

3FBA, este presenta dos pozos de igual energía, mientras que el 4FBA y el BA tienen cuatro. Podría suponerse en este caso que los métodos monodimensionales podrían ser adecuados para interpretar el desdoblamiento, sin embargo, dado que las moléculas tienen dos rotores que presentan cierto grado de acoplamiento, es preferible emplear un método como el 2D-NS que incluye dicho acoplamiento.

En el caso del 3FBA hay cuatro mínimos con distinta energía, que denominamos de menor a mayor energía como M1, M2, M3 y M4, de forma que M1 es el mínimo absoluto (ver Figura 1). Además, la interconversión desde M1 a M1* (donde el asterisco hace referencia a su enantiómero) presenta dos etapas, una primera donde se produce la conversión M1→ M3, con una barrera calculada en 525 cm^{-1} y una energía para M3 de 284 cm^{-1} y una segunda que se corresponderá con M3→ M1*. Este proceso también sucede para la conversión de M2 a M2*, pero en este caso el intermedio es M4.

Si analizamos los momentos de inercia reducidos de ambos rotores nos encontramos con una enorme diferencia en cuanto a su valor. El grupo -CH_2OH presenta un momento de inercia reducido en torno a 18 amu $Å^2$ mientras que en el caso del grupo -OH el valor es de 0.8 amu $Å^2$. Dado que el momento de inercia es para el movimiento rotacional el análogo a la masa para el movimiento lineal, un giro en torno al rotor del grupo -OH es más susceptible de experimentar efecto túnel que un mismo giro en torno al otro rotor. Lógicamente, esta consideración es válida tanto para el 3FBA como para el 4FBA o el BA.

También se pueden representar las funciones de onda del estado fundamental y el primer

estado excitado con el fin de comprobar que efectivamente la diferencia de energía entre niveles se corresponde con la transición M1 → M1*. Efectivamente, la representación de las mismas corrobora que el desdoblamiento obtenido se corresponde con dicha transición, ya que, ambas funciones se encuentran localizadas exclusivamente sobre los pozos M1 y M1*. Siendo la primera de ellas simétrica y la segunda antisimétrica con respecto a la transición M1 → M1*. Dicho tránsito supone una variación de 86° para el rotor -CH_2OH y de 116° para el -OH. El cálculo del desdoblamiento para la molécula del 3FBA mediante el método 2D-NS ofrece un valor de 0.02 MHz, relativamente alejado del valor experimental de 0.82 MHz.

Para el 3FBA además podemos postular la existencia de un segundo desdoblamiento debido al tránsito M2 → M2*, ya que, de forma similar a la conversión M1 → M1*, la representación de las función de onda del segundo y tercer estado excitado y la diferencia de energía así lo sugieren. Por desgracia, en este caso no contamos con datos experimentales para poder comparar nuestros resultados.

En el caso del 4FBA, el giro en torno al rotor -CH_2OH da lugar a dos conformaciones indistinguibles, y por consiguiente, cualquier giro de 180° nos lleva a una conformación idéntica a la inicial. Tendremos, por tanto, cuatro pozos isoenergéticos en la superficie de energía potencial; dos son conformaciones indistinguibles de M1 y las otras dos lo son del enantiómero M1*. Para este caso el desdoblamiento calculado es de 429 MHz. El análisis de las funciones de onda correspondientes resulta nuevamente de gran ayuda, ya que nos permite discernir por condiciones de simetría qué conversión es la responsable del desdoblamiento, sugiriendo que el tránsito M1→ M1* es directo a diferencia del que ocurre en la molécula de 3FBA.

Dada la similitud entre las estructuras del BA y el 4FBA, obtenemos unas superficies de energía potencial muy similares y todas aquellas consideraciones realizadas para el 4FBA con respecto a su simetría continúan siendo válidas para el BA. El valor del desdoblamiento calculado mediante el método 2D-NS para esta última molécula es de 453 MHz, un valor muy similar al experimental.

Capítulo 3

Este capítulo puede considerarse el núcleo central de esta tesis, tanto por el volumen de resultados, como por el contenido teórico del mismo, que tiene como resultado el diseño de un nuevo método para el cálculo de funciones rovibracionales.

Dicho capítulo consiste en el estudio de 20 moléculas que presentan dos rotaciones internas, si bien, a diferencia de los capítulos anteriores, nos centramos en la función rovibracional y en el cálculo de las funciones termodinámicas. Al término del mismo, se incluye una comparación entre los resultados obtenidos con los distintos métodos y una explicación razonada sobre las diferencias encontradas.

La selección de los 20 sistemas estudiados se ha realizado tratando de representar todas las situaciones posibles, esto es: sistemas con rotores prácticamente independientes (poco acoplamiento), sistemas con acoplamiento fuerte y sistemas donde uno de los rotores está unido directamente al otro (rotación compuesta).

La sección dedicada a la metodología incluye el desarrollo matemático del método 2D-NS,

realizando especial hincapié en cómo incorporar la función de partición rovibracional teniendo en cuenta la anarmonicidad, lo que da lugar a dos variantes del método 2D-NS dependiendo de la estrategia seguida. Aunque ambas variantes incluyen la anarmonicidad debida a las torsiones, la primera de ellas, a la que llamamos GS2D-NS (del inglés *Global Separability Two-Dimensional Non Separable*) asume que es posible separar los grados de libertad torsionales del resto de grados de libertad de forma global. La segunda variante, resulta algo más precisa debido a que considera la variación tanto de la rotación externa como de los 3N-8 grados de libertad restantes en relación con las dos torsiones. Esta segunda variante lleva por nombre E2D-NS (del inglés *Extended Two-Dimensional Non Separable*). Además, en este mismo capítulo, se incluye una breve descripción del resto de métodos considerados en este estudio.

A la hora de valorar los resultados, se han comparado por separado las funciones de partición torsionales (de forma similar a lo realizado en el capítulo 1) de las rovibracionales. En cuanto a las primeras, el método desarrollado por Pitzer & Gwinn ofrece unos resultados comparables al método 2D-NS, mostrándose en todas las situaciones como un método más preciso que el método que no incluye acoplamientos. Esto pone de manifiesto la importancia de considerar el acoplamiento entre torsiones. Por tanto, en aquellos casos donde la aplicación del método 2D-NS resulta muy costoso desde un punto de vista computacional, el método de Pitzer & Gwinn es probablemente la mejor alternativa.

A la hora de comparar las funciones de partición rovibracionales resulta esencial considerar como se calcula la energía del punto cero (ZPE). En el caso del método E2D-NS, esta se obtiene como la suma entre las contribuciones de los 3N-8 grados de libertad que excluyen las torsiones más la energía del estado fundamental obtenida con el método 2D-NS. De forma general, dicha ZPE es ligeramente menor que la obtenida empleando la aproximación del oscilador armónico. Esto implica que a temperaturas bajas el valor de la función de partición rovibracional E2D-NS sea ligeramente mayor que la función de partición armónica. Esta tendencia suele invertirse conforme la temperatura aumenta si existen otros mínimos próximos en energía al mínimo global.

Se observa cierta diferencia entre las funciones obtenidas mediante los métodos E2D-NS y GS2D-NS durante todo el intervalo de temperaturas considerado, lo cual sugiere que incorporar la anarmonicidad torsional sobre la función de partición armónica puede conllevar un error considerable.

Las funciones de partición rovibracionales obtenidas mediante los métodos MC-HO (armónico multiconformacional) y MS-T(U) (método multiestructural sin acoplamiento entre rotores) ofrecen resultados comparables a la función E2D-NS a temperaturas del orden de 200 K. Sin embargo, a temperaturas mayores de 300 K los valores obtenidos se desvían sustancialmente de los obtenidos con el método E2D-NS. Para este último intervalo de temperaturas, el MS-T(C) (método multiestructural con acoplamiento entre rotores) es el que ofrece los resultados más similares a los obtenidos con el método E2D-NS.

También se calculan las funciones termodinámicas a partir de las funciones de partición rovibracionales para poder comparar los resultados con los datos experimentales disponibles. Dicha comparación sitúa al método E2D-NS como el que aporta resultados más precisos. El segundo mejor método es el MS-T(C), seguido del método GS2D-NS que ofrece unos resultados ligeramente peores que el método MS-T(C).

De forma general, en aquellos casos donde la obtención de la función de partición E2D-NS resulte muy compleja el método MS-T(C) resulta la alternativa más idónea.

Capítulo 4

Este último capítulo se centra en el estudio teórico mediante la teoría variacional del estado de transición de la reacción de abstracción de hidrógeno en la molécula de etanol mediante hidrógeno atómico. Además, se analizan los efectos cinéticos isotópicos y se consideran todas las conformaciones posibles (reactivos, productos y estados de transición). Para realizar dichos cálculos, se empleará la teoría variacional del estado de transición de caminos múltiples (MP-CVT). La teoría canónica variacional (CVT) se puede considerar una versión refinada de la teoría convencional del estado de transición (TST), ya que incorpora efectos cuánticos y tiene en cuenta la posibilidad de que el cuello de botella de la reacción no esté localizado en el estado de transición (efecto variacional).

Dado que los datos experimentales son en disolución acuosa, los cálculos de estructura electrónica incluyen un modelo de continuo que simula el disolvente. La anarmonicidad debida a las torsiones se incluye empleando el método 2D-NS. Las distintas conformaciones para los mínimos y estados de transición pueden ser representadas mediante proyecciones de Newman de la forma:

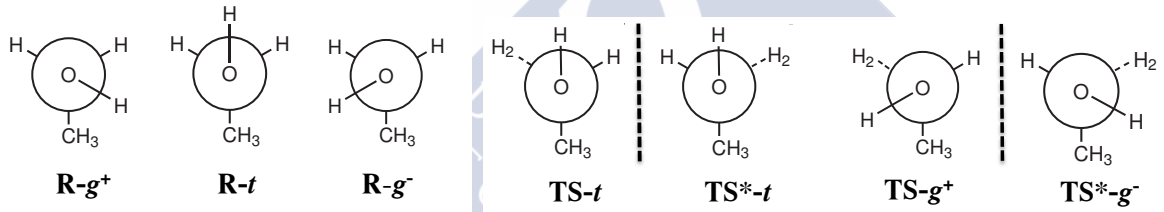

Además, atendiendo a las distintas sustituciones isotópicas estudiadas experimentalmente, tendremos 4 reacciones posibles, que denominamos R1, R2, R3 y R4, siendo R1 la reacción sin sustituciones isotópicas y, por tanto, la que emplearemos como referencia para calcular los KIEs:

$$H + CH_3CH_2OH \longrightarrow H_2 + CH_3CHOH \quad (R1)$$

$$H + CD_3CD_2OH \longrightarrow HD + CD_3CDOH \quad (R2)$$

$$D + CH_3CH_2OD \longrightarrow DH + CH_3CHOD \quad (R3)$$

$$D + CD_3CD_2OD \longrightarrow D_2 + CD_3CDOD \quad (R4)$$

De forma general, las constantes de velocidad de reacción obtenidas mediante el método MP-CVT resultan más parecidas a las experimentales que aquellas obtenidas con MP-TST.

Los KIEs calculados para los ratios R1/R2, R1/R3 y R1/R4, son muy próximos a los valores experimentales cuando se tiene en cuenta el efecto túnel y los efectos variacionales. Además se ofrece un desglose de los ratios atendiendo a las distintas contribuciones

(traslación, anarmonicidad debida a las torsiones, rotación, vibración, efecto variacional y efecto túnel), así como la contribución individual por parte de cada uno de los estados de transición posibles. De esta forma, resulta posible entender qué contribución tiene más peso en cada una de las sustituciones isotópicas.

Por último, se deduce teóricamente que la contribución porcentual de cada uno los estados de transición (siempre y cuando sean interconvertibles entre si) con respecto al KIE total, es constante, independientemente de la sustitución isotópica considerada.

USC
UNIVERSIDADE
DE SANTIAGO
DE COMPOSTELA

Introduction

This PhD dissertation deals with the development and testing of methods able to evaluate internal rotor and rotational vibrational partition functions of molecules with two torsional modes. The main method discussed in the Dissertation includes both the kinetic and potential couplings and is called Two-Dimensional Non Separable (2D-NS). Its description is included in the Theoretical Background section in the Appendix.

Chapter 1 considers two molecular systems, one with weak coupling between rotors and the other with strong coupling. The 2D-NS partition function and several monodimensional and bidimensional partition functions were calculated and compared. The main idea was to test if the other methods are able to handle both situations as the 2D-NS does.

Chapter 2 explores the possibilities that the method provides by studying three molecules presenting two hindered internal rotors for which experimental tunneling splittings have been reported. The analysis of the wavefunctions were important tools to get insight into the tunneling mechanism. Furthermore, the calculation of the ground vibrational state energy levels by the 2D-NS method allowed us to test its accuracy for the prediction of this kind of phenomena.

Chapter 3 includes an extensive study of twenty molecules with two hindered internal rotations. The 2D-NS method is used to calculate the hindered rotation partition functions and the results are compared with several of the most popular monodimensional and bidimensional methods. During this chapter the 2D-NS method is extended to obtain the rovibrational partition function, and this leads to two different methods, which differ in the global separability assumption of the torsional degrees of freedom. In the same manner, and as for the bidimensional partition functions, a comparison between several methods was also included. In order to evaluate the accuracy of the methods, rovibrational partition functions were used to calculate ideal-gas standard-state thermodynamic functions. The calculated values were compared to experimental data available in the scientific literature.

Chapter 4 comprises a study of the kinetic isotope effects (KIEs) for the hydrogen abstraction reaction from ethanol by atomic hydrogen in aqueous solution at room temperature. Multipath canonical variational transition state theory accounted for tunneling and variational effects. The anarmonicity due to the torsions was incorporated through the 2D-NS method. All possible transition states were incorporated to the study and their contribution to the torsional, rovibrational, translational, and tunneling KIEs factors was individually analyzed. The results were compared to the available experimental data.

Chapter 5 summarizes the conclusions.

USC
UNIVERSIDADE
DE SANTIAGO
DE COMPOSTELA

Chapter 1

Quantum Treatment for Internal Rotations

The link to the scientific publication is:

http://link.springer.com/article/10.1007%2Fs00894-014-2190-z

Publication Information:

Luis Simón-Carballido, Antonio Fernández-Ramos. Calculation of the two-dimensional non-separable partition function for two molecular systems. *J. Mol. Model.*, 2014, **20**, 2190.
IMPACT FACTOR: 1.438
DOI: 10.1007/s00894-014-2190-z

USC
UNIVERSIDADE
DE SANTIAGO
DE COMPOSTELA

Chapter 2

Hindered Rotor Tunneling Splittings

The link to the scientific publication is:

`http://pubs.rsc.org/en/Content/ArticleLanding/2016/CP/C5CP05307B#!divAbstract`

Publication Information:

Tiago Vinicius Alves, Luis Simón-Carballido, Fernando Rei Ornellas Antonio Fernández-Ramos. Hindered rotor tunneling splittings: an application of the two-dimensional non-separable method to benzyl alcohol and two of its fluorine derivatives. *Phys. Chem. Chem. Phys.*, 2016, **18**, 8945-8953.
IMPACT FACTOR: 4.449
DOI: 10.1039/c5cp05307b

USC
UNIVERSIDADE
DE SANTIAGO
DE COMPOSTELA

Chapter 3

Calculating Torsional and Rotational-vibrational Partition Functions

3.1 Introduction

The calculation of rovibrational partition functions in flexible molecules is specially challenging if the goal is to calculate accurate thermodynamic functions or thermal rate constants. Recent theoretical studies show that these objectives can be achieved by accounting for torsional anharmonicity [1] and multiple reaction paths [2, 3, 4, 5, 6]. This work is concerned with the first of these two issues. An accurate calculation of rovibrational partition functions involves a good description of the coupling between the tops themselves and between those tops and the other degrees of freedom. However, it is quite common to calculate the rovibrational partition function within the rigid-rotor harmonic oscillator (RRHO) approximation, because it allows the separation of rotation and vibration, i.e,

$$Q_{\mathrm{rv}}^{\mathrm{RRHO}} = Q_{\mathrm{rot}} Q_{\mathrm{vib}} \tag{3.1}$$

In general, this approximation is good at low temperatures because in this case the partition function is well described by a few levels belonging to the global minimum of the potential energy surface. However, as temperature rises, the torsional motions that correspond to low frequency vibrational modes, are excited till high vibrational states and some molecules may have enough energy to overcome the torsional barriers and populate other minima of the potential energy surface. Therefore, the methods dealing with hindered rotations should, on one side, include the anharmonicity due to the torsions (plus the coupling), and on the other side, incorporate this deviation from the harmonic behavior in the total rovibrational partition function.

In the spirit of Eq. 3.1, the harmonic rovibrational partition function of a molecule with J conformers (distinguishable minima) which can be reached by internal rotations can be

written as

$$Q_{\rm rv}^{\rm MC-H} = \sum_{j=1}^{J} Q_j^{\rm RRHO} \tag{3.2}$$

where MC-H means multiconformer harmonic, because $Q_j^{\rm RRHO}$ uses the same RRHO approximation as Eq. 3.1, but for each of the conformers, i.e.,

$$Q_{\rm rv,j}^{\rm RRHO} = Q_{{\rm rot},j} Q_j^{\rm HO} e^{-\beta U_j} \tag{3.3}$$

The Boltzmann factor of Eq. 3.3 takes into account the difference in energy, U_j, between conformer j and the conformer corresponding to the global minimum. Noticed that, for a flexible molecule, Eq. 3.2 should be more accurate than Eq. 3.1 because it accounts for all the local minima of the molecule and not just for the absolute minimum.

It is possible to go a step further by analyzing in more detail the torsional potential of the molecule. Specifically, the torsions can be treated as coupled hindered rotors instead of harmonic oscillators, and the coupling between the torsions and the other degrees of freedom can be also included. The works of Pitzer and Gwinn (PG) [7] and Kilpatrick and Pitzer (KP) [8] addressed the problem of how to calculate torsional partition functions even in situations involving strongly coupled torsions. Much of the later research is based on finding approximations and/or improvements to these two seminal works. Some of that research effort will be discussed in Section 2. However, there are still aspects which were not discussed in depth in those two papers, but that are important to obtain accurate rovibrational partition functions, i.e., how to account for anharmonicity in systems with distinguishible multiple torsional minima, how to incorporate the torsional partition function into the total rovibrational partition function of Eq. 3.2, and how accurate are some of the available methods which already incorporate torsional anharmonicity into the rovibrational partition function. These issues are also discussed in Section 2, and different methods are compared for a set of molecules in Section 4; this comparison also includes experimenal data of themodynamic functions [9]. The computational details are described in Section 3, and Section 5 concludes.

As benchmark for the torsional partition function we use the two dimensional non separable (2D-NS) method [10]; it evaluates the torsional partition function by solving the two dimensional Schrödinger equation with a coupled potential, which has been fitted to Fourier series. The 2D-NS method is compared with some one dimensional methods, as well as, with the torsional PG method. For the rovibrational partition function we use as benchmark the extended classical hindered rotor method of Vansteenkiste *et al.* [11], but corrected for quantum effects with the 2D-NS method. We call this method extended two dimensional non separable (E2D-NS) method. It is compared with other multiconformational methods, like the multistructural uncoupled [MS-T(U)] [12], and the multistructural coupled [MS-T(C)] approximations [13]. Finally, the available experimental thermochemical data [9] are compared with theoretical data obtained by some of the methods that include torsional anharmonicity in the evaluation of the rovibrational partition function.

For the comparison among different methods we consider a series of 20 molecules, each of them with two hindered rotors. The name of the molecules and the rotating groups are listed

in Table 3.1 and depicted in Fig. 3.1. The relative energies of the local torsional minima with respect to the global minimum are given in Table 3.2. There are molecules with nearly independent (separable) rotors, as for instance **S17**, molecules in which the two torsions seem quite coupled, as **S7**, and molecules involving compound rotation (one rotating group is attached to the other rotating group), as **S2**, **S8** and **S19**. There are also different types of rotors: symmetric tops (no off-balance term during rotation) as the methyl group, slightly asymmetric tops as the -OH group, and very asymmetric tops as the -COH and the -CFH_2 groups. Therefore, the set of molecules includes all type of situations, from the separable (or nearly separable) torsions with constant reduced moments of inertia to the coupled torsions with reduced moments of inertia that change substantially with the internal rotation.

Table 3.1: List of the molecules considered in this study.

System	Empirical formula	Chemical name	Rotating tops
S1	$C_2H_2O_3$	Oxo-acetic acid	-COH, -OH
S2	$C_2H_4O_2$	Vinyl hydroperoxide	-OOH, -OH
S3	$C_2H_4O_2$	Hydroxyacetaldehyde	-COH, -OH
S4	C_2H_6O	Ethanol	-OH, -CH_3
S5	$C_3H_4O_2$	2-Propenoic acid	-CH=CH_2, -OH
S6	$C_3H_4O_2$	Malonaldehyde	-COH, -OH
S7	C_3H_5FO	3-Fluoro-2-propenol	-OH, -CH_2F
S8	C_3H_6O	Methoxy ethene	-O-CH_3, -CH_3
S9	C_3H_6O	Propen-3-ol	-CH_2-OH, -OH
S10	C_3H_6O	2-Propenol	-OH, -CH_3
S11	C_3H_6O	(*Z*)-1-Propenol	-OH, -CH_3
S12	C_4H_6O	Methacrolein	-COH, -CH_3
S13	C_4H_6O	(*Z*) 1,3-butadien-1-ol	-CH=CH_2, -OH
S14	C_4H_6O	1,3-Butadien-2-ol	-CH=CH_2, -OH
S15	C_4H_6O	(*Z*) 2-butenal	-COH, -CH_3
S16	C_4H_8	1-butene	-CH_2-CH_3, -CH_3
S17	C_4H_8	(*Z*) 2-butene	-CH_3, -CH_3
S18	C_5H_6O	(2*E*)-penta-2,4-dienal	-CH=CH_2, -COH
S19	C_7H_8O	Benzyl alcohol	-CH_2-OH, -OH
S20	C_7H_8O	2-Methyl-phenol	-OH, -CH_3

3.2 Methodology

Firstly, this section briefly outlines some general aspects about torsions, having as background the works of PG and KP, because most of the work discussed after is related to their work. Secondly, some one-dimensional methods to treat torsional anharmonicity are discussed. This Section continues with a description of two-dimensional methods dealing with coupled torsions, and concludes with an explanation of how to incorporate torsional anharmonicity in the calculation of rovibrational partition functions.

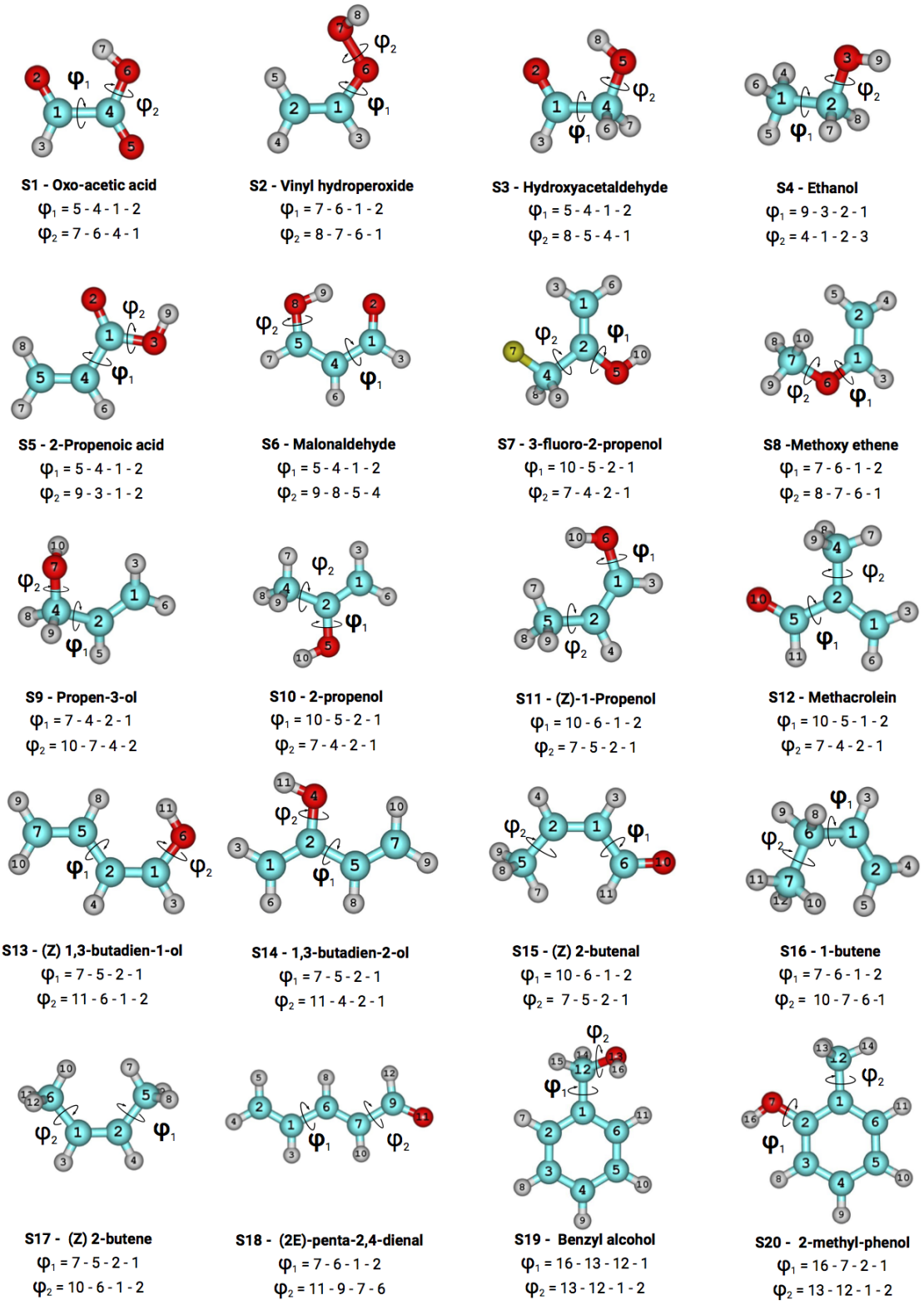

Figure 3.1: Molecules studied in this work. The two dihedral angles indicate the atoms involved in each torsional motion. Light gray, red, cyan and yellow represent hydrogen, oxygen, carbon and fluorine atoms, respectively.

Table 3.2: Some parameters of interest for the conformers of the 20 systems studied, i.e., total number of wells, the symmetry numbers for internal rotation and the energy difference between conformers U_j (in cm^{-1}). It also indicates the two torsional angles ϕ_1, ϕ_2 of a given conformer and if that conformer has an enantiomer. For the other enantiomer $\phi_1 \rightarrow 360 - \phi_1$ and $\phi_2 \rightarrow 360 - \phi_2$.

System	*Wells*	σ_1, σ_2	*Conformer*	*Enantiomer?*	$[\phi_1, \phi_2]$	U_j
$S1$	4	1,1	S1-M1	No	180,0	0
			S1-M2	No	180,180	337
			S1-M3	No	0,180	787
			S1-M4	No	0,0	3334
$S2$	6	1,1	S2-M1	Yes	359,118	0
			S2-M2	Yes	199,109	535
			S2-M3	Yes	200,231	556
$S3$	4	1,1	S3-M1	No	0,0	0
			S3-M2	No	180,180	1189
			S3-M3	Yes	194,79	1295
			S3-M4	No	0,180	2023
$S4$	9	1,3	S4-M1	No	180,60	0
			S4-M2	Yes	61,57	42
$S5$	5	1,1	S5-M1	No	0,0	0
			S5-M2	No	180,0	88
			S5-M3	No	0,180	2278
			S5-M4	Yes	158,171	2614
$S6$	4	1,1	S6-M1	No	0,0	0
			S6-M2	No	180,0	3641
			S6-M3	No	180,180	3695
			S6-M4	No	0,180	4789
$S7$	7	1,1	S7-M1	No	0,0	0
			S7-M2	Yes	199,142	50
			S7-M3	Yes	6,242	439
			S7-M4	Yes	156,354	1273
$S8$	9	1,3	S8-M1	No	0,60	0
			S8-M2	Yes	171,57	958
$S9$	9	1,1	S9-M1	Yes	6,60	0
			S9-M2	Yes	124,302	3
			S9-M3	No	0,180	202
			S9-M4	Yes	130,171	490
			S9-M5	Yes	123,65	576
$S10$	6	1,3	S10-M1	No	0,0	0
			S10-M2	No	180,0	781
$S11$	6	1,3	S11-M1	No	0,0	0
			S11-M2	No	180,0	209
$S12$	6	1,3	S12-M1	No	180,0	0
			S12-M2	No	0,0	1158
$S13$	5	1,1	S13-M1	No	180,0	0
			S13-M2	No	180,180	146
			S13-M3	Yes	39,6	233
			S13-M4	No	0,180	916
$S14$	7	1,1	S14-M1	No	180,0	0
			S14-M2	Yes	170,158	653
			S14-M3	Yes	30,2	1069
			S14-M4	Yes	41,198	1577
$S15$	9	1,3	S15-M1	No	180,0	0
			S15-M2	No	0,0	324
			S15-M3	No	0,60	325
$S16$	9	1,3	S16-M1	No	0,60	0
			S16-M2	Yes	239,61	25
$S17$	9	3,3	S17-M1	No	0,0	0
$S18$	6	1,1	S18-M1	No	180,180	0
			S18-M2	No	180,0	534
			S18-M3	Yes	27,179	1088
			S18-M4	Yes	30,0	1700
$S19$	6	2,1	S19-M1	Yes	36,59	0
			S19-M2	No	0,180	328
$S20$	6	1,3	S20-M1	No	180,60	0
			S20-M2	No	0,60	158

3.2.1 General aspects about torsions

In the most simple case the torsions are separable and can be treated as independent rotors. Under those conditions the torsional partition function $Q_{\text{tor}}^{\text{X}}$ within a given approximation X and associated to t torsions is given by:

$$Q_{\text{tor}}^{\text{X}} = \prod_{\tau=1}^{t} q_{\tau}^{\text{X}} \tag{3.4}$$

where q_{τ}^{X}, $\tau = 1, \ldots, t$ are the partition functions that correspond to each of the torsions (hereafter, the undercase letter q will refer to the partition function of just one torsional mode).

In the 1940's PG accurately calculated the one-dimensional torsional partition function for a torsional potential having M-fold symmetry with only one term in the cosine, i.e.,

$$V_{\tau}(\phi_{\tau}) = \frac{1}{2} W_{\tau}(1 - \cos(M_{\tau}\phi_{\tau})) \tag{3.5}$$

ϕ_{τ} being the torsional angles and M_{τ} the periodicity. For the potential of Eq. 3.5, usually called reference PG potential (RPG), the torsional frequencies $\overline{\omega}_{\tau}$ can be related to the reduced moments of inertia I_{τ} of the minimum of the potential and to the barrier height W_{τ} by:

$$\overline{\omega}_{\tau} = \frac{1}{M_{\tau}} \left(\frac{W_{\tau}}{2I_{\tau}} \right)^{1/2} \tag{3.6}$$

Each of the one-dimensional Schrödinger equations is of the type:

$$-\frac{\hbar^2}{2I_{\tau}} \frac{d^2\Phi_{\tau}}{d\Phi_{\tau}^2} + V_{\tau}\Phi_{\tau} = E\Phi_{\tau} \tag{3.7}$$

which are reduced to Mathieu differential equations when the potential is the one of Eq. 3.5. PG solved the Mathieu equations and the results where tabulated. They also solved the Schrödinger equation when the potential has several cosine terms (in this case is called Hill equation), i.e.,

$$V_{\tau}(\phi_{\tau}) = a_{0,\tau} + \sum_{n_{\tau}=1}^{N_{\tau}} a_{n,\tau} \cos(n_{\tau}\phi_{\tau})) \tag{3.8}$$

However, the solution of the Mathieu and Hill differential equations is far from trivial, so PG also presented a useful expression for complex cases, which approximates the quantum torsional partition function to the product of the classical partition function $Q_{\text{cl,tor}}^{(\text{C})}$ by a coefficient $F^{\text{TPG(C)}}$ that takes into account quantum effects. In the most general case the classical partition function is considered coupled (C), and the torsional PG expression [TPG(C)] is given by:

$$Q_{\text{tor}}^{\text{TPG(C)}} = Q_{\text{cl,tor}}^{(\text{C})} F^{\text{TPG(C)}} \tag{3.9}$$

The coefficient is given by the ratio:

$$F^{\mathrm{TPG(C)}} = \frac{Q_{\mathrm{tor}}^{\mathrm{HO(C)}}}{Q_{\mathrm{tor}}^{\mathrm{CHO(C)}}} \tag{3.10}$$

The quantum and classical harmonic-oscillator partition functions due to the two coupled torsions $\eta = 1, 2$ are given by:

$$Q_{\mathrm{tor}}^{\mathrm{HO(C)}} = \prod_{\eta=1}^{2} \frac{e^{-\beta\hbar\overline{\omega}_\eta/2}}{1 - e^{-\beta\hbar\overline{\omega}_\eta}}, \tag{3.11}$$

and

$$Q_{\mathrm{tor}}^{\mathrm{CHO(C)}} = \prod_{\eta=1}^{2} \frac{1}{\beta\hbar\overline{\omega}_\eta} \tag{3.12}$$

respectively (hereafter the Greek letters τ and η indicate uncoupled and coupled torsional frequencies, respectively).

Hereafter, the harmonic partition functions with the subscript tor are calculated using pure torsional frequencies or torsional potentials in the case of classical partition functions. If normal-mode frequencias are used the subscript nm will be added to the partition function. Torsional frequencies are written with an overline ($\overline{\omega}$ to distinguish them from normal-mode frequencies ω. Also the following superscripts for harmonic partition functions will be used along the paper: quantum harmonic oscillator (HO), classical harmonic oscillator (CHO), multi-conformer harmonic oscillator (MC-HO) and multi-conformer classical harmonic oscillator (MC-CHO). Moreover, the superscripts, for different approximations, may include a U or a C between parentheses to indicate uncoupled or coupled torsions, respectively, in cases that both of them are discussed.

The coupled torsional frequencies, as well as, the classical partition functions are calculated from expressions obtained by KP and summarized below. KP devised a method which includes the full kinetic and potential energy coupling between torsions and between those torsions and the external rotation of the molecule. For the particular case of two hindered rotations with dihedral angles ϕ_1 and ϕ_2, the exact classical partition function for the hindered rotor plus overall rotation is given by:

$$Q_{\mathrm{cl}}^{\mathrm{FC}} = \frac{8\pi^2}{\sigma_{\mathrm{tor}}\sigma_{\mathrm{rot}}} \left(\frac{1}{2\pi\beta\hbar^2}\right)^{5/2} \int_0^{2\pi}\int_0^{2\pi} d\phi_1 d\phi_2 |\mathbf{S}(\phi_1,\phi_2)|^{1/2} \mathrm{e}^{-\beta \mathrm{V}(\phi_1,\phi_2)}, \tag{3.13}$$

where $Q_{\mathrm{cl}}^{\mathrm{FC}}$ means fully coupled (FC) classical partition function, $\beta = k_{\mathrm{B}}T$, k_{B} is Boltzmann constant, T is temperature; $\hbar$ is Planck constant divided by 2π; σ_{rot} is the symmetry number for overall rotation [14]; $\sigma_{\mathrm{tor}} = \sigma_{\mathrm{tor},1}\sigma_{\mathrm{tor},2}$ is the product of the symmetry numbers for internal rotation $\sigma_{\mathrm{tor},1}$ and $\sigma_{\mathrm{tor},2}$ about the dihedral angles ϕ_1 and ϕ_2, respectively; $V(\phi_1,\phi_2)$ is the torsional potential; $|\mathbf{S}(\phi_1,\phi_2)|$ is the determinant of the $\mathbf{S}$ matrix, which after a congruent

transformation (see Ref. 8) is given by:

$$\mathbf{S} = \begin{pmatrix} I_1^{\rm rot} & 0 & 0 & 0 & 0 \\ 0 & I_2^{\rm rot} & 0 & 0 & 0 \\ 0 & 0 & I_3^{\rm rot} & 0 & 0 \\ 0 & 0 & 0 & I_1 & -\Lambda_{12} \\ 0 & 0 & 0 & -\Lambda_{12} & I_2 \end{pmatrix} \tag{3.14}$$

Therefore the determinant of the **S** matrix can be written as:

$$|\mathbf{S}| = |\mathbf{D}| \prod_{i=1}^{3} I_i^{\rm rot} \tag{3.15}$$

where $I_i^{\rm rot}$ accounts for each of the three principal moments of inertia. The matrix **D** accounts for the kinetic energy couplings between the two torsions and between the torsions and the external rotation:

$$\mathbf{D} = \begin{pmatrix} I_1 & -\Lambda_{12} \\ -\Lambda_{12} & I_2 \end{pmatrix} \tag{3.16}$$

The reduced moments of inertia of the two torsions are I_1 and I_2, and Λ_{12} is the coupling. For the 20 systems studied in this work, they are given in Table 3.3. The reduced moments of inertia I_1 and I_2 can also be obtained by the method of Pitzer [15] and they are commonly used in the evaluation of partition functions which consider torsions as separable ($\Lambda_{12} = 0$). In general, a very good approximation is to assume that the principal moments of inertia do not change with the torsional angles, so we use the ones of the absolute minimum. In that case Eq. 3.13 is approximated to:

$$Q_{\rm cl}^{\rm FC} \cong Q_{\rm rot} Q_{\rm cl,tor}^{\rm (C)} \tag{3.17}$$

where

$$Q_{\rm rot} = \frac{8\pi^2}{\sigma_{\rm rot}} \left(\frac{1}{2\pi\hbar^2\beta} \right)^{3/2} \sqrt{I_1^{\rm rot} I_2^{\rm rot} I_3^{\rm rot}} \tag{3.18}$$

is the rotational partition function, and

$$Q_{\rm cl,tor}^{\rm (C)} = \frac{1}{\sigma_{\rm tor}} \frac{1}{2\pi\beta\hbar^2} \int_0^{2\pi} \int_0^{2\pi} d\phi_1 d\phi_2 |\mathbf{D}(\phi_1,\phi_2)|^{1/2} {\rm e}^{-\beta {\rm V}(\phi_1,\phi_2)}, \tag{3.19}$$

is the classical torsional partition function which enters Eq. 3.9; $|\mathbf{D}(\phi_1,\phi_2)|$ being the determinant of the **D** matrix. The torsional frequencies are calculated as the eigenvalues of the secular determinant:

$$|\mathbf{K} - \overline{\omega}_\eta^2 \mathbf{D}| = 0 \tag{3.20}$$

being

$$\mathbf{K} = \begin{pmatrix} \frac{\partial^2 V}{\partial \phi_1^2} & \frac{\partial^2 V}{\partial \phi_1 \partial \phi_2} \\ \frac{\partial^2 V}{\partial \phi_1 \partial \phi_2} & \frac{\partial^2 V}{\partial \phi_2^2} \end{pmatrix} \tag{3.21}$$

the force constant matrix $\mathbf{K}$ of the torsional potential at the global minimum. In the PG and KP works the $Q_{\rm tor}^{\rm TPG(C)}$ partition function is only calculated at the global minimum of the torsional potential, because it is assumed that the other wells have torsional frequencies similar to the global minimum. There is not a unique way to calculate $\mathbf{K}$, in the 2D-NS method is obtained from the two-dimensional torsional Fourier series potential, frequencies $\overline{\omega}_\eta$ in Table 3.4 and hereafter. If the frequencies are obtained from the force constants associated to the torsions, which were calculated from the electronic structure calculations, they are given by $\overline{\omega}_\eta^{\rm (C)}$ in Table 3.4 and are used in the MS-T(C) method.

The PG coefficient of Eq. 3.9 can be seen as a quantum correction to the classical partition function, but the expression can also be written as

$$Q_{\rm tor}^{\rm TPG(C)} = \frac{Q_{\rm cl,tor}^{\rm (C)}}{Q_{\rm tor}^{\rm CHO(C)}} Q_{\rm tor}^{\rm HO(C)} \tag{3.22}$$

so it can also be seen as an anharmonic correction to the harmonic oscillator torsional partition function (i.e., as the ratio between the fully coupled classical partition function and the classical limit of the harmonic oscillator partition function).

There is not a unique way to incorporate multiple torsional wells into the torsional partition function of Eq. 3.9. One possibility is to substitute the HO and CHO partition functions by multiconformer partition functions. The multiconformer HO and CHO partition functions are

$$Q_{\rm tor}^{\rm MC-HO(C)} = \sum_{j=1}^{J} e^{-\beta U_j} \prod_{\eta=1}^{2} \frac{e^{-\beta\hbar\overline{\omega}_{j,\eta}/2}}{1-e^{-\beta\hbar\overline{\omega}_{j,\eta}}}, \tag{3.23}$$

and

$$Q_{\rm tor}^{\rm MC-CHO(C)} = \sum_{j=1}^{J} e^{-\beta U_j} \prod_{\eta=1}^{2} \frac{1}{\beta\hbar\overline{\omega}_{j,\eta}}, \tag{3.24}$$

respectively. The torsional frequencies, $\overline{\omega}_{j,\eta}$ with $\eta = 1, 2$, are calculated for each well j through Eq. 3.20. The difference in energy between the absolute minimum and the well j is given by U_j. A similar equation to Eq. 3.9 but taking into account multiple wells would be:

$$Q_{\rm tor}^{\rm MC-TPG(C)} = Q_{\rm cl,tor}^{\rm (C)} \frac{Q_{\rm tor}^{\rm MC-HO(C)}}{Q_{\rm tor}^{\rm MC-CHO(C)}} \tag{3.25}$$

which can be considered an extension of the PG expression to take into account multiple wells.

3.2.2 One-dimensional methods

The classical partition function of Eq. 3.19 considers that torsions are non-separable. However, many available methods assume that the two dimensional partition function can be written as a product of two one-dimensional partition functions that correspond to each

Table 3.3: List of the reduced moments of inertia I_j, couplings Λ, and product of the principal moments of inertia I_A, I_B, I_C. The units of the moments of inertia and couplings are amu·Å^2.

Conformer	I_1, I_2	Λ	$I_A I_B I_C$
S1-M1	6.957, 0.786	-3.540E-01	7.408E+05
S1-M2	6.362, 0.768	-7.676E-02	7.875E+05
S1-M3	6.548, 0.783	3.765E-01	8.086E+05
S1-M4	6.492, 0.719	-1.791E-01	8.215E+05
S2-M1	3.823, 0.842	-2.964E-01	1.919E+05
S2-M2	7.047, 0.806	5.399E-02	1.459E+05
S2-M3	7.011, 0.824	8.101E-02	1.415E+05
S3-M1	4.383, 0.784	-5.110E-01	2.009E+05
S3-M2	5.902, 0.743	2.854E-01	1.779E+05
S3-M3	5.953, 0.727	-4.161E-02	1.892E+05
S3-M4	3.844, 0.741	1.276E-01	2.157E+05
S4-M1	0.736, 2.590	-2.687E-02	4.544E+04
S4-M2	0.732, 2.593	1.577E-01	4.767E+04
S5-M1	8.511, 0.796	-4.270E-01	8.419E+05
S5-M2	8.199, 0.779	4.403E-02	8.338E+05
S5-M3	8.534, 0.728	2.565E-01	8.560E+05
S5-M4	8.233 0.746	3.942E-01	8.763E+05
S6-M1	6.577, 0.854	-4.670E-01	7.155E+05
S6-M2	6.888, 0.719	8.457E-02	9.609E+05
S6-M3	6.990, 0.739	-7.100E-04	9.392E+05
S6-M4	5.632, 0.735	2.832E-01	9.064E+05
S7-M1	0.761, 10.87	4.897E-01	1.192E+06
S7-M2	0.777, 13.13	-4.468E-01	1.118E+06
S7-M3	0.753, 13.18	2.138E-01	1.211E+06
S7-M4	0.740, 10.82	-2.447E-01	1.212E+06
S8-M1	4.217, 2.979	-1.501E+00	2.131E+05
S8-M2	6.972, 2.494	-5.130E-01	1.631E+05
S9-M1	5.002, 0.779	-4.683E-01	2.679E+05
S9-M2	7.301, 0.739	-1.891E-01	2.605E+05
S9-M3	4.898, 0.742	-1.024E-01	2.572E+05
S9-M4	7.190, 0.758	2.283E-01	2.463E+05
S9-M5	7.204, 0.760	-3.750E-01	2.605E+05
S10-M1	0.743, 2.937	6.738E-02	2.715E+05
S10-M2	0.737, 2.930	-1.029E-01	2.743E+05
S11-M1	0.738, 2.880	-1.050E-01	2.871E+05
S11-M2	0.736, 2.919	8.350E-02	2.764E+05
S12-M1	6.704, 3.040	-7.911E-01	1.094E+06
S12-M2	6.748, 2.960	3.883E-01	1.110E+06
S13-M1	8.845, 0.732	-6.034E-02	1.073E+06
S13-M2	8.861, 0.744	3.419E-01	1.047E+06
S13-M3	8.699, 0.788	-4.561E-01	1.045E+06
S13-M4	6.924, 0.737	1.191E-01	1.063E+06
S14-M1	8.542, 0.744	4.087E-02	9.690E+05
S14-M2	8.391, 0.763	3.622E-01	9.958E+05
S14-M3	8.410, 0.763	-3.683E-01	1.070E+06
S14-M4	8.813, 0.745	2.010E-01	1.086E+06
S15-M1	7.282, 2.971	5.953E-01	1.178E+06
S15-M2	5.933, 3.038	-7.152E-01	1.115E+06
S15-M3	6.352, 3.028	-7.085E-01	1.015E+06
S16-M1	5.367, 2.954	-1.301E+00	3.333E+05
S16-M2	7.690, 2.817	-4.068E-01	3.241E+05
S17-M1	2.920, 2.920	-5.071E-02	3.672E+05
S18-M1	8.799, 8.205	-4.506E+00	2.510E+06
S18-M2	7.729, 4.817	-2.583E+00	3.776E+06
S18-M3	5.545, 6.784	-2.079E+00	3.668E+06
S18-M4	8.539, 7.117	-5.086E+00	3.246E+06
S19-M1	16.089, 0.799	-7.513E-01	1.475E+07
S19-M2	15.098, 0.773	3.998E-01	1.443E+07
S20-M1	0.765, 3.057	4.656E-02	1.285E+07
S20-M2	0.774, 3.043	-2.810E-02	1.295E+07

Table 3.4: For each system list of TES frequencies $\overline{\omega}_{j,\tau}^{\mathrm{TES}}$; uncoupled $\overline{\omega}_{j,\tau}$ and coupled $\overline{\omega}_{j,\eta}$ torsional frequencies obtained from Eq. 3.20 by using the one-dimensional and two dimensional Fourier series potentials, respectively; uncoupled $\overline{\omega}_{j,\tau}^{(\mathrm{U})}$ and coupled $\overline{\omega}_{j,\eta}^{(\mathrm{C})}$ torsional frequencies obtained from Eq. 3.20 by using the harmonic force constants at the minima; normal-mode frequencies ω_j. The zero-point energy (ZPE) due to the torsions calculated by the TES and 2D-NS methods is also indicated. All the frequencies and ZPEs are given in cm^{-1}.

System	Conformer	$\mathrm{ZPE}^{\mathrm{TES}}$	$\mathrm{ZPE}^{\mathrm{2D-NS}}$	$\overline{\omega}_{j,\tau}^{\mathrm{TES}}$	$\overline{\omega}_{j,\tau}$	$\overline{\omega}_{j,\eta}$	$\overline{\omega}_{j,\tau}^{(\mathrm{U})}$	$\overline{\omega}_{j,\eta}^{(\mathrm{C})}$	ω_j
$S1$	S1-M1	369.9	366.2	156.0, 582.8	157.0, 618.9	153.4, 599.5	193.5, 657.7	177.8, 658.0	168.4, 668.0
	S1-M2				*, 614.6	98.6, 589.8	111.5, 601.8	111.0, 602.6	100.4, 667.8
	S1-M3					92.4, 592.2	93.5, 601.5	92.9, 611.7	92.7, 677.3
	S1-M4				74.0, *	78.5, 428.4	80.4, 461.3	80.4, 463.0	80.1, 430.5
$S2$	S2-M1	191.6	184.8	247.4, 135.8	256.0, 179.6	236.6, 181.1	252.4, 198.4	252.5, 197.5	248.8, 176.3
	S2-M2					268.6, 81.4	102.9, 268.5	89.1, 274.5	75.8, 260.9
	S2-M3				135.3,*	234.3, 69.4	90.7, 240.2	89.1, 241.4	64.9, 227.9
$S3$	S3-M1	266.4	319.3	252.9, 280.0	263.0, 285.3	201.6, 404.8	285.1, 403.6	229.4, 411.6	198.0, 392.6
	S3-M2				104.6, *	86.7, 233.9	92.2, 231.9	91.1, 232.4	86.4, 227.9
	S3-M3					81.9, 295.1	87.6, 293.3	85.5, 293.6	81.4, 285.7
	S3-M4				*,245.7	178.0, 259.5	202.4, 223.2	176.8, 248.3	165.6, 242.2
$S4$	S4-M1	255.9	255.2	261.9, 249.9	300.4, 259.6	294.9, 240.6	278.6, 259.6	288.2, 248.2	284.1, 241.3
	S4-M2				296.3,*	296.9, 265.0	287.6, 269.8	292.6, 266.5	284.2, 262.3
$S5$	S5-M1	356.9	357.6	119.1, 594.6	118.3, 775.3	118.3, 606.1	125.7, 603.5	125.6, 611.9	119.1, 641.6
	S5-M2				106.8,*	106.6, 565.0	129.5, 574.8	126.9, 576.0	112.7, 590.0
	S5-M3				*, 493.8	94.5, 473.5	100.1, 457.5	97.5, 462.7	94.2, 428.3
	S5-M4					90.5, 479.4	124.7, 477.7	124.6, 482.8	94.5, 489.6
$S6$	S6-M1	468.5	448.1	212.9, 724.0	213.3, 717.9	209.4, 696.7	321.1, 895.7	288.5, 896.1	271.5, 900.2
	S6-M2				151.1,*	147.5, 466.0	169.0, 475.3	168.6, 475.5	152.7, 542.5
	S6-M3					148.1, 337.1	168.6, 337.8	168.6, 339.9	153.1, 264.4
	S6-M4				*,415.2	137.7, 435.0	160.2, 418.4	156.3, 421.5	142.6, 475.7
$S7$	S7-M1	228.5	231.9	353.8, 103.2	362.4, 104.2	369.3, 104.2	379.7, 114.4	381.2, 110.6	373.4, 108.5
	S7-M2					433.1, 112.2	435.2, 128.6	435.7, 123.3	425.3, 118.2
	S7-M3				*. 89.3	390.0, 88.4	396.5, 101.4	396.9, 101.0	398.9, 90.7
	S7-M4				185.1, *	223.5, 105.8	243.4, 116.5	246.1, 115.2	217.0, 112.4
$S8$	S8-M1	230.0	242.7	228.1, 231.8	237.8, 247.1	241.9, 251.9	257.0, 263.5	246.6, 266.0	240.9, 261.3
	S8-M2				62.5,*	14.3, 157.2	63.3, 157.1	52.1, 166.3	28.2, 164.1
$S9$	S9-M1	222.3	228.6	165.0, 279.6	233.5, 303.7	180.2, 312.8	194.1, 316.1	190.6, 317.0	183.2, 302.6
	S9-M2				132.8,*	120.5, 350.1	139.7, 343.5	138.3, 343.6	118.8, 337.5
	S9-M3				*,233.8	161.5, 249.8	183.3, 222.1	152.7, 248.0	150.5, 244.9
	S9-M4					112.3, 257.0	121.6, 255.0	121.2, 255.3	111.1, 250.5
	S9-M5				122.1,*	107.4, 228.1	115.6, 226,6	110.3, 236.3	101.7, 222.9
$S10$	S10-M1	292.2	292.9	409.5, 174.9	419.3, 180.9	419.6, 180.8	432.8, 187.9	432.9, 185.8	423.8, 180.8
	S10-M2				221.9,*	232.8, 176.7	242.7, 205.3	250.3, 199.8	214.7, 169.3
$S11$	S11-M1	201.3	211.6	348.0, 54.6	365.0, 53.4	381.4, 52.7	383.9, 69.7	386.9, 66.5	329.2, 48.6
	S11-M2				174.6,*	210.4, 108.5	228.9, 120.6	231.0, 113.0	199.4, 99.1
$S12$	S12-M1	144.3	145.3	153.8, 134.7	154.1, 141.9	159.6, 139.2	188.3, 159.7	198.4, 153.9	179.1, 146.1
	S12-M2				107.9,*	149.4, 106.9	113.7, 147.4	113.6, 147.4	111.9, 144.8
$S13$	S13-M1	231.4	236.4	110.5, 352.3	112.0, 360.7	107.2, 372.8	116.8, 386.8	111.5, 389.2	102.0, 290.8
	S13-M2				*, 245.7	127.9, 257.0	143,0, 258.3	142.6, 259.0	131.4, 215.7
	S13-M3				137.6,*	134.2, 519.5	188.3, 558.6	174.4, 559.0	153.9, 595.8
	S13-M4					93.6, 301.3	119.2, 317.2	111.7, 322.3	107.5, 274.8
$S14$	S14-M1	243.6	243.6	135.4, 351.7	135.8, 358.8	135.7, 358.9	159.1, 376.1	153.4, 379.2	143.9, 370.0
	S14-M2				*, 274.8	126.9, 279.6	162.4, 347.6	162.3, 349.7	141.0, 255.5
	S14-M3				102.4,*	102.0, 405.6	115.3, 407.9	115.0, 411.0	102.1, 383.3
	S14-M4					121.8, 306.0	131.8, 314.8	131.7, 315.9	123.7, 293.3
$S15$	S15-M1	135.4	136.7	130.1, 140.6	131.1, 147.9	122.0, 160.0	146.2, 149.7	136.0, 162.1	119.8, 158.0
	S15-M2				54.1, *	26.5, 146.0	110.3, 109.7	63.1, 153.3	13.6, 133.9
	S15-M3					40.4, 157.1	170.7, 182.8	116.6, 209.9	105.8, 196.2
$S16$	S16-M1	203.8	193.1	155.1, 252.6	158.7, 260.8	142.6, 304.6	171.7, 264.9	171.4, 271.5	166.5, 267.4
	S16-M2				109.6,*	109.4, 233.4	118.6, 264.9	118.0, 240.9	106.6, 228.5
$S17$	S17-M1	122.3	123.3	122.3, 122.3	129.3, 129.3	128.2, 130.5	132.3, 132.3	127.6, 136.6	120.8, 132.1
$S18$	S18-M1	135.9	154.3	132.1, 139.6	132.4, 139.9	108.2, 201.7	152.5, 168.0	128.3, 235.3	203.5, 278.7
	S18-M2				*, 144.4	118.6, 192.6	167.1, 163.7	135.7, 222.3	126.6, 258.2
	S18-M3				121.9,*	117.0, 174.3	137.8, 184.9	131.2, 206.4	125.2, 277.4
	S18-M4					86.3, 190.9	116.8, 129.4	95.0, 210.1	80.9, 203.3
$S19$	S19-M1	216.2	182.5	85.6, 346.8	128.9, 457.2	53.3, 327.6	64.2, 421.8	61.3, 325.4	54.7, 320.9
	S19-M2				*, 260.7	15.8, 228.0	41.5, 220.3	29.9, 220.3	8.0, 180.9
$S20$	S20-M1	229.8	226.7	341.1, 118.6	356.9, 122.5	349.1, 122.2	336.8, 97.3	337.6, 96.4	343.6, 90.6
	S20-M2				280.2,*	275.4, 163.1	286.8, 163.6	287.1, 162.5	289.4, 158.5

of the two torsions, as indicated by Eq. 3.4. Under this assumption the classical partition function for each of the torsions is given by:

$$q_{\mathrm{cl},\tau} = \sqrt{\frac{I_\tau k_B T}{2\pi\hbar^2}} \int_0^{2\pi/\sigma_{\mathrm{tor},\tau}} d\phi_\tau \exp(-\beta V_\tau[\phi_\tau]) \tag{3.26}$$

The integral of Eq. 3.26 can be solved analytically when the potential is well represented by the reference PG (RPG) potential of Eq. 3.5. In that case the reference classical (RC) partition function equals:

$$q_\tau^{\mathrm{RC}} = q_\tau^{\mathrm{FR}} \exp(-\beta W_\tau/2) I_0(\beta W_\tau/2) \tag{3.27}$$

where I_0 is a modified Bessel function of the first kind, Q_τ^{FR} is the classical free-rotor partition function of rotation τ given by

$$q_\tau^{\mathrm{FR}} = \frac{1}{\sigma_{\mathrm{tor},\tau}} \left(\frac{2\pi I_\tau}{\beta\hbar^2}\right)^{1/2} \tag{3.28}$$

and W_τ is the barrier height. One approximation that avoids the calculation of barrier heights is through their estimate from Eq. 3.6. The reduced moment of inertia is calculated at the equilibrium geometry, and the torsional frequency can be assumed, in the roughest approximation, to be equal to the normal mode frequency with the large torsional component. This is a good approximation if the torsion is not coupled.

Notice that most of the potentials will be more complicated than that of Eq. 3.5. In those cases we use an effective barrier height, W_τ^{eff}, which is obtained as the half sum of the left and right barriers that connect the absolute minimum with other minima. i.e.,

$$W_\tau^{\mathrm{eff}} = (W_\tau^L + W_\tau^R)/2 \tag{3.29}$$

The general expression of Eq. 3.9 for the case of the RPG potential that we use in this work is given by:

$$q_\tau^{\mathrm{RPG}} = q_\tau^{\mathrm{RC}} \frac{q_\tau^{\mathrm{HO}}}{q_\tau^{\mathrm{CHO}}} \tag{3.30}$$

where

$$q_\tau^{\mathrm{HO}} = \frac{e^{-\beta\hbar\overline{\omega}_\tau/2}}{1 - e^{-\beta\hbar\overline{\omega}_\tau}}, \tag{3.31}$$

and

$$q_\tau^{\mathrm{CHO}} = \frac{1}{\beta\hbar\overline{\omega}_\tau} \tag{3.32}$$

In this work, the torsional frequency $\overline{\omega}_\tau$ of each hindered rotor in the RPG method is calculated from Eq. 3.6 using the the effective barrier obtained from Eq. 3.29 and the reduced moment of inertia of the equilibrium geometry. There are several other approximations to calculate two of the unknowns of Eq. 3.6, which were extensively discussed in Ref. 16.

A correction to the approximate quantum correction of q_τ^{RPG}, which reproduces the tabulated data by PG obtained from the solution of the Schrödinger equation for the RPG potential, was proposed by Ayala and Schlegel (AS) [17]:

$$q_\tau^{\mathrm{AS}} = \frac{1 + P_{2,\tau} \exp(-\beta W_\tau/2)}{1 + P_{1,\tau} \exp(-\beta W_\tau/2)} q_\tau^{\mathrm{RPG}} \tag{3.33}$$

where $P_{1,\tau}$ and $P_{2,\tau}$ are fifth order polynomials. In this work the RPG and AS partition functions make use of the effective barriers obtained from Eq. 3.29 and of the reduced moments of inertia calculated at the absolute minimum. Therefore, the calculation of these two partition functions require the geometries, frequencies of the absolute minimum and torsional barrier heights about this minimum.

Truhlar [18], and Chuang and Truhlar [19] (CT) recommended a partition function that uses normal-mode frequencies and avoids the calculation of barrier heights. It includes all the conformational minima about a given rotation:

$$q_{\tau,\mathrm{nm}}^{\mathrm{CT}} = q_{\tau,\mathrm{nm}}^{\mathrm{MC-HO}} \tanh\left(\frac{q_\tau^{\mathrm{FR}}}{q_{\tau,\mathrm{nm}}^{\mathrm{MC-CHO}}}\right) \tag{3.34}$$

At low temperatures, Eq. 3.34 tends to the multi-conformer normal-mode harmonic oscillator (MC-HO) partition function, i.e.,

$$q_{\tau,\mathrm{nm}}^{\mathrm{MC-HO}} = \sum_{j=1}^{J_\tau} q_{j,\tau,\mathrm{nm}}^{\mathrm{HO}} e^{-\beta U_{j,\tau}} \tag{3.35}$$

where J_τ is the number of distinguishable minima along ϕ_τ and $U_{j,\tau}$ the relative energy of minimum j with regards to the absolute minimum. Eq. 3.34 tends to the classical multi-conformer harmonic oscillator (MC-CHO) partition function at intermediate temperatures, i.e.,

$$q_{\tau,\mathrm{nm}}^{\mathrm{MC-CHO}} = \sum_{j=1}^{J_\tau} q_{j,\tau,\mathrm{nm}}^{\mathrm{CHO}} e^{-\beta U_{j,\tau}} \tag{3.36}$$

and to the free-rotor partition function at high temperatures.

Whereas the CT method can still grasp some of the features of a general potential, a good performance of the RPG and AS methods is essentially limited to cases in which the RPG potential is accurate. An extension of the RPG method, called segmented RPG (SRPG), accounts for the characteristics of the potential. It uses pure torsional frequencies and involves the calculation of the classical partition function of Eq. 3.26 as a sum of segmented reference classical (SRC) partition functions with the PG quantum correction at each well along ϕ_τ, i.e.,

$$q_\tau^{\mathrm{SRPG}} = \sum_{j=1}^{J_\tau} \exp(-\beta U_{j,\tau}) \frac{q_{j,\tau}^{\mathrm{HO}}}{q_{j,\tau}^{\mathrm{CHO}}} q_{j,\tau}^{\mathrm{SRC}} \tag{3.37}$$

where the segmented reference classical partition function at each well is given by:

$$q_{j,\tau}^{\mathrm{SRC}} = q_{j,\tau}^{\mathrm{FR}} \times \left[\frac{\phi_{j,\tau,\mathrm{eq}} - \phi_{j,\tau}^{L}}{2\pi} \exp\left(-\beta W_{j,\tau}^{L}/2\right) I_0(\beta W_{j,\tau}^{L}/2) + \frac{\phi_{j,\tau}^{R} - \phi_{j,\tau,\mathrm{eq}}}{2\pi} \exp\left(-\beta W_{j,\tau}^{R}/2\right) I_0(\beta W_{j,\tau}^{R}/2) \right], \tag{3.38}$$

and

$$q_{j,\tau}^{\mathrm{FR}} = \frac{1}{\sigma_{\mathrm{tor},\tau}} \left(\frac{2\pi I_{j,\tau}}{\beta \hbar^2} \right)^{1/2} \tag{3.39}$$

represents the free rotor partition function at well j. The total SRC partition function is:

$$q_{\tau}^{\mathrm{SRC}} = \sum_{j=1}^{J_\tau} q_{j,\tau}^{\mathrm{SRC}} \tag{3.40}$$

The evaluation of the SRPG partition function requires geometries and torsional barrier heights that surround each of the wells, $W_{j,\tau}^{L}$ and $W_{j,\tau}^{R}$ being the left and right barrier heights located at the $\phi_{j,\tau}^{L}$ and $\phi_{j,\tau}^{R}$ torsional angles. The position of each well is given by $\phi_{j,\tau,\mathrm{eq}}$.

The SRPG method requires almost the same computational effort, but it is less accurate, than the methods that require the knowledge of the one-dimensional potential along each torsional angle. If the one-dimensional potential is available for torsion ϕ_τ, it is possible to calculate the TPG partition function as:

$$q_{\tau}^{\mathrm{TPG}} = q_{\mathrm{cl},\tau} \frac{q_{\tau}^{\mathrm{HO}}}{q_{\tau}^{\mathrm{CHO}}} \tag{3.41}$$

where

$$q_{\tau}^{\mathrm{HO}} = \frac{e^{-\beta\hbar\overline{\omega}_\tau/2}}{1 - e^{-\beta\hbar\overline{\omega}_\tau}}, \tag{3.42}$$

and

$$q_{\tau}^{\mathrm{CHO}} = \frac{1}{\beta\hbar\overline{\omega}_\tau} \tag{3.43}$$

For the case of two hindered rotors the uncoupled torsional PG partition function is given by:

$$Q_{\mathrm{tor}}^{\mathrm{TPG(U)}} = \prod_{\tau=1}^{2} q_{\tau}^{\mathrm{TPG}} \tag{3.44}$$

In this case the HO and CHO torsional frequencies are calculated from the one-dimensional potential, i.e.,

$$\overline{\omega}_\tau = \sqrt{\frac{k_\tau}{I_\tau}} \tag{3.45}$$

where the force constant k_τ, which is given by

$$k_\tau = \left(\frac{d^2 V_\tau}{d\phi^2} \right)_{\phi_\tau = \phi_{\tau,\mathrm{eq}}} \tag{3.46}$$

as well as the reduced moment of inertia are calculated at the global minimum. In the same way it is also possible to calculate the multi-conformer torsional HO and CHO partition functions, which are given by Eqs. 3.35 and 3.36, respectively, but using torsional instead of normal-mode frequencies.

The calculation of the energy levels by directly solving the Mathieu or Hill differential equations resulting from the substitution of the one dimensional potentials into the Schrödinger equation of Eq. 3.7 is very laborious. However, nowadays the energy levels are obtained through the variational theorem, which is a straightforward procedure. This method is called torsional eigenvalue summation (TES). In the study of internal rotations, it is common to use as trial function a linear combination of functions which are solution of the Schrödinger equation for the particle in a ring:

$$\Phi_\tau(\phi_\tau) = \frac{1}{\sqrt{2\pi}} \sum_{k=-K}^{K} c_{\tau,k} e^{ik\phi_\tau}, \tag{3.47}$$

where K is of the order of one hundred. The TES partition function is obtained from:

$$q_\tau^{\mathrm{TES}} = \frac{1}{\sigma_\tau} \sum_j e^{-\beta\varepsilon_{j,\tau}} \tag{3.48}$$

being $\sigma_{\mathrm{tor},\tau}$ the symmetry number for internal rotation, and $\varepsilon_{j,\tau}$ are the eigenvalues (energies) after diagonalization of the secular matrices resulting from applying the variational method to the Schrödinger equation.

3.2.3 Two-dimensional methods for coupled torsions

In the previous subsection torsions in two dimensions were calculated as the product of the two one-dimensional partition functions, but they can also be calculated from the coupled potential. One example of the latter is the TPG(C) partition function. A quantum version of the TPG(C) for two coupled torsions is the 2D-NS method [10, 20], in which the torsional partition function is evaluated by directly solving the two-dimensional Schrödinger equation with full coupling in the kinetic, T_{tor} and potential energy terms, $V_{\mathrm{tor}}(\phi_1, \phi_2)$, i.e.:

$$\left\{ T_{\mathrm{tor}}\left(\frac{\partial}{\partial\phi_1}, \frac{\partial}{\partial\phi_2}\right) + V_{\mathrm{tor}}(\phi_1, \phi_2) \right\} \Phi(\phi_1, \phi_2) = E\Phi(\phi_1, \phi_2) \tag{3.49}$$

The kinetic energy is given by Eq. 8 of Ref. 10. The potential is fitted to Fourier series of the type:

$$\begin{aligned} V_{\mathrm{tor}}(\phi_1, \phi_2) =& V_1(\phi_1) + V_2(\phi_2) + \\ & \sum_{l_1=1}^{L_1} \sum_{l_2=1}^{L_2} c_{l_1 l_2} \cos(l_1\phi_1) \cos(l_2\phi_2) + \sum_{l_1'=1}^{L_1'} \sum_{l_2'=1}^{L_2'} c'_{l_1' l_2'} \sin(l_1'\phi_1) \sin(l_2'\phi_2) \end{aligned} \tag{3.50}$$

where $V_1(\phi_1)$ and $V_2(\phi_2)$ are one-dimensional potentials of the type of Eq. 3.8. The parameters $c_{l_1 l_2}$ and $c'_{l_1' l_2'}$, as well as, the parameters for the one-dimensional potentials are obtained

from the fitting. The potential of Eq. 3.50 may also include odd terms involving $\sin(n_1\phi_1)$, $\sin(n_2\phi_2)$, $\cos(l_1\phi_1)\sin(l_2\phi_2)$ or $\sin(l'_1\phi_1)\sin(l'_2\phi_2)$ functions, but they are seldom needed to obtain a good fit.

Eq. 3.49 is solved by the variational method. The trial function is built as the product of two one-dimensional wave functions, which are solution of the Schrödinger equation for the particle in a ring, i.e.,

$$\Phi(\phi_1,\phi_2) = \frac{1}{2\pi}\sum_{k_1=-K}^{K}\sum_{k_2=-K}^{K} c_{k_1,k_2} e^{ik_1\phi_1} e^{ik_2\phi_2} \tag{3.51}$$

The 2D-NS partition function for hindered rotors is just the direct sum of the eigenvalues E_j obtained from Eq. 3.49 divided by the symmetry number due to the torsions, $\sigma_{\rm tor}$:

$$Q_{\rm tor}^{\rm 2D-NS} = \frac{1}{\sigma_{\rm tor}}\sum_j e^{-\beta E_j} \tag{3.52}$$

and, therefore, it can also be used to calculate the tunneling splitting of the lowest vibrational level due to torsional motion [21].

3.2.4 The rovibrational partition function with torsional anharmonicity

In the previous Sections we have discussed different methods to treat torsions, but they need to be integrated into the total rovibrational partition function to be operative. The most straightforward way to incorporate anharmonicity due to hindered rotors into the harmonic rovibrational partition function of Eq. 3.2 would be to remove the normal-modes associated to the torsions and multiply the resulting partition function by the torsional partition function using a given approximation, i.e.,

$$Q^{\rm X} = Q_{\rm tor}^{\rm X}\frac{Q^{\rm MC-H}}{Q_{\rm tor,nm}^{\rm MC-HO}} \tag{3.53}$$

where the subscript nm in the MC-HO partition function indicates that is based on normal modes and X indicates any method to treat torsional modes. Normal-mode torsional frequencies may be coupled between them or with other vibrational degrees of freedom, so, unfortunately, this procedure is not very accurate.

Vansteenkiste *et al.* [11] proposed a way to incorporate the rovibrational partition function into the torsional partition function, so it is possible to account for the variation of the vibrational non-torsional degrees of freedom with the t torsions:

$$\begin{aligned} Q_{\rm rv}^{\rm EHR} =& \frac{8\pi^2}{\sigma_{\rm tor}\sigma_{\rm rot}}\left(\frac{1}{2\pi\beta\hbar^2}\right)^{3/2+t/2}\int_0^{2\pi}\int_0^{2\pi},\cdots,\int_0^{2\pi} d\phi_1 d\phi_2,\cdots,d\phi_{\rm t}\times \\ & |\mathbf{S}(\phi_1,\phi_2,\cdots\phi_{\rm t})|^{1/2} {\rm e}^{-\beta {\rm V}(\phi_1,\phi_2,\cdots,\phi_{\rm t})} \overline{\overline{\rm Q}}^{\rm HO}(\phi_1,\phi_2,\cdots,\phi_{\rm t}) \end{aligned} \tag{3.54}$$

The extended hindered rotor (EHR) partition function of Eq. 3.54 treats all the vibrational degrees of freedom, with the exception of the t torsions, quantum mechanically. The vibrational partition function $\overline{\overline{Q}}^{\mathrm{HO}}$ refers to the product of the individual vibrational harmonic 3N-6-t nontorsional vibrations and is given by:

$$\overline{\overline{Q}}^{\mathrm{HO}}(\phi_1, \phi_2, \cdots, \phi_{\mathrm{t}}) = \prod_{\overline{\overline{m}}=1}^{3N-6-t} \frac{e^{-\beta\hbar\overline{\overline{\omega}}_{\overline{\overline{m}}}/2}}{1 - e^{-\beta\hbar\overline{\overline{\omega}}_{\overline{\overline{m}}}}} \tag{3.55}$$

where the frequencies $\overline{\overline{\omega}}_{\overline{\overline{m}}}$ were calculated using nonredundant internal coordinates as detailed in Ref. 13.

In the case of two torsions ($t = 2$) the EHR partition function is given by:

$$Q_{\mathrm{rv}}^{\mathrm{EHR}} = \frac{8\pi^2}{\sigma_{\mathrm{tor}}\sigma_{\mathrm{rot}}} \left(\frac{1}{2\pi\beta\hbar^2}\right)^{5/2} \int_0^{2\pi}\int_0^{2\pi} d\phi_1 d\phi_2 |\mathbf{S}(\phi_1, \phi_2)|^{1/2} \mathrm{e}^{-\beta \mathrm{V}(\phi_1,\phi_2)} \overline{\overline{\mathrm{Q}}}^{\mathrm{HO}}(\phi_1, \phi_2) \tag{3.56}$$

The interpolation of the $\overline{\overline{Q}}^{\mathrm{HO}}$ partition function at different values of the two torsional angles is discussed in the Computational details Section.

Quantum effects due to the torsions can be incorporated into the partition function of Eq. 3.56 as the ratio between quantum and classical torsional partition functions through a PG multiplicative coefficient like the one of Eq. 3.10, i.e.,

$$Q_{\mathrm{rv}}^{\mathrm{EX}} = F^{\mathrm{X}} Q_{\mathrm{rv}}^{\mathrm{EHR}} \tag{3.57}$$

where X indicates the method used to calculate the two dimensional torsional partition function. It is also possible to use multiconformational partition functions

$$F^{\mathrm{MC-TPG(C)}} = \frac{\overline{Q}_{\mathrm{tor}}^{\mathrm{MC-HO(C)}}}{\overline{Q}_{\mathrm{tor}}^{\mathrm{MC-CHO(C)}}} \tag{3.58}$$

or the 2D-NS partition funcion, that does not invoke the harmonic approximation. In this case the $F^{\mathrm{2D-NS}}$ is given by:

$$F^{\mathrm{2D-NS}} = \frac{Q_{\mathrm{tor}}^{\mathrm{2D-NS}}}{Q_{\mathrm{tor,cl}}^{(\mathrm{C})}} \tag{3.59}$$

and therefore the extended 2D-NS method (E2D-NS) is given by:

$$Q_{\mathrm{rv}}^{\mathrm{E2D-NS}} = F^{\mathrm{2D-NS}} Q_{\mathrm{rv}}^{\mathrm{EHR}} \tag{3.60}$$

The E2D-NS method, in addition to the quantum effects due to the torsions, includes the variation of the external rotation and of the 3N-8 vibrational degrees of freedom with the two torsions, as well as, the coupling between torsions. The partition function obtained from Eq. 3.60 is more accurate than the partition function obtained by the expression [10]:

$$Q_{\mathrm{rv}}^{\mathrm{GS2D-NS}} = \alpha_{\mathrm{tor}}^{\mathrm{2D-NS}} Q_{\mathrm{rv}}^{\mathrm{MC-H}} \tag{3.61}$$

The coefficient $\alpha_{\rm tor}^{\rm 2D-NS}$ accounts for deviations of the multiconformational RRHO partition function due to torsional anharmonicity:

$$\alpha_{\rm tor}^{\rm 2D-NS} = \frac{Q_{\rm tor}^{\rm 2D-NS}}{Q_{\rm tor}^{\rm MC-HO(C)}} \tag{3.62}$$

The problem with Eq. 3.61 is that assumes global separability of the torsional degrees of freedom, so we call the method GS2D-NS. This approximation is not involved in the calculation of the E2D-NS partition function.

Another possibility which has been explored recently, is to correct for anharmonicity at each of the distinguishable wells of the potential energy surface, i.e.,

$$Q_{\rm rv}^{\rm MS-T(Y)} = \sum_{j=1}^{J} Q_j^{\rm RRHO} Y_j^{\rm A} \tag{3.63}$$

where A indicates the following two approaches: (i) the uncoupled multistructural method with torsional anharmonicity [MS-T(U)]; and (ii) coupled multistructural method with torsional anharmonicity [MS-T(C)]. $Y_j^{\rm A}$ is calculated from the ratio between the classical anharmonic and classical harmonic oscillator torsional partition functions and is given by:

$$Y_j^{\rm MS-T(U)} = Z_j \prod_{\tau=1}^{t} f_{j,\tau} = Z_j \prod_{\tau=1}^{t} \frac{q_{j,\tau}^{\rm RC(U)}}{q_{j,\tau}^{\rm CHO(U)}} \tag{3.64}$$

in the uncoupled version, and by

$$Y_j^{\rm MS-T(C)} = \prod_{\eta=1}^{t} f_{j,\eta} = \prod_{\eta=1}^{t} \frac{q_{j,\eta}^{\rm RC(C)}}{q_{j,\eta}^{\rm CHO(C)}} \tag{3.65}$$

in the coupled approximation. The definitions of Z_j, the classical $q_{j,\tau}^{\rm RC(U)}$ and $q_{j,\eta}^{\rm RC(C)}$, and the classical harmonic $q_{j,\tau}^{\rm CHO(U)}$ partition functions and $q_{j,\eta}^{\rm CHO(C)}$ are described below.

The main difference between the method of Eq. 3.63 and E2D-NS is that the latter is a global method, in the sense that it needs a knowledge of the whole torsional potential, whereas Y_j^A is a local coefficient based on estimates of the anharmonicity in the surroundings of the wells. As a result the evaluation of the E2D-NS partition function is quite expensive in computer time (since the number of electronic structure calculations increases exponentially with the number of torsions), and difficult to extend beyond two or three coupled torsions. These two issues are not too important for the extension of the MS-T(Y) methods to higher dimensions.

The classical harmonic oscillator partition function in the MS-T(U) method is given by:

$$q_{\rm j,\tau}^{\rm CHO} = \frac{1}{\beta\hbar\overline{\omega}_{j,\tau}^{\rm (U)}} \tag{3.66}$$

and the torsional frequencies of each well are calculated as:

$$\overline{\omega}_{j,\tau}^{(\mathrm{U})} = \sqrt{\frac{k_{j,\tau}}{I_{j,\tau}}} \tag{3.67}$$

where $I_{j,\tau}$ and $k_{j,\tau}$ are the reduced moment of inertia and internal-coordinate force constant, respectively, for torsion τ in the well j. Assuming that the potential at the surroundings of a given minimum is well represented by a PG reference potential, i.e., by the potential of Eq. 3.5, for minimum j we have the expression:

$$V_{j,\tau}(\phi_\tau) = U_j + \frac{1}{2}W_{j,\tau}^{(\mathrm{U})}[1 - \cos M_{j,\tau}(\phi_\tau - \phi_{j,\tau,\mathrm{eq}})]; \quad \frac{-\pi}{M_{j,\tau}} \leq \phi_\tau - \phi_{j,\tau,\mathrm{eq}} \leq \frac{\pi}{M_{j,\tau}} \tag{3.68}$$

with $\phi_{j,\tau,\mathrm{eq}}$ being the torsional angle ϕ_τ at the equilibrium position. With the type of potential of Eq. 3.68 the barrier height is given by an expression similar to Eq. 3.6, i.e.,

$$W_{j,\tau}^{(\mathrm{U})} = \frac{2I_{j,\tau}[\overline{\omega}_{j,\tau}^{(\mathrm{U})}]^2}{M_{j,\tau}^2} \tag{3.69}$$

The RC(U) partition function is similar to Eq. 3.27 but for well j, that is,

$$q_{j,\tau}^{\mathrm{RC(U)}} = \frac{\sigma_{\mathrm{tor},\tau}}{M_{j,\tau}} q_{\tau,j}^{\mathrm{FR}} \exp\Big(-\beta W_{j,\tau}^{(\mathrm{U})}/2\Big) I_0(\beta W_{j,\tau}^{(\mathrm{U})}/2) \tag{3.70}$$

It should be noticed that $\sigma_{\mathrm{tor},\tau}/M_{j,\tau}$ removes the torsional symmetry number of the free-rotor partition function and establishes the domain of well j through the local periodicity parameter $M_{j,\tau}$. This parameter is calculated through a Voronoi tessellation scheme [1]. Finally, the Z_j factor is given by

$$Z_j = g_j + (1 - g_j) Z_j^{\mathrm{int}} Z_j^{\mathrm{coup}} \tag{3.71}$$

The factor Z_j^{int} takes into account the coupling between torsions. It is given by the ratio between the coupled and uncoupled CHO partition functions:

$$Z_j^{\mathrm{int}} = \frac{\prod_{\eta=1}^{t} \overline{\omega}_{j,\eta}^{(\mathrm{C})}}{\prod_{\tau=1}^{t} \overline{\omega}_{j,\tau}^{(\mathrm{U})}} \tag{3.72}$$

where the product of the coupled torsional frequencies $\overline{\omega}_{j,\eta}^{(\mathrm{C})}$ is calculated as:

$$\prod_{\eta=1}^{t} \overline{\omega}_{j,\eta}^{(\mathrm{C})} = \frac{\prod_{m=1}^{F} \omega_{j,m}}{\prod_{\overline{\overline{m}}=1}^{F-t} \overline{\overline{\omega}}_{j,\overline{\overline{m}}}} \tag{3.73}$$

F being the number of vibrational degrees of freedom of the system; $\omega_{j,m}$ represents the normal mode frequencies at well j and $\overline{\overline{\omega}}_{j,\overline{\overline{m}}}$ are the nontorsional frequencies calculated in nonredundant internal coordinates. Both, the uncoupled $\overline{\omega}_{j,\tau}^{(\mathrm{U})}$ and the coupled $\overline{\omega}_{j,\eta}^{(\mathrm{C})}$ torsional

frequencies are calculated from the force constants Hessian evaluated at each of the wells, whereas the uncoupled $\varpi_{j,\tau}$ and coupled $\varpi_{j,\eta}$ torsional frequencies used in the TPG and 2D-NS partition functions were obtained from Eqs. 3.6 and 3.20, respectively, and the force constants were obtained from the Fourier series orsional potentials of Eqs. 3.8 and 3.50, respectively.

On the other hand, the Z_j^{coup} term incorporates the coupling in the reduced moments of inertia through the ratio:

$$Z_j^{\text{coup}} = \left(\frac{|\mathbf{D}_j|}{\prod_{\tau=1}^{t} I_{j,\tau}} \right)^{1/2} \tag{3.74}$$

The factor g_j tends to the unity at low temperatures, where the rovibrational coupling is small and tends to zero at high temperatures. It is given by a switching function similar to the one used in the CT method of Eq. 3.34:

$$g_j = \prod_{\tau=1}^{t} \tanh \left(\frac{\sigma_{\text{tor},\tau}}{M_{j,\tau}} \frac{q_{j,\tau}^{\text{FR}}}{q_{j,\tau}^{\text{CHO(U)}}} \right)^{1/t} \tag{3.75}$$

However, a given torsion may reach the high temperature limit at different rate than other torsion, if the barriers they have to overcome are different. The coupled multistructural method with torsional anharmonicity [MS-T(C)] solves this problem by removing the Z_j term and incorporating the couplings into the $F_j^{\text{MS-T(C)}}$ coefficient. For the evaluation of the $q_j^{\text{CHO(C)}}$ partition function is enough to know the product of the coupled torsional frequencies, whereas the evaluation of the reference coupled classical partition function about each well requires the calculation of coupled barrier heights, which are obtained from the eigenvalues $\tilde{\lambda}_{j,\eta}$ of the equation:

$$\tilde{\mathbf{F}}_j^{\text{tor}} = \mathbf{L}_j \mathbf{F}_j^{\text{tor}} \mathbf{L}_j \tag{3.76}$$

The force constant matrix in internal coordinates associated to the torsions $\mathbf{F}_j^{\text{tor}}$ includes the coupling between the torsions, and $\mathbf{L}_j$ is a diagonal matrix with elements given by $1/M_{j,\tau}$. The coupled torsional barriers are given by

$$W_{j,\eta}^{(\text{C})} = 2\tilde{\lambda}_{j,\eta}, \tag{3.77}$$

and the product of $q_{j,\tau}^{\text{RC(C)}}$, which we call here $Q^{\text{RC(C)}}$, is given by:

$$Q^{\text{RC(C)}} = \prod_{\eta=1}^{t} q_{j,\eta}^{\text{RC(C)}} = Z_j^{\text{coup}} \prod_{\tau=1}^{t} \frac{\sigma_{\text{tor},\tau}}{M_{j,\tau}} q_{\tau,j}^{\text{FR}} \prod_{\eta=1}^{t} \exp\Big(-\beta W_{j,\eta}^{(\text{C})}/2\Big) I_0(\beta W_{j,\eta}^{(\text{C})}/2) \tag{3.78}$$

It should be noticed that neither $W_{j,\tau}^{(\text{U})}$ nor $W_{j,\eta}^{(\text{C})}$ correspond to calculated torsional barriers by electronic structure methods, but to effective torsional barriers. Thus, the multistructural reference classical coupled torsional-rotational partition function [MS-RC(C)] given by

$$Q^{\text{MS-RC(C)}} = \sum_{j=1}^{J} Q_{j,\text{rot}} \prod_{\eta=1}^{t} q_{j,\eta}^{\text{RC(C)}} \tag{3.79}$$

may not reach the same high temperature limit than the classical fully coupled partition function of Eq. 3.13.

3.3 Computational Details

All the electronic structure calculations were performed at the MPWB1K method [22], with the augmented polarized double-ζ basis set, 6-31+G(d,p) [23]. This level of calculation performs well for nonmetallic thermochemical data and thermochemistry [24]. The energies, geometries and normal-mode frequencies of all the stationary points are listed in the Supporting Information. The 2D-NS method needs the construction of a global two-dimensional torsional potential energy surfaces for each molecule. Each point is obtained by partial optimization, i.e., all the internal coordinates of the molecule were optimized except the two torsions that were kept frozen. For the scan about the torsion we used a stepsize of 10° (although, in general converged results are obtained with a stepsize of 15°). The elements of the $\mathbf{D}_j$ matrix were calculated for each for the geometries as described in Ref. 8 and implemented in Ref. 12. The normal-mode frequencies calculated at each of the stationary points and the projected normal mode frequencies (after removal of the torsional degrees of freedom) were obtained with the program Ms-Tor [12] and scaled by 0.964 [25].

The two-dimensional torsional potential energy grid obtained from the electronic structure calculations was fitted to Fourier series, i.e. to a potential given by Eq. 3.50. The contour plots of those two-dimensional surfaces are displayed in Figs. 3.2 and 3.3. All classical partition functions that needed integration were evaluated by the trapezoidal rule with a stepsize of 1°. The $\mathbf{D}$ matrix was also fitted to Fourier series having the same terms as the potential. All the fits to Fourier series were carried out by the GNUplot program [26].

The evaluation of the $\overline{\overline{Q}}^{\mathrm{HO}}$ partition function at different values of the two torsional angles, needed in the calculation of the EHR partition function, involved the following steps: (i) Evaluation of the force constants matrix (Hessian) at the stationary points (minima, transition states and maxima); (ii) removal of the torsional frequencies; (iii) interpolation of $\overline{\overline{Q}}^{\mathrm{HO}}$ at non-stationary structures. Step (i) is straightforward because the search is directly carried out on the fitted Fourier series potential; once the stationary points are located the Hessian can be evaluated by standard quantum chemistry programs. Step (ii) involves the separation of torsions from the other degrees of freedom. This is achieved by a transformation of the Cartesian coordinates Hessian into a internal coordiantes Hessian in which the torsions are explicitely and uniquely defined (no redundances) and removed from the the rest of the 3N-8 degrees of freedom by using the procedure described in Ref. 13. This allows the calculation of $\overline{\overline{\omega}}_{\overline{\overline{m}}}$ and ,therefore, of $\overline{\overline{Q}}^{\mathrm{HO}}$ at the stationary points. For Step (iii), first we divide each of the two-dimensional surfaces into Delaunay triangles using the software package TRIPACK of Renka [27]. The vertices of the triangles correspond to stationary points, so at these locations the rovibrational partition function is available. For a given point at the edge or inside the triangle we approximate the partition function by the one at the vertex with the shortest distance between the point an the vertex.

The eigenvalues needed to obtain the 2D-NS partition functions were calculated with the JADAMILU software [28]. All the one-dimensional and two-dimensional torsional partition functions, as well as the multidimensional rovibrational partition functions were obtained by the HR2D program [29].

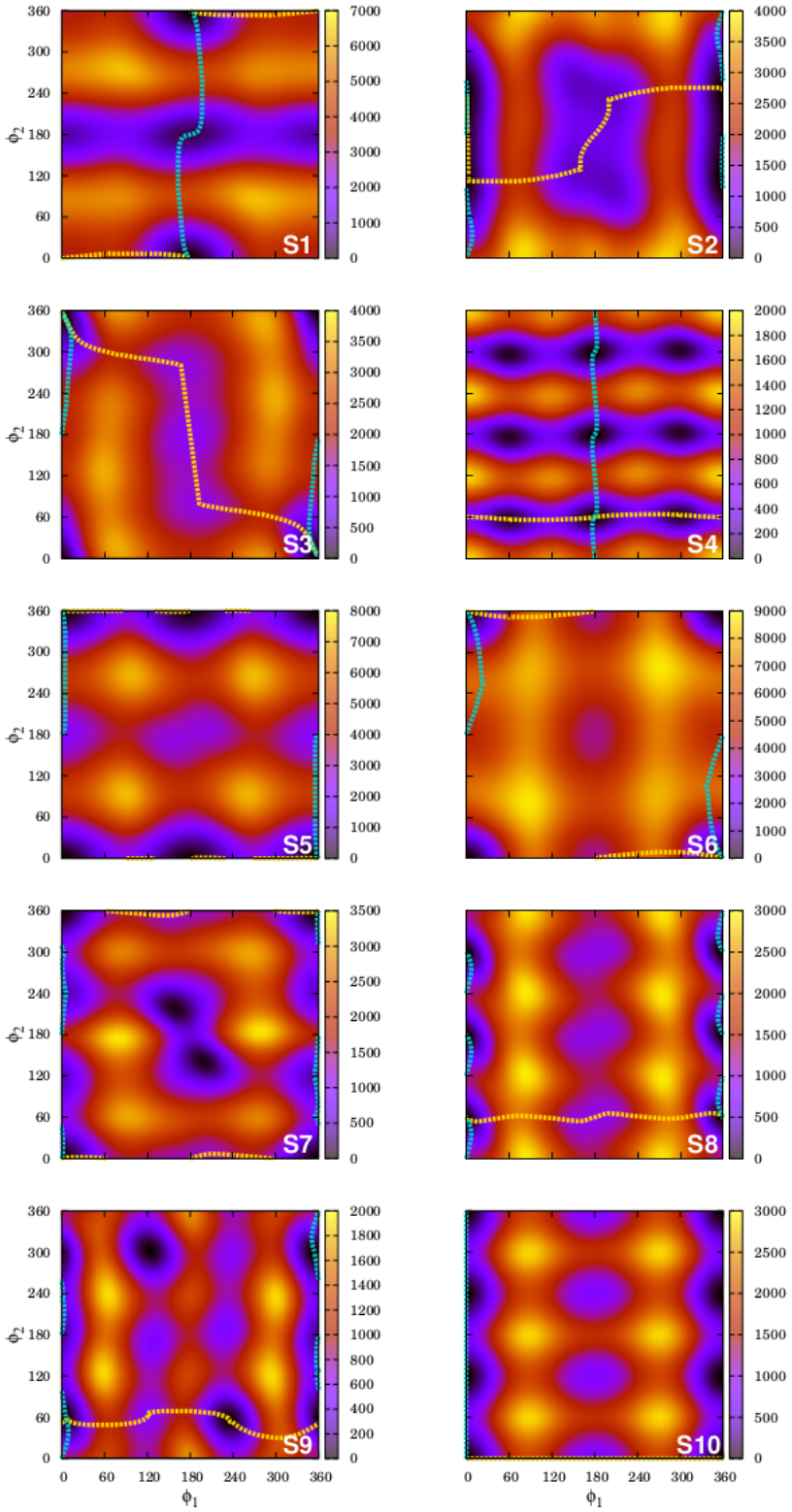

Figure 3.2: Contour plots for molecules **S1** to **S10**. The green and yellow dotted lines indicate the one-dimensional paths about ϕ_1 and ϕ_2, respectively.

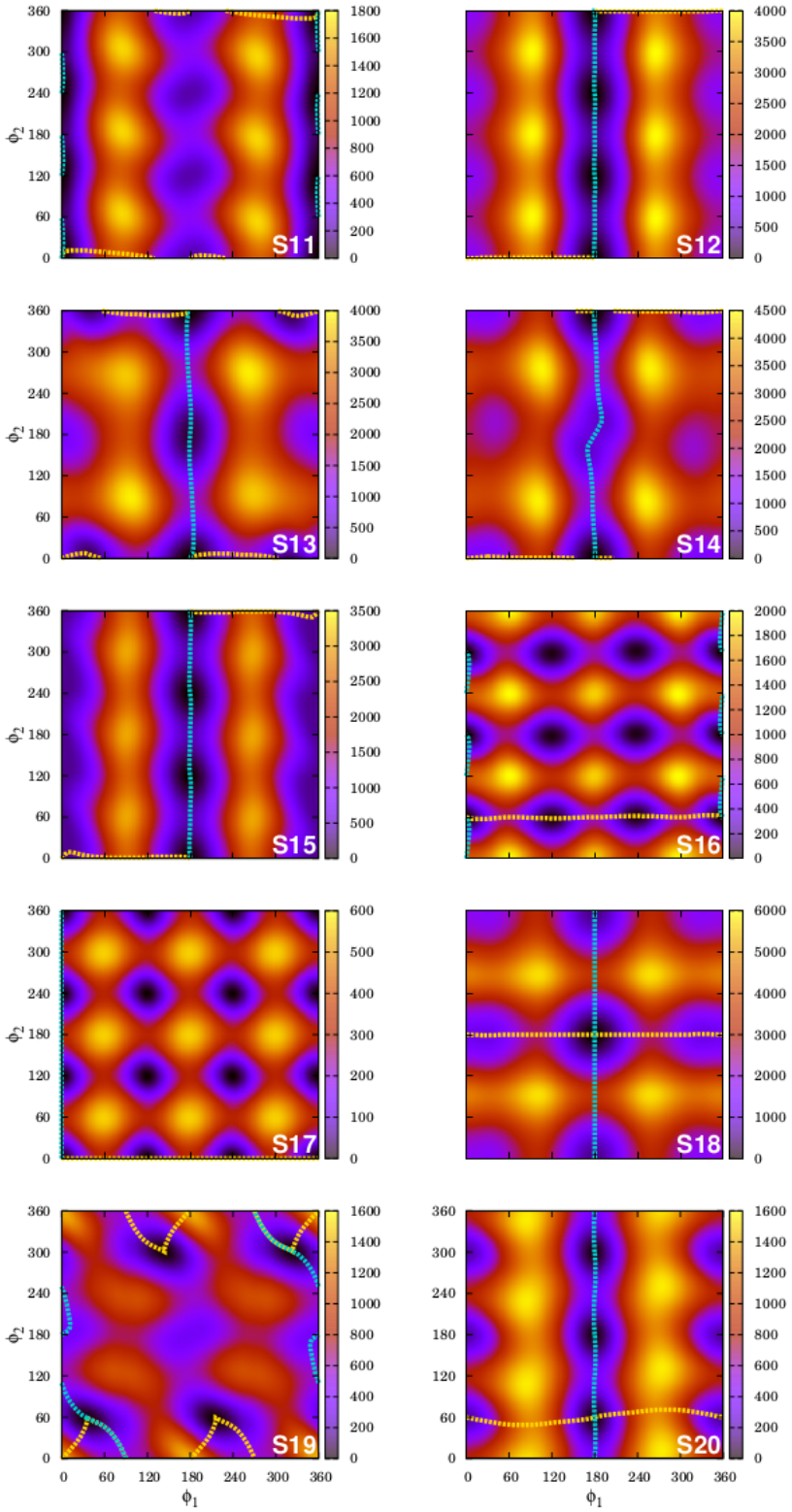

Figure 3.3: Same as 3.2 but for molecules **S11** to **S20**.

The MS-T(U) and MS-T(C) partition functions were calculated with the Ms-Tor program [12]. For each molecule all the electronic structure geometries and frequencies of the conformations are listed in the Supporting Information. All the electronic structure calculations were performed using the *Gaussian09* [30] program.

3.4 Results and Discussion

For the systems studied, two types of comparison are performed for the partition functions at temperatures between 100 and 2500 K. On one hand, we make comparisons between two-dimensional torsional partition functions. Specifically, the 2D-NS method of Eq. 3.52 is compared with the one and two dimensional torsional partition functions of several separable methods given by Eq. 3.4 and described in Section 2. The comparison is extended to non-separable methods as TPG(C) and MC-TPG(C). Deviations from the benchmark calculations for the set of $N_\mathrm{s} = 20$ molecules $\mathbf{S}\ell$ ($\ell = 1, 2, \ldots, 20$) at a given temperature T are given by the mean unsigned percentage error (MUPE):

$$\mathrm{MUPE-TQ-X}(T) = \frac{100}{N_\mathrm{s}} \sum_{\ell=1}^{N_\mathrm{s}} \left| \frac{Q_\mathrm{tor}^{\mathrm{2D-NS}}(\ell, T) - Q_\mathrm{tor}^{\mathrm{X}}(\ell, T)}{Q_\mathrm{tor}^{\mathrm{2D-NS}}(\ell, T)} \right| \tag{3.80}$$

where X indicates the method that is compared with the 2D-NS method. The expression inside the sum of Eq. 3.80 yields the percentage error (PE) of each individual system.

On the other hand, we compare rovibrational partition functions, i.e., those obtained with MS-T(U) and MS-T(C) with the E2D-NS method. As for the case of torsional partition functions, we also calculate the MUPEs at each tempererature, which in this case are given by:

$$\mathrm{MUPE-Q-X'}(T) = \frac{100}{N_\mathrm{s}} \sum_{\ell=1}^{N_\mathrm{s}} \left| \frac{Q^{\mathrm{E2D-NS}}(\ell, T) - Q^{\mathrm{X}}(\ell, T)}{Q^{\mathrm{E2D-NS}}(\ell, T)} \right| \tag{3.81}$$

where X' indicates the method that is compared with the E2D-NS method.

Finally, we compare the MC-HO, MS-T(U), MS-T(C) and E2D-NS methods with the available standard-state (pressure of 1 bar) gas-phase experimental values of entropy S°, heat capacity at constant pressure C_p°, entalphy $H^\circ - H_0^\circ$ and Gibbs free energy $G^\circ - H_0^\circ$. Both the entalphy and the free energy are referred to the enthalpy at $T = 0$ K (H_0°). For the set of systems for which there are experimental data $N_{\mathrm{s}'}$, the MUPE for the free energy is calculated as:

$$\mathrm{MUPE-G-X'}(T) = \frac{100}{N_{\mathrm{s}'}} \sum_{\ell'=1}^{N_{\mathrm{s}'}} \left| \frac{\exp\left[(-G_{0,\mathrm{exp}}^\circ - H_{0,\mathrm{exp}}^\circ)/RT\right] - \exp\left[-(G_0^{\circ,\mathrm{X}'} - H_0^{\circ,\mathrm{X}'})/RT\right]}{\exp\left[-(G_{0,\mathrm{exp}}^\circ - H_{0,\mathrm{exp}}^\circ)/RT\right]} \right| \tag{3.82}$$

The reason for calculating MUPE-G in this manner is due to the connection of Gibbs free energy with thermochemical and chemical kinetics parameters. MUPE-H is calculated in a

similar manner as MUPE(G), and MUPE(S) is calculated as:

$$\mathrm{MUPE-S-X'}(T) = \frac{100}{N_{\mathrm{s}'}} \sum_{\ell'=1}^{N_{\mathrm{s}'}} \left| \frac{\exp\left(S^{\circ}_{0,\mathrm{exp}}/R\right) - \exp\left(S_0^{\circ,\mathrm{X}'}/R\right)}{\exp\left[S^{\circ}_{0,\mathrm{exp}}/R\right]} \right| \tag{3.83}$$

In the case of the heat capacity at constant pressure, the MUPE(HC) is simply calculated as:

$$\mathrm{MUPE-Cp-X'}(T) = \frac{100}{N_{\mathrm{s}'}} \sum_{\ell'=1}^{N_{\mathrm{s}'}} \left| \frac{C^{\circ}_{p,\mathrm{exp}} - C_p^{\circ,\mathrm{X}'})}{C^{\circ}_{p,\mathrm{exp}}} \right| \tag{3.84}$$

3.4.1 Torsional partition functions

The individual PEs for some torsional partition functions at temperatures 150, 300, 500, 1000 and 2500 K are listed in Tables 3.5, 3.6, 3.7, 3.8 and 3.9, respectively. Hindered rotor partition functions described in Section 2 that require very little information about the torsional PES and that assume that the two torsions are separable can be obtained by the CT (Eq. 3.34), the RPG (Eq. 3.30) and AS (Eq. 3.33) approximations; the last two need information of the barrier heights about the minima, but they assume that the barriers can be calculated from Eq. 3.6 and that the torsional frequencies are well represented by normal-mode frequencies, so the three methods only need information about the minima.

Table 3.5: Percentage errors at $T = 150$ K of several torsional partition functions when compared with those obtained by the 2D-NS method.

System	$Q_{\mathrm{tor}}^{\mathrm{CT}}$	$Q_{\mathrm{tor}}^{\mathrm{RPG}}$	$Q_{\mathrm{tor}}^{\mathrm{SRPG}}$	$Q_{\mathrm{tor}}^{\mathrm{TPG(U)}}$	$Q_{\mathrm{tor}}^{\mathrm{TES}}$	$Q_{\mathrm{tor}}^{\mathrm{TPG(C)}}$
S1	43	-141	19	19	6	8
S2	22	17	43	15	8	7
S3	-14	-335	-42	-42	-50	-10
S4	13	-11	12	12	-4	8
S5	27	-79	30	16	6	8
S6	75	-145	22	35	18	5
S7	53	-40	73	47	45	-2
S8	11	-121	2	-8	-16	19
S9	-3	-28	10	20	3	9
S10	12	-75	13	5	-1	5
S11	-39	-88	-2	-10	-23	8
S12	28	-62	21	1	-1	3
S13	-68	-187	10	-10	-20	5
S14	15	-90	59	2	0	3
S15	-10	-44	27	8	5	4
S16	19	22	20	24	20	15
S17	22	2	2	5	0	6
S18	70	-243	24	-24	-24	0
S19	-57	7	13	34	-1	9
S20	-23	-57	3	6	-4	9

Table 3.6: Same as Table 3.5 but for $T = 300$ K.

System	$Q_{\text{tor}}^{\text{CT}}$	$Q_{\text{tor}}^{\text{RPG}}$	$Q_{\text{tor}}^{\text{SRPG}}$	$Q_{\text{tor}}^{\text{TPG(U)}}$	$Q_{\text{tor}}^{\text{TES}}$	$Q_{\text{tor}}^{\text{TPG(C)}}$
S1	38	-111	18	20	15	4
S2	-6	0	29	11	9	2
S3	5	-288	-28	-13	-16	0
S4	18	-8	4	2	-4	4
S5	18	-74	21	8	4	3
S6	57	-185	9	18	11	2
S7	56	-64	61	50	49	0
S8	5	-121	-1	-4	-7	8
S9	6	-20	2	11	5	5
S10	13	-78	8	2	-1	3
S11	-30	-54	-5	-16	-22	4
S12	30	-69	18	0	-1	1
S13	-64	-120	-11	-32	-37	1
S14	10	-179	33	1	0	2
S15	-62	-16	31	10	8	2
S16	22	23	16	20	18	5
S17	32	2	2	4	2	3
S18	64	-241	19	-21	-21	0
S19	-33	15	11	12	-1	5
S20	-11	-36	-3	-2	-7	4

Table 3.7: Same as Table 3.5 but for $T = 500$ K.

System	$Q_{\text{tor}}^{\text{CT}}$	$Q_{\text{tor}}^{\text{RPG}}$	$Q_{\text{tor}}^{\text{SRPG}}$	$Q_{\text{tor}}^{\text{TPG(U)}}$	$Q_{\text{tor}}^{\text{TES}}$	$Q_{\text{tor}}^{\text{TPG(C)}}$
S1	45	-62	28	29	27	2
S2	-41	5	28	11	10	1
S3	26	-198	-6	6	5	2
S4	22	-7	0	-1	-5	2
S5	16	-70	17	5	3	2
S6	49	-197	5	12	8	1
S7	53	-53	51	45	44	1
S8	-23	-74	9	9	8	4
S9	15	-6	3	12	9	3
S10	15	-65	6	0	-3	2
S11	-23	-33	-6	-15	-18	2
S12	31	-64	16	0	0	2
S13	-59	-85	-25	-44	-47	1
S14	3	-149	22	1	0	1
S15	-99	-2	30	7	7	1
S16	28	24	14	19	18	2
S17	32	1	1	2	2	1
S18	61	-192	16	-25	-25	0
S19	-17	20	13	9	3	4
S20	0	-22	-4	-4	-6	2

Table 3.8: Same as Table 3.5 but for $T = 1000$ K.

System	$Q_{\text{tor}}^{\text{CT}}$	$Q_{\text{tor}}^{\text{RPG}}$	$Q_{\text{tor}}^{\text{SRPG}}$	$Q_{\text{tor}}^{\text{TPG(U)}}$	$Q_{\text{tor}}^{\text{TES}}$	$Q_{\text{tor}}^{\text{TPG(C)}}$
S1	57	-13	40	41	40	1
S2	-69	12	30	12	11	1
S3	51	-59	22	29	28	2
S4	26	-5	-2	-3	-4	1
S5	20	-60	14	4	3	1
S6	47	-194	6	9	8	1
S7	35	-30	38	32	32	1
S8	-63	-15	17	21	20	1
S9	17	6	3	13	12	1
S10	16	-34	4	-2	-3	2
S11	-12	-16	-4	-10	-11	1
S12	28	-42	13	-1	-1	0
S13	-39	-53	-31	-42	-43	1
S14	-12	-67	12	0	0	1
S15	-92	4	23	3	2	0
S16	35	21	10	17	17	1
S17	26	1	1	1	1	0
S18	55	-102	14	-29	-29	0
S19	-10	16	10	6	5	1
S20	11	-9	-2	-2	-2	1

Table 3.9: Same as Table 3.5 but for $T = 2500$ K.

System	$Q_{\text{tor}}^{\text{CT}}$	$Q_{\text{tor}}^{\text{RPG}}$	$Q_{\text{tor}}^{\text{SRPG}}$	$Q_{\text{tor}}^{\text{TPG(U)}}$	$Q_{\text{tor}}^{\text{TES}}$	$Q_{\text{tor}}^{\text{TPG(C)}}$
S1	57	9	38	37	37	1
S2	-36	15	29	14	14	0
S3	40	-5	20	26	26	0
S4	22	-3	-3	-2	-3	0
S5	27	-27	12	4	4	1
S6	63	-67	33	33	33	1
S7	1	-10	25	17	17	0
S8	-23	7	9	19	19	0
S9	14	9	1	11	11	0
S10	8	-12	1	-2	-2	0
S11	-3	-6	-2	-4	-4	0
S12	21	-13	8	0	0	0
S13	-13	-24	-19	-23	-23	0
S14	-26	-18	5	1	0	0
S15	-43	5	15	1	1	0
S16	32	15	3	13	13	0
S17	15	1	1	1	1	0
S18	47	-46	9	-30	-30	0
S19	-6	7	5	3	3	0
S20	13	-2	-1	0	0	0

For the systems studied there is no much difference between the RPG and AS methods. With the approximations indicated above both methods overestimate the torsional partition function and lead to very large errors. MUPEs below 25% are only obtained at about $T =$ 2000 K. The results improve substantially, and the two MUPEs are below 25% at$T \leq 700$ K when calculated for systems having methyl groups. This is not surprising because methyl groups usually are well represented by potentials of the type of Eq. 3.5. Actually, for **S17** the PE is about 3% between 150 and 2500 K. For the rest of systems in which one of the tops is a methyl group the resulting PE is due to the other rotating top. The largest deviations are for systems which have very large barriers about the absolute minimum. Usually, it involves rotations about the -COH (systems **S1**, **S3**, **S6**) and -CH=CH_2 (systems **S13** and **S18**); both rotating groups are asymmetric and sometimes with a strong variation of the reduced moments of inertia and strong coupling between the torsions. The AS and RPG methods also have difficulty with -OH tops as for instance in **S3**, **S11** and **S13**, and therefore the range of applicability of these two methods is limited to systems well represented by one well with a given periodicity.

The CT method performs better than the AS and RPG methods at low temperatures, but it makes use of normal-mode frequencies, which may not represent well the pure torsional modes. This is, for instance, the case of **S13** for which the two normal mode frequencies with the largest torsional character are 102.0 and 290.8 cm^{-1}, whereas the $\overline{\omega}_{j,\eta}$ frequencies are 107.2 and 372.8 cm^{-1}, respectively. At high temperatures the RPG and AS methods yield smaller MUPEs than the CT method when compared to the 2D-NS method. In the case of the CT method the errors are probably due to difficulties handling correctly the intermediate regimes between the harmonic oscillator and the free rotor.

More sophisticated one-dimensional methods gather more information about the two-dimensional torsional potential than just the conformational minima, but they still assume separability between torsions. Additionally, with the exception of segmented methods, it is common to consider that there is no variation of the reduced moments of inertia with the torsional angles and that they have the value calculated at the absolute minimum. Starting from the absolute minimum, one of the main problems is to build one-dimensional potentials that incorporate the main features of the torsional PES. In this work, for each torsional angle, we have located the transition states that by following the minimum energy path (MEP) lead to the absolute minimum on one side and to other minimum on the other side of the MEP. The procedure continues with the location of the transition state that connects this last minimum with other minimum and so on until a period of 360 degrees is completed. Those paths are displayed in Figs. 3.2 and 3.3. The evaluation of the MEP based on the two-dimensional Fourier series PES is straightforward and it does not require further electronic structure calculations. The one-dimensional potentials may leave minima unexplored and the importance of their contribution will be reflected in the partition function. Other approach would be to scan one of the torsions and leave the other torsion frozen. However, this procedure yields poorer results than the one based on the MEP.

For system **S1** the absolute minimum located at $(\phi_{1,\mathrm{eq}}, \phi_{2,\mathrm{eq}})$ equals $(180°, 0°)$; for the construction of the potential about $\phi_{1,\mathrm{eq}}$ the transition states that lead to this minimum are located at $(66°, 7°)$ and at $(294°, -7°)$. When the MEP is followed in the opposite direction

both transition states lead to the minimum located at $(0°, 0°)$ or at $(360°, 0°)$, which has an energy of 3334 cm^{-1}. On the other hand, the potential about ϕ_2 passes through the minimum located at $(180°, 180°)$ with an energy of 337 cm^{-1}. However, none of the two potentials pass through the minimum at $(0°, 180°)$ with an energy of 787 cm^{-1}. In general the two orientations of the -COH group (at 0° and at 180°) lead to quite different energies because both conformations correspond to distinct chemical environments. For this reason methods based on a given periodicity of the potential, as the RPG or AS methods, fail to produce accurate partition functions for this top. Also the methods based on one-dimensional paths, as the TPG(U), TES and SRPG methods, yield large PEs at high temperature for this case (the MUPEs are displayed in Fig. 3.4.

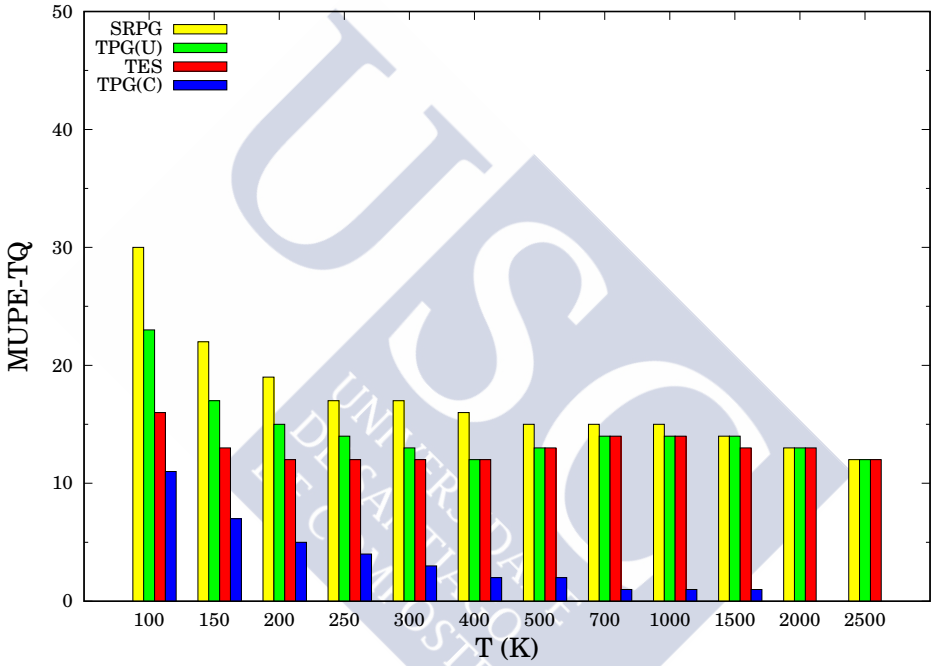

Figure 3.4: MUPE-TQ calculated by Eq. 3.87 for several torsional partition functions at different temperatures (the 2D-NS method is used as reference).

The SRPG method only needs the barrier heights between the minima and assumes a potential based on the RPG approximation for each of the minima. Usually, as is the case in this work, the barrier heights needed to apply Eq. 3.37 are taken from the electronic structure calculations, but they could be obtained from Eq. 3.6. Therefore the SRPG method, which only applies the RPG approximation locally, is more accurate that the RPG and AS methods. However, if the barriers are calculated by electronic structure methods, it is better to use the TES method, because with slightly more computational effort it is possible to obtain the one dimensional potentials (fitted to Fourier series), and with them at hand, it is straightforward to solve the Schrödinger equation. At low temperatures the TES method performs better than the SRPG method, but at high temperatures both methods yield similar MUPEs. One notable exception at high temperatures is molecule **S18** for which there is a strong variation

in the reduced moments of inertia between different minima (for instance between **S18-M1** and **S18-M2**) and the SRPG method, which includes the reduced moments of inertia of each minima, performs better than the TES method. The fact that at high temperature the MUPEs for SRPG and TES are similar indicates that, for each torsional mode, the classical partition function of Eq. 3.40 mimics well the one-dimensional classical partitions of Eq. 3.26. This result indicates that a modified version of Eq. 3.40 could be a good replacement of the two-dimensional classical partition function. This is the idea of Eq. 3.78, which extends the reference classical PG approximation to all the wells of the PES and considers effective torsional barriers to account for the coupling between torsions.

Within this context, it is interesting to compare the multistructural reference classical rotational-torsional partition function $Q^{\mathrm{MS-RC(C)}}$ of Eq. 3.79 to the $Q^{(\mathrm{U})}_{\mathrm{cl,rt}}$ partition function, which is given by

$$Q^{(\mathrm{U})}_{\mathrm{cl,rt}} = Q_{\mathrm{rot}} \prod_{\tau=1}^{t} q_{\mathrm{cl},\tau}, \tag{3.85}$$

and to the full classical partition function of Eq. 3.13 (taken as benchmark). In Eq. 3.85 the rotational partition function is evaluated at the absolute minimum. The comparison shows that at $T < 700$ K the MUPEs are slightly lower for $Q^{(\mathrm{U})}_{\mathrm{cl,rt}}$ than for $Q^{\mathrm{MS-C(C)}}$ at $T < 700$ K; for instance at $T = 300$ K the MUPEs are 11% and 14%, respectively. Only above 1000 K $Q^{\mathrm{RC(C)}}$ is clearly better than $Q^{(\mathrm{U})}_{\mathrm{cl,rt}}$ and at $T = 2500$ K the MUPEs are 12% and 8% for the latter and the former partition functions, respectively. The largest PE at both low and high temperatures using $Q^{\mathrm{MS-RC(C)}}$ correspond to system **S6** with PEs of 44% and 27% at 150 and 2500 K, respectively. The advantage of the classical partition function $Q^{\mathrm{MS-RC(C)}}$ over $Q^{(\mathrm{U})}_{\mathrm{cl,rt}}$ is that the former only needs information about the minima.

The TPG(U) method, which is based on the $Q^{(\mathrm{U})}_{\mathrm{cl,tor}}$ partition function, yields MUPEs with values between the TES and SRPG methods. It converges to the TES method at high temperatures because both make use of the same classical partition function, but at low temperatures it approximates the quantum effects by just the ratio between the quantum and classical harmonic oscillator partition functions calculated at the absolute minimum. The torsional frequencies are obtained by direct derivation of the one-dimensional Fourier series potentials. The TPG(U) and TES methods basically require the same computational effort so the latter should be chosen as the preferred method in detriment of the former.

It should be noticed that the one-dimensional potentials were obtained from the two-dimensional potential, which it has been previously fitted to Fourier series. Therefore, here we are assuming that the two-dimensional potential is available. If that is the case then it is possible to calculate the TPG(C) partition functions. In this method quantum effects are incorporated into the 2D classical partition function using the PG approximation as in the TPG(U) method. However, the torsional frequencies are obtained from Eq. 3.20 including full coupling between the torsions. The largest MUPE of the TPG(C) partition functions when compared with those of the 2D-NS method occurs at $T = 150$ K with a value of 7% and a maximum PE of 19% for molecule **S8**. At $T = 300$ K the MUPE reduces to 3% and with a maximum PE of 8% for molecule **S8**. Therefore, the TPG(C) method is a very good alternative to the 2D-NS method, that avoids the problem of solving directly the Schrödinger

equation.

3.4.2 Rovibrational partition functions

The zero-point energy (ZPE) of the E2D-NS partition function is given by the contribution of the 3N-8 nontorsional degrees of freedom plus the lowest energy level obtained by direct diagonalization of the 2D-NS torsional partition function. For molecules like **S1**, **S2** or **S6** this ZPE is quite different from the one obtained from the normal-modes analysis (see Table 3.10). In general, the normal mode frequencies associated to the torsions are lowered when coupled torsional frequencies are being considered, so at very low temperatures the E2D-NS partition function may be larger (more density of states) than the harmonic oscillator one. As temperature rises this effect may reverse quite fast (the E2D-NS partition function becomes lower than the MC-H partition function) if there are other minima available, and the barriers between them are not too high, so they can be easily reached. This is for instance the case of molecule **S2** that has a barrier between the two degenerate minima of only 116 cm^{-1}. On the other hand, **S1** and **S6** have large barrier heights between the lowest energy minima with the lowest energy and the each well behaves close to a harmonic oscillator, but in the case of E2D-NS method with lower frequencies than the normal mode frequencies associated to the torsions. The effect of having different ZPE thresholds shows in the MUPEs. Thus, the MUPE at $T = 150$ K is 19% for the MC-H and the MS-T(U) methods and 21% for the MS-T(C) method. At $T = 300$ K the MUPE increases to 21% and 24% for the MC-H and MS-T(U) methods, respectively, but it decreases to 15% for the MS-T(C) method.

It is also interesting to know the effect of the variation of the ZPE on the 3N-8 degrees of freedom on the EHR partition function by comparing the results with a EHR partition function with invariant ZPE and principal moments of inertia given by the absolute minimum geometry. This one-well EHR partition function (EHR-1W) is given by:

$$Q_{\rm rv}^{\rm EHR-1W} = \frac{8\pi^2}{\sigma_{\rm tor}\sigma_{\rm rot}}\left(\frac{1}{2\pi\beta\hbar^2}\right)^{5/2} Q_{\rm rot}\overline{\overline{Q}}^{\rm HO}\int_0^{2\pi}\int_0^{2\pi} d\phi_1 d\phi_2 |\mathbf{D}(\phi_1,\phi_2)|^{1/2} {\rm e}^{-\beta {\rm V}(\phi_1,\phi_2)} \quad (3.86)$$

As expected, at low temperatures both results are quite similar, except for molecules **S7** and **S9** with PEs of 18% and 20% at $T = 150$ K. The reason is that these two molecules present very low energy minima with values of 50 (**M2-S7**) and 3 cm^{-1} (**M2-S9**) with respect to their absolute minima **M1-S7** and **M1-S9**, respectively. The ZPE increases this difference in the case of **M2-S7** by 35 cm^{-1} and in the case of **M2-S7** by 27 cm^{-1} so the EHR-1W partition function is larger than the normal EHR partition function of Eq. 3.56. For the rest of molecules the PEs are smaller or even negligible, so at $T = 150$ K the MUPE is only 4%. At $T = 300$ K the MUPE is still 4% but at higher temperatures starts to increase and at $T = 1000$ K is 9% and at $T = 2500$ K is 16%. As temperature increases the MUPE also increases because the normal EHR partition function starts to have important contributions from the transition states and maxima. In general, these stationary points have lower ZPEs than the minima resulting in a reduction of the classical potential and therefore in the increase of the normal EHR partition function with respect to the EHR-1W partition function. It should be also mentioned that Pitzer [8] and KP indicated that the variation with geometry

Table 3.10: Zero-point energies (in kcal/mol) of the absolute minimun of each system obtained by the harmonic oscillator (HO) and the E2D-NS approximations.

System	ZPE-HO	ZPE-E2D-NS
$S1$	27.37	27.24
$S2$	37.50	37.41
$S3$	38.21	38.26
$S4$	49.73	49.71
$S5$	42.11	42.09
$S6$	42.37	42.01
$S7$	48.40	48.37
$S8$	53.07	53.04
$S9$	52.96	52.91
$S10$	52.64	52.60
$S11$	52.79	52.80
$S12$	55.67	55.61
$S13$	56.27	56.29
$S14$	56.05	56.00
$S15$	55.85	55.84
$S16$	67.35	67.27
$S17$	66.96	66.95
$S18$	59.12	59.10
$S19$	83.00	82.99
$S20$	82.19	82.23

of the ZPE and the **D** matrix may roughly compensate, so to perform the calculations at the absolute minimum only may be a good approximation. However, our calculations indicate that the MUPEs are similar to the ones obtained using the EHR-1W approximation at low temperatures and larger than those at high temperatures (10% $T = 1000$ K and 18% at $T = 2500$ K).

Quantum effects on the EHR partition function were included as the ratio between the quantum 2D-NS and the torsional classical partition function. However, if the 2D-NS partition function is not available quantum effects can be incorporated through any of the methods discussed in the previous Subsection. At $T = 150$ K the MUPEs associated to the PG coefficients given by the TPG(C), MC-TPG(C) and TES methods with respect to $F^{\mathrm{2D-NS}}$ are 6, 5 and 5%, respectively. The small difference between the TPG(C) and MC-TPG(C) methods shows that quantum effects can successfully be reproduced by the ratio between the quantum and classical harmonic oscillator at the global minimum. The MUPEs decrease to less than 3% at $T = 300$ K. It is also interesting to build a PG coefficient using the frequencies obtained from Eq. 3.20 (also called the KP method) but using the harmonic oscillator force constants instead of the ones obtained from the Fourier torsional potential. Using these frequencies the MUPEs are 11 and 4% at 150 and 300 K, respectively. The largest error is due to system **S6** with PEs of 59 and 26% at 150 and 300 K, respectively (if this system is removed from the calculation of the MUPE, the latter is reduced to 8% at $T = 150$ K). On average quantum effects decrease the classical partition function by about 80% at $T = 150$ K, but only by 15%

at $T = 300$ K. Therefore, if we are not interested on the evaluation of the partition function at very low temperatures, it is sufficient to calculate the PG coefficient from the torsional frequencies at the absolute minimum from the latter method just described.

The effect of including a global correction to the torsional anharmonicity can be checked by comparing the GS2D-NS partition function of Eq. 3.61 with that obtained by the E2D-NS method. At $T = 150$ K the PEs are quite large for systems **S1**, **S6** and **20** with values of 33%, 70% and 47%, respectively, and the MUPE is 14%. As temperature increases the MUPE remains constant but increases slightly at very high temperatures reaching 17% at $T = 2500$ K (see Fig. 3.5). These results indicate that to incorporate torsional anharmonicity on top of the MC-H partition function, even when full couplings in the kinetic and potential energies are taken into account, may lead to substantial errors. Some of us have used Eq. 3.61 to study the the hydrogen abstraction from ethanol by atomic hydrogen [31], but for the ethanol molecule, the MUPE between the E2D-NS and the GS2D-NS partition functions is always between 6 and 8% in the whole range of temperatures studied in this work.

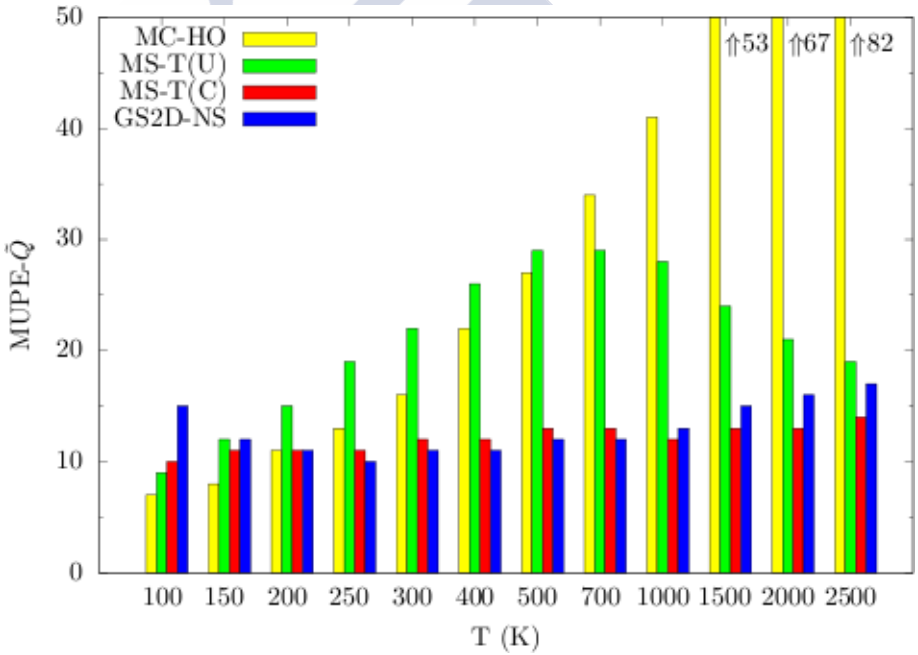

Figure 3.5: MUPE-$\tilde{Q}$ calculated by Eq. 3.87 for several rovibrational partition functions at different temperatures (the E2D-NS method is used as reference).

Hereafter, to establish a more direct comparison of the E2D-NS method with other methods that evaluate the rovibrational partition function but have different thresholds for the ZPEs. In these cases, we think that is more useful to work with rovibrational partition functions that are referred to the ZPE of the absolute minimum, instead of to the bottom of the potential. In this way anharmonic effects due to the ZPE are removed. In this case the

MUPE is calculated as:

$$\mathrm{MUPE}-\tilde{\mathrm{Q}}-\mathrm{X}'(T)=\frac{100}{N_{\mathrm{s}}}\sum_{\ell=1}^{N_{\mathrm{s}}}\left|\frac{\tilde{Q}^{\mathrm{E2D-NS}}(\ell,T)-\tilde{Q}^{\mathrm{X}}(\ell,T)}{\tilde{Q}^{\mathrm{E2D-NS}}(\ell,T)}\right| \tag{3.87}$$

where the tilde in the partition function indicates that the calculations are referred to the ZPE of the absolute minimum. When comparing MUPE-Q and MUPE-$\tilde{\mathrm{Q}}$ there is an increase of the former with respect to the latter by about 10% at $T = 150$ K. This difference is reduced to only 3% at $T = 300$ K. Moreover, ZPE 'exclusive' partition functions can also be used in the comparison between theoretical and experimental thermodynamic functions, i.e., the entropy and the constant-pressure heat capacity are independent of the ZPE of the system and the free energy and the enthalpy are always referred to a reference state, which in general is the value of the entalphy at $T = 0$ K, so the effect of the ZPE is also removed in this case.

Flexible molecules have multiple torsional minima, so it is important to establish whether we need to incorporate all the minima, as in the multiconformer approximation of Eq. 3.2, or it is enough to consider just the absolute minimum. The comparison with the E2D-NS results shows that even at low temperatures the one-well approximation yields larger MUPEs than the MC-H approximation. For instance at $T = 150$ K the MC-H MUPE is 8% whereas the one-well HO MUPE is 19%. At $T = 500$ K the MUPE in the latter increases to 45% whereas in the former is 27%. Only at $T = 2500$ K the situation reverses, but at this temperature the harmonic approximation is very poor in bot cases with MUPEs larger than 60%.

The two multistructural methods incorporate torsional anharmonicity by quotients between the reference classical partition function and the classical harmonic oscillator partition function for each of the wells. It would be more accurate to define a quotient between the full quantum partition function and the quantum harmonic oscillator partition, because in this case nonclassical effects are automatically included. We have calculated the ratio between quantum and classical partition functions by

$$F=\frac{Q_{\mathrm{tor}}^{\mathrm{2D-NS}}/Q_{\mathrm{tor}}^{\mathrm{MC-HO(C)}}}{Q_{\mathrm{cl,tor}}^{(\mathrm{C})}/Q_{\mathrm{tor}}^{\mathrm{MC-CHO(C)}}} \tag{3.88}$$

and this coefficient is below 10% at $T = 150$ K and below 5% at $T = 300$ K. The exception is system **S8** for which at $T = 150$ K the PE is 23%. Therefore, the quotient between classical and classical harmonic oscillator partition functions provides a good account of deviations from the harmonic approximation except at very low temperatures.

Fig. 3.5 shows that at $T \leq 200$ K the harmonic oscillator and the MC-T(U) (which involves uncoupled torsions) partition functions agree quite well with the E2D-NS method. Notice that at those temperatures the MC-H partition function seem as good as anharmonic methods, but at room temperature the MUPE is already 16%. As temperature increases the harmonic oscillator partition function deviates substantially from the benchmark results, the MUPE being 82% at $T = 2500$ K. In general the harmonic approximation leads to partition functions which are too high (with the exception of molecules **S1** and **S6** discussed above). The reason being that the density of states is larger for the harmonic than for the anharmonic

methods, because the space available to the molecular system is more reduced that when torsional anharmonicity is included. Surprisingly the MC-H partition functions yield values with smaller MUPEs than the obtained by the MC-T(U) method at temperatures $T \leq 500$ K. The best results are obtained with the MS-T(C) method, which improves substantially the MS-T(U) method above $T = 200$ K. The largest MUPE for the MS-T(C) is 14% an occurs at $T = 2500$ K.

In general, methyl groups are weakly coupled to other torsions, and the torsional potential has a periodicity of 120°. One would expect a better performance of the anharmonic methods with respect to the benchmark results when the MUPE only includes this type of tops. This is the case for the MS-T(C) for which the MUPE drops to 7% at $T = 2500$ K. However, the MS-T(U) method performs worse for molecules having methyl groups than for the whole set. Specifically, the MUPE reaches its highest value of 41% at $T = 500$ K [the MUPE for the MS-T(C) at this temperature is 9%]. At $T = 500$ K the largest PE is for system **S15** with a value of 169%; the two rotating tops of this molecule are the -CH_3 and the -COH groups, with torsional barriers with regards to the absolute minimum of 419 and 2508 cm^{-1}, respectively. The two barriers for internal rotation are very different, so both tops reach the high temperature limit at very different thresholds. This situation cannot be handle properly by the switching function of Eq. 3.75, but it is properly taken into account by the MS-T(C) method, so the PE decreases till 1%.

3.4.3 Comparison with thermodynamic functions

Experimental values for thermodynamic functions are available for systems **S4**, **S16** and **S17** for temperatures in the interval between 100 and 2500 K and for **S5** and **S20** in the interval between 100 and 1500 K [9]. The MUPEs, as calculated from Eqs. 3.82 to 3.84, are displayed in Fig. 3.6. The calculated free energies by the GS2D-NS method yield MUPE-Gs larger than 20% at temperatures below $T = 700$ K. Those values are also larger than the obtained by the MS-T(C), so taking into account that the GS2D-NS method is computationally more demanding, the latter approximation is not pursued further. The values of C_p are not too sensitive to the method employed. In this case the MS-T(U), MS-T(C) and E2D-NS methods yield similar errors in the whole interval of temperatures studied. At temperatures between 100 and 700 K the E2D-NS method is substantially better than the rest, when compared with the experimental values of free energies, enthalpies and entropies. MS-T(C) is the second best method. This result indicate that to account for torsional coupling is important in the evaluation of thermodynamic functions.

3.5 Conclusions

In this work we have compared several methodologies using as benchmark the 2D-NS and E2D-NS methods to test the accuracy of the calculated torsional and rovibrational partition functions, respectively. For that comparison we have used a set of 20 molecules presenting two hindered rotors. From the results obtained and the comparison with experimental

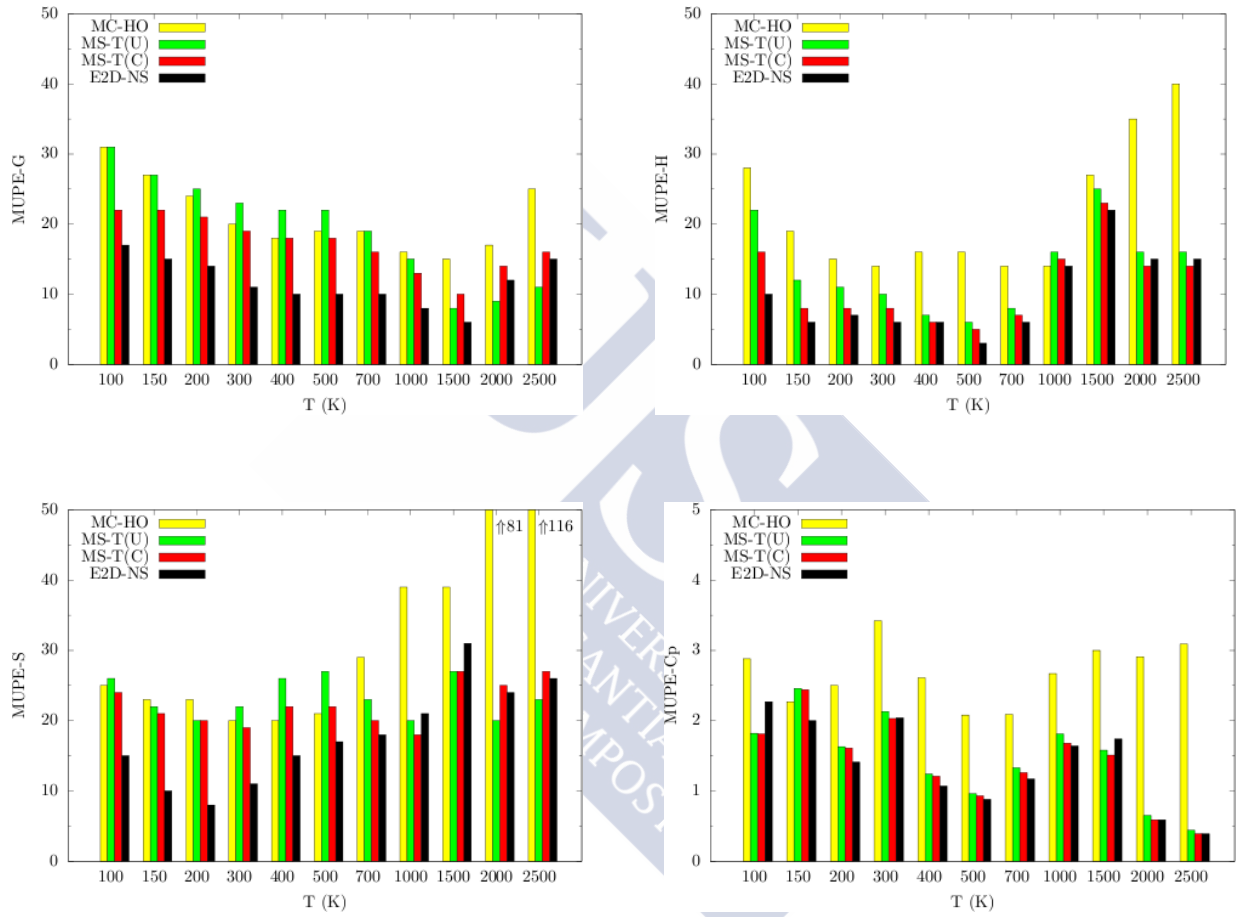

Figure 3.6: MUPEs obtained from the comparison between gas-phase standard-state experimental thermodynamic functions (as indicated by Eqs. 3.82 to 3.84) and those obtained from different theoretical methods described in the main text.

thermodynamic functions we draw the following conclusions:

i) The RPG and AS methods only yield relatively good results when the potential has a given periodicity, as is the case of the methyl groups.

ii) The TPG(C) method yields the lowest values of MUPE-TQ when compared with the 2D-NS method and it is a good alternative to the latter if the solution of the two dimensional Schrödinger equation is too cumbersome. The TES, TPG(U) and SRPG battery of methods become less accurate as we progress in the sequence at low and intermediate temperatures, although the three of them lead to the same high temperature limit (with MUPEs of 12% at $T = 2500$ K). The TPG(C) method is much better than the TPG(U) method, which shows the importance of taking into account the coupling between torsions.

iii) The multistructural reference classical rotational-torsional partition function $Q^{\mathrm{MS-RCC(C)}}$ when compared to the full coupled rotational-torsional partition function $Q^{\mathrm{FC(C)}}$ yiels MUPEs between 15 and 8% in the interval of temperatures between 100 and 2500 K.

iv) The accuracy of given rovibrational partition function depends not only on the accuracy of the anharmonic torsional partition functions but also on its implementation. Thus the global torsional separability approximation, as in the GS2D-NS method, does not improve the MS-T(C) results despite the fact that the method uses the 2D-NS method to calculate the torsional partition function.

v) When calculating rovibrational partition function at room temperature or below, the multiconformer harmonic approximation seems as good as any of the approximated methods described in this work. However, the comparison with the experimental thermodynamic functions shows that approximations which include torsional anharmonicity and coupling perform better than the harmonic approximation also at low temperatures.

vi) Overall, the E2D-NS method chosen as benchmark for the comparison of the systems studied is also the method with the smallest MUPEs when compared with the available experimental thermodynamic functions.

vii) If the E2D-NS method is not affordable, the MS-T(C) method is the best option to calculate rovibrational partition functions including torsional anharmonicity. It only needs information about the conformational minima, which a highly desirable characteristic when dealing with molecules having three or more hindered rotors.

USC
UNIVERSIDADE
DE SANTIAGO
DE COMPOSTELA

Chapter 4

Kinetic Isotope Effects in Multipath VTST

The link to the scientific publication is:

http://pubs.acs.org/doi/abs/10.1021/acs.jpcb.5b09671

Publication Information:

Luis Simón-Carballido, Tiago Vinicius Alves, Agnieszka Dybala-Defratyka, Antonio Fernández-Ramos. Kinetic Isotope Effects in Multipath VTST: Application to a Hydrogen Abstraction Reaction. *J. Phys. Chem. B*, 2016, **120**, 1911–1918.
IMPACT FACTOR: 3.187
DOI: 10.1021/acs.jpcb.5b09671

USC
UNIVERSIDADE
DE SANTIAGO
DE COMPOSTELA

Bibliography

[1] J. Zheng, T. Yu, E. Papajak, I. M. Alecu, S. L. Mielke, and D. G. Truhlar. Practical methods for including torsional anharmonicity in thermochemical calculations on complex molecules: The internal-coordinate multi-structural approximation. *Phys. Chem. Chem. Phys.*, 13(23):10885–10907, 2011.

[2] R. Meana-Pañeda and A. Fernández-Ramos. Tunneling and conformational flexibility play critical roles in the isomerization mechanism of vitamin D. *J. Am. Chem. Soc.*, 134:346–354 , 2012.

[3] T. Yu, J. Zheng, and D. G. Truhlar. Multi-path variational transition state theory: rate constant of the 1,4-hydrogen shift isomerization of the 2-cyclohexylethyl radical. *J. Phys. Chem. A*, 116:297–308, 2012.

[4] I. M. Alecu and D. G. Truhlar. Computational study of the reactions of methanol with the hydroperoxyl and methyl radicals. 2. Accurate thermal rate constants. *J. Phys. Chem. A*, 115(51):14599–14611, 2011.

[5] J. Zheng and D. G. Truhlar. Including torsional anharmonicity in canonical and microcanonical reaction path calculations. *J. Chem. Theory Comput.*, 9:2875, 2013.

[6] J. Zheng, T. Yu, and D. G. Truhlar. Multi-structural thermodynamics of C-H bond dissociation in hexane and isohexane yielding seven isomeric hexyl radicals. *Phys. Chem. Chem. Phys.*, 13(43):19318, 2011.

[7] K. S. Pitzer and W. D. Gwinn. Energy levels and thermodynamic functions for molecules with internal rotations. I. Rigid frame with attached tops. *J. Chem. Phys.*, 10:428–440, 1942.

[8] J. E. Kilpatrick and K. S. Pitzer. Energy levels and thermodynamics functions for molecules with internal rotation. III. Compound rotation. *J. Chem. Phys.*, 17:1064, 1949.

[9] M. Frenkel, K. N. Marsh, R. C. Wilhoit, G. J. Kabo, and G. N. Roganov. Thermodynamics of organic compounds in the gas. Thermodynamics Research Center, College Station, TX, 1994.

[10] A. Fernández-Ramos. Accurate treatment of two-dimensional non-separable hindered internal rotors. *J. Chem. Phys.*, 138:134112, 2013.

[11] P. Vansteenkiste, D. Van Neck, V. Van Speybroeck, and M. Waroquier. An extended hindered-rotor model with incorporation of coriolis and vibrational-rotational coupling for calculating partition functions and derived quantities. *J. Chem. Phys.*, 125:049902, 2006.

[12] J. Zheng, S. L. Mielke, K. L. Clarkson, and D. G. Truhlar. Mstor: A program for calculating partition functions, free energies, enthalpies, entropies, and heat capacities of complex molecules including torsional anharmonicity. *Comput. Phys. Commun.*, 183: 1803, 2012.

[13] J. Zheng and D. G. Truhlar. Quantum thermochemistry: multistructural method with torsional anharmonicity based on a coupled torsional potential. *J. Chem. Theory Comput.*, 9:1356–1367, 2013.

[14] A. Fernández-Ramos, B. A. Ellingson, R. Meana-Pañeda, and J. M. C. Marques, and D. G. Truhlar. Symmetry numbers and chemical reaction rates. *Theor. Chem. Acc.*, 118:813–826, 2007.

[15] K. S. Pitzer. Energy levels and thermodynamic functions for molecules with internal rotations. II. Unsymmetrical tops attached to a rigid frame. *J. Chem. Phys.*, 14:239–243, 1946.

[16] B. A. Ellingson, V. A. Lynch, S. L. Mielke, and D. G. Truhlar. Statistical thermodynamics of bond torsional modes: Tests of separable, almost-separable, and improved Pitzer–Gwinn approximations. *J. Chem. Phys.*, 125:84305, 2006.

[17] P. Y. Ayala and H. B. Schlegel. Identification and treatment of internal rotation in normal mode vibrational analysis. *J. Chem. Phys.*, 108:2314, 1998.

[18] D. G. Truhlar. A simple approximation for the vibrational partition function of a hindered internal rotation. *J. Comput. Chem.*, 12(2):266, 1991.

[19] Y. Y. Chuang and D. G. Truhlar. Statistical thermodynamics of bond torsional modes. *J. Chem. Phys.*, 112(3):1221, 2000.

[20] L. Simón-Carballido and A. Fernández-Ramos. Calculation of the two-dimensional non-separable partition function for two molecular systems. *J. Mol. Model.*, 20(2190):2190, 2014.

[21] T. V. Alves, L. Simón-Carballido, F. R. Ornellas, and A. Fernández-Ramos. Hindered rotor tunneling splittings: an application of the two-dimensional non-separable method to benzyl alcohol and two of its fluorine derivatives. *Phys. Chem. Chem. Phys.*, 18: 8945–8953, 2016.

[22] Y. Zhao, B. J. Lynch, and D. G. Truhlar. Hybrid meta Density Functional Theory methods for Thermochemistry, Thermochemical Kinetics, and noncovalent interactions: The MPW1B95 and MPWB1K models and comparative assessments for hydrogen bonding and van der Waals interactions. *J. Phys. Chem A*, 108:6908–6918, 2004.

[23] W. J. Hehre, R. Ditchfield, and J. A. Pople. Self-consistent molecular orbital methods. XII. Further extensions of Gaussian-type basis sets for use in molecular orbital studies of organic molecules. *J. Chem. Phys.*, 56(5):2257–2261, 1972.

[24] Y. Zhao, N. E. Schultz, and D. G. Truhlar. Design of density functionals by combining the method of constant satisfaction with parametrization for thermochemistry, thermochemical kinetics, and noncovalent interactions. *J. Chem. Theory Comput.*, 2:364–382, 2006.

[25] I. M. Alecu, J. Zheng, Y. Zhao, and D. G. Truhlar. Computational thermochemistry: Scale factor databases and scale factors for vibrational frequencies obtained from electronic model chemistries. *J. Chem. Theory Comput.*, 6:2872–2887, 2010.

[26] Gnuplot 4.4: an interactive plotting program. http://gnuplot.sourceforge.net/, March 2010.

[27] R. J. Renka. Tripack, a constrained two-dimensional delaunay triangulation package. *ACM Transactions on Mathematical Software*, 22:1–8, 1996.

[28] M. Bollhöfer and Y. Notay. Jadamilu: a software code for computing selected eigenvalues of large sparse symmetric matrices. *Comput. Phys. Commun.*, 177:951, 2007.

[29] A. Fernández-Ramos. HR2D version 1.0, Universidade de Santiago de Compostela, Santiago de Compostela, 2012.

[30] M. J. Frisch, G. W. Trucks, H. B. Schlegel, G. E. Scuseria, M. A. Robb, J. R. Cheeseman, G. Scalmani, V. Barone, B. Mennucci, G. A. Petersson, H. Nakatsuji, M. Caricato, X. Li, H. P. Hratchian, A. F. Izmaylov, J. Bloino, G. Zheng, J. L. Sonnenberg, M. Hada, M. Ehara, K. Toyota, R. Fukuda, J. Hasegawa, M. Ishida, T. Nakajima, Y. Honda, O. Kitao, H. Nakai, T. Vreven, J. A. Montgomery Jr., J. E. Peralta, F. Ogliaro, M. Bearpark, J. J. Heyd, E. Brothers, K. N. Kudin, V. N. Staroverov, R. Kobayashi, J. Normand, K. Raghavachari, A. Rendell, J. C. Burant, S. S. Iyengar, J. Tomasi, M. Cossi, N. Rega, J. M. Millam, M. Klene, J. E. Knox, J. B. Cross, V. Bakken, C. Adamo, J. Jaramillo, R. Gomperts, R. E. Stratmann, O. Yazyev, A. J. Austin, R. Cammi, C. Pomelli, J. W. Ochterski, R. L. Martin, K. Morokuma, V. G. Zakrzewski, G. A. Voth, P. Salvador, J. J. Dannenberg, S. Dapprich, A. D. Daniels, O. Farkas, J. B. Foresman, J. V. Ortiz, J. Cioslowski, and D. J. Fox. Gaussian09, Gaussian, Inc., Wallingford CT, 2009.

[31] R. Meana-Pañeda and A. Fernández-Ramos. Accounting for conformational flexibility and torsional anharmonicity in the H + CH_3CH_2OH hydrogen abstraction reactions: A

multi-path variational transition state theory study. *J. Chem. Phys.*, 140(17):174303, 2014.

[32] M. L. Edinoff and J. G. Aston. The rotational entropy of nonrigid polyatomic molecules. *J. Chem. Phys.*, 3:379–383, 1935.

Appendix A

Theoretical Background

A.1 Moment of Inertia

Angular velocity can be considered as a measure of the speed of the rotation, or in other words, as a rate of change in the angle describing the rotation movement. It is usually expressed by the greek letter ω, and is obtained through the equation:

$$\boldsymbol{\omega} = \frac{d\phi}{dt}\boldsymbol{u} \tag{A.1}$$

bold letters represent vectors. In this equation $\boldsymbol{u}$ is the unitary vector along the axis of rotation, ϕ is the angle and t is time. Angular velocities are usually expressed as rad/s. The direction of $\boldsymbol{u}$ is along the axis of the rotation.

As a curiosity, the same equations involved in the equations on linear motion are valid for angular motion but interchanging the linear magnitudes by the rotational analogues. The five fundamental equations of linear and angular motion (both with constant acceleration) are:

$$\begin{aligned}
s &= s_0 + v_0 t + 1/2 a t^2 & \phi &= \phi_0 + \omega_0 t + 1/2 \alpha t^2 \\
s &= s_0 + 1/2(v + v_0)t & \phi &= \phi_0 + 1/2(\omega + \omega_0)t \\
s &= s_0 + vt - (1/2)at^2 & \phi &= \phi_0 + \omega t - (1/2)\alpha t^2 \\
v &= v_0 + at & \omega &= \omega_0 + \alpha t \\
v^2 &= v_0^2 + 2a(s - s_0) & \omega^2 &= \omega_0^2 + 2\alpha(\phi - \phi_0)
\end{aligned} \tag{A.2}$$

where s is displacement, ϕ angular displacement, v velocity, ω angular velocity, a acceleration, α angular acceleration. Subscript zero (0) refers to the initial value of a given magnitude.

The moment of inertia is the analogous of mass for linear movement. The same way mass appears on the Newton's second law for dimensionless bodies, moment of inertia appears for rigid bodies. Let's write down both equations:

$$\begin{aligned}
\boldsymbol{F} &= \frac{d\boldsymbol{p}}{dt} = \frac{dm}{dt}\boldsymbol{v}\frac{d\boldsymbol{v}}{dt}m = m\boldsymbol{a} \\
\boldsymbol{\tau} &= \frac{d\boldsymbol{L}}{dt} = \frac{dI}{dt}\boldsymbol{\omega}\frac{d\boldsymbol{\omega}}{dt}I = I\boldsymbol{\alpha}
\end{aligned} \tag{A.3}$$

where F corresponds to the magnitude force, p to momentum, I to moment of inertia and τ to torque.

Logically, torque is the analogue of force for rotational movement. This kind of analogy between linear and rotational movements extends through a lot of magnitudes such as kinetic and potential energy, work or power but we will focus on the moment of inertia.

The same way mass can be thought as the resistance a body offers against being accelerated, moment of inertia gives us an idea of how difficult is to rotate a body around an axis. The mathematical formula that describes the moment of inertia for a rigid body is:

$$I = \int x^2 dm \tag{A.4}$$

where x is the distance from the point considered to the axis of rotation and m is the mass.

On the International System of Units (SI), the moment of inertia is expressed by the units kg$\cdot$ m^2, though, in our case, when talking about molecules amu $\cdot$ Å^2 is more suitable. The application of this formula usually carries the need of expressing the infinitesimal amount of mass, dm, as a function of the density of the body, ρ. For that general situation in which the density of the body can be considered constant, the following equation is valid:

$$dm = \rho dV \tag{A.5}$$

Let's put a pair of examples on how to determine the moment of inertia. First, let's consider a thin disk of radius R and mass M, the axis of rotation is set perpendicular to the disk and passes through its center as seen in Fig. A.1. The disk has no volume. Its superficial

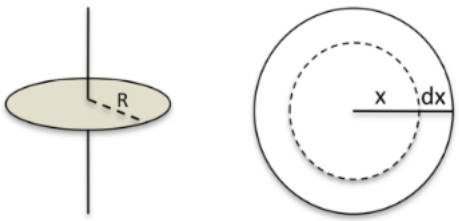

Figure A.1: Representation of the elements involved in the calculation of the moment of inertia of a disk.

density will be:

$$\rho = \frac{M}{\pi R^2} \tag{A.6}$$

We consider now an element of mass, dm, that is at a distance x away from the axis and width dx. This element can be considered as a rectangle of length $2\pi x$ and a width of dx, and dm can be expressed as:

$$dm = \rho dA = \frac{M}{\pi R^2} 2\pi x dx \tag{A.7}$$

Therefore, its moment of inertia around the axis of rotation is given by:

$$I = \int_0^R \frac{2Mx}{R^2} x^2 dx = \left[\frac{MX^4}{2R^2}\right]_0^R = \frac{MR^2}{2} \tag{A.8}$$

If we know the moment of inertia about an axis that crosses through the center of masses of a system, it is possible to obtain with a simple calculation the moment of inertia about another parallel axis. This can be achieved by the Steiner's theorem:

$$I = I_{cm} + Md^2 \tag{A.9}$$

where I_{cm} refers to the moment of inertia across the center of masses, M is the total mass and d represents the distance between the two axis considered.

Unfortunately, since molecules can not be considered as continuous distributions of mass with constant density, the Eq. A.4 is not adequate. Molecules are better described as a system of particles, since the volume of the atoma is negligible compared with the volume of the molecule. In these situations, the equation of the moment of inertia contains a sum instead of an integral:

$$I = \sum_i m_i r_i^2 \tag{A.10}$$

with m_i being the mass of particle i and r_i the distance to the axis.

However, for polyatomic molecules it is better to use the tensor of inertia. The first step in order to calculate the moment of inertia of a molecule is to translate our coordinate system to the center of mass. The center of mass can be calculated using the formula:

$$R_{\mathrm{CM}} = \frac{\sum_i m_i r_i}{\sum_i m_i} \tag{A.11}$$

where r_i are the distances between the atoms and the axis considered, and R_{CM} are the coordinates of the center of mass.

The inertia tensor is given by this matrix:

$$\begin{pmatrix} I_{xx} & I_{xy} & I_{xz} \\ I_{yx} & I_{yy} & I_{yz} \\ I_{zx} & I_{zy} & I_{zz} \end{pmatrix}$$

And its elements are:

$$\begin{pmatrix} \sum_i m_i y_i^2 + z_i^2 & -\sum_i m_i (x_i y_i) & -\sum_i m_i (x_i z_i) \\ -\sum_i m_i (y_i x_i) & \sum_i m_i x_i^2 + z_i^2 & -\sum_i m_i (y_i z_i) \\ -\sum_i m_i (z_i x_i) & -\sum_i m_i (z_i y_i) & \sum_i m_i x_i^2 + y_i^2 \end{pmatrix}$$

This matrix is then diagonalized in order to obtain the principal moments of inertia (which are the eigenvalues). By doing this we can define a new Cartesian coordinates system where its tensor of inertia is given by:

$$\begin{pmatrix} I_a & 0 & 0 \\ 0 & I_b & 0 \\ 0 & 0 & I_c \end{pmatrix}$$

where I_a, I_b and I_c are the principal moments of inertia of the molecule. The determination of the moment of inertia of a molecule is key in order to obtain its thermodynamical properties since I_i appears in the rotational partition function. For instance, the classical rotational partition function is given by:

$$Q_{\text{rot}} = \frac{\pi^{1/2}(8\pi^2 kT)^{3/2}(I_a I_b I_c)^{1/2}}{\sigma h^3} \tag{A.12}$$

where σ is the rotational symmetry number, T is the temperature, k is the Boltzmann constant and h is the Planck constant.

All molecules exhibit rotational movement, although rotation can be limited to only two degrees of freedom in the case of linear molecules instead of the usual three. For non-linear polyatomic molecules there are $3N$ degrees of freedom, with N being the number of atoms. Three of those are associated with the translation, another three are the rotations and the rest are usually considered as internal vibrations. Although this approach is correct, there is one type of vibration quite common that could be best described as an internal rotation.

Let's consider a molecule with a terminal group -CH_3 or -OH; any of those groups can rotate around its bond as seen in Fig. A.2.

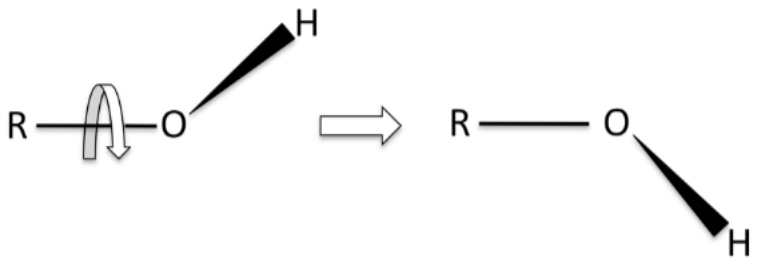

Figure A.2: Schematic representation of the internal rotation through a terminal -OH group.

This kind of movement usually presents a low frequency mode associated to it. There is not a unique formula to correctly describe hindered rotations, since this kind of movement may present very different characteristics from one to another. The shape of the potential, the steepness or the barrier height between wells, can make a huge difference about how it should be treated.

If we consider V_0 as the barrier height, at high temperatures when $kT >> V_0$ the typical free rotor approach should be quite good since the barrier height is negligible with respect to the energy of the molecules, thus resulting in a seemingly free rotor movement. Whereas at low temperatures, the harmonic oscillator should be a reasonable approach since the molecules are "trapped" within a given well. Although any of these treatments can work quite well in some ranges they usually fail to describe the internal rotation when a big range of temperatures is considered. Therefore, in order to solve this problem a hindered rotor model is needed. There are several well known methods developed under certain approximations for attempting to calculate precise hindered rotation partition functions, such as Truhlar [12, 13], or Ayala & Schlegel [17], though the pioneer method is the one from Pitzer and coworkers.

A.2 Reduced Moment of Inertia

In the forties, Pitzer and coworkers describe in a series of papers, Pitzer and Gwinn [7], Pitzer [15], Kilpatrick and Pitzer [8], a mathematical methodology able to calculate the energy levels and partition functions of molecules presenting hindered rotors.

Those molecules whose moments of inertia for the overall rotation can be considered independent from the internal rotation are considered as symmetrical tops. Pitzer and Gwinn [7] refers to this kind of molecules which can be considered as a rigid frame with attached symmetrical tops.

One of the first key concepts described on this paper is the reduced moment of inertia for the internal rotation, which is given by the equation:

$$I_m = A_m(1 - \sum_{i=1}^{3} A_m \lambda_{mi}^2 / I_i) \tag{A.13}$$

being A_m the moment of inertia of the mth top itself, λ_{mi} the direction cosine between the axis of the mth top and the ith principal axis of the whole molecule, I_m the moment of inertia for the rotation of the mth and I_i the moment of inertia of the whole molecule about this axis.

With several tops within the molecule, the following aproximation can be made:

$$I_m = I_m^0 - (1/2) \sum_{m' \neq m}{}' \Lambda_{mm'}^2 / I_{m'}^0 \tag{A.14}$$

and $\Lambda_{mm'}$ is obtained by the following equation:

$$\Lambda_{mm'} = A_m A_{m\prime} \sum_{i=1}^{3} \lambda_{mi} \lambda_{m'i} / I_i \tag{A.15}$$

All these equations are accurate for those cases where the potential adjusts to the following equation:

$$V_{(\phi_1,\phi_2\ldots\phi_N)} = \sum_{m=1}^{N}(1/2)V_m(1-\cos n_m\phi_m) \tag{A.16}$$

where V_m is the barrier height of the potential for the mth top and n_m is the number of potential minima per revolution.

The latter potential expression is still correct when the coupling between rotors is weak. Tops like the methyl group that present an axis of symmetry fall into the category of symmetrical tops. However, there are some tops that present an internal rotation capable of altering the moments of inertia of the overall rotation. This kind of tops fall into the category of unsymmetrical tops, although Pitzer makes a distinction between them attending to their nature:

1. Balanced tops: rotors whose center of gravity lies on the axis of rotation.

2. Small off-balance tops: rotors in which the internal rotation has little effect on the moment of inertia of the overall rotation. Groups like -OH, -NH_2 or -CH_2D fall under this category.

3. Large off-balance tops: rotors without axis of symmetry that possess atoms with considerably different masses that do not lie on the axis of rotation. This includes rotors such as -CH_2Cl or -CHO.

It should be noticed that those changes in the moment of inertia of the overall rotation also provoke a change in the vibrations. According to Pitzer, for the equilibrium geometries, those changes usually compensate each other when movements are treated classically.

For unsymmetrical tops we have a different set of equations that differ a bit from those proposed for the symmetrical tops. The first consideration is to look for the z axis of each top as the axis of rotation with x passing through the center of masses of the top. Then, in order to obtain the reduced moment of inertia it is easier to consider just those atoms that do not lie on the axis of rotation of the mth top. Under this considerations we define the following magnitudes:

$$\begin{aligned} A_m &= \sum_i m_i(x_i^2+y_i^2) \\ B_m &= \sum_i m_i x_i z_i \\ C_m &= \sum_i m_i y_i z_i \\ U_m &= \sum_i m_i x_i \end{aligned} \tag{A.17}$$

where A_m is the moment of inertia about the z axos for top mth, B_m and C_m are the xy and the yz products of inertia respectively, and U_m is the off balance factor. There is a matrix that relates the axes of the mth top (x, y, z) and the principal axes (1,2,3):

$$\begin{pmatrix} \alpha_m^{1x} & \alpha_m^{2x} & \alpha_m^{3x} \\ \alpha_m^{1y} & \alpha_m^{2y} & \alpha_m^{3y} \\ \alpha_m^{1z} & \alpha_m^{2z} & \alpha_m^{3z} \end{pmatrix}$$

where α_m^{ij} are the direction cosines between the axes of the mth top (x, y, z) and the axes of the whole molecule (1, 2, 3).

If we define the vector that binds the center of gravity of the whole molecule to the origin of coordinates of the mth top as $\boldsymbol{r_m}$, One can obtain a similar set of formulas like those given for symmetrical tops. It should be noticed that these new equations can still be used for symmetrical tops since most of the new terms will be zero for those molecules.

Now Λ is obtained through this equation:

$$\Lambda_{mm'} = \sum_i \left\{ \frac{\alpha_m^{iy}\alpha_{m'}^{iy}U_m U_{m'}}{M} + \frac{\beta_m^i \beta_{m'}^i}{I_i} \right\} \tag{A.18}$$

with β_m^i being:

$$\beta_m^i = \alpha_m^{iz}A_m - \alpha_m^{ix}B_m - \alpha_m^{iy}C_m + U_m(\alpha_m^{i-1,y}r_m^{i+1} - \alpha_m^{i+1,y}r_m^{i-1}) \tag{A.19}$$

It should be noticed that due to the cyclic nature of the axes numeration if $i = 1$ then $i - 1 = 3$ and, in the same way, if $i = 3$ then $i + 1 = 1$. The reduced moment of inertia for an unsymmetrical top is as follows:

$$I_m = A_m - \Lambda_{mn} = A_m - \sum_i \left\{ \frac{(\alpha_m^{iy}U_m)^2}{M} + \frac{(\beta_m^i)^2}{I_i} \right\} \tag{A.20}$$

In cases in which there are several tops Eq. A.14 can be used but $\Lambda_{mm'}$ should be obtained from Eq. A.18. Some of these equations or very similar ones can still be applied when considering composed tops instead of single tops.

Kilpatrick and Pitzer [8] considers not just a top attached to a basic rigid frame but a top attached to a rotating group. If we consider a molecule with two symmetric tops, the rotational kinetic matrix for the equilibrium geometry would be as follows:

$$S = \begin{pmatrix} I_{xx} & 0 & 0 & \lambda_{x1}A_1 & \lambda_{x2}A_2 \\ 0 & I_{yy} & 0 & \lambda_{y1}A_1 & \lambda_{y2}A_2 \\ 0 & 0 & I_{zz} & \lambda_{z1}A_1 & \lambda_{z2}A_2 \\ \lambda_{x1}A_1 & \lambda_{y1}A_1 & \lambda_{z1}A_1 & A_1 & 0 \\ \lambda_{x2}A_2 & \lambda_{y2}A_2 & \lambda_{z2}A_2 & 0 & A_2 \end{pmatrix} \tag{A.21}$$

The diagonalization of the S matrix about the elements I_{xx}, I_{yy} and I_{zz} leads to a new matrix of the form:

$$\begin{pmatrix} I_{xx} & 0 & 0 & 0 & 0 \\ 0 & I_{yy} & 0 & 0 & 0 \\ 0 & 0 & I_{zz} & 0 & 0 \\ 0 & 0 & 0 & I_1 & -\Lambda_{12} \\ 0 & 0 & 0 & -\Lambda_{12} & I_2 \end{pmatrix} \tag{A.22}$$

The D matrix is the submatrix that includes the reduced moments of inertia of the two tops:

$$D = \begin{pmatrix} I_1 & -\Lambda_{12} \\ -\Lambda_{12} & I_2 \end{pmatrix} \tag{A.23}$$

Both the reduced moments of inertia (I_i) and the coupling terms (Λ_{ij}) are independent of the orientation of the axes of the molecule.

In order to obtain the kinetic energy of the internal rotation we need to set an appropiate coordinate system. Let's consider a Cartesian coordinates axes (0) fixed in space, then we should consider another set of cartesian axes (1) fixed with respect some part of our molecule which will be denoted as a rigid group. This group will be the basic frame to which the rotations of the other groups of atoms will be related. If we have another set of atoms linked to (1) then it would be possible to consider another set of Cartesian coordinates axes (2) related to the first order frame (1) in the same way (1) is related to (0). One can include additional frames under this premises. It should be notice that only (1) is allowed to have both rotation and translation movement with respect to (0) while second order (or higher) frame (2) are just allowed to rotate with respect to (1).

If we consider two frames m and n the relation between the position vectors of their axes is given by:

$$\boldsymbol{\xi_m} = \boldsymbol{\alpha_{mn}}\boldsymbol{\xi_n} \tag{A.24}$$

or in the matrix form:

$$\begin{pmatrix} \xi_m^x \\ \xi_m^y \\ \xi_m^z \end{pmatrix} = \begin{pmatrix} {\alpha_{mn}}^{xx} & {\alpha_{mn}}^{xy} & {\alpha_{mn}}^{xz} \\ {\alpha_{mn}}^{yx} & {\alpha_{mn}}^{yy} & {\alpha_{mn}}^{yz} \\ {\alpha_{mn}}^{zx} & {\alpha_{mn}}^{zy} & {\alpha_{mn}}^{zz} \end{pmatrix} \begin{pmatrix} \xi_n^x \\ \xi_n^y \\ \xi_n^z \end{pmatrix} \tag{A.25}$$

${\alpha_{mn}}^{xy}$ being the direction cosine of the angle of the x axis of frame m and the y axis of frame n.

This rotation matrix is orthonormal so its transpose is equal to its inverse:

$$\boldsymbol{\alpha_{mn}}^{-1} = \boldsymbol{\alpha_{mn}}' \tag{A.26}$$

it also satisfies that:

$${\alpha_{mn}}^{xx} = {\alpha_{mn}}^{yy}{\alpha_{mn}}^{zz} - {\alpha_{mn}}^{zy}{\alpha_{mn}}^{yz} \tag{A.27}$$

Let's r_{10} be the 1×3 column matrix that includes the coordinates of frame (1) with respect to (0). Accordingly, we will also have $r_{\mathrm{n,n-1}}$ with n being the total number of frames. In the same manner, the coordinates of an atom placed on frame n are represented on a $1 \times$

3 column matrix, r_{n}, with x_n, y_n and z_n as its elements. Since the atom belongs to the frame n, x_n, y_n and z_n remain constant (since only rotation is allowed). In the same way, we can relate the same atom to the frame it is attached (*n-1*) by the coordinates $x_{\mathrm{n-1}}$. Generally, any atom in frame n has *n+1* set of coordinates we can refer to. We will refer to the angular velocities of frame n with respect to frame *n-1* as ${\omega_n}^x$, ${\omega_n}^y$ and ${\omega_n}^z$, at the same time, we will set the axes in a way the frame can only rotate around its z axis, so that only ${\omega_n}^z$ is different from zero. Considering Eq. A.24, the relation between two sets of coordinates is given by:

$$\boldsymbol{x_{n-1}} = \boldsymbol{\alpha'_{n,n-1}} \boldsymbol{x_n} + \boldsymbol{r_{n,n-1}} \tag{A.28}$$

Given that the next relation is valid as shown by Frazer, Duncan & Collar:

$$\boldsymbol{\alpha_{n,n-1}} \partial/\partial t(\boldsymbol{\alpha_{n,n-1}}^{\boldsymbol{-1}}) = \partial/\partial t(\boldsymbol{\alpha_{n,n-1}}) \boldsymbol{\alpha_{n,n-1}}^{\boldsymbol{-1}} = \begin{pmatrix} 0 & -{\omega_n}^z & {\omega_n}^y \\ {\omega_n}^z & 0 & -{\omega_n}^x \\ -{\omega_n}^y & {\omega_n}^x & 0 \end{pmatrix} \tag{A.29}$$

we can write the following equality:

$$\begin{pmatrix} 0 & -{\omega_n}^z & {\omega_n}^y \\ {\omega_n}^z & 0 & -{\omega_n}^x \\ -{\omega_n}^y & {\omega_n}^x & 0 \end{pmatrix} \begin{pmatrix} x_n \\ y_n \\ z_n \end{pmatrix} = - \begin{pmatrix} 0 & -z_n & y_n \\ z_n & 0 & -x_n \\ -y_n & x_n & 0 \end{pmatrix} \begin{pmatrix} {\omega_n}^x \\ {\omega_n}^y \\ {\omega_n}^z \end{pmatrix} \tag{A.30}$$

We will refer to the latter equation using matrix notation:

$$\boldsymbol{\Omega_n x_n} = \boldsymbol{X_n \omega_n} \tag{A.31}$$

Now we can write the derivatives with respect to time from Eq. A.28 as:

$$\frac{\partial}{\partial t}(\boldsymbol{x_{n-1}}) = \frac{\partial}{\partial t}(\boldsymbol{\alpha'_{n,n-1}}) \boldsymbol{x_n} + \boldsymbol{\alpha'_{n,n-1}} \frac{\partial}{\partial t}(\boldsymbol{x_n}) \tag{A.32}$$

at the same time, from Eq. A.29 we get that:

$$\frac{\partial}{\partial t}(\boldsymbol{\alpha'_{n,n-1}}) = \boldsymbol{\alpha'_{n,n-1}} \boldsymbol{\Omega_n} \tag{A.33}$$

combining these equations we get to the regular expression of the velocidity of an atom placed on a fixed frame n:

$$v = \frac{\partial}{\partial t}(\boldsymbol{x_0}) = \frac{\partial}{\partial t}(\boldsymbol{r_{10}}) - \boldsymbol{\alpha'_{10}} \boldsymbol{X_1 \omega_1} - \boldsymbol{\alpha'_{10}} \boldsymbol{\alpha'_{21}} \boldsymbol{X_2 \omega_2} \ldots - \boldsymbol{\alpha'_{10}} \boldsymbol{\alpha'_{21}} \ldots \boldsymbol{\alpha'_{n,n-1}} \boldsymbol{X_n \omega_n} \tag{A.34}$$

The kinetic energy is given by the summation over all the atoms following the formula:

$$2T = \sum m \boldsymbol{v'v} \tag{A.35}$$

If we consider $\frac{\partial}{\partial t}(\boldsymbol{r_{10}})$ as $\mathbf{u}$, the total kinetic energy for a 3 frame molecule can be written as the matrix equation:

$$2T = (\boldsymbol{u'}, \boldsymbol{\omega_1'}, \boldsymbol{\omega_2'}, \boldsymbol{\omega_3'}) \sum m \begin{pmatrix} \boldsymbol{E} & -\boldsymbol{\alpha_{10}'X_1} & -\boldsymbol{\alpha_{20}'X_2} & -\boldsymbol{\alpha_{30}'X_3} \\ -\boldsymbol{X_1'\alpha_{10}} & \boldsymbol{X_1'X_1} & \boldsymbol{X_1'\alpha_{21}'X_2} & \boldsymbol{X_1'\alpha_{31}'X_3} \\ -\boldsymbol{X_2'\alpha_{20}} & \boldsymbol{X_2'\alpha_{21}X_1} & \boldsymbol{X_2'X_2} & \boldsymbol{X_2'\alpha_{32}'X_3} \\ -\boldsymbol{X_3'\alpha_{30}} & \boldsymbol{X_3'\alpha_{31}X_1} & \boldsymbol{X_3'\alpha_{32}X_2} & \boldsymbol{X_3'X_3} \end{pmatrix} \begin{pmatrix} \boldsymbol{u} \\ \boldsymbol{\omega_1} \\ \boldsymbol{\omega_2} \\ \boldsymbol{\omega_3} \end{pmatrix} \tag{A.36}$$

Since $\mathbf{u}$, $\boldsymbol{\omega_1}$, $\boldsymbol{\omega_2}$ and $\boldsymbol{\omega_3}$ are all 1×3 matrices, we can express the above square matrix as a 12×12 matrix. But this matrix can also be reduced into a 8×8 matrix if we consider that the elements ω_2^x, ω_2^y, ω_3^x and ω_3^y are all zero. This new 8×8 matrix will take into account 3 translation movements, 3 overall rotations, and two internal rotations from frames (2) and (3). From now on we will denote with a star those magnitudes that have no contribution from higher ordered groups.

The next step will be to deepen on the submatrix obtained from the kinetic energy general equation. The first diagonal term ends up being:

$$\sum mE = \begin{pmatrix} M^* & 0 & 0 \\ 0 & M^* & 0 \\ 0 & 0 & M^* \end{pmatrix} \tag{A.37}$$

with m being the mass of the group considered. When considering the contribution from higher ordered groups, the complete kinetic energy matrix is:

$$\begin{pmatrix} M & 0 & 0 \\ 0 & M & 0 \\ 0 & 0 & M \end{pmatrix}$$

The second diagonal term considered would be $\sum m\boldsymbol{X_1'X_1}$:

$$\begin{aligned} &\sum m \begin{pmatrix} 0 & z & -y \\ -z & 0 & x \\ y & -x & 0 \end{pmatrix} \begin{pmatrix} 0 & -z & y \\ z & 0 & -x \\ -y & x & 0 \end{pmatrix} \\ &= \begin{pmatrix} \sum m(z^2+y^2) & -\sum mxy & -\sum mxz \\ -\sum mxy & \sum m(z^2+x^2) & -\sum myz \\ -\sum mxz & -\sum myz & \sum m(y^2+x^2) \end{pmatrix} \\ &= \begin{pmatrix} I_{xx}^* & -I_{xy}^* & -I_{xz}^* \\ -I_{xy}^* & I_{yy}^* & -I_{yz}^* \\ -I_{xz}^* & -I_{yz}^* & I_{zz}^* \end{pmatrix} \end{aligned} \tag{A.38}$$

When talking about the complete kinetic energy, the term is the sum of all the matrices of this form, one from each frame, resulting in:

$$\begin{pmatrix} I_{xx} & -I_{xy} & -I_{xz} \\ -I_{xy} & I_{yy} & -I_{yz} \\ -I_{xz} & -I_{yz} & I_{zz} \end{pmatrix}$$

Next diagonal term is $\sum m\boldsymbol{X_2'X_2}$, but is preferable to include $\boldsymbol{\omega_2}$ since only ω_2^z is non zero. So in this case we get:

$$\sum m(0,0,\omega_2^z)X_2'X_2\begin{pmatrix}0\\0\\\omega_2^z\end{pmatrix} = \omega_2^z\sum(x^2+y^2)\omega_2^z = \omega_2^z A_2^*\omega_2^z \tag{A.39}$$

where A_2^* is the moment of inertia of the second ordered group around its own z axis.

In this case, as it was stated before, there is no contribution from higher order groups attached to this one. If we consider all the atoms from higher order groups (all of them treated as a rigid body) and evaluate the rotational contribution to the kinetic energy matrix, we obtain A_2 which is the moment of inertia of the second order group plus the higher order groups around the z axis of frame (2). For the fourth diagonal term, $\sum m\boldsymbol{X_3'X_3}$, we get an analogous result with A_3 being the contribution of the rotation ω_3^z.

Since our kinetic matrix is symmetric, we will now focus only on the off-diagonal terms that lie below the diagonal elements. The first of these is, $-\sum m\boldsymbol{X_1'\alpha_{10}}$, where the elements of $\sum m\boldsymbol{X_1}$ are zero. For the second term $-\sum m\boldsymbol{X_2'\alpha_{20}}$ we repeat the strategy and include the $\boldsymbol{\omega_2}$ elements in order to reduce the dimension of the matrix from 3×3 to 3×1. Since only ω_2^z is non zero the equation for this term becomes:

$$-(0,0,\omega_2^z)\sum m\begin{pmatrix}0 & z_2 & -y_2\\ -z_2 & 0 & x_2\\ y_2 & -x_2 & 0\end{pmatrix}\boldsymbol{\alpha_{20}u} = -\omega_2^z(U_2^y,-U_2^x,0)\boldsymbol{\alpha_{20}u} \tag{A.40}$$

In the latter equation, U^x $(\sum mx)$, represents the off-balance factor in the x direction. Consequently, the third off-diagonal term will be $-\omega_3^z(U_3^y,-U_3^x,0)\boldsymbol{\alpha_{30}u}$. These first three off-diagonal terms represent the interaction between the translation of the whole molecule and the rotation of the distinct frame rotations. The next term involves the interaction between two rotation movements $\boldsymbol{\omega_1}$ and $\boldsymbol{\omega_2}$:

$$\begin{aligned}
&\boldsymbol{\omega_1'}\sum m\boldsymbol{X_1'\alpha_{21}'X_2'\omega_2}\\
&=\boldsymbol{\omega_1'}\sum m\begin{pmatrix}0 & z_1 & -y_1\\ -z_1 & 0 & x_1\\ y_1 & -x_1 & 0\end{pmatrix}\begin{pmatrix}{\alpha_{21}}^{xx} & {\alpha_{21}}^{yx} & {\alpha_{21}}^{zx}\\ {\alpha_{21}}^{xy} & {\alpha_{21}}^{yy} & {\alpha_{21}}^{zy}\\ {\alpha_{21}}^{xz} & {\alpha_{21}}^{yz} & {\alpha_{21}}^{zz}\end{pmatrix}\begin{pmatrix}0 & z_2 & -y_2\\ -z_2 & 0 & x_2\\ y_2 & -x_2 & 0\end{pmatrix}\begin{pmatrix}0\\0\\\omega_2^z\end{pmatrix}\\
&=\boldsymbol{\omega_1'}\sum m\begin{pmatrix}z_1(y_2\alpha^{xy}-x_2\alpha^{yy})-y_1(y_2\alpha^{xz}-x_2\alpha^{yz})\\ x_1(y_2\alpha^{xz}-x_2\alpha^{yz})-z_1(y_2\alpha^{xx}-x_2\alpha^{yx})\\ y_1(y_2\alpha^{xz}-x_2\alpha^{yx})-x_1(y_2\alpha^{xy}-x_2\alpha^{yy})\end{pmatrix}\omega_2^z
\end{aligned} \tag{A.41}$$

The next step is to get rid of x_1, y_1 and z_1. This can be accomplished by the use of Eq. A.28:

$$\begin{aligned}
x_1 &= \alpha_{21}^{xx}x_2+\alpha_{21}^{yx}y_2+\alpha_{21}^{zx}z_2+r_{21}^x\\
y_1 &= \alpha_{21}^{xy}x_2+\alpha_{21}^{yy}y_2+\alpha_{21}^{zy}z_2+r_{21}^y\\
z_1 &= \alpha_{21}^{xz}x_2+\alpha_{21}^{yz}y_2+\alpha_{21}^{zz}z_2+r_{21}^z
\end{aligned} \tag{A.42}$$

Since Eq. A.27 implies that any element of $\boldsymbol{\alpha_{nm}}$ is equal to its own cofactor. In order to reduce the previous equations for the kinetic energy, Pitzer defines a new interaction element, β, as follows:

$$\begin{aligned}
\beta_{21}^x =& \alpha_{21}^{zx}A_2 - \alpha_{21}^{xx}B_2 - \alpha_{21}^{yx}C_2 + (\alpha_{21}^{yz}r_{21}^y - \alpha_{21}^{yy}r_{21}^z)U_2^x \\
&+ (\alpha_{21}^{xy}r_{21}^z - \alpha_{21}^{xz}r_{21}^y)U_2^y \\
\beta_{21}^y =& \alpha_{21}^{zy}A_2 - \alpha_{21}^{xy}B_2 - \alpha_{21}^{yy}C_2 + (\alpha_{21}^{yx}r_{21}^z - \alpha_{21}^{yz}r_{21}^x)U_2^x \\
&+ (\alpha_{21}^{xz}r_{21}^x - \alpha_{21}^{xx}r_{21}^z)U_2^y \\
\beta_{21}^z =& \alpha_{21}^{zz}A_2 - \alpha_{21}^{xz}B_2 - \alpha_{21}^{yz}C_2 + (\alpha_{21}^{yy}r_{21}^x - \alpha_{21}^{yx}r_{21}^y)U_2^x \\
&+ (\alpha_{21}^{xx}r_{21}^y - \alpha_{21}^{xy}r_{21}^x)U_2^y
\end{aligned} \tag{A.43}$$

where the terms B_n and C_n are the xy and yz cross products of inertia, respectively. Then the interaction kinetic energy between ω_1 and ω_2 can be rewritten on a reduced manner as:

$$\boldsymbol{\omega_1'} \sum m \boldsymbol{X_1'\alpha_{21}'X_2'\omega_2} = \boldsymbol{\omega_1'} \begin{pmatrix} \beta_{21}^x \\ \beta_{21}^y \\ \beta_{21}^z \end{pmatrix} \omega_2^z \tag{A.44}$$

The interaction element of the kinetic energy matrix between ω_l^i and ω_n^z is therefore β_{nl}^i. In the same way, the interaction between ω_2^z and ω_3^z can be described with the Eq. A.44 as:

$$(0,0,\omega_2^z) \sum m \boldsymbol{X_2'\alpha_{32}'X_3} \begin{pmatrix} 0 \\ 0 \\ \omega_3^z \end{pmatrix} = \omega_2^z \beta_{32}^z \omega_3^z \tag{A.45}$$

We have now described all the elements of the kinetic matrix, but there are still some simplifications to be done. First off, we can remove from the S matrix those rows and columns that relate to translation. This can be done by a diagonalization about elements of $\boldsymbol{u}$. This process is easier if we place the origin of frame (1) at the instantaneous center of gravity of the molecule. By doing this, U_1^x, U_1^y and U_1^z are all zero, though the change in the coordinate system will also change the values of I and β that correspond to ω_1^x, ω_1^y or ω_1^z.

So, let's first consider the total kinetic matrix for a system with 3 frames where (3) is attached to (2), and (2) is attached to (1):

$$\begin{pmatrix}
M & 0 & 0 & & \alpha_{10}' \begin{pmatrix} 0 & U_1^z & -U_1^y \\ -U_1^z & 0 & U_1^x \\ U_1^y & -U_1^x & 0 \end{pmatrix} & & \alpha_{20}^{yx}U_2^x & \alpha_{30}^{yx}U_3^x \\
0 & M & 0 & & & & \alpha_{20}^{yy}U_2^x & \alpha_{30}^{yy}U_3^x \\
0 & 0 & M & & & & \alpha_{20}^{yz}U_2^x & \alpha_{30}^{yz}U_3^x \\
\begin{pmatrix} 0 & -U_1^z & U_1^y \\ U_1^z & 0 & -U_1^x \\ -U_1^y & U_1^x & 0 \end{pmatrix} \alpha_{10} & & I_{xx} & -I_{xy} & -I_{xz} & & \beta_{21}^x & \beta_{31}^x \\
& & -I_{xy} & I_{yy} & -I_{yz} & & \beta_{21}^y & \beta_{31}^y \\
& & -I_{xz} & -I_{yz} & I_{zz} & & \beta_{21}^z & \beta_{31}^z \\
\alpha_{20}^{yx}U_2^x & \alpha_{20}^{yy}U_2^x & \alpha_{20}^{yz}U_2^x & & \beta_{21}^x & \beta_{21}^y & \beta_{21}^z & & A_2 & \beta_{3,2}^z \\
\alpha_{30}^{yx}U_3^x & \alpha_{30}^{yy}U_3^x & \alpha_{30}^{yz}U_3^x & & \beta_{31}^x & \beta_{31}^y & \beta_{31}^z & & \beta_{3,2}^z & A_3
\end{pmatrix} \tag{A.46}$$

If we set the origin of frame (1) at the center of masses and then proceed to make a diagonalization of the kinetic matrix we get to the S matrix:

$$\boldsymbol{w'_n}\begin{pmatrix} I_{xx} & I_{xy} & I_{xz} & \beta^x_{21} & \beta^x_{31} \\ I_{xy} & I_{yy} & I_{yz} & \beta^y_{21} & \beta^y_{31} \\ I_{xz} & I_{yz} & I_{zz} & \beta^z_{21} & \beta^z_{31} \\ \beta^x_{21} & \beta^y_{21} & \beta^z_{21} & J_2 & \beta^z_{32}-\psi^z_{32} \\ \beta^x_{31} & \beta^y_{31} & \beta^z_{31} & \beta^z_{32}-\psi^z_{32} & J_3 \end{pmatrix}\boldsymbol{w_n} = (S) \tag{A.47}$$

where $\boldsymbol{\omega_n} = (\omega^x_1, \omega^y_1, \omega^z_1, \omega^z_2, \omega^z_3)$ and the new terms J and ψ are

$$J_n = A_n - (U^x_n)^2 M^{-1} \tag{A.48}$$

$$\psi_{mn} = U^x_m U^x_n(\alpha^{yx}_{m1}\alpha^{yx}_{n1} + \alpha^{yy}_{m1}\alpha^{yy}_{n1} + \alpha^{yz}_{m1}\alpha^{yz}_{n1})M^{-1} \tag{A.49}$$

We can take a look now into a different molecule squeme. Let's consider now the case proposed by Pitzer where instead of just three frames there are four; a frame (2a) attached to frame (1), (3) attached to (2a) and another frame (2b) attached to (1). In this scenario we get a slighty different S matrix:

$$\boldsymbol{w'_n}\begin{pmatrix} I_{xx} & I_{xy} & I_{xz} & \beta^x_{2a,1} & \beta^x_{2b,1} & \beta^x_{31} \\ I_{xy} & I_{yy} & I_{yz} & \beta^y_{2a,1} & \beta^y_{2b,1} & \beta^y_{31} \\ I_{xz} & I_{yz} & I_{zz} & \beta^z_{2a,1} & \beta^z_{2b,1} & \beta^z_{31} \\ \beta^x_{2a,1} & \beta^y_{2a,1} & \beta^z_{2a,1} & J_2 a & -\psi_{2b,2a} & -\psi_3, 2a \\ \beta^x_{2b,1} & \beta^y_{2b,1} & \beta^z_{2b,1} & -\psi_{2b,2a} & J_{2b} & \beta^z_{3,2b}-\psi^z_{3,2b} \\ \beta^x_{31} & \beta^y_{31} & \beta^z_{31} & -\psi_{3,2a} & \beta^z_{3,2a}-\psi^z_{3,2a} & J_3 \end{pmatrix}\boldsymbol{w_n} = (S) \tag{A.50}$$

where $\boldsymbol{\omega_n} = (\omega^x_1, \omega^y_1, \omega^z_1, \omega^z_{2a}, \omega^z_{2b}, \omega^z_3)$

All the thermodynamic properties with respect to the internal rotation of a molecule can be obtained through this S matrix. The elements of this matrix are constant in cases where all rotating groups can be considered as symmetric tops. The diagonalization of matrix A.47 about the elements $I_x x$, $I_y y$ and $I_z z$ results in the D matrix A.23, which is the matrix of the kinetic energy for internal rotation.

In those cases where the off-diagonal elements are small it is usually a good aproximation to consider the diagonal elements as the pure reduced moments of inertia since low off-diagonal values can be related to a low coupling between rotors. In this situations one can treat both internal rotations separately. The potential energy is usually expressed by a power series about the equilibrium point:

$$V = \frac{1}{2}\sum_m\sum_{m'} b_{mm'}\phi_m\phi_{m'} + \frac{1}{3!}\sum_m\sum_{m'}\sum_{m''} c_{mm'm''}\phi_m\phi_{m'}\phi_{m''} + \cdots \tag{A.51}$$

with $b_{mm'}$ and $c_{mm'm''}$ being:

$$b_{mm'} = \left(\frac{\partial^2 V}{\partial\phi_m \partial\phi_{m'}}\right)_e \tag{A.52}$$

$$c_{mm'm''} = \left(\frac{\partial^3 V}{\partial\phi_m \partial\phi_{m'} \partial\phi_{m''}}\right)_e \tag{A.53}$$

where e refers to the equilibrium geometry, so the ϕ_m coordinates are all related to it. In those cases where only the first sum of Eq. A.51 is evaluated the result is the usual harmonic oscillator aproximation. Frequencies of the t rotors are obtained through the resolution of the determinantal equations:

$$\begin{bmatrix} b_{11} - 4\pi^2\nu^2 D_{11} & b_{12} - 4\pi^2\nu^2 D_{12} & \cdots & b_{1t} - 4\pi^2\nu^2 D_{1t} \\ b_{21} - 4\pi^2\nu^2 D_{21} & b_{22} - 4\pi^2\nu^2 D_{22} & \cdots & b_{2t} - 4\pi^2\nu^2 D_{2t} \\ \cdots & \cdots & \cdots & \cdots \\ b_{t1} - 4\pi^2\nu^2 D_{t1} & b_{t2} - 4\pi^2\nu^2 D_{t2} & \cdots & b_{tt} - 4\pi^2\nu^2 D_{tt} \end{bmatrix} = 0 \tag{A.54}$$

From which energy can be determined as a sum of t members:

$$E = \sum_{\tau=1}^{t} (n_\tau + \frac{1}{2}) h\nu_\tau \tag{A.55}$$

Logically, under the harmonic oscillator aproximation the partition function can be obtained as a product:

$$Q_{\text{tor}}^{\text{HO(C)}} = \prod_{\tau=1}^{t} \frac{1}{1 - e^{-h\nu_\tau/kT}} \tag{A.56}$$

At the same time, the classical partition function for the harmonic oscillator can be written as:

$$Q_{\text{tor}}^{\text{CHO(C)}} = \frac{(kT/h)^t}{\prod_\tau \nu_\tau} \tag{A.57}$$

The Pitzer & Gwinn method for calculating the partition function uses the ratio between the last two:

$$Q_{\text{tor}}^{\text{TPG(C)}} = Q_{\text{cl,tor}}^{\text{(C)}} \frac{Q_{\text{tor}}^{\text{HO(C)}}}{Q_{\text{tor}}^{\text{CHO(C)}}} \tag{A.58}$$

In those cases with high temperatures the ratio has to be near to 1, resulting in $Q_{\text{tor}}^{\text{TPG(C)}} = Q_{\text{cl,tor}}^{\text{(C)}}$.

In order to obtain the exact classical partition function ($Q_{\text{cl,tor}}^{\text{(C)}}$) one may refer to the Edinoff & Aston theorem [32] which offers a solution for those molecules with unsymmetrical tops.

Let's consider a molecule with several tops and a fixed center of gravity. Angular coordinates α_n (with t being the number of tops) will be used to define the distinct tops orientation relative to the frame. There will be t sets of axes (x_i, y_i, z_i) for each of those tops. On a similar way, we can denote I_{xi}, I_{yi} and I_{zi} as the moment of inertia, and ω_{xi}, ω_{yi} and ω_{zi} as the angular velocities. Rotational kinetic energy may be written as:

$$T = (1/2) \sum_{i=1}^{t} (I_{xi}\omega_{xi}^2 + I_{yi}\omega_{yi}^2 + I_{zi}\omega_{zi}^2) \tag{A.59}$$

or as a function of its velocities:

$$2T = \sum_{i,j=1}^{t} A_{ij}\dot{x}_i\dot{x}_j \tag{A.60}$$

where t is the number of degrees of freedom and $A_{ij} = f_{ij}(x_1, x_2, ..., x_r)$. If matrix A is not singular then, the Hamiltonian can be written as a function of its momentum:

$$2T = \sum_{i,j=1}^{t} B_{ij}p_ip_j \tag{A.61}$$

with p referring to the momentum magnitude and B_{ij} as the cofactor of A_{ij} so $(A)\times(B) = (1)$. The rotational partition function is then obtained through an integration over the momentum which can vary from $-\infty$ to $+\infty$ and the space coordinates which can vary from α_i to β_i:

$$Q^{(\mathrm{C})}_{\mathrm{cl,tor}} = \frac{1}{h}\int_{-\infty}^{+\infty}\cdots\int_{-\infty}^{+\infty}\int_{\alpha_t}^{\beta_t}\cdots\int_{\alpha_1}^{\beta_1} e^{-1/2kT\sum_{i=1}^{t} B_{ij}p_ip_j} dp_1\cdots dp_t dx_1\cdots dx_t \tag{A.62}$$

which can be converted into:

$$Q^{(\mathrm{C})}_{\mathrm{cl,tor}} = \frac{1}{h}\int_{-\infty}^{+\infty}\cdots\int_{-\infty}^{+\infty}\int_{\alpha_t}^{\beta_t}\cdots\int_{\alpha_1}^{\beta_1} e^{-1/2kT\sum_{i=1}^{t} D_ip_{i'}^2} dp'_i\cdots dp'_t dx_1\cdots dx_t \tag{A.63}$$

the integration over the momentum yields the following equation:

$$Q^{(\mathrm{C})}_{\mathrm{cl,tor}} = \frac{(2\pi kT)^{t/2}}{h}\int_{\alpha_t}^{\beta_t}\cdots\int_{\alpha_1}^{\beta_1}\left(\frac{1}{D_1D_2\cdots D_t}\right)^{1/2} dx_1\cdots dx_t \tag{A.64}$$

and as shown by Edinoff & Aston, this equation becomes:

$$Q^{(\mathrm{C})}_{\mathrm{cl,tor}} = [(2\pi kT)^{t/2}/h^t]\int_{\alpha_t}^{\beta_t}\cdots\int_{\alpha_1}^{\beta_1}[A]^{(1/2)}dx_1\cdots dx_t \tag{A.65}$$

where [A] is the determinant of matrix (A).

The mathematical proof behind this mathematical deduction will be quoted next: Let $\Phi = \sum_{i,j=1}^{t} B_{ij}p_ip_j$ be a real positive quadratic form with nonsingular matrix (B). If the P's are subjected to a homogeneous linear transformation with the matrix (C) the new quadratic form in, say, the p''s, has the matrix $(C)^\dagger(B)(C)$ with $(C)^\dagger$ being the transposed matrix. In the case of Φ, it can be reduced by a real orthogonal transformation in r variables to the form: $\sum_{i=1}^{t} D_ip_i'^2$. The Jacobian of the transformation is 1. The integrand is positive and the limits of integration are from $-\infty$ to $+\infty$. This first part of the theorem permits the conversion from Eq. A.62 into Eq. A.63. The integration over the momentum then yields Eq. A.64 and since $D_1D_2\cdots D_t = [C]^\dagger[B][C] = [B]$ and for a real orthogonal matrix $[C]^\dagger = [C]^{-1} = 1$ so Eq. A.64 becomes Eq. A.65.

A.3 Particle in a Ring

For a particle that spins around a ring without the influence of an external potential, the Hamiltonian is given by:

$$\widehat{H}(\phi) = -\frac{\hbar^2}{2I}\frac{d^2}{d\phi^2} \tag{A.66}$$

With ϕ being the rotation angle. Therefore, the time independet Schrödinger equation is:

$$\widehat{H}(\phi)\varphi(\phi) = -\frac{\hbar^2}{2I}\frac{d^2}{d\phi^2}\varphi(\phi) = E\varphi(\phi) \tag{A.67}$$

which has as a general solution $\varphi(\phi) = e^{\lambda\phi}$. Therefore:

$$\begin{aligned} &\frac{d}{d\phi}e^{\lambda\phi} = \lambda e^{\lambda\phi}\,; \qquad \frac{d^2}{d\phi^2} = \lambda^2 e^{\lambda\phi} = \lambda^2\varphi(\phi) \\ &-\frac{\hbar^2}{2I}\lambda^2\varphi(\phi) = \varphi(\phi)E\,; \qquad \lambda^2 = -\frac{2EI}{\hbar^2} \\ &\lambda = \pm\frac{i}{\hbar}\sqrt{2EI}\,; \qquad \varphi(\phi) = e^{\pm\frac{i}{\hbar}\sqrt{2EI}\phi} \end{aligned} \tag{A.68}$$

Once the particle completes a loop the wavefunctions have to be the same $\varphi(\phi) = \varphi(\phi + 2\pi)$.

$$\varphi(\phi) = e^{\pm\frac{i}{\hbar}\sqrt{2EI}\phi} = e^{\pm\frac{i}{\hbar}\sqrt{2EI}(\phi+2\pi)}$$

If $m = \frac{\sqrt{2EI}}{\hbar}$, then $\varphi(\phi) = e^{\pm im\phi}e^{\pm 2\pi im}$ and because $e^{\pm\pi im} = 1$ due to Euler's relation:

$$e^{i\phi} = cos\phi + isen\phi \tag{A.69}$$

and

$$e^{\pm 2\pi im} = cos(+2\pi m) \pm isen\phi = 1 \tag{A.70}$$

the unnormalized wavefunction is given by:

$$\varphi(\phi) = e^{\pm im\phi} \tag{A.71}$$

This equality is satisfied if m can take entire values (both positive and negative) since the cosine function it's an even function and at the same time, we get rid of the sine function. Our wavefunction becomes:

$$\varphi(\phi) = Ne^{\pm im\phi} \tag{A.72}$$

where N is the normalization constant, $N = 1/2\pi$, and $m = (0, \pm1, \pm2, ...)$. The energy is given by:

$$m = \frac{\sqrt{2EI}}{\hbar} \rightarrow m^2 = \frac{2EI}{\hbar^2} \rightarrow E = \frac{m^2\hbar^2}{2I} \tag{A.73}$$

All energy levels are doubly degenerated with the exception of $m = 0$. This degeneracy responds to the dual character of the rotation movement since the particle can rotate clockwise or counterclockwise. If we consider a molecule with a single hindered rotor, the Hamiltonian can be written as:

$$\widehat{H} = -\frac{\hbar^2}{2I_1}\frac{d^2}{d\phi_1^2} + V(\phi_1) \tag{A.74}$$

where I_1 is the momento of inertia and the potential can be fitted to a Fourier series of the type:

$$V(\phi_1) = a_0 + \sum_{l=1} a_l\, cos(l\phi_1) + \sum_{l'=1} b_{l'}\, sin(l'\phi_1) \tag{A.75}$$

The trial wavefunctions are expressed as a linear combination between all the possible states. This means we have to consider both positive and negative values for the quantum number m previously described.

$$\Phi_1(\phi_1) = N \sum_{m=-m_{\mathrm{MAX}}}^{m_{\mathrm{MAX}}} C_m e^{im\phi_1} = \sum_m C_m \varphi_m(\phi_1) \tag{A.76}$$

In order to obtain the energy we applied the variational method, which is usually represented by the equation:

$$E\Psi = \frac{\langle\Psi|\widehat{H}|\Psi\rangle}{\langle\Psi|\Psi\rangle} \tag{A.77}$$

Combining Eq. A.74 into Eq. A.75 we obtain the following expression for the Hamiltonian $\widehat{H}$:

$$\widehat{H} = -\frac{\hbar^2}{2I_1}\frac{d^2}{d\phi_1^2} + a_0 + \sum_{l=1} a_l\, cos(l\phi_1) + \sum_{l'=1} b_{l'}\, sin(l'\phi_1) \tag{A.78}$$

where each of the elements of the secular matrix obey the general formula:

$$H_{mn} = \langle m|\, \widehat{H}\, |n\rangle = \langle \varphi_m(\phi_1)|\, \widehat{H}\, |\varphi_n(\phi_1)\rangle \tag{A.79}$$

The Schrödinger equation for H_{mn} is:

$$\int_0^{2\pi} \varphi_m^*(\phi_1)\widehat{H}\varphi_n(\phi_1)d\phi_1 = \int_0^{2\pi} \varphi_m^*(\phi_1)\left(-\frac{\hbar^2}{2I_1}\right)\frac{d^2}{d\phi_1^2}\varphi_n(\phi_1)d\phi_1 \tag{A.80}$$

$$+ a_0 \int_0^{2\pi} \varphi_m^*(\phi_1)\varphi_n(\phi_1)d\phi_1 \tag{A.81}$$

$$+ \sum_{l=1} \int_0^{2\pi} \varphi_m^*(\phi_1) a_l\, cos(l\phi_1)\varphi_n(\phi_1)d\phi_1 \tag{A.82}$$

$$+ \sum_{l_1'=1} \int_0^{2\pi} \varphi_m^*(\phi_1) b_{l'}\, sin(l'\phi_1)\varphi_n(\phi_1)d\phi_1 \tag{A.83}$$

We solve each term separately. Term A.80 is given by:

$$\begin{aligned}(A.80) &= \int_0^{2\pi} N^* e^{-im\phi_1}\left(-\frac{\hbar^2}{2I_1}\right)\frac{d^2}{d\phi^2}Ne^{in\phi_1}d\phi_1 \\ &= N^2\int_0^{2\pi}\frac{n^2\hbar^2}{2I_1}e^{-im\phi_1}e^{in\phi_1}d\phi_1 \\ &= \frac{n^2\hbar^2}{2I_1}\int_0^{2\pi}N^2e^{i(n-m)\phi_1}d\phi_1 \qquad (A.84)\end{aligned}$$

$$\begin{aligned}\text{we have used;}\quad &\frac{d}{d\phi_1}Ne^{in\phi_1} = inNe^{in\phi_1} \\ &\frac{d^2}{d\phi_1^2}Ne^{in\phi_1} = -n^2Ne^{in\phi_1}\end{aligned}$$

Considering the values that the quantum numbers m and n can take, we arrive to two possible situations: m and n having equal or distinct values. First we consider the situation in which $m \neq n$:

$$\begin{aligned}\int_0^{2\pi} e^{i(n-m)\phi_1}d\phi_1 &= \int_0^{2\pi} cos(n-m)\phi_1 d\phi_1 + i\int_0^{2\pi} sin(n-m)\phi_1 d\phi_1 \\ &= \frac{1}{n-m}sin(n-m)\phi_1\Big]_0^{2\pi} - \frac{i}{n-m}cos(n-m)\phi_1\Big]_0^{2\pi} \\ &= \frac{1}{n-m}(sin(2\pi) - sin(0) - i(cos(2\pi) - cos(0)) = 0 \qquad (A.85)\end{aligned}$$

If $m = n$ then:

$$\int_0^{2\pi} e^{i(n-m)\phi_1}d\phi_1 = 1 \qquad (A.86)$$

The integration of Eq. A.85 is usually expressed as:

$$(A.85) = \frac{n^2\hbar^2}{2I_1}\delta_{mn} \qquad (A.87)$$

where δ_{mn} is the delta function of Kronecker ($\delta_{mn} = 0$ if $m \neq n$ and $\delta_{mn} = 1$ if $m = n$).

In the same way, Term A.81 reduces to:

$$(A.81) = a_0\delta_{mn} \qquad (A.88)$$

The solution of the integration of Term A.82 is a bit more complex:

$$\begin{aligned}(A.82) &= \int_0^{2\pi} \varphi_m^* a_l \, cos(l\phi_1)\varphi_n d\phi_1 \\ &= \int_0^{2\pi} N^* e^{-im\phi_1} a_l \, cos(l\phi_1) N e^{in\phi_1} d\phi_1 \\ &= a_l N^2 \int_0^{2\pi} e^{i(n-m)\phi_1} cos(l\phi_1) d\phi_1 \\ &= a_l N^2 \left[\underbrace{\int_0^{2\pi} cos((n-m)\phi_1) cos(l\phi_1) d\phi_1}_{\text{A}} + \underbrace{\int_0^{2\pi} sin((n-m)\phi_1) cos(l\phi_1) d\phi_1}_{\text{B}} \right]\end{aligned}$$

It should be reminded that these integrals have as general solution:

$$\int cos(ax)cos(bx)dx = \frac{sin(x(a-b))}{2(a-b)} + \frac{sin(x(a+b))}{2(a+b)}; \quad a^2 \neq b^2$$
$$\int sin(ax)cos(bx)dx = -\frac{cos(x(a-b))}{2(a-b)} - \frac{cos(x(a+b))}{2(a+b)}; \quad a^2 \neq b^2$$

Therefore in our case, Term (A) can be expressed as:

$$(A) = \frac{sin((n-m)-l)\phi_1}{2((n-m)-l)} + \frac{sin((n-m)+l)\phi_1}{2((n-m)+l)} \Bigg]_0^{2\pi} \tag{A.89}$$

If we now define k_1 and k_2 as:

$$k_1 = n - m - l$$
$$k_2 = n - m + l$$

then Term (A) becomes:

$$(A) = \frac{sin(k_1 2\pi)}{2k_1} + \frac{sin(k_2 2\pi)}{2k_2} \tag{A.90}$$

and since k_1 and k_2 can only take entire values and $sin(n2\pi) = 0$, both summands of the latter equation are zero if:

$$(n-m)^2 \neq l^2 \tag{A.91}$$

For Term (B) we arrive into a similar expression:

$$\begin{aligned}(B) &= -\frac{cos((n-m)-l)\phi_1}{2((n-m)-l)} - \frac{cos((n-m)+l)\phi_1}{2((n-m)+l)} \Bigg]_0^{2\pi} \\ &= -\frac{cos(k_1 2\pi)}{2k_1} - \frac{cos(k_2 2\pi)}{2k_2} + \frac{cos(0)}{2k_1} + \frac{cos(0)}{2k_2}\end{aligned} \tag{A.92}$$

and since both $cos(n2\pi) = 1$ and $cos(0) = 1$ Term (B) is also zero if:

$$(n-m)^2 \neq l^2 \tag{A.93}$$

if $(n-m)^2 = l^2 \rightarrow l = \pm(n-m)$, because l has always a positive value. In this case Term (A) if given by:

$$\int_0^{2\pi} cos(\pm(n-m)\phi_1)cos(l\phi_1)d\phi_1$$
$$= \int_0^{2\pi} cos(\pm l\phi_1)cos(l\phi_1)d\phi_1 \tag{A.94}$$

Since the cosine function is even; $cos(ax) = cos(-ax)$ or $cos(x) - cos(-x) = 0$. This kind of integral offers the next solution:

$$\int_0^{2\pi} cos(\pm ax)cos(ax)dx = \int_0^{2\pi} cos(ax)cos(ax)dx$$
$$= \int_0^{2\pi} cos^2(ax)dx = \frac{x}{2} + \frac{1}{4a}sin(2ax) \tag{A.95}$$

Therefore Term A.94 becomes:

$$\frac{\phi_1}{2} + \frac{1}{4l}sin(2l\phi_1)\Big]_0^{2\pi} = \pi \tag{A.96}$$

Since the sine function is an odd; $-sin(x) = sin(-x)$ or $sin(x) + sin(-x) = 0$. We obtain the next result for Term (B):

$$\int_0^{2\pi} sin(\pm l\phi_1)cos(l\phi_1)d\phi_1 = 0 \tag{A.97}$$

In summary, Term A.82 can be expressed as:

$$(A.82) \ = a_l N^2 \pi = a_l \frac{1}{2\pi}\pi = \frac{a_l}{2} \tag{A.98}$$

Since $l = \pm(n-m) = |m-n|$, we use the following expression for Term A.82:

$$a_l \langle m| \, cos(l\phi_1) \, |n\rangle = \frac{a_l}{2}\delta_{|m-n|,l} \tag{A.99}$$

Term A.83 is given by:

$$(A.83) \ = \int_0^{2\pi} N^2 b_{l'} e^{-in\phi_1} sin(l'\phi_1) e^{im\phi_1} d\phi_1$$
$$= N^2 b_{l'} \int_0^{2\pi} e^{i(n-m)\phi_1} sin(l'\phi_1)d\phi_1$$
$$= N^2 b_{l'} \left[\underbrace{\int_0^{2\pi} cos((n-m)\phi_1)sin(l'\phi_1)d\phi_1}_{\text{C}} + i \underbrace{\int_0^{2\pi} sin((n-m)\phi_1)sin(l'\phi_1)d\phi_1}_{\text{D}} \right]$$

Term (C) is zero for both cases in which $(n-m)^2 = l^2$ and $(n-m)^2 \neq l^2$; the reasoning under this fact is the same that was stated for Term (B).
For term (D), we have a non zero result for those cases in which $(n-m)^2 = l^2$, but this time the reasoning is a bit different than for Term (A). In this case due to the odd parity of the sine function we obtain the following expression:

$$i\int_0^{2\pi} sin(\pm(n-m)\phi_1)sin(l'\phi_1)d\phi_1 = \pm i\pi \tag{A.100}$$

Term A.83 becomes:

$$\begin{aligned}(A.83) \;&= \frac{1}{2\pi}b_{l'}(\pm i)\pi\delta_{|m-n|,l'} = \frac{b'_l}{2}i(\pm)\delta_{|m-n|,l'} \\ &= -sig(m-n)i\frac{b'_l}{2}\delta_{|m-n|,l'} \qquad (A.101)\\ \text{where;}\quad &sig(x) = -1,\ \text{If } x<0 \\ &sig(x) = 1,\ \text{If } x>0\end{aligned}$$

Finally, the matrix element of H_{mn} of Eq. A.79 can be rewritten as:

$$H_{mn} = \left(\frac{n^2\hbar^2}{2I_1} + a_0\right)\delta_{mn} + \frac{a_l}{2}\delta_{|m-n|,l} - sig(m-n)i\frac{b'_l}{2}\delta_{|m-n|,l'} \tag{A.102}$$

For molecules with 2 rotors (2D) whose rotation is expressed by the coordinates ϕ_1 and ϕ_2, the Hamiltonian is quite similar to the one of 1D rotors:

$$\widehat{H} = \underbrace{-\frac{\hbar^2}{2}\left(\frac{\partial^2}{I_1\partial\phi_1^2} + \frac{\partial^2}{I_2\partial\phi_2^2}\right)}_{\widehat{T}} + V(\phi_1,\phi_2) \tag{A.103}$$

where $\widehat{T}$ stands for the kinetic energy operator and th matrix elements lead to the following terms:

$$\langle mj|\,\widehat{T}\,|nk\rangle = \left(\frac{n^2\hbar^2}{2I_1} + \frac{n^2\hbar^2}{2I_2}\right)\delta_{mn}\delta_{jk} \tag{A.104}$$

Like in the 1D equations, the kinetic energy matrix is diagonal. The potential operator also gives analogous terms to the 1D case:

$$\begin{aligned}\langle mj|\,V(\phi_1)\,|nk\rangle &= \left(\frac{a_l}{2}\delta_{|m-n|,l} - sig(m-n)i\frac{b'_l}{2}\delta_{|m-n|,l'}\right)\delta_{jk} \\ \langle mj|\,V(\phi_2)\,|nk\rangle &= \left(\frac{a'_t}{2}\delta_{|j-k|,t} - sig(j-k)i\frac{b'_{t'}}{2}\delta_{|j-k|,t'}\right)\delta_{mn} \qquad (A.105)\end{aligned}$$

If we consider a cross term of the type; $c_{lt}\,cos(l\phi_1)\,cos(t\phi_2)$, the matrix element is given by:

$$\begin{aligned}&c_{lt}\,\langle mj|\,cos(l\phi_1)\,cos(t\phi_2)\,|nk\rangle = c_{lt}\,\langle m|\,cos(l\phi_1)\,|n\rangle\,\langle j|\,cos(t\phi_2)\,|k\rangle \\ =&c_{lt}\left(\frac{\delta_{|m-n|,l}}{2}\frac{\delta_{|j-k|,t}}{2}\right) = \frac{c_{lt}}{4}\delta_{|m-n|,l}\delta_{|j-k|,t} \qquad (A.106)\end{aligned}$$

Though we've just considered a term of the type $cos(x)\ cos(y)$, the solution for other combinations is quite similar. For instance:

$$\begin{aligned} & c'_{l't'} \langle mj| sin(l'\phi_1)sin(t'\phi_2) |nk\rangle = c'_{l't'} \langle m| sin(l'\phi_1) |n\rangle \langle j| sin(t'\phi_2) |k\rangle \\ =& c'_{l't'} \left(-sig(m-n)\frac{i}{2}\delta_{|m-n|,l'}\right)\left(-sig(j-k)\frac{i}{2}\delta_{|j-k|,t'}\right) \\ =& c'_{l't'} sig(m-n)sig(j-k)\left(-\frac{1}{4}\right)\delta_{|m-n|,l'}\delta_{|j-k|,t'} \end{aligned} \tag{A.107}$$

A.4 2D-NS Methodology

The Hamiltonian for two torsions, ϕ_1 and ϕ_2, that are coupled can be written as:

$$H_{\text{tor}}\left(\tfrac{\partial}{\partial\phi_1}, \tfrac{\partial}{\partial\phi_2}; \phi_1, \phi_2\right) = T_{\text{tor}}\left(\tfrac{\partial}{\partial\phi_1}, \tfrac{\partial}{\partial\phi_2}\right) + V_{\text{tor}}(\phi_1, \phi_2) \tag{A.108}$$

where the kinetic energy T_{tor} is given by Eq. 8 of Ref. 10. The potential energy $V_{\text{tor}}(\phi_1, \phi_2)$ is split into three terms

$$V_{\text{tor}}(\phi_1, \phi_2) = V_1(\phi_1) + V_2(\phi_2) + V^{\text{2D}}(\phi_1, \phi_2), \tag{A.109}$$

and each of them is fitted to Fourier series:

$$V_1(\phi_1) = a_0 + \sum_{M=1}^{M_{\max}} a_M \cos(M\phi_1) + \sum_{M'=1}^{M'_{\max}} a'_{M'} \sin(M'\phi_1), \tag{A.110}$$

$$V_2(\phi_2) = b_0 + \sum_{N=1}^{N_{\max}} b_N \cos(N\phi_2) + \sum_{N'=1}^{N'_{\max}} b'_{N'} \sin(N'\phi_2), \tag{A.111}$$

and

$$\begin{aligned} V_{\text{tor}}(\phi_1, \phi_2) = & V_1(\phi_1) + V_2(\phi_2) + \\ & \sum_{L_1=1}^{L_{1,\max}} \sum_{L_2=1}^{L_{2,\max}} c_{L_1L_2} \cos(L_1\phi_1)\cos(L_2\phi_2) + \\ & \sum_{P_1=1}^{P_{1,\max}} \sum_{P_2=1}^{P_{2,\max}} d_{P_1P_2} \sin(P_1\phi_1)\sin(P_2\phi_2) + \\ & \sum_{L'_1=1}^{L'_{1,\max}} \sum_{L'_2=1}^{L'_{2,\max}} c'_{L'_1L'_2} \cos(L'_1\phi_1)\sin(L'_2\phi_2) + \\ & \sum_{P'_1=1}^{P'_{1,\max}} \sum_{P'_2=1}^{P'_{2,\max}} d'_{P'_1P'_2} \sin(P'_1\phi_1)\cos(P'_2\phi_2) \end{aligned} \tag{A.112}$$

where a_0, b_0, $a_M(M = 1, \ldots, M_{\max})$, $a'_{M'}(M' = 1, \ldots, M'_{max})$, $b_N(N = 1, \ldots, N_{\max})$, and $b'_{N'}(N' = 1, \ldots, N'_{\max})$ are fitting parameters of the one-dimensional potential. Also $c_{L_1 L_2}$, $L_1 = 1, \ldots, L_{1,\max}$, $L_2 = 1, \ldots, L_{2,\max}$, $d_{P_1 P_2}$, $P_1 = 1, \ldots, P_{1,\max}$, $P_2 = 1, \ldots, P_{2,\max}$, $c'_{L'_1 L'_2}$, $d'_{L'_1 L'_2}$, $L'_1 = 1, \ldots, L'_{1,\max}$, $L'_2 = 1, \ldots, L'_{2,\max}$, and $d'_{P'_1 P'_2}$, $P'_1 = 1, \ldots, P'_{1,\max}$, $P'_2 = 1, \ldots, P'_{2,\max}$ are fitting parameters, and $L_{1,\max}$, $L_{2,\max}$, $L'_{1,\max}$, $L'_{2,\max}$, $P_{1,\max}$, $P_{2,\max}$, $P'_{1,\max}$, and $P'_{2,\max}$ indicate the largest number of each series. It should be noticed that the potentials $V_1^{1\mathrm{D}}(\phi_1)$ and $V_2^{1\mathrm{D}}(\phi_2)$ are different from the potentials $V_1(\phi_1)$ and $V_2(\phi_2)$, because the former potentials correspond to one-dimensional potentials obtained by scanning one of the torsional angles while fixing the other, whereas the later are simply fitting potentials that, together with the potential of Eq. A.112, minimize the root mean square of residuals with respect to the electronic structure calculations.

It is possible to solve the Schrödinger equation by the variational method using the product of two wavefunctions, and each of them is a linear combinations of the wavefunctions which are solution of the Schrödinger equation for the particle in a ring, i. e.,

$$\Phi(\phi_1, \phi_2) = \Phi_1(\phi_1)\Phi_2(\phi_2) \tag{A.113}$$

being

$$\Phi_1(\phi_1) = \frac{1}{\sqrt{2\pi}} \sum_{k=-k_{\max}}^{k_{\max}} c_{1,k} e^{ik\phi_1}, \tag{A.114}$$

and

$$\Phi_2(\phi_2) = \frac{1}{\sqrt{2\pi}} \sum_{n=-n_{\max}}^{n_{\max}} c_{2,n} e^{in\phi_2} \tag{A.115}$$

The trial wavefunction of Eq. A.113 is used together with the Hamiltonian of Eq. A.108 to obtain the eigenvalues. Thus, the 2D-NS quantum partition function obtained from the direct sum of the eigenvalues is given by

$$Q_{\mathrm{tor}}^{2\mathrm{D}-\mathrm{NS}} = \frac{1}{\sigma_{\mathrm{tor}}} \sum_j e^{-\beta E_{\mathrm{tor},j}} \tag{A.116}$$

where

$$\sigma_{\mathrm{tor}} = \sigma_1 \sigma_2 \tag{A.117}$$

being σ_1 and σ_2 the symmetry numbers associated to the internal rotation about ϕ_1 and ϕ_2, respectively, and $E_{\mathrm{tor},j}$ the j-th eigenvalue.

A.5 Thermodynamic Functions

In order to obtain the different thermodynamic functions it is necessary to calculate the derivatives of the partition function, because the formulas for internal energy (U) and entropy (S) are respectively,

$$U = k_B T^2 \frac{\partial ln Q}{\partial T} \tag{A.118}$$

and

$$S = \frac{U}{T} + k_B \, lnQ \tag{A.119}$$

where k_B is the to the Boltzmann constant, T the temperature and Q the partition function. Now, we write down the same expression as a function of β:

$$\beta = \frac{1}{k_B T} \rightarrow \frac{\partial \beta}{\partial T} = -\frac{1}{k_B T^2} \rightarrow \frac{\partial T}{\partial \beta} = -\frac{1}{k_B \beta^2} \tag{A.120}$$

so, U and S become:

$$U = \frac{1}{k_B}\frac{1}{\beta^2}\frac{\partial lnQ}{\partial \beta}\frac{\partial \beta}{\partial T} = \frac{1}{k_B}\frac{1}{\beta^2}\frac{\partial lnQ}{\partial \beta}\left(-k_B\beta^2\right) = -\left(\frac{\partial lnQ}{\partial \beta}\right) \tag{A.121}$$

$$S = -k_B\beta\left(\frac{\partial lnQ}{\partial \beta}\right) + k_B \, lnQ \tag{A.122}$$

Most of the partition functions considered in this section have been already defined in Chapter 3. The $Q^{\mathrm{GS2D-NS}}$ is obtained as:

$$Q_{\mathrm{rv}}^{\mathrm{GS2D-NS}} = \alpha_{\mathrm{tor}}^{\mathrm{2D-NS}} Q_{\mathrm{rv}}^{\mathrm{MC-H}} \tag{A.123}$$

where $\alpha_{\mathrm{tor}}^{\mathrm{2D-NS}}$ is given by:

$$\alpha_{\mathrm{tor}}^{\mathrm{2D-NS}} = \frac{Q_{\mathrm{tor}}^{\mathrm{2D-NS}}}{Q_{\mathrm{tor}}^{\mathrm{MC-HO(C)}}} \tag{A.124}$$

where $Q_{\mathrm{tor}}^{\mathrm{2D-NS}}$ was described in the previous section and $Q_{\mathrm{tor}}^{\mathrm{MC-HO(C)}}$ is the multiconformer harmonic oscillator torsional partition function:

$$Q_{\mathrm{tor}}^{\mathrm{MC-HO(C)}} = \sum_{j=1}^{J} e^{-\beta U_j} \prod_{\eta=1}^{t} \frac{e^{-\beta\hbar\overline{\omega}_{j,\eta}/2}}{1 - e^{-\beta\hbar\overline{\omega}_{j,\eta}}}, \tag{A.125}$$

with $\overline{\omega}_{j,\eta)}$ being the projected frequencies, J is the total number of conformers, t is the total number of torsions, j and η refer to the number of a given conformer and the number of a given torsion, respectively. $Q_{\mathrm{rv}}^{\mathrm{MC-H}}$ is the multiconformer harmonic rovibrational partition function:

$$Q_{\mathrm{rv}}^{\mathrm{MC-H}} = \sum_{j}^{J} Q_i^{\mathrm{RRHO}} = \sum_{j}^{J} Q_{\mathrm{rot},j} Q_j^{\mathrm{HO}} e^{-\beta U_j} \tag{A.126}$$

where U_j is the energy difference between the conformer j and the global minimum. $Q_{\mathrm{rot},j}$ is the rotational partition function for conformer j and Q_j^{HO} is the harmonic oscillator partition function for conformer j, both these function were already defined in Chapter 3.

Then, the derivatives of the multiconformational partition function are obtained as it follows:

$$-\frac{\partial ln Q_{\mathrm{rv}}^{\mathrm{GS2D-NS}}}{\partial\beta} = -\frac{\partial ln(\alpha_{\mathrm{tor}}^{\mathrm{2D-NS}} Q_{\mathrm{rv}}^{\mathrm{MC-H}})}{\partial\beta} = -\frac{\partial ln\left(\frac{Q_{\mathrm{tor}}^{\mathrm{2D-NS}}}{Q_{\mathrm{tor}}^{\mathrm{MC-HO(C)}}} Q_{\mathrm{rv}}^{\mathrm{MC-H}}\right)}{\partial\beta}$$
$$= -\underbrace{\left(\frac{\partial ln Q_{\mathrm{tor}}^{\mathrm{2D-NS}}}{\partial\beta}\right)}_{\mathrm{T_1}} + \underbrace{\left(\frac{\partial ln Q_{\mathrm{tor}}^{\mathrm{MC-HO(C)}}}{\partial\beta}\right)}_{\mathrm{T_2}} - \underbrace{\left(\frac{\partial ln Q_{\mathrm{rv}}^{\mathrm{MC-H}}}{\partial\beta}\right)}_{\mathrm{T_3}} \tag{A.127}$$

Term $\mathrm{T_1}$, can be obtained as:

$$(\mathrm{T_1}) = \frac{1}{Q_{\mathrm{tor}}^{\mathrm{2D-NS}}}\frac{\partial Q_{\mathrm{tor}}^{\mathrm{2D-NS}}}{\partial\beta} = \frac{1}{Q_{\mathrm{tor}}^{\mathrm{2D-NS}}}\frac{\partial}{\partial\beta}\left(\sum_i e^{-E_i\beta}\right)$$
$$= -\frac{1}{Q_{\mathrm{tor}}^{\mathrm{2D-NS}}}\sum_i (E_i)e^{-E_i\beta} \tag{A.128}$$

In the case of Term $\mathrm{T_2}$, $Q_{\mathrm{tor}}^{\mathrm{MC-HO(C)}}$ can be rewritten as:

$$Q_{\mathrm{tor}}^{\mathrm{MC-HO(C)}} = \sum_{j=1}^{J} e^{-\beta U_j}\prod_{\eta}^{t} q_{j,\eta}^{\mathrm{HO}} \tag{A.129}$$

The partition function is of the type $Q^* = \sum_j^J f_1(\beta)\prod_{\eta=1}^t f_2(\beta)$. From now on, for the sake of a easier comprehension we will refer to the term $\prod_{\eta=1}^t f_2(\beta)$ as $F_2(\beta)$. This kind of derivatives can be solved in the following manner:

$$-\frac{\partial ln Q^*}{\partial\beta} = -\frac{1}{Q^*}\frac{\partial Q^*}{\partial\beta} = -\frac{1}{Q^*}\frac{\partial\sum_{j=1}^J f_1(\beta)F_2(\beta)}{\partial\beta} = -\frac{1}{Q^*}\sum_{j=1}^{J}\frac{\partial}{\partial\beta}\left[f_1(\beta)F_2(\beta)\right]$$
$$= -\frac{1}{Q^*}\left[f_1'(\beta)F_2(\beta) + f_1(\beta)F_2'(\beta)\right] \tag{A.130}$$

The derivative $f_1'(\beta)$ is:

$$f_1(\beta) = e^{-\beta U_i} \rightarrow f_1'(\beta) = (-U_j)f_1(\beta) \tag{A.131}$$

For the evaluation of $F_2'(\beta)$ there are some considerations to be made first:

$$F_2(\beta) = \prod_{\eta=1}^{t} f_2(\beta) \rightarrow F_2'(\beta) = \frac{\partial}{\partial\beta}\prod_{\eta=1}^{t} f_2(\beta) = F_2(\beta)\frac{\partial ln}{\partial\beta}\left(\prod_{\eta=1}^{t} f_2(\beta)\right)$$
$$= F_2(\beta)\frac{\partial}{\partial\beta}\sum_{\eta=1}^{t} ln\, f_2(\beta) = F_2(\beta)\sum_{\eta=1}^{t}\frac{\partial ln}{\partial\beta}\left[f_2(\beta)\right] = F_2(\beta)\sum_{\eta=1}^{t}\frac{1}{f_2(\beta)}\frac{\partial f_2(\beta)}{\partial\beta}$$

If $f_2(\beta) = q_{j,\eta}^{\mathrm{HO}}$, then;

$$\frac{\partial f_2(\beta)}{\partial \beta} = \frac{\partial}{\partial \beta}\left[\frac{e^{-c_1\beta}}{1-e^{-c_2\beta}}\right] = \frac{(-c_1)e^{-c_1\beta}(1-e^{-c_2\beta}) - e^{-c_1\beta}c_2e^{-c_2\beta}}{(1-e^{-c_2\beta})^2}$$

where $c_1 = \hbar\bar{\omega}_{j,\eta}/2$ and $c_2 = \hbar\bar{\omega}_{j,\eta}$, so $c_2 = 2c_1$;

$$\frac{\partial f_2(\beta)}{\partial \beta} = \frac{-c_1e^{-c_1\beta} + c_1e^{-c_1\beta}e^{-c_2\beta} - 2c_1e^{-c_1\beta}e^{-c_2\beta}}{(1-e^{-c_2\beta})^2} = \frac{-c_1e^{-c_1\beta}(1+e^{-c_2\beta})}{(1-e^{-c_2\beta})^2}$$

So we can now evaluate $\frac{1}{f_2(\beta)}\frac{\partial f_2(\beta)}{\partial \beta}$;

$$\frac{1}{f_2(\beta)}\frac{\partial f_2(\beta)}{\partial \beta} = \frac{1-e^{c_2\beta}}{e^{-c_1\beta}}(-c_1)\frac{e^{-c_1\beta}(1+e^{-c_2\beta})}{(1-e^{-c_2\beta})^2} = -c_1\frac{1+e^{c_2\beta}}{1-e^{-c_2\beta}} \tag{A.132}$$

Now, we can finally express $F_2'(\beta)$ as:

$$F_2'(\beta) = -\sum_{\eta=1}^{t}\frac{\hbar\bar{\omega}_{j,\eta}}{2}\left(\frac{1+e^{-\hbar\beta\bar{\omega}_{j,\eta}}}{1-e^{-\hbar\beta\bar{\omega}_{j,\eta}}}\right) \tag{A.133}$$

Once we know the form of both derivatives $f_1'(\beta)$ and $F_2'(\beta)$, the term T_2 can be written as:

$$-\frac{\partial ln Q_{\mathrm{tor}}^{\mathrm{MC-HO(C)}}}{\partial \beta} = \frac{1}{Q_{\mathrm{tor}}^{\mathrm{MC-HO(C)}}}\left[\sum_{j=1}^{J}U_je^{-\beta U_j}\prod_{\eta=1}^{t}q_{j,\eta}^{HO} + e^{-\beta U_j}\sum_{\eta=1}^{t}\frac{\hbar\bar{\omega}_{j,\eta}}{2}\left(\frac{1+e^{-\hbar\beta\bar{\omega}_{j,\eta}}}{1-e^{-\hbar\beta\bar{\omega}_{j,\eta}}}\right)\right] \tag{A.134}$$

The same strategy applies to obtain Term T_3.

$$-\frac{\partial ln Q_{\mathrm{rv}}^{\mathrm{MC-H}}}{\partial \beta} = -\frac{\partial ln}{\partial \beta}\sum_{j}^{J}Q_j^{\mathrm{RRHO}} = -\frac{1}{Q_{\mathrm{rv}}^{\mathrm{MC-H}}}\sum_{j}^{J}\frac{\partial}{\partial \beta}Q_j^{\mathrm{RRHO}} \tag{A.135}$$

We shall now focus on the derivative of Q_j^{RRHO}. Therefore:

$$\frac{\partial}{\partial \beta}Q_j^{\mathrm{RRHO}} = \frac{\partial}{\partial \beta}\left(Q_{\mathrm{rot},j}Q_j^{\mathrm{HO}}e^{-\beta U_j}\right) = \frac{\partial}{\partial \beta}\left(Q_{\mathrm{rot},j}Q_j^{\mathrm{HO}}\right)e^{-\beta U_j} - U_j\left(Q_{\mathrm{rot},j}Q_j^{\mathrm{HO}}\right)e^{-\beta U_j}$$

where

$$\frac{\partial}{\partial \beta}\left(Q_{\mathrm{rot},j}Q_j^{\mathrm{HO}}\right) = \frac{Q_{\mathrm{rot},j}}{\partial \beta}Q_j^{\mathrm{HO}} + Q_{\mathrm{rot},j}\frac{\partial Q_j^{\mathrm{HO}}}{\partial \beta} = \left(\frac{\partial ln Q_{\mathrm{rot},j}}{\partial \beta} + \frac{\partial ln Q_j^{\mathrm{HO}}}{\partial \beta}\right)Q_{\mathrm{rot},j}Q_j^{\mathrm{HO}}$$

where Q_{rot} can be written as seen in Chapter 3 as:

$$Q_{\text{rot}} = \frac{8\pi^2}{\sigma_{\text{rot}}} \left(\frac{1}{2\pi\hbar^2\beta} \right)^{3/2} \sqrt{I_1^{\text{rot}} I_2^{\text{rot}} I_3^{\text{rot}}} \tag{A.136}$$

where I_1^{tor}, I_2^{tor} and I_3^{tor} are the principal moments of inertia and σ_{rot} is the symmetry number for external rotation. Then $Q_{\text{rot},j}$ can be written as $Q_{\text{rot},j} = c_{\text{rot}}\beta^{-3/2}$ where:

$$c_{\text{rot}} = \frac{8\pi^2}{\sigma_{\text{rot}}} \left(\frac{1}{2\pi\hbar^2} \right)^{3/2} \sqrt{I_1^{\text{rot}} I_2^{\text{rot}} I_3^{\text{rot}}}$$

Therefore:

$$\frac{\partial ln Q_{\text{rot},j}}{\partial\beta} = \frac{1}{Q_{\text{rot},j}} \frac{\partial}{\partial\beta} \left(c_{\text{rot}}\beta^{-3/2} \right) = \frac{1}{Q_{\text{rot},j}} (-c_{\text{rot}}) \frac{3}{2} \beta^{-5/2} = \frac{-c_{\text{rot}}(3/2)\beta^{-5/2}}{c_{\text{rot}}\beta^{-3/2}} = -\frac{3}{2}\frac{1}{\beta}$$

and

$$\frac{\partial ln Q_j^{\text{HO}}}{\partial\beta} = -\sum_{\tau=1}^{F} \frac{\hbar\omega_\tau}{2} \left(\frac{1 + e^{-\hbar\omega_\tau\beta}}{1 - e^{-\hbar\omega_\tau\beta}} \right)$$

Now it is possible to rearrange terms to obtain a new expression for Term T_3:

$$-\frac{ln Q_{\text{rv}}^{\text{MC-H}}}{\partial\beta} = \frac{1}{Q_{\text{rv}}^{\text{MC-H}}} \sum_{j=1}^{J} \left\{ \left[\frac{3}{2\beta} + \sum_{\tau=1}^{F} \frac{\hbar\omega_\tau}{2} \left(\frac{1 + e^{-\hbar\omega_\tau\beta}}{1 - e^{-\hbar\omega_\tau\beta}} \right) + U_j \right] Q_{\text{rot},j} Q_j^{\text{HO}} e^{-\beta U_j} \right\} \tag{A.137}$$

For the case of the $Q_{\text{rv}}^{\text{E2D-NS}}$ we have that:

$$Q_{\text{rv}}^{\text{E2D-NS}} = \frac{Q_{\text{tor}}^{\text{2D-NS}}}{Q_{\text{tor,cl}}^{(\text{C})}} Q_{\text{rv}}^{\text{EHR}} \tag{A.138}$$

where $Q_{\text{tor,cl}}$ is the classical torsional partition function:

$$Q_{\text{cl,tor}}^{(\text{C})} = \frac{1}{\sigma_{\text{tor}}} \frac{1}{2\pi\beta\hbar^2} \int_0^{2\pi} \int_0^{2\pi} d\phi_1 d\phi_2 |\mathbf{D}(\phi_1, \phi_2)|^{1/2} \mathrm{e}^{-\beta \mathrm{V}(\phi_1, \phi_2)} \tag{A.139}$$

and $Q_{\text{rv}}^{\text{EHR}}$ is the extended hindered rotor partition function presented in Chapter 3:

$$Q_{\text{rv}}^{\text{EHR}} = \frac{8\pi^2}{\sigma_{\text{tor}}\sigma_{\text{rot}}} \left(\frac{1}{2\pi\beta\hbar^2} \right)^{5/2} \int_0^{2\pi} \int_0^{2\pi} d\phi_1 d\phi_2 |\mathbf{S}(\phi_1, \phi_2)|^{1/2} \mathrm{e}^{-\beta \mathrm{V}(\phi_1, \phi_2)} \overline{\overline{Q}}^{\text{HO}}(\phi_1, \phi_2) \tag{A.140}$$

where $\overline{\overline{Q}}^{\text{HO}}$ is the product of the 3N-8 individual vibrational harmonic nontorsional vibrations:

$$\overline{\overline{Q}}^{\text{HO}}(\phi_1, \phi_2, \cdots, \phi_{\text{t}}) = \prod_{\overline{\overline{m}}=1}^{3N-6-t} \frac{e^{-\beta\hbar\overline{\overline{\omega}}_{\overline{\overline{m}}}/2}}{1 - e^{-\beta\hbar\overline{\overline{\omega}}_{\overline{\overline{m}}}}} \tag{A.141}$$

In this situation, the derivatives are:

$$-\frac{\partial ln Q_{\mathrm{rv}}^{\mathrm{E2D-NS}}}{\partial\beta} = -\underbrace{\left(\frac{\partial ln Q_{\mathrm{tor}}^{\mathrm{2D-NS}}}{\partial\beta}\right)}_{\mathrm{T}_4} + \underbrace{\left(\frac{\partial ln Q_{\mathrm{tor,cl}}^{(\mathrm{C})}}{\partial\beta}\right)}_{\mathrm{T}_5} - \underbrace{\left(\frac{\partial ln Q_{\mathrm{rv}}^{\mathrm{EHR}}}{\partial\beta}\right)}_{\mathrm{T}_6} \tag{A.142}$$

Term T_4 is the same as term T_1 and has already been solved. Term T_5 is:

$$\frac{\partial ln Q_{\mathrm{tor,cl}}^{(\mathrm{C})}}{\partial\beta} = \frac{1}{Q_{\mathrm{tor,cl}}^{(\mathrm{C})}}\frac{\partial Q_{\mathrm{tor,cl}}^{(\mathrm{C})}}{\partial\beta} = \frac{1}{Q_{\mathrm{tor,cl}}^{(\mathrm{C})}}\frac{\partial}{\partial\beta}\frac{C}{\beta}\int_0^{2\pi}\int_0^{2\pi} d\phi_1 d\phi_2 |\mathbf{D}(\phi_1,\phi_2)|^{1/2}\mathrm{e}^{-\beta \mathrm{V}(\phi_1,\phi_2)} \tag{A.143}$$

with C being

$$C = \frac{1}{\sigma_{\mathrm{tor}}}\frac{1}{2\pi\hbar^2} \tag{A.144}$$

Therefore, the derivative becomes:

$$\begin{aligned}\frac{\partial Q_{\mathrm{tor,cl}}^{(\mathrm{C})}}{\partial\beta} =& C\left(-\frac{1}{\beta^2}\int\int |\mathbf{D}(\phi_1,\phi_2)|^{1/2}\mathrm{e}^{-\beta \mathrm{V}(\phi_1,\phi_2)}\mathrm{d}\phi_1\mathrm{d}\phi_2\right.\\ &\left.-\frac{1}{\beta}\int\int \frac{V(\phi_1,\phi_2)}{\beta}e^{-\beta V(\phi_1,\phi_2)}|\mathbf{D}(\phi_1,\phi_2)|^{1/2}\mathrm{d}\phi_1\mathrm{d}\phi_2\right)\\ =& -\frac{C}{\beta}\left(\int\int |\mathbf{D}(\phi_1,\phi_2)|^{1/2}\mathrm{e}^{-\beta \mathrm{V}(\phi_1,\phi_2)}\left(\frac{1}{\beta}+\mathrm{V}(\phi_1,\phi_2)\right)\mathrm{d}\phi_1\mathrm{d}\phi_2\right)\end{aligned} \tag{A.145}$$

Term T_5 can be written as:

$$\frac{\partial ln Q_{\mathrm{tor,cl}}^{(\mathrm{C})}}{\partial\beta} = -\frac{1}{Q_{\mathrm{tor,cl}}^{(\mathrm{C})}}\frac{C}{\beta}\left(\int\int |\mathbf{D}(\phi_1,\phi_2)|^{1/2}\mathrm{e}^{-\beta \mathrm{V}(\phi_1,\phi_2)}\left(\frac{1}{\beta}+\mathrm{V}(\phi_1,\phi_2)\right)\mathrm{d}\phi_1\mathrm{d}\phi_2\right) \tag{A.146}$$

Term T_6 is:

$$\frac{\partial ln Q_{\mathrm{rv}}^{\mathrm{EHR}}}{\partial\beta} = \frac{1}{Q_{\mathrm{rv}}^{\mathrm{EHR}}}\frac{\partial Q_{\mathrm{rv}}^{\mathrm{EHR}}}{\partial\beta} \tag{A.147}$$

where

$$\begin{aligned}\frac{\partial Q_{\mathrm{rv}}^{\mathrm{EHR}}}{\partial\beta} =& \frac{\partial}{\partial\beta}\frac{C'}{\beta^{5/2}}\int_0^{2\pi}\int_0^{2\pi} d\phi_1 d\phi_2 |\mathbf{S}(\phi_1,\phi_2)|^{1/2}\mathrm{e}^{-\beta \mathrm{V}(\phi_1,\phi_2)}\overline{\overline{\mathrm{Q}}}^{\mathrm{HO}}(\phi_1,\phi_2)\\ =& -\frac{5C'}{2\beta^{7/2}}\int_0^{2\pi}\int_0^{2\pi} d\phi_1 d\phi_2 |\mathbf{S}(\phi_1,\phi_2)|^{1/2}\mathrm{e}^{-\beta \mathrm{V}(\phi_1,\phi_2)}\overline{\overline{\mathrm{Q}}}^{\mathrm{HO}}(\phi_1,\phi_2)\\ &-\frac{C'}{\beta^{5/2}}\int_0^{2\pi}\int_0^{2\pi} V(\phi_1,\phi_2) d\phi_1 d\phi_2 |\mathbf{S}(\phi_1,\phi_2)|^{1/2}\mathrm{e}^{-\beta \mathrm{V}(\phi_1,\phi_2)}\overline{\overline{\mathrm{Q}}}^{\mathrm{HO}}(\phi_1,\phi_2)\\ &+\frac{C'}{\beta^{5/2}}\int_0^{2\pi}\int_0^{2\pi} d\phi_1 d\phi_2 |\mathbf{S}(\phi_1,\phi_2)|^{1/2}\mathrm{e}^{-\beta \mathrm{V}(\phi_1,\phi_2)}\frac{\partial\overline{\overline{\mathrm{Q}}}^{\mathrm{HO}}(\phi_1,\phi_2)}{\partial\beta}\end{aligned} \tag{A.148}$$

with C' being

$$C' = \frac{8\pi^2}{\sigma_{\rm tor}\sigma_{\rm rot}} \left(\frac{1}{2\pi\hbar^2}\right)^{5/2} \tag{A.149}$$

$\frac{\partial \overline{\overline{Q}}^{\rm HO}}{\partial \beta}$ is solved in the usual manner:

$$\frac{\partial ln \overline{\overline{Q}}^{\rm HO}}{\partial \beta} = -\sum_{\overline{\overline{m}}=1}^{3N-6-t} \frac{\hbar\overline{\overline{\omega}}_{\overline{\overline{m}}}}{2} \left(\frac{1+e^{-\hbar\beta\hbar\overline{\overline{\omega}}_{\overline{\overline{m}}}}}{1-e^{-\hbar\beta\hbar\overline{\overline{\omega}}_{\overline{\overline{m}}}}}\right) \tag{A.150}$$

If we consider that:

$$\epsilon(\phi_1,\phi_2) = d\phi_1 d\phi_2 |\mathbf{S}(\phi_1,\phi_2)|^{1/2} {\rm e}^{-\beta {\rm V}(\phi_1,\phi_2)} \overline{\overline{\rm Q}}^{\rm HO}(\phi_1,\phi_2) \tag{A.151}$$

then, Term $\rm T_6$ is given by:

$$\frac{\partial ln Q_{\rm rv}^{\rm EHR}}{\partial \beta} = -\frac{1}{Q_{\rm rv}^{\rm EHR}} \frac{C}{\beta^{5/2}} \int_0^{2\pi}\int_0^{2\pi} \left[\frac{5}{2\beta} + V(\phi_1,\phi_2) + \sum_{\overline{\overline{m}}=1}^{3N-6-t} \frac{\hbar\overline{\overline{\omega}}_{\overline{\overline{m}}}}{2} \left(\frac{1+e^{-\hbar\beta\hbar\overline{\overline{\omega}}_{\overline{\overline{m}}}}}{1-e^{-\hbar\beta\hbar\overline{\overline{\omega}}_{\overline{\overline{m}}}}}\right)\right] \epsilon(\phi_1,\phi_2) \tag{A.152}$$

USC
UNIVERSIDADE
DE SANTIAGO
DE COMPOSTELA

Appendix B

Supporting Information for Chapter 1

This section includes several tables of interest of the chapter entitled "Quantum treatment for internal rotations".

Table B.1: Parameters (in 100/amu·Å^2) used to fit by Fourier series the $d_{\tau\varsigma}$ elements of the inverse of the **D** matrix for system **S1**.

Parameters	$\tau = 1, \varsigma = 1$	$\tau = 1, \varsigma = 2$	$\tau = 2, \varsigma = 2$
$a_0^{\tau\varsigma}$	133.3640	-0.7680	34.2162
$a_1^{\tau\varsigma}$	-0.1766	3.937	-0.1181
$a_2^{\tau\varsigma}$	2.1210	-0.0504	0.0790
$a_3^{\tau\varsigma}$	-0.6731	-0.0052	0.0037
$a_4^{\tau\varsigma}$	0.0516	-0.0238	0.0010
$a_5^{\tau\varsigma}$	-0.01736	0.0053	-0.0009
$a_6^{\tau\varsigma}$	0.02900	-0.0002	0.0000
$a_7^{\tau\varsigma}$	-0.0047	0.0005	-0.0000
$a_8^{\tau\varsigma}$	0.0043	0.0004	-0.0000
$a_9^{\tau\varsigma}$	-0.0012	-0.0001	-0.0000
$b_1^{\tau\varsigma}$	...	...	...
$b_2^{\tau\varsigma}$	...	...	...
$b_3^{\tau\varsigma}$	0.0029	0.0094	-0.0872
$b_4^{\tau\varsigma}$	...	...	...
$b_5^{\tau\varsigma}$	...	...	...
$b_6^{\tau\varsigma}$	0.0025	-0.0011	0.0086
$b_7^{\tau\varsigma}$	...	...	...
$b_8^{\tau\varsigma}$	...	...	...
$b_9^{\tau\varsigma}$	-0.0029	0.0006	-0.0021

Table B.2: Parameters (in 100/amu·Å^2) used to fit by Fourier series the cross-term parameters of the $d_{\tau\varsigma}$ elements of the inverse of the **D** matrix for system **S1**.

Parameters	$\tau = 1, \varsigma = 1$	$\tau = 1, \varsigma = 2$	$\tau = 2, \varsigma = 2$
$c_{11}^{\tau\varsigma}$, $d_{11}^{\tau\varsigma}$	...	...	...
$c_{12}^{\tau\varsigma}$, $d_{12}^{\tau\varsigma}$	...	...	...
$c_{13}^{\tau\varsigma}$, $d_{13}^{\tau\varsigma}$	0.1825, 0.1091	-0.0079, -0.1981	0.0223, -0.0070
$c_{14}^{\tau\varsigma}$, $d_{14}^{\tau\varsigma}$	...	...	...
$c_{15}^{\tau\varsigma}$, $d_{15}^{\tau\varsigma}$	...	...	...
$c_{16}^{\tau\varsigma}$, $d_{16}^{\tau\varsigma}$	-0.0241, -0.0038	0.0055, 0.0220	-0.0030, -0.0007
$c_{21}^{\tau\varsigma}$, $d_{21}^{\tau\varsigma}$	...	...	...
$c_{22}^{\tau\varsigma}$, $d_{22}^{\tau\varsigma}$	...	...	...
$c_{23}^{\tau\varsigma}$, $d_{23}^{\tau\varsigma}$	-0.0324, -0.1464	-0.0062, 0.0176	-0.0079, 0.0042
$c_{24}^{\tau\varsigma}$, $d_{24}^{\tau\varsigma}$	...	...	...
$c_{25}^{\tau\varsigma}$, $d_{25}^{\tau\varsigma}$	...	...	...
$c_{26}^{\tau\varsigma}$, $d_{26}^{\tau\varsigma}$	0.0140, 0.0085	-0.0032, -0.0011	0.0020, -0.0020
$c_{31}^{\tau\varsigma}$, $d_{31}^{\tau\varsigma}$	...	...	...
$c_{32}^{\tau\varsigma}$, $d_{32}^{\tau\varsigma}$	...	...	...
$c_{33}^{\tau\varsigma}$, $d_{33}^{\tau\varsigma}$	0.0301, 0.0368	0.0026, -0.0097	0.0063, -0.0056
$c_{34}^{\tau\varsigma}$, $d_{34}^{\tau\varsigma}$	...	...	...
$c_{35}^{\tau\varsigma}$, $d_{35}^{\tau\varsigma}$	...	...	...
$c_{36}^{\tau\varsigma}$, $d_{36}^{\tau\varsigma}$	-0.0149, -0.0024	-0.0006, 0.0028	-0.0009, 0.0005
$c_{41}^{\tau\varsigma}$, $d_{41}^{\tau\varsigma}$	...	...	...
$c_{42}^{\tau\varsigma}$, $d_{42}^{\tau\varsigma}$	...	...	...
$c_{43}^{\tau\varsigma}$, $d_{43}^{\tau\varsigma}$	0.0268, -0.0508	0.0012, 0.0047	-0.0002, 0.0004
$c_{44}^{\tau\varsigma}$, $d_{44}^{\tau\varsigma}$	...	...	...
$c_{45}^{\tau\varsigma}$, $d_{45}^{\tau\varsigma}$	...	...	...
$c_{46}^{\tau\varsigma}$, $d_{46}^{\tau\varsigma}$	0.0118, 0.0049	-0.0018, -0.0009	0.0003, -0.0008
$c_{51}^{\tau\varsigma}$, $d_{51}^{\tau\varsigma}$	...	...	...
$c_{52}^{\tau\varsigma}$, $d_{52}^{\tau\varsigma}$	...	...	...
$c_{53}^{\tau\varsigma}$, $d_{53}^{\tau\varsigma}$	...	...	...
$c_{54}^{\tau\varsigma}$, $d_{54}^{\tau\varsigma}$	...	...	...
$c_{55}^{\tau\varsigma}$, $d_{55}^{\tau\varsigma}$	...	...	...
$c_{56}^{\tau\varsigma}$, $d_{56}^{\tau\varsigma}$	...	...	...
$c_{61}^{\tau\varsigma}$, $d_{61}^{\tau\varsigma}$	...	...	...
$c_{62}^{\tau\varsigma}$, $d_{62}^{\tau\varsigma}$	...	...	...
$c_{63}^{\tau\varsigma}$, $d_{63}^{\tau\varsigma}$	...	...	...
$c_{64}^{\tau\varsigma}$, $d_{64}^{\tau\varsigma}$	...	...	...
$c_{65}^{\tau\varsigma}$, $d_{65}^{\tau\varsigma}$	...	...	...
$c_{66}^{\tau\varsigma}$, $d_{66}^{\tau\varsigma}$	...	...	...

Table B.3: Parameters (in 100/amu·Å^2) used to fit by Fourier series the one-dimensional parameters of the $d_{\tau\varsigma}$ elements of the inverse of the **D** matrix for system **S2**.

Parameters	$\tau = 1, \varsigma = 1$	$\tau = 1, \varsigma = 2$	$\tau = 2, \varsigma = 2$
$a_0^{\tau\varsigma}$	132.7440	-0.7726	8.1629
$a_1^{\tau\varsigma}$	-0.5927	3.8996	0.0206
$a_2^{\tau\varsigma}$	2.3319	-0.0682	0.0657
$a_3^{\tau\varsigma}$	-0.6475	-0.0147	-0.0021
$a_4^{\tau\varsigma}$	0.0306	-0.0190	0.0008
$a_5^{\tau\varsigma}$	-0.0301	0.0049	-0.0001
$a_6^{\tau\varsigma}$	0.0214	-0.0012	-0.0002
$a_7^{\tau\varsigma}$	-0.0021	0.0009	0.0002
$a_8^{\tau\varsigma}$	0.0041	-0.0001	0.0000
$a_9^{\tau\varsigma}$	-0.0021	0.0001	0.0000
$b_1^{\tau\varsigma}$	0.9004	1.8142	0.3410
$b_2^{\tau\varsigma}$	0.0543	0.1482	0.7379
$b_3^{\tau\varsigma}$	0.0049	0.1345	0.0023
$b_4^{\tau\varsigma}$	0.0274	-0.0457	0.0617
$b_5^{\tau\varsigma}$	-0.0035	0.0041	-0.0271
$b_6^{\tau\varsigma}$	-0.0132	-0.0118	0.0091
$b_7^{\tau\varsigma}$	...	...	...
$b_8^{\tau\varsigma}$	...	...	...
$b_9^{\tau\varsigma}$	...	...	...

Table B.4: Parameters (in 100/amu·Å^2) used to fit by Fourier series the cross-term parameters of the $d_{\tau\varsigma}$ elements of the inverse of the **D** matrix for system **S2**.

Parameters	$\tau = 1, \varsigma = 1$	$\tau = 1, \varsigma = 2$	$\tau = 2, \varsigma = 2$
$c_{11}^{\tau\varsigma}$, $d_{11}^{\tau\varsigma}$	-0.8502, 1.3157	0.8623, -2.1001	-0.0198, 0.0832
$c_{12}^{\tau\varsigma}$, $d_{12}^{\tau\varsigma}$	0.5643, -1.2409	-0.0735, 0.1623	0.0703, -0.1004
$c_{13}^{\tau\varsigma}$, $d_{13}^{\tau\varsigma}$	0.2090, 0.3687	0.1116, -0.4693	-0.0075, 0.0140
$c_{14}^{\tau\varsigma}$, $d_{14}^{\tau\varsigma}$	-0.0667, -0.0506	0.0569, 0.1052	-0.0079, -0.0097
$c_{15}^{\tau\varsigma}$, $d_{15}^{\tau\varsigma}$	...	...	...
$c_{16}^{\tau\varsigma}$, $d_{16}^{\tau\varsigma}$	...	...	...
$c_{21}^{\tau\varsigma}$, $d_{21}^{\tau\varsigma}$	0.4814, -0.5299	0.0180, -0.0017	0.0852, -0.1146
$c_{22}^{\tau\varsigma}$, $d_{22}^{\tau\varsigma}$	-0.1383, 0.1440	-0.0331, 0.0411	-0.0231, 0.0334
$c_{23}^{\tau\varsigma}$, $d_{23}^{\tau\varsigma}$	0.3187, -0.6594	0.0183, 0.0099	0.0109, -0.0201
$c_{24}^{\tau\varsigma}$, $d_{24}^{\tau\varsigma}$	0.0348, -0.0065	-0.0087, -0.0077	0.0020, -0.0036
$c_{25}^{\tau\varsigma}$, $d_{25}^{\tau\varsigma}$	...	...	...
$c_{26}^{\tau\varsigma}$, $d_{26}^{\tau\varsigma}$	...	...	...
$c_{31}^{\tau\varsigma}$, $d_{31}^{\tau\varsigma}$	-0.1711, 0.1545	0.0613, -0.0381	-0.0028, 0.0089
$c_{32}^{\tau\varsigma}$, $d_{32}^{\tau\varsigma}$	0.2228, -0.2415	-0.0032, -0.0269	0.0013, -0.0148
$c_{33}^{\tau\varsigma}$, $d_{33}^{\tau\varsigma}$	-0.1907, 0.2703	-0.0041, 0.0044	-0.0045, 0.0061
$c_{34}^{\tau\varsigma}$, $d_{34}^{\tau\varsigma}$	0.0394, -0.0169	0.0060, -0.0057	-0.0042, 0.0019
$c_{35}^{\tau\varsigma}$, $d_{35}^{\tau\varsigma}$	...	...	...
$c_{36}^{\tau\varsigma}$, $d_{36}^{\tau\varsigma}$	...	...	...
$c_{41}^{\tau\varsigma}$, $d_{41}^{\tau\varsigma}$	0.0315, -0.0162	-0.0077, 0.0306	-0.0016, 0.0021
$c_{42}^{\tau\varsigma}$, $d_{42}^{\tau\varsigma}$	-0.0265, 0.0165	0.0053, -0.0043	-0.0010, 0.0018
$c_{43}^{\tau\varsigma}$, $d_{43}^{\tau\varsigma}$	0.1294, -0.1548	0.0045, 0.0082	0.0002, -0.0004
$c_{44}^{\tau\varsigma}$, $d_{44}^{\tau\varsigma}$	-0.0262, 0.0221	-0.0072, 0.0024	-0.0003, 0.0016
$c_{45}^{\tau\varsigma}$, $d_{45}^{\tau\varsigma}$	...	...	...
$c_{46}^{\tau\varsigma}$, $d_{46}^{\tau\varsigma}$	...	...	...
$c_{51}^{\tau\varsigma}$, $d_{51}^{\tau\varsigma}$	-0.0198, 0.0087	-0.0001, -0.0068	0.0001, -0.0005
$c_{52}^{\tau\varsigma}$, $d_{52}^{\tau\varsigma}$	0.0047, 0.0065	-0.0032, 0.0025	-0.0004, 0.0003
$c_{53}^{\tau\varsigma}$, $d_{53}^{\tau\varsigma}$	-0.0501, 0.0732	0.0025, -0.0055	0.0004, -0.0006
$c_{54}^{\tau\varsigma}$, $d_{54}^{\tau\varsigma}$	0.0073, -0.0050	0.0023, -0.0010	0.0002, -0.0001
$c_{55}^{\tau\varsigma}$, $d_{55}^{\tau\varsigma}$	...	...	...
$c_{56}^{\tau\varsigma}$, $d_{56}^{\tau\varsigma}$	...	...	...
$c_{61}^{\tau\varsigma}$, $d_{61}^{\tau\varsigma}$	0.0133, -0.0054	0.0001, 0.0014	0.0006, 0.0000
$c_{62}^{\tau\varsigma}$, $d_{62}^{\tau\varsigma}$	0.0020, -0.0045	0.0013, 0.0003	0.0002, 0.0001
$c_{63}^{\tau\varsigma}$, $d_{63}^{\tau\varsigma}$	0.0158, -0.0249	-0.0017, 0.0028	-0.0003, 0.0005
$c_{64}^{\tau\varsigma}$, $d_{64}^{\tau\varsigma}$	0.0007, -0.0018	-0.0005, 0.0002	0.0001, 0.0000
$c_{65}^{\tau\varsigma}$, $d_{65}^{\tau\varsigma}$	...	...	...
$c_{66}^{\tau\varsigma}$, $d_{66}^{\tau\varsigma}$	...	...	...

Table B.5: Parameters (in cm^{-1}) for the one-dimensional potentials of the two systems.

Parameter	S1	S2
a_0	1131.7	683.6
a_1	-263.1	120.3
a_2	-773.2	-731.4
a_3	-118.4	-149.8
a_4	31.2	108.7
a_5	-4.9	-28.5
a_6	2.3	10.2
a_7	-1.3	-22.5
a_8	0.5	16.8
a_9	-0.3	-4.1
b_0	344.4	486.2
b_1	2.2	127.4
b_2	3.6	-279.1
b_3	-359.9	-332.9
b_4	-2.6	16.0
b_5	-1.3	-71.2
b_6	18.1	71.3
b_7	-0.0	-11.6
b_8	-0.0	-6.5
b_9	-1.4	7.2

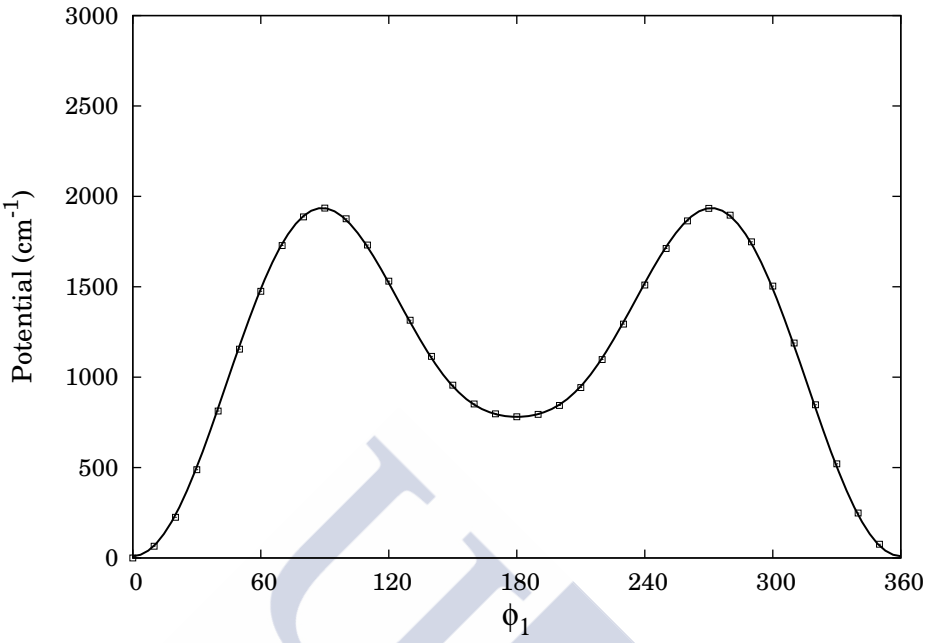

Figure B.1: One dimensional potential for rotation about ϕ_1 in **S1**.

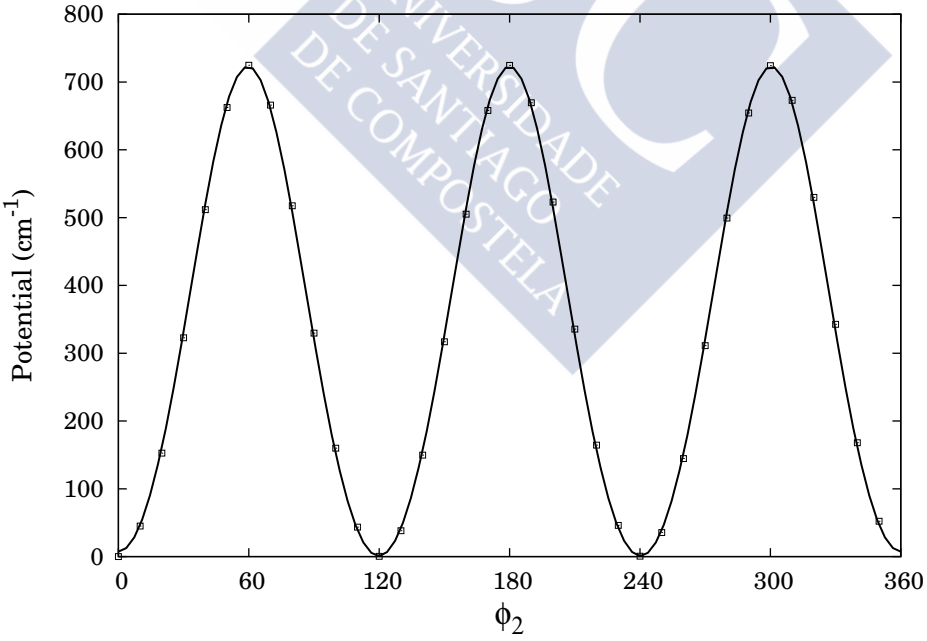

Figure B.2: One dimensional potential for rotation about ϕ_2 in **S1**.

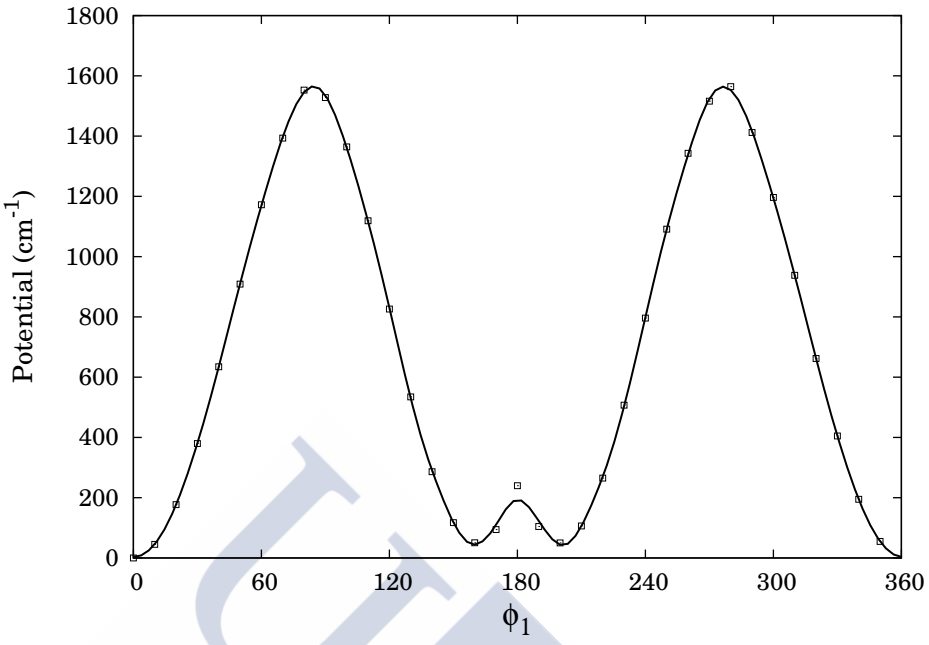

Figure B.3: One dimensional potential for rotation about ϕ_1 in **S2**.

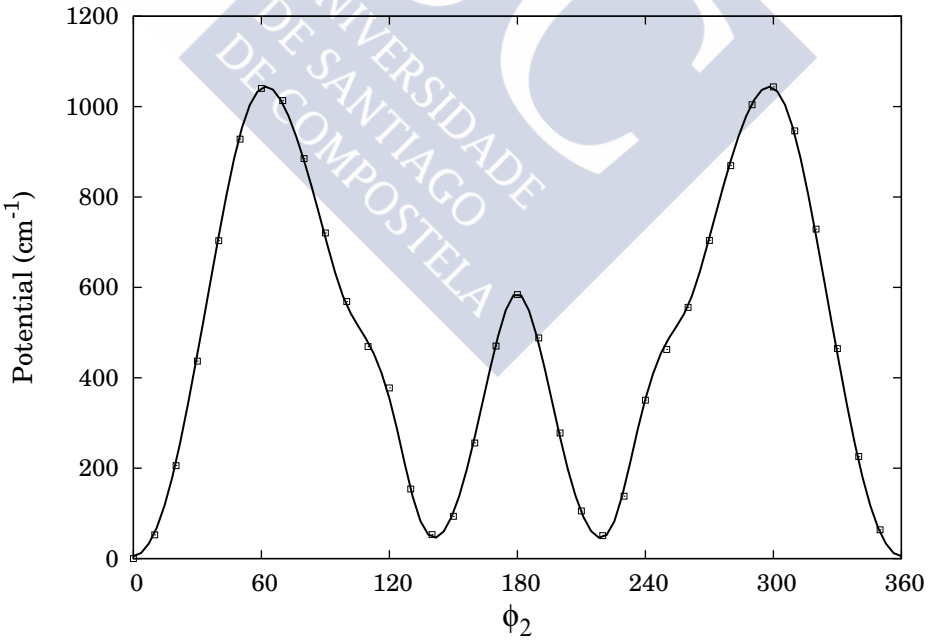

Figure B.4: One dimensional potential for rotation about ϕ_2 in **S2**.

USC
UNIVERSIDADE
DE SANTIAGO
DE COMPOSTELA

Appendix C

Supporting Information for Chapter 2

This section includes several tables of interest of the chapter entitled "Hindered Rotor Tunneling Splittings".

Table C.1: Parameters (in 100/amu·Å^2) used to fit by Fourier series the one-dimensional parameters of $d_{\tau\varsigma}$ elements of the inverse of **D** matrix for system **3FBA**.

Parameter	τ=1,ς=1	τ=1,ς=2	τ=2,ς=2
$a_0^{\tau\varsigma}$	5.6091	-2.5027	127.3530
$a_1^{\tau\varsigma}$	0.3477	-0.2082	-0.0659
$a_2^{\tau\varsigma}$	0.5095	-0.4828	0.8277
$a_3^{\tau\varsigma}$	0.0280	-0.0085	-0.0117
$a_4^{\tau\varsigma}$	0.0399	-0.0375	0.0153
$a_5^{\tau\varsigma}$	-0.0002	0.0011	-0.0008
$a_6^{\tau\varsigma}$	0.0004	0.0008	-0.0122
$b_1^{\tau\varsigma}$	0.2335	-6.1262	4.3689
$b_2^{\tau\varsigma}$	0.1511	-0.0761	3.8746
$b_3^{\tau\varsigma}$	0.0005	-0.1265	0.7214
$b_4^{\tau\varsigma}$	0.0098	-0.0237	0.1290
$b_5^{\tau\varsigma}$	0.0004	-0.0055	0.0282
$b_6^{\tau\varsigma}$	0.0001	-0.0004	0.0152

Table C.2: Parameters (in 100/amu·Å^2) used to fit by Fourier series the cross-term parameters of $d_{\tau\varsigma}$ elements of the inverse of **D** matrix for system **3FBA**.

Parameter	τ=1,ς=1	τ=1,ς=2	τ=2,ς=2
$c_{11}^{\tau\varsigma}$,$d_{11}^{\tau\varsigma}$	0.0245, -0.0039	-0.0153, -0.4117	0.0584, 0.2311
$c_{12}^{\tau\varsigma}$,$d_{12}^{\tau\varsigma}$	0.0013, 0.0227	-0.0015, -0.0048	0.1942, -0.0266
$c_{13}^{\tau\varsigma}$,$d_{13}^{\tau\varsigma}$	0.0013, -0.0004	-0.0076, -0.0057	0.0200, -0.0235
$c_{14}^{\tau\varsigma}$,$d_{14}^{\tau\varsigma}$	0.0008, 0.0004	-0.0010, 0.0001	0.0088, -0.0009
$c_{15}^{\tau\varsigma}$,$d_{15}^{\tau\varsigma}$	0.0001, 0.0000	-0.0002, -0.0002	0.0013, -0.0013
$c_{16}^{\tau\varsigma}$,$d_{16}^{\tau\varsigma}$	0.0002, 0.0000	0.0001, 0.0001	-0.0002, -0.0013
$c_{21}^{\tau\varsigma}$,$d_{21}^{\tau\varsigma}$	0.0937, -0.0720	-0.2166, -0.2465	1.0097, -0.1383
$c_{22}^{\tau\varsigma}$,$d_{22}^{\tau\varsigma}$	0.0410, -0.0054	-0.0786, 0.0534	0.7274, -0.6456
$c_{23}^{\tau\varsigma}$,$d_{23}^{\tau\varsigma}$	0.0130, -0.0152	-0.0429, 0.0358	0.2680, -0.2639
$c_{24}^{\tau\varsigma}$,$d_{24}^{\tau\varsigma}$	0.0037, -0.0032	-0.0135, 0.0129	0.0986, -0.1211
$c_{25}^{\tau\varsigma}$,$d_{25}^{\tau\varsigma}$	0.0009, -0.0011	-0.0039, 0.0045	0.0304, -0.0339
$c_{26}^{\tau\varsigma}$,$d_{26}^{\tau\varsigma}$	0.0000, -0.0002	-0.0009, 0.0011	0.0066, -0.0080
$c_{31}^{\tau\varsigma}$,$d_{31}^{\tau\varsigma}$	0.0029, -0.0046	-0.0007, -0.0174	-0.0043, 0.0269
$c_{32}^{\tau\varsigma}$,$d_{32}^{\tau\varsigma}$	0.0036, -0.0019	-0.0003, -0.0001	0.0161, -0.0055
$c_{33}^{\tau\varsigma}$,$d_{33}^{\tau\varsigma}$	0.0008, -0.0015	-0.0005, -0.0001	0.0024, -0.0044
$c_{34}^{\tau\varsigma}$,$d_{34}^{\tau\varsigma}$	0.0000, -0.0002	0.0001, 0.0000	0.0021, -0.0003
$c_{35}^{\tau\varsigma}$,$d_{35}^{\tau\varsigma}$	-0.0001, 0.0000	0.0000, -0.0001	-0.0001, 0.0007
$c_{36}^{\tau\varsigma}$,$d_{36}^{\tau\varsigma}$	-0.0003, 0.0000	0.0001, -0.0001	-0.0006, 0.0009
$c_{41}^{\tau\varsigma}$,$d_{41}^{\tau\varsigma}$	0.0117, -0.0184	-0.0228, 0.0114	0.1012, -0.1265
$c_{42}^{\tau\varsigma}$,$d_{42}^{\tau\varsigma}$	0.0177, -0.0160	-0.0273, 0.0295	0.2055, -0.2350
$c_{43}^{\tau\varsigma}$,$d_{43}^{\tau\varsigma}$	0.0090, -0.0099	-0.0206, 0.0217	0.1953, -0.2049
$c_{44}^{\tau\varsigma}$,$d_{44}^{\tau\varsigma}$	0.0036, -0.0038	-0.0118, 0.0119	0.1130, -0.1133
$c_{45}^{\tau\varsigma}$,$d_{45}^{\tau\varsigma}$	0.0012, -0.0012	-0.0052, 0.0050	0.0516, -0.0495
$c_{46}^{\tau\varsigma}$,$d_{46}^{\tau\varsigma}$	0.0001, -0.0003	-0.0019, 0.0019	0.0169, -0.0166
$c_{51}^{\tau\varsigma}$,$d_{51}^{\tau\varsigma}$	-0.0006, 0.0004	0.0007, 0.0002	-0.0002, -0.0008
$c_{52}^{\tau\varsigma}$,$d_{52}^{\tau\varsigma}$	0.0001, -0.0003	0.0001, -0.0001	-0.0011, 0.0003
$c_{53}^{\tau\varsigma}$,$d_{53}^{\tau\varsigma}$	0.0003, -0.0003	0.0001, 0.0000	-0.0009, -0.0012
$c_{54}^{\tau\varsigma}$,$d_{54}^{\tau\varsigma}$	0.0002, -0.0001	0.0000, 0.0000	0.0010, -0.0002
$c_{55}^{\tau\varsigma}$,$d_{55}^{\tau\varsigma}$	0.0000, 0.0000	-0.0001, 0.0000	0.0005, -0.0005
$c_{56}^{\tau\varsigma}$,$d_{56}^{\tau\varsigma}$	0.0001, 0.0000	-0.0001, 0.0000	0.0009, -0.0007
$c_{61}^{\tau\varsigma}$,$d_{61}^{\tau\varsigma}$	-0.0004, -0.0004	0.0011, -0.0005	-0.0216, 0.0116
$c_{62}^{\tau\varsigma}$,$d_{62}^{\tau\varsigma}$	0.0019, -0.0018	-0.0017, 0.0019	0.0075, -0.0027
$c_{63}^{\tau\varsigma}$,$d_{63}^{\tau\varsigma}$	0.0023, -0.0021	-0.0032, 0.0026	0.0240, -0.0209
$c_{64}^{\tau\varsigma}$,$d_{64}^{\tau\varsigma}$	0.0011, -0.0010	-0.0023, 0.0019	0.0218, -0.0201
$c_{65}^{\tau\varsigma}$,$d_{65}^{\tau\varsigma}$	0.0003, -0.0003	-0.0012, 0.0009	0.0132, -0.0113
$c_{66}^{\tau\varsigma}$,$d_{66}^{\tau\varsigma}$	0.0001, 0.0000	-0.0006, 0.0003	0.0058, -0.0042

Table C.3: Parameters (in 100/amu·Å^2) used to fit by Fourier series the one-dimensional parameters of $d_{\tau\varsigma}$ elements of the inverse of **D** matrix for system **4FBA**.

Parameter	τ=1,ς=1	τ=1,ς=2	τ=2,ς=2
$a_0^{\tau\varsigma}$	5.9708	-2.3557	127.0170
$a_2^{\tau\varsigma}$	0.2385	-0.2530	0.7348
$a_4^{\tau\varsigma}$	0.0127	-0.0142	0.0094
$a_6^{\tau\varsigma}$	-0.0011	0.0022	-0.0135
$b_1^{\tau\varsigma}$	0.2146	-6.0986	4.2882
$b_2^{\tau\varsigma}$	0.1474	-0.0672	3.9607
$b_3^{\tau\varsigma}$	-0.0013	-0.1269	0.7125
$b_4^{\tau\varsigma}$	0.0092	-0.0225	0.1307
$b_5^{\tau\varsigma}$	0.0002	-0.0053	0.0288
$b_6^{\tau\varsigma}$	-0.0002	-0.0001	0.0154

Table C.4: Parameters (in 100/amu·Å^2) used to fit by Fourier series the cross-term parameters of $d_{\tau\varsigma}$ elements of the inverse of **D** matrix for system **4FBA**.

Parameter	τ=1,ς=1	τ=1,ς=2	τ=2,ς=2
$c_{21}^{\tau\varsigma}$,$d_{21}^{\tau\varsigma}$	0.0645, -0.0520	-0.1827, -0.0393	0.9801, -0.4901
$c_{22}^{\tau\varsigma}$,$d_{22}^{\tau\varsigma}$	0.0322, -0.0164	-0.0787, 0.0644	0.6530, -0.7048
$c_{23}^{\tau\varsigma}$,$d_{23}^{\tau\varsigma}$	0.0105, -0.0140	-0.0353, 0.0398	0.2770, -0.2886
$c_{24}^{\tau\varsigma}$,$d_{24}^{\tau\varsigma}$	0.0026, -0.0029	-0.0120, 0.0137	0.1014, -0.1288
$c_{25}^{\tau\varsigma}$,$d_{25}^{\tau\varsigma}$	0.0007, -0.0009	-0.0036, 0.0046	0.0312, -0.0369
$c_{26}^{\tau\varsigma}$,$d_{26}^{\tau\varsigma}$	-0.0001, -0.0002	-0.0007, 0.0012	0.0065, -0.0091
$c_{41}^{\tau\varsigma}$,$d_{41}^{\tau\varsigma}$	0.0054, -0.0103	-0.0170, 0.0281	0.1018, -0.1541
$c_{42}^{\tau\varsigma}$,$d_{42}^{\tau\varsigma}$	0.0119, -0.0123	-0.0250, 0.0276	0.1918, -0.2291
$c_{43}^{\tau\varsigma}$,$d_{43}^{\tau\varsigma}$	0.0068, -0.0072	-0.0192, 0.0211	0.1907, -0.2024
$c_{44}^{\tau\varsigma}$,$d_{44}^{\tau\varsigma}$	0.0031, -0.0031	-0.0116, 0.0115	0.1092, -0.1095
$c_{45}^{\tau\varsigma}$,$d_{45}^{\tau\varsigma}$	0.0012, -0.0009	-0.0051, 0.0047	0.0497, -0.0465
$c_{46}^{\tau\varsigma}$,$d_{46}^{\tau\varsigma}$	0.0003, -0.0003	-0.0021, 0.0017	0.0162, -0.0148
$c_{61}^{\tau\varsigma}$,$d_{61}^{\tau\varsigma}$	-0.0007, 0.0007	0.0017, -0.0006	-0.0236, 0.0127
$c_{62}^{\tau\varsigma}$,$d_{62}^{\tau\varsigma}$	0.0007, -0.0007	-0.0008, 0.0009	0.0063, -0.0012
$c_{63}^{\tau\varsigma}$,$d_{63}^{\tau\varsigma}$	0.0014, -0.0012	-0.0029, 0.0022	0.0253, -0.0244
$c_{64}^{\tau\varsigma}$,$d_{64}^{\tau\varsigma}$	0.0009, -0.0006	-0.0025, 0.0022	0.0234, -0.0207
$c_{65}^{\tau\varsigma}$,$d_{65}^{\tau\varsigma}$	0.0003, -0.0002	-0.0014, 0.0011	0.0133, -0.0124
$c_{66}^{\tau\varsigma}$,$d_{66}^{\tau\varsigma}$	0.0003, -0.0001	-0.0008, 0.0005	0.0067, -0.0053

Table C.5: Parameters (in 100/amu·Å^2) used to fit by Fourier series the one-dimensional parameters of $d_{\tau\varsigma}$ elements of the inverse of **D** matrix for system **BA**.

Parameter	τ=1,ς=1	τ=1,ς=2	τ=2,ς=2
$a_0^{\tau\varsigma}$	6.2942	-2.6735	127.4790
$a_2^{\tau\varsigma}$	0.3952	-0.3970	0.8124
$a_4^{\tau\varsigma}$	0.0278	-0.0261	0.0140
$a_6^{\tau\varsigma}$	-0.0007	0.0019	-0.0135
$b_1^{\tau\varsigma}$	0.2382	-6.1209	4.2365
$b_2^{\tau\varsigma}$	0.1486	-0.0648	3.6205
$b_3^{\tau\varsigma}$	-0.0001	-0.1200	0.7007
$b_4^{\tau\varsigma}$	0.0099	-0.0235	0.1196
$b_5^{\tau\varsigma}$	0.0003	-0.0051	0.0271
$b_6^{\tau\varsigma}$	0.0000	-0.0002	0.0147

Table C.6: Parameters (in 100/amu·Å^2) used to fit by Fourier series the cross-term parameters of $d_{\tau\varsigma}$ elements of the inverse of **D** matrix for system **BA**.

Parameter	τ=1,ς=1	τ=1,ς=2	τ=2,ς=2
$c_{21}^{\tau\varsigma}$,$d_{21}^{\tau\varsigma}$	0.0853,232.4840	-0.2020, -0.1402	0.9854, -0.2897
$c_{22}^{\tau\varsigma}$,$d_{22}^{\tau\varsigma}$	0.0388,132.4760	-0.0786, 0.0579	0.6369, -0.6237
$c_{23}^{\tau\varsigma}$,$d_{23}^{\tau\varsigma}$	0.0126, 25.1012	-0.0375, 0.0368	0.2517, -0.2607
$c_{24}^{\tau\varsigma}$,$d_{24}^{\tau\varsigma}$	0.0033, 6.4150	-0.0123, 0.0131	0.0902, -0.1150
$c_{25}^{\tau\varsigma}$,$d_{25}^{\tau\varsigma}$	0.0009, 0.7867	-0.0035, 0.0044	0.0276, -0.0332
$c_{26}^{\tau\varsigma}$,$d_{26}^{\tau\varsigma}$	0.0000, -0.2078	-0.0007, 0.0012	0.0059, -0.0090
$c_{41}^{\tau\varsigma}$,$d_{41}^{\tau\varsigma}$	0.0090, 20.5502	-0.0195, 0.0216	0.0995, -0.1433
$c_{42}^{\tau\varsigma}$,$d_{42}^{\tau\varsigma}$	0.0158, 36.5011	-0.0264, 0.0291	0.1908, -0.2234
$c_{43}^{\tau\varsigma}$,$d_{43}^{\tau\varsigma}$	0.0086, 21.9533	-0.0198, 0.0215	0.1856, -0.1953
$c_{44}^{\tau\varsigma}$,$d_{44}^{\tau\varsigma}$	0.0035, 10.0673	-0.0116, 0.0115	0.1052, -0.1056
$c_{45}^{\tau\varsigma}$,$d_{45}^{\tau\varsigma}$	0.0012, 2.7850	-0.0049, 0.0047	0.0479, -0.0436
$c_{46}^{\tau\varsigma}$,$d_{46}^{\tau\varsigma}$	0.0001, 0.3223	-0.0019, 0.0016	0.0147, -0.0136
$c_{61}^{\tau\varsigma}$,$d_{61}^{\tau\varsigma}$	-0.0007, -0.4765	0.0016, -0.0006	-0.0258, 0.0127
$c_{62}^{\tau\varsigma}$,$d_{62}^{\tau\varsigma}$	0.0014, 3.5145	-0.0011, 0.0015	0.0052, -0.0018
$c_{63}^{\tau\varsigma}$,$d_{63}^{\tau\varsigma}$	0.0020, 4.3241	-0.0031, 0.0025	0.0236, -0.0245
$c_{64}^{\tau\varsigma}$,$d_{64}^{\tau\varsigma}$	0.0011, 1.5230	-0.0024, 0.0022	0.0228, -0.0197
$c_{65}^{\tau\varsigma}$,$d_{65}^{\tau\varsigma}$	0.0004, 0.3095	-0.0015, 0.0011	0.0134, -0.0124
$c_{66}^{\tau\varsigma}$,$d_{66}^{\tau\varsigma}$	0.0003, -0.2564	-0.0008, 0.0005	0.0072, -0.0046

Table C.7: Parameters (in cm^{-1}) for the one-dimensional potentials of the three systems.

Parameter	3FBA	4FBA	BA
a_0	557.84	548.16	521.13
a_1	-22.67	-	-
a_2	19.79	77.53	79.50
a_3	4.18	-	-
a_4	-6.96	-5.53	-10.04
a_5	0.30	-	-
a_6	-2.65	-2.59	-7.64
b_1	3.16	11.35	-39.49
b_2	56.83	46.97	22.30
b_3	193.75	194.43	187.20
b_4	-2.45	-2.12	-2.43
b_5	0.02	0.06	0.12
b_6	1.50	1.52	1.32

Table C.8: Coupling parameters (in cm^{-1}) for the three systems.

Parameter	3FBA	4FBA	BA
a_0	557.84	548.16	521.13
a_1	-22.67	-	-
c_{11}, d_{11}	19.80, -0.46	- , -	- , -
c_{12}, d_{12}	7.63, -7.44	- , -	- , -
c_{11}, d_{11}	19.80, -0.46	- , -	- , -
c_{12}, d_{12}	7.63, -7.44	- , -	- , -
c_{13}, d_{13}	1.58, -2.19	- , -	- , -
c_{14}, d_{14}	0.31, -0.32	- , -	- , -
c_{15}, d_{15}	-0.02, 0.02	- , -	- , -
c_{16}, d_{16}	-0.01, 0.05	- , -	- , -
c_{21}, d_{21}	249.57, -195.93	250.87, -210.77	232.48, -190.44
c_{22}, d_{22}	146.34, -232.31	153.82, -241.96	132.48, -213.06
c_{23}, d_{23}	28.60, -27.16	30.29, -28.71	25.10, -22.34
c_{24}, d_{24}	8.53, -9.56	9.46, -10.41	6.41, -7.99
c_{25}, d_{25}	1.19, -2.28	1.31, -2.48	0.79, -2.01
c_{26}, d_{26}	0.24, -0.17	0.29, -0.31	-0.21, 0.25
c_{31}, d_{31}	1.24, -2.61	- , -	- , -
c_{32}, d_{32}	1.10, -1.43	- , -	- , -
c_{33}, d_{33}	0.02, 0.19	- , -	- , -
c_{34}, d_{34}	-0.06, 0.10	- , -	- , -
c_{35}, d_{35}	-0.08, 0.08	- , -	- , -
c_{36}, d_{36}	-0.15, 0.15	- , -	- , -
c_{41}, d_{41}	24.33, -30.76	22.22, -29.55	20.55, -25.92
c_{42}, d_{42}	44.36, -44.61	41.28, -41.75	36.50, -40.15
c_{43}, d_{43}	23.87, -25.69	23.36, -25.33	21.95, -23.96
c_{44}, d_{44}	10.95, -11.08	10.45, -10.59	10.07, -9.66
c_{45}, d_{45}	3.44, -3.41	3.38, -3.28	2.78, -3.21
c_{46}, d_{46}	0.66, -0.78	0.72, -0.87	0.32, -0.31
c_{51}, d_{51}	0.14, -0.13	- , -	- , -
c_{52}, d_{52}	-0.01, -0.01	- , -	- , -
c_{53}, d_{53}	-0.23, 0.06	- , -	- , -
c_{54}, d_{54}	-0.04, 0.07	- , -	- , -
c_{55}, d_{55}	-0.11, 0.10	- , -	- , -
c_{56}, d_{56}	-0.04, 0.11	- , -	- , -
c_{61}, d_{61}	0.03, -0.29	-0.09, -0.42	-0.48, 1.39
c_{62}, d_{62}	3.19, -4.01	3.48, -4.30	3.51, -4.10
c_{63}, d_{63}	5.11, -4.75	5.38, -4.94	4.32, -4.72
c_{64}, d_{64}	2.24, -2.04	2.31, -2.12	1.52, -1.83
c_{65}, d_{65}	0.76, -0.81	0.91, -0.92	0.31, -0.72
c_{66}, d_{66}	0.15, -0.24	0.22, -0.28	-0.26, 0.15

Table C.9: Parameters (in cm^{-1}) for the one-dimensional LRP 1D-potentials of the three systems.

Parameter	3FBA	4FBA	BA
a_0	310.64	315.76	340.07
a_1	-43.55	-	-
a_2	90.39	193.81	249.48
a_3	-6.37	-	-
a_4	188.29	119.15	61.92
a_5	29.55	-	-
a_6	-102.68	-191.88	-223.91
a_7	12.62	-	-
a_8	-115.66	-91.28	-51.77
a_9	-6.82	-	-
a_{10}	-62.32	-10.60	3. 77
a_{11}	-13.33	-	-
a_{12}	-10.96	9.23	2.72
a_{13}	-6.21	-	-
a_{14}	8.13	0.38	-0.46
a_{15}	2.18	-	-
a_{16}	3.65	-2.23	-0.25
a_{17}	2.59	-	-
a_{18}	-2.08	1.18	2.56
a_{19}	-	-	-
a_{20}	-	0.42	-1.77
a_{21}	-	-	-
a_{22}	-	-1.21	0.66
a_{23}	-	-	-
a_{24}	-	0.30	0.12
a_{25}	-	-	-
a_{26}	-	-0.04	0.31
a_{27}	-	-	-
a_{28}	-	0.19	-0.41
a_{29}	-	-	-
a_{30}	-	-0.39	-0.38
a_{31}	-	-	-
a_{32}	-	0.17	0.06
a_{33}	-	-	-
a_{34}	-	0.36	-0.41
a_{35}	-	-	-
a_{36}	-	-0.23	-0.17
a_{37}	-	-	-
a_{38}	-	-0.26	-0.24
a_{39}	-	-	-
a_{40}	-	-0.22	-0.26
a_{41}	-	-	-
a_{42}	-	-0.57	0.09

Table C.10: Parameters (in cm^{-1}) for the one-dimensional MEP 1D-potentials of the three systems.

Parameter	3FBA	4FBA	BA
a_0	270.84	260.44	266.22
a_1	-45.67	-	-
a_2	57.77	159.53	199.28
a_3	-3.72	-	-
a_4	238.55	217.94	206.62
a_5	14.21	-	-
a_6	-1.36	-56.09	-64.20
a_7	19.98	-	-
a_8	-20.06	-27.21	-27.62
a_9	15.85	-	-
a_{10}	-18.36	-22.01	-24.20
a_{11}	11.87	-	-
a_{12}	-12.38	-19.78	-24.06
a_{13}	9.03	-	-
a_{14}	-8.43	-17.08	-17.17
a_{15}	8.37	-	-
a_{16}	-8.40	-16.02	-18.24
a_{17}	7.75	-	-
a_{18}	-8.15	-15.05	-14.37
a_{19}	-	-	-
a_{20}	-6.79	-14.20	-15.03
a_{21}	-	-	-
a_{22}	-6.20	-13.38	-13.29
a_{23}	-	-	-
a_{24}	-5.47	-11.84	-11.79
a_{25}	-	-	-
a_{26}	-5.71	-11.68	-11.03
a_{27}	-	-	-
a_{28}	-4.59	-9.80	-8.96
a_{29}	-	-	-
a_{30}	-4.44	-9.71	-9.07
a_{31}	-	-	-
a_{32}	-3.65	-9.16	-7.20
a_{33}	-	-	-
a_{34}	-3.71	-8.23	-6.32
a_{35}	-	-	-
a_{36}	-2.82	-7.39	-5.49
a_{37}	-	-	-
a_{38}	-2.79	-5.79	-4.57
a_{39}	-	-	-
a_{40}	-2.26	-4.55	-3.53
a_{41}	-	-	-
a_{42}	-1.91	-4.76	-3.27

Table C.11: Splittings (in MHz) of the three systems.

	LRP	MEP
3FBA	0.10	0.17
4FBA	2.75	1.16
BA	44.75	6.94

Table C.12: 3FBA 1D splittings for LRP potential.

Level	Energy / (cm^{-1})
0^-	48.233758326967
0^+	48.233761858612
1^-	97.044699973137
1^+	97.044699978114

Table C.13: 3FBA 1D splittings for MEP potential.

Level	Energy / (cm^{-1})
0^-	38.718023887157
0^+	38.718029873557
1^-	86.164753074931
1^+	86.164757470385

Table C.14: 4FBA 1D splittings for LRP potential.

Level	Energy / (cm^{-1})
0^+0^+	48.629385737616
0^+0^-	48.629386325438
0^-0^-	48.629477594516
0^-0^+	48.629478235747

Table C.15: 4FBA 1D splittings for MEP potential.

Level	Energy / (cm^{-1})
0^+0^+	35.952445172150
0^+0^-	35.952445207477
0^-0^-	35.952484080135
0^-0^+	35.952484635106

Table C.16: Benzil-alcohol 1D splittings for LRP potential.

Level	Energy / (cm^{-1})
0^+0^+	45.474093162051
0^+0^-	45.474095860494
0^-0^+	45.475586311217
0^-0^-	45.475589934062

Table C.17: Benzil-alcohol 1D splittings for MEP potential.

Level	Energy / (cm^{-1})
0^+0^+	35.546354662426
0^+0^-	35.546355694849
0^-0^+	35.546586381599
0^-0^-	35.546595640431

Appendix D

Supporting Information for Chapter 3

This section includes several tables of interest of the chapter entitled "Calculating Torsional and Rotational-vibrational Partition Functions".

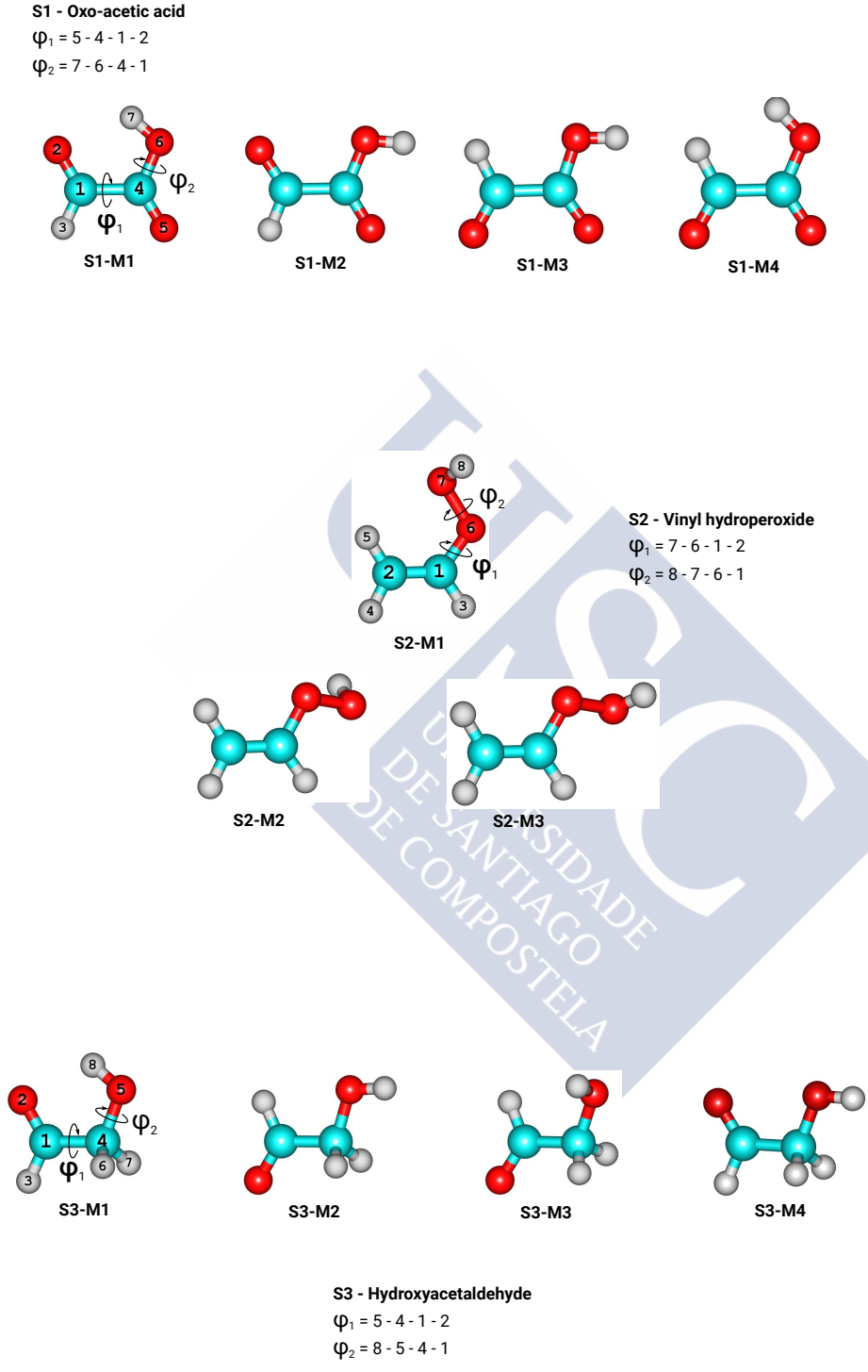

Figure D.1: Conformations of the molecules **S1**, **S2** and **S3**.

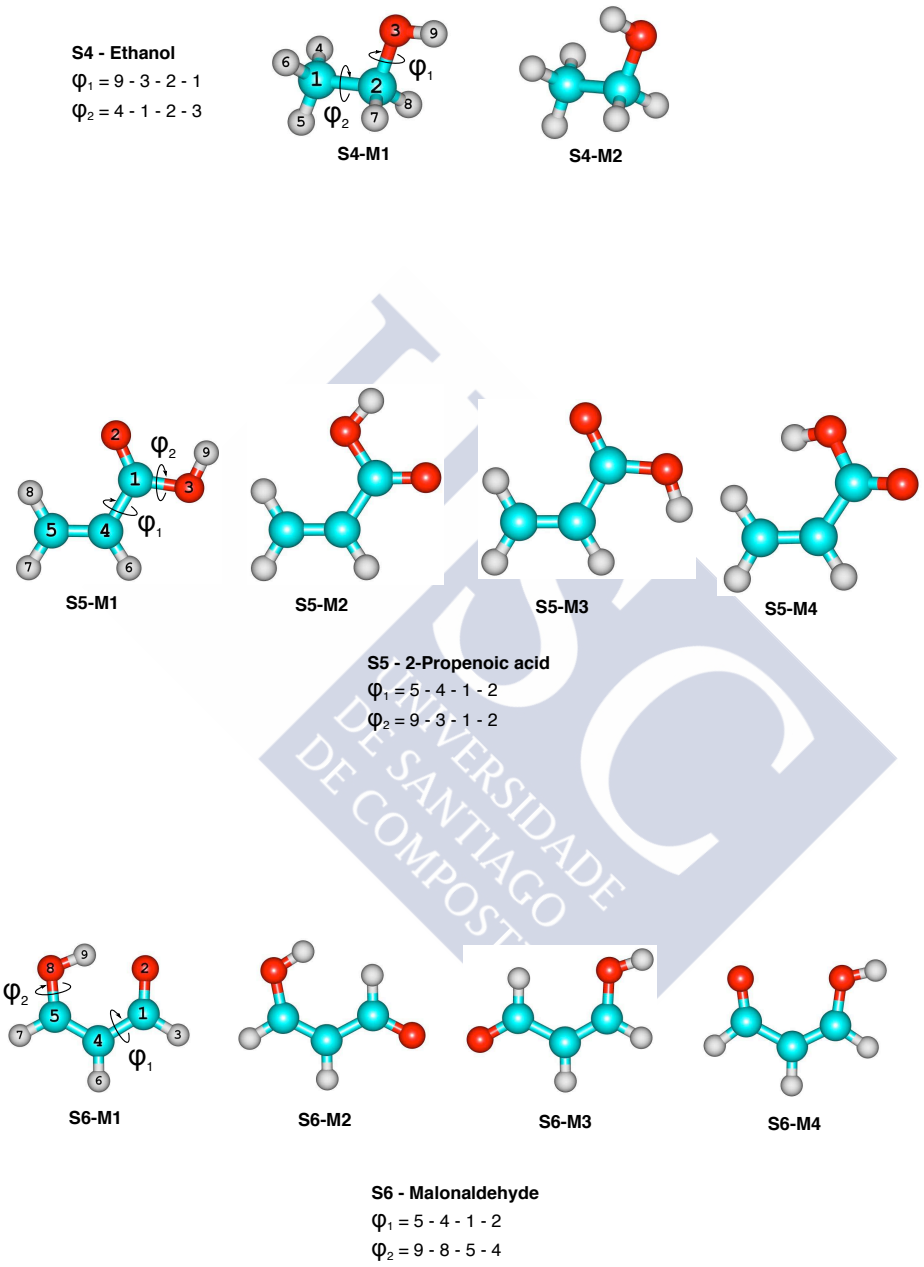

Figure D.2: Conformations of the molecules **S4**, **S5** and **S6**.

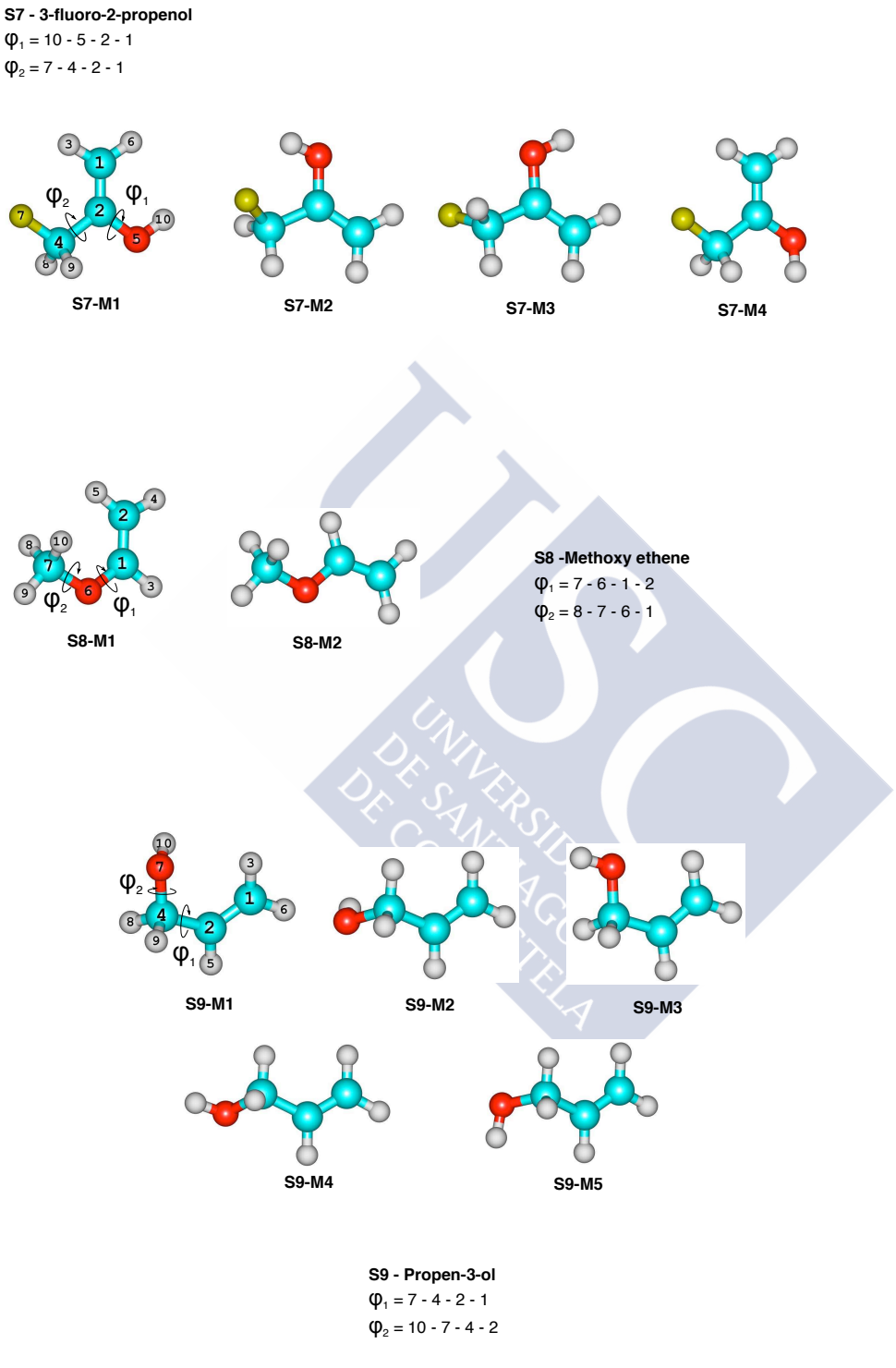

Figure D.3: Conformations of the molecules **S7**, **S8** and **S9**.

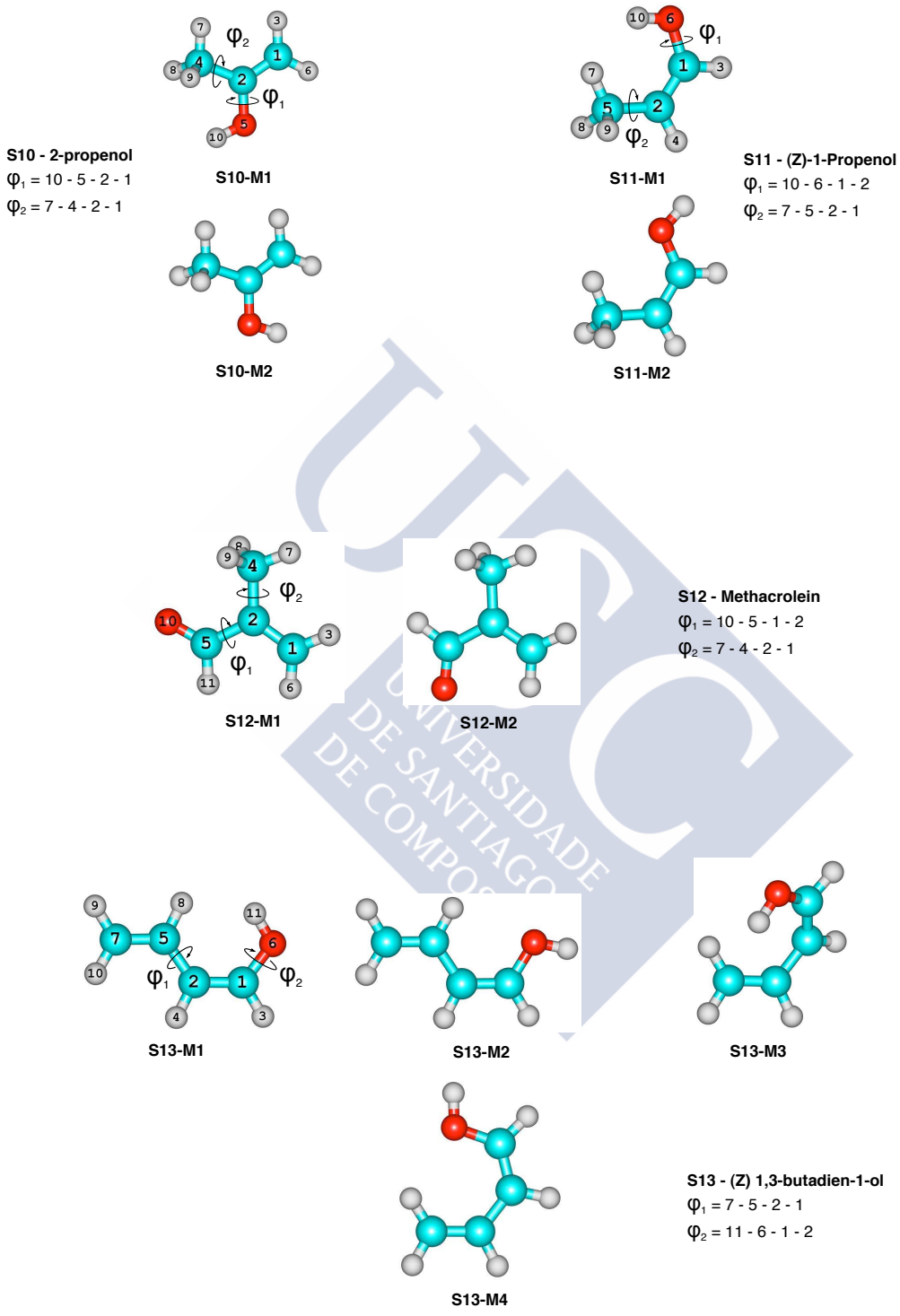

Figure D.4: Conformations of the molecules **S10**, **S11**, **S12** and **S13**.

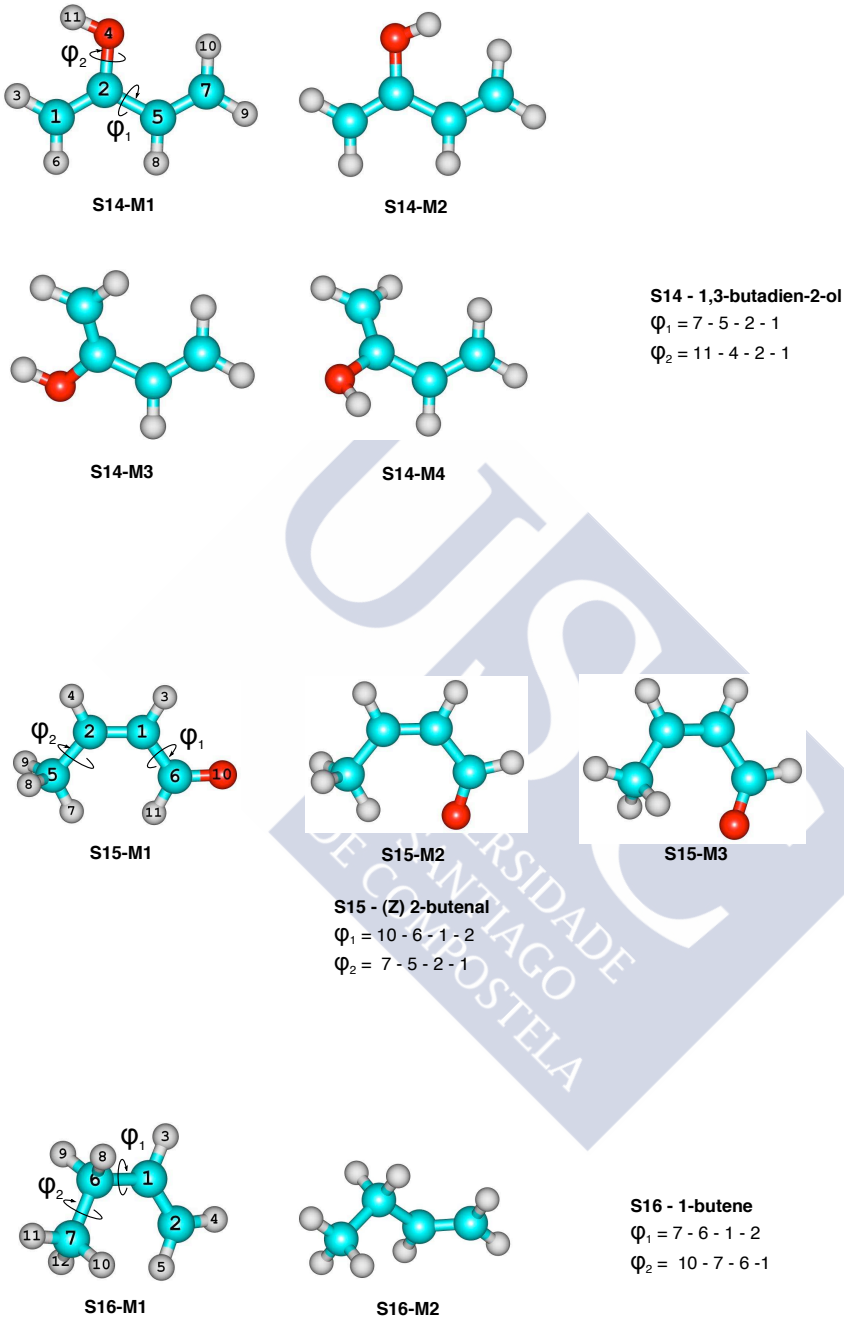

Figure D.5: Conformations of the molecules **S15**, **S16** and **S17**.

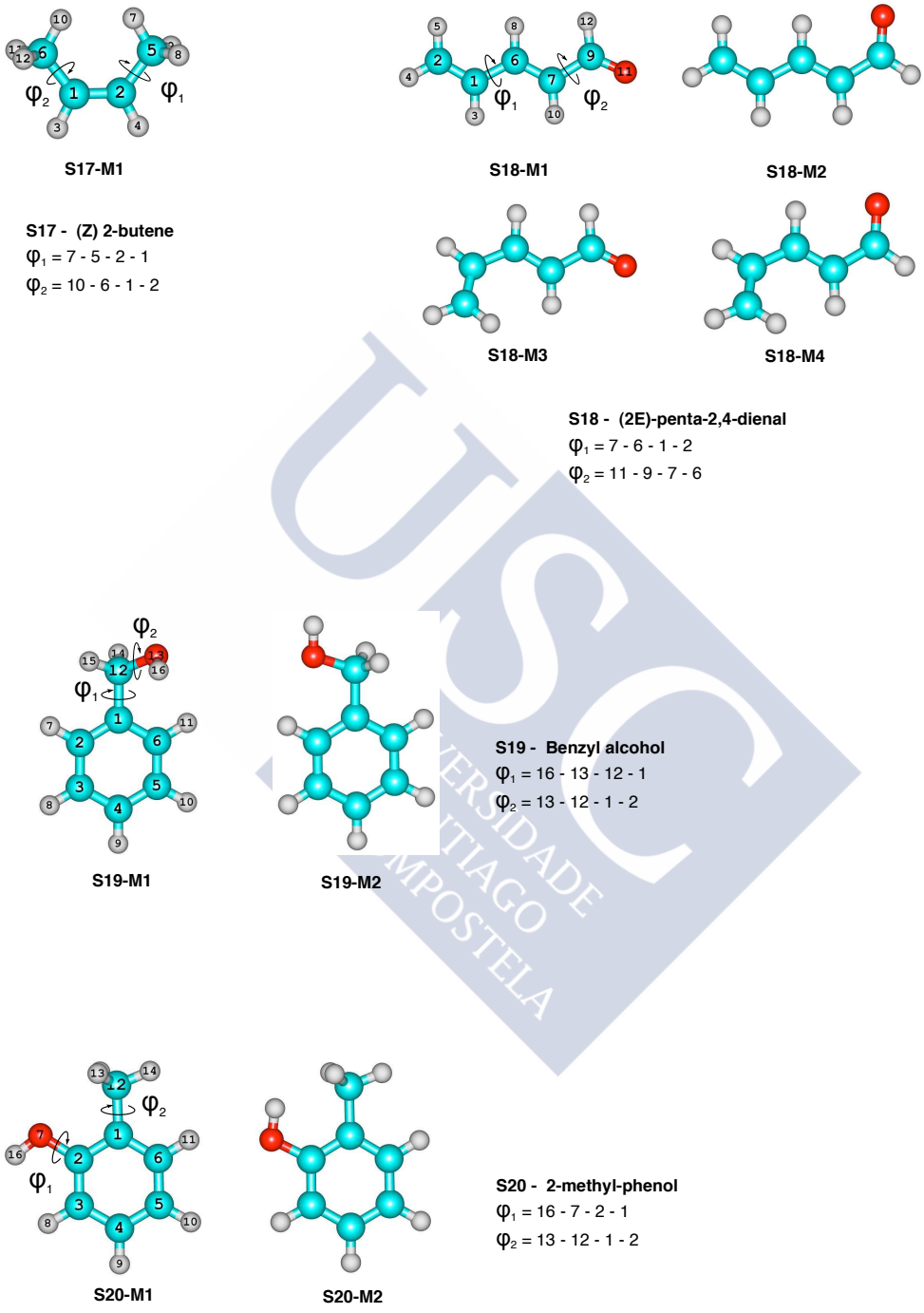

Figure D.6: Conformations of the molecules **S18**, **S19** and **S20**.

Table D.1: Thermodynamic functions at 298.15 K obtained with E2D-NS method for all the systems studied in this work. G^{o}_{m}, E^{o}_{m} and H^{o}_{m} are expressed in kcal/mol, S^{o}_{m} and $C_{p,m}$, in cal/mol·K.

System	$\Delta^{T}_{0}G^{o}_{m}$	$\Delta^{T}_{0}E^{o}_{m}$	$\Delta^{T}_{0}H^{o}_{m}$	S^{o}_{m}	$C_{p,m}$
S1	-17.615	3.341	3.934	72.274	19.539
S2	-17.385	3.316	3.909	71.420	18.860
S3	-16.804	2.968	3.560	68.303	18.356
S4	-16.575	2.849	3.441	67.134	15.635
S5	-17.922	3.288	3.881	73.128	19.379
S6	-17.304	3.008	3.600	70.113	18.214
S7	-18.476	3.800	4.392	76.700	22.275
S8	-16.855	3.266	3.859	69.475	20.906
S9	-17.980	3.466	4.058	73.916	19.831
S10	-16.925	3.232	3.825	69.594	20.401
S11	-17.567	3.343	3.935	72.119	19.033
S12	-18.098	3.685	4.278	75.048	21.627
S13	-18.399	3.900	4.493	76.779	22.816
S14	-17.800	3.768	4.360	74.328	24.751
S15	-18.490	3.906	4.499	77.107	21.281
S16	-17.908	3.435	4.027	73.573	20.486
S17	-17.373	3.474	4.067	71.908	19.380
S18	-18.927	4.299	4.892	79.891	26.142
S19	-20.621	4.722	5.315	86.987	29.318
S20	-19.845	4.776	5.369	84.566	30.668

Table D.2: Thermodynamic functions, G^{o}_{m} and H^{o}_{m} (in kcal/mol), obtained through four different methods (MC-HO, MS-T(U), MS-T(C) and E2D-NS) at 100 K. Experimental values are also listed when available.

System	MC-HO		MST-(U)		MS-T(C)		E2D-NS		Exp.	
	$\Delta_0^T G^{o}_{m}$	$\Delta_0^T H^{o}_{m}$	$\Delta_0^T G^{o}_{m}$	$\Delta_0^T H^{o}_{m}$	$\Delta_0^T G^{o}_{m}$	$\Delta_0^T H^{o}_{m}$	$\Delta_0^T G^{o}_{m}$	$\Delta_0^T H^{o}_{m}$	$\Delta_0^T G^{o}_{m}$	$\Delta_0^T H^{o}_{m}$
S1	-7.690	1.475	-7.694	1.481	-7.675	1.476	-7.693	1.477	...	...
S2	-7.598	1.485	-7.626	1.522	-7.591	1.515	-7.581	1.506	...	...
S3	-7.355	1.376	-7.361	1.382	-7.312	1.388	-7.384	1.401	...	...
S4	-7.239	1.424	-7.275	1.464	-7.264	1.464	-7.258	1.455	-7.276	1.449
S5	-7.833	1.529	-7.839	1.536	-7.810	1.534	-7.846	1.529	-7.897	1.536
S6	-7.609	1.361	-7.611	1.363	-7.566	1.363	-7.628	1.388	...	...
S7	-7.974	1.643	-7.988	1.658	-7.977	1.656	-7.987	1.675	...	...
S8	-7.350	1.405	-7.358	1.416	-7.348	1.413	-7.359	1.415	...	...
S9	-7.829	1.521	-7.856	1.557	-7.827	1.559	-7.822	1.573	...	...
S10	-7.388	1.385	-7.403	1.402	-7.392	1.402	-7.399	1.406	...	...
S11	-7.698	1.611	-7.751	1.613	-7.621	1.592	-7.638	1.572	...	...
S12	-7.788	1.570	-7.804	1.589	-7.763	1.589	-7.831	1.620	...	...
S13	-7.924	1.687	-7.937	1.703	-7.871	1.705	-7.921	1.700	...	...
S14	-7.714	1.481	-7.725	1.494	-7.704	1.494	-7.725	1.500	...	...
S15	-7.980	1.929	-8.021	1.993	-7.877	1.774	-7.930	1.769	...	...
S16	-7.851	1.474	-7.871	1.499	-7.795	1.542	-7.805	1.550	-7.742	1.606
S17	-7.376	1.598	-7.443	1.662	-7.418	1.661	-7.467	1.678	-7.536	1.667
S18	-8.122	1.742	-8.128	1.748	-8.015	1.750	-8.107	1.746	...	...
S19	-8.874	1.926	-8.911	1.986	-8.790	1.852	-8.856	1.847	...	...
S20	-8.502	1.788	-8.548	1.827	-8.524	1.826	-8.480	1.797	-8.452	1.798

Table D.3: Same as Table D.2 but at 300 K.

System	MC-HO		MST-(U)		MS-T(C)		E2D-NS		Exp.	
	$\Delta_0^T G_\mathrm{m}^\mathrm{o}$	$\Delta_0^T H_\mathrm{m}^\mathrm{o}$	$\Delta_0^T G_\mathrm{m}^\mathrm{o}$	$\Delta_0^T H_\mathrm{m}^\mathrm{o}$	$\Delta_0^T G_\mathrm{m}^\mathrm{o}$	$\Delta_0^T H_\mathrm{m}^\mathrm{o}$	$\Delta_0^T G_\mathrm{m}^\mathrm{o}$	$\Delta_0^T H_\mathrm{m}^\mathrm{o}$	$\Delta_0^T G_\mathrm{m}^\mathrm{o}$	$\Delta_0^T H_\mathrm{m}^\mathrm{o}$
S1	-17.723	3.901	-17.748	3.944	-17.703	3.934	-17.748	3.970	...	...
S2	-17.602	4.062	-17.724	4.151	-17.624	4.086	-17.535	3.935	...	...
S3	-16.843	3.538	-16.874	3.595	-16.791	3.632	-16.931	3.594	...	...
S4	-16.619	3.419	-16.747	3.485	-16.723	3.483	-16.699	3.470	-16.717	3.435
S5	-18.029	3.895	-18.055	3.925	-17.995	3.924	-18.058	3.917	-18.170	3.931
S6	-17.352	3.553	-17.358	3.559	-17.268	3.562	-17.434	3.634	...	...
S7	-18.543	4.349	-18.609	4.430	-18.581	4.419	-18.618	4.434	...	...
S8	-17.045	4.232	-17.101	4.290	-17.014	4.078	-16.984	3.897	...	...
S9	-18.054	3.993	-18.175	4.092	-18.114	4.080	-18.116	4.095	...	...
S10	-16.997	3.811	-17.070	3.910	-17.041	3.887	-17.053	3.863	...	...
S11	-17.872	4.036	-17.970	4.001	-17.689	3.985	-17.700	3.971	...	...
S12	-18.092	4.258	-18.166	4.341	-18.086	4.344	-18.237	4.318	...	...
S13	-18.519	4.460	-18.579	4.528	-18.451	4.535	-18.541	4.535	...	...
S14	-17.885	4.362	-17.941	4.446	-17.894	4.422	-17.938	4.406	...	...
S15	-18.996	4.902	-19.123	4.868	-18.582	4.650	-18.633	4.538	...	...
S16	-18.034	3.914	-18.129	4.024	-18.022	4.067	-18.045	4.065	-17.981	4.131
S17	-17.253	4.141	-17.445	4.145	-17.393	4.146	-17.498	4.107	-17.588	4.052
S18	-19.088	4.890	-19.114	4.925	-18.897	4.947	-19.075	4.940	...	...
S19	-20.937	5.545	-21.088	5.591	-20.648	5.357	-20.782	5.369	...	...
S20	-20.020	5.374	-20.162	5.431	-20.113	5.429	-20.001	5.425	-19.943	5.403

Table D.4: Same as Table D.2 but at 700 K.

System	MC-HO		MST-(U)		MS-T(C)		E2D-NS		Exp.	
	$\Delta_0^T G_m^o$	$\Delta_0^T H_m^o$	$\Delta_0^T G_m^o$	$\Delta_0^T H_m^o$	$\Delta_0^T G_m^o$	$\Delta_0^T H_m^o$	$\Delta_0^T G_m^o$	$\Delta_0^T H_m^o$	$\Delta_0^T G_m^o$	$\Delta_0^T H_m^o$
S1	-50.777	13.393	-50.969	13.568	-50.858	13.575	-51.073	13.751	...	...
S2	-50.932	14.082	-51.208	13.812	-50.876	13.741	-50.483	13.712	...	...
S3	-48.615	14.244	-48.871	14.304	-48.727	14.296	-48.895	14.165	...	...
S4	-47.178	12.529	-47.508	12.403	-47.452	12.403	-47.396	12.348	-47.406	12.466
S5	-51.895	14.737	-52.074	14.961	-51.930	14.950	-52.066	14.956	-52.358	14.875
S6	-49.605	13.926	-49.642	13.977	-49.439	13.984	-50.005	14.230	...	...
S7	-54.312	16.531	-54.670	16.722	-54.557	16.652	-54.651	16.652	...	...
S8	-50.788	16.175	-50.622	15.436	-50.118	15.271	-49.832	15.350	...	...
S9	-52.209	15.112	-52.531	14.897	-52.369	14.884	-52.417	14.903	...	...
S10	-49.703	15.367	-50.076	15.481	-49.934	15.391	-49.876	15.321	...	...
S11	-51.740	14.964	-51.764	14.506	-51.127	14.592	-51.191	14.642	...	...
S12	-53.280	16.959	-53.619	17.090	-53.456	17.136	-53.623	16.834	...	...
S13	-54.565	17.123	-54.869	17.309	-54.573	17.297	-54.845	17.471	...	...
S14	-53.529	18.149	-53.880	18.360	-53.709	18.306	-53.719	18.222	...	...
S15	-56.102	17.165	-56.051	16.457	-54.687	16.619	-54.664	16.625	...	...
S16	-52.365	16.080	-52.783	16.182	-52.586	16.218	-52.642	16.191	-52.570	16.294
S17	-50.900	16.379	-51.089	15.769	-50.976	15.785	-51.153	15.721	-51.294	15.715
S18	-57.364	19.632	-57.589	19.935	-57.137	20.002	-57.484	19.846	...	...
S19	-63.850	23.700	-63.990	23.088	-62.744	23.073	-63.074	23.038	...	...
S20	-61.586	23.716	-61.909	23.498	-61.793	23.503	-61.610	23.610	-61.439	23.712

Table D.5: Same as Table D.2 but at 1500 K.

System	MC-HO		MST-(U)		MS-T(C)		E2D-NS		Exp.	
	$\Delta_0^T G_m^o$	$\Delta_0^T H_m^o$	$\Delta_0^T G_m^o$	$\Delta_0^T H_m^o$	$\Delta_0^T G_m^o$	$\Delta_0^T H_m^o$	$\Delta_0^T G_m^o$	$\Delta_0^T H_m^o$	$\Delta_0^T G_m^o$	$\Delta_0^T H_m^o$
S1	-134.454	38.627	-135.057	38.696	-134.827	38.687	-135.670	39.168	...	...
S2	-136.323	41.307	-136.048	39.769	-135.337	39.797	-134.768	40.419	...	...
S3	-132.038	42.317	-132.105	41.071	-131.764	41.022	-132.130	41.143	...	...
S4	-126.871	41.262	-127.009	40.024	-126.896	40.035	-126.737	40.027	-127.041	40.501
S5	-141.049	46.880	-141.828	47.204	-141.466	47.102	-141.842	47.246	-141.754	45.638
S6	-135.786	48.512	-136.201	49.316	-135.702	49.114	-137.394	49.713	...	...
S7	-149.419	51.334	-150.092	50.599	-149.777	50.549	-150.002	50.583	...	...
S8	-140.707	49.450	-138.752	47.204	-137.681	47.245	-137.494	47.917	...	...
S9	-142.511	48.338	-142.391	46.759	-142.059	46.781	-142.217	46.864	...	...
S10	-137.645	48.968	-138.173	47.979	-137.781	47.942	-137.674	48.051	...	...
S11	-141.252	48.031	-140.182	46.096	-139.027	46.434	-139.304	46.645	...	...
S12	-148.886	54.925	-149.470	54.167	-149.193	54.245	-149.318	54.348	...	...
S13	-151.615	54.574	-152.383	54.360	-151.718	54.324	-152.649	54.759	...	...
S14	-151.028	56.404	-151.718	55.728	-151.323	55.731	-151.393	55.974	...	...
S15	-154.772	54.359	-153.161	51.995	-150.675	52.684	-150.918	53.353	...	...
S16	-146.206	55.316	-146.849	54.415	-146.483	54.471	-146.579	54.453	-146.644	54.827
S17	-143.410	55.615	-142.467	53.464	-142.261	53.518	-142.562	53.449	-142.991	53.766
S18	-162.622	62.113	-163.416	62.055	-162.545	62.148	-163.267	62.514	...	...
S19	-186.393	79.535	-185.243	77.150	-182.754	77.550	-183.399	77.470	...	...
S20	-181.620	79.653	-181.558	78.160	-181.328	78.194	-181.153	78.479	-181.133	79.137

Table D.6: Same as Table D.2 but at 2500 K.

System	MC-HO		MST-(U)		MS-T(C)		E2D-NS		Exp.	
	$\Delta_0^T G_m^o$	$\Delta_0^T H_m^o$	$\Delta_0^T G_m^o$	$\Delta_0^T H_m^o$	$\Delta_0^T G_m^o$	$\Delta_0^T H_m^o$	$\Delta_0^T G_m^o$	$\Delta_0^T H_m^o$	$\Delta_0^T G_m^o$	$\Delta_0^T H_m^o$
S1	-259.593	74.264	-260.456	73.509	-260.061	73.487	-261.873	74.214	...	...
S2	-265.497	80.800	-263.461	77.466	-262.387	77.595	-261.972	78.588	...	...
S3	-259.118	82.079	-257.929	79.156	-257.337	79.108	-258.030	79.195	...	...
S4	-250.832	85.075	-249.746	82.044	-249.576	82.071	-249.309	82.076	-250.239	82.875
S5	-279.002	93.207	-280.219	92.285	-279.553	92.202	-280.434	92.923	...	...
S6	-272.356	97.845	-273.476	97.889	-272.505	97.722	-275.953	98.947	...	...
S7	-297.015	101.838	-297.150	99.317	-296.622	99.318	-297.039	99.416	...	...
S8	-280.979	99.165	-275.589	95.050	-274.000	95.251	-274.178	96.033	...	...
S9	-283.217	97.950	-281.408	94.439	-280.908	94.501	-281.231	94.606	...	...
S10	-275.566	98.696	-275.281	95.838	-274.631	95.899	-274.572	96.153	...	...
S11	-280.890	97.571	-277.249	93.570	-275.621	94.149	-276.242	94.426	...	...
S12	-299.947	110.714	-299.942	108.188	-299.539	108.293	-299.971	108.900	...	...
S13	-304.115	109.886	-304.921	108.377	-303.803	108.391	-305.670	108.894	...	...
S14	-304.442	111.968	-304.657	109.554	-304.036	109.610	-304.402	110.136	...	...
S15	-309.262	109.792	-304.390	105.208	-300.839	106.351	-301.837	107.493	...	...
S16	-296.785	115.186	-296.764	112.523	-296.219	112.617	-296.362	112.582	-296.815	113.253
S17	-292.326	115.492	-288.769	111.341	-288.474	111.439	-288.928	111.368	-289.944	111.980
S18	-329.224	123.669	-330.103	122.109	-328.744	122.246	-330.376	123.226	...	...
S19	-386.130	162.054	-381.960	157.335	-378.222	158.174	-379.233	158.058	...	...
S20	-378.265	162.206	-376.649	158.820	-376.302	158.896	-376.219	159.243	...	...

Table D.7: Thermodynamic functions, S^{o}_{m} and $C_{p,m}$ (in cal/mol·K), obtained through four different methods (MC-HO, MS-T(U), MS-T(C) and E2D-NS) at 100 K. Experimental values are also listed when available.

System	MC-HO		MST-(U)		MS-T(C)		E2D-NS		Exp.	
	S^{o}_{m}	$C_{p,m}$	S^{o}_{m}	$C_{p,m}$	S^{o}_{m}	$C_{p,m}$	S^{o}_{m}	$C_{p,m}$	S^{o}_{m}	$C_{p,m}$
S1	61.100	13.135	61.166	13.245	61.012	13.167	61.135	13.365	...	...
S2	60.550	13.729	60.990	14.265	60.704	14.001	60.580	13.129	...	...
S3	58.208	11.416	58.292	11.478	58.003	11.619	58.554	11.526	...	...
S4	57.755	11.127	58.261	11.525	58.187	11.514	58.088	11.442	58.167	11.219
S5	62.416	12.512	62.502	12.605	62.293	12.603	62.498	12.584	62.894	12.507
S6	59.804	11.549	59.825	11.570	59.526	11.577	60.109	11.813	...	...
S7	64.109	14.178	64.310	14.420	64.219	14.421	64.410	14.423	...	...
S8	58.364	12.597	58.495	12.914	58.401	12.584	58.491	12.349	...	...
S9	62.330	13.156	62.757	13.700	62.576	13.677	62.638	13.646	...	...
S10	58.490	11.979	58.704	12.259	58.628	12.239	58.698	12.299	...	...
S11	62.055	13.331	62.427	13.122	61.421	13.104	61.404	13.063	...	...
S12	62.385	14.164	62.618	14.476	62.351	14.477	63.005	14.551	...	...
S13	64.077	14.959	64.268	15.188	63.842	15.220	64.141	15.200	...	...
S14	61.298	13.608	61.457	13.817	61.318	13.780	61.506	13.808	...	...
S15	66.061	18.434	66.757	18.833	64.339	16.810	64.665	16.071	...	...
S16	62.165	12.955	62.463	13.357	62.250	13.359	62.368	13.310	62.321	13.482
S17	59.827	13.798	60.703	14.141	60.530	14.132	60.966	13.938	61.350	13.253
S18	65.759	16.275	65.841	16.366	65.101	16.430	65.691	16.486	...	...
S19	71.995	18.774	72.650	19.539	70.948	17.768	71.355	17.828	...	...
S20	68.599	17.500	69.164	17.743	69.002	17.725	68.516	17.780	68.329	17.947

Table D.8: Same as Table D.7 but at 300 K.

System	MC-HO		MST-(U)		MS-T(C)		E2D-NS		Exp.	
	$S_{\mathrm{m}}^{\mathrm{o}}$	$C_{\mathrm{p,m}}$	$S_{\mathrm{m}}^{\mathrm{o}}$	$C_{\mathrm{p,m}}$	$S_{\mathrm{m}}^{\mathrm{o}}$	$C_{\mathrm{p,m}}$	$S_{\mathrm{m}}^{\mathrm{o}}$	$C_{\mathrm{p,m}}$	$S_{\mathrm{m}}^{\mathrm{o}}$	$C_{\mathrm{p,m}}$
S1	72.080	18.862	72.307	19.246	72.124	19.257	72.395	19.589	...	...
S2	72.213	19.909	72.916	19.849	72.368	19.544	71.564	18.909	...	...
S3	67.936	18.144	68.228	18.786	68.079	19.120	68.414	18.527	...	...
S4	66.792	15.728	67.439	15.710	67.356	15.701	67.231	15.691	67.170	15.652
S5	73.077	19.230	73.269	19.473	73.062	19.481	73.249	19.479	73.671	19.641
S6	69.683	17.862	69.725	17.906	69.433	17.922	70.227	18.357	...	...
S7	76.304	21.949	76.797	22.559	76.665	22.410	76.838	22.386	...	...
S8	70.922	24.536	71.304	23.787	70.307	22.396	69.605	20.972	...	...
S9	73.491	19.844	74.225	19.938	73.980	19.845	74.039	19.905	73.657	18.250
S10	69.361	20.433	69.931	21.142	69.761	20.866	69.721	20.469	...	...
S11	73.027	19.289	73.236	18.876	72.247	18.965	72.237	19.106	...	...
S12	74.500	21.946	75.023	22.391	74.768	22.447	75.182	21.725	...	...
S13	76.596	22.328	77.025	22.759	76.620	22.762	76.921	22.930	...	...
S14	74.158	24.799	74.623	25.506	74.387	25.269	74.482	24.870	...	...
S15	79.661	22.134	79.968	20.865	77.443	21.749	77.239	21.374	...	...
S16	73.160	20.055	73.846	20.649	73.630	20.628	73.701	20.573	73.707	20.550
S17	71.315	20.559	71.965	19.576	71.797	19.599	72.019	19.491	72.134	19.252
S18	79.925	25.902	80.130	26.245	79.479	26.405	80.053	26.260	...	...
S19	88.273	30.126	88.928	29.247	86.682	29.417	87.170	29.476	...	...
S20	84.649	30.594	85.308	30.549	85.138	30.547	84.756	30.823	84.486	30.593

Table D.9: Same as Table D.7 but at 700 K.

System	MC-HO		MST-(U)		MS-T(C)		E2D-NS		Exp.	
	S^{o}_{m}	$C_{p,m}$	S^{o}_{m}	$C_{p,m}$	S^{o}_{m}	$C_{p,m}$	S^{o}_{m}	$C_{p,m}$	S^{o}_{m}	$C_{p,m}$
S1	91.672	27.506	92.195	27.648	92.048	27.680	92.605	28.065	...	...
S2	92.877	29.251	92.886	27.896	92.311	28.006	91.706	28.952	...	...
S3	89.798	31.556	90.251	30.388	90.032	30.078	90.083	30.554	...	...
S4	85.296	28.852	85.588	27.931	85.507	27.942	85.348	28.054	85.531	28.401
S5	95.189	33.480	95.764	34.120	95.543	34.029	95.746	34.091	96.047	33.059
S6	90.759	32.927	90.884	33.207	90.605	33.171	91.765	33.559	...	...
S7	101.205	36.978	101.989	36.626	101.727	36.570	101.861	36.587	...	...
S8	95.662	34.546	94.368	32.534	93.412	32.923	93.117	34.346	...	...
S9	96.173	34.286	96.325	32.922	96.076	32.962	96.171	33.113	95.117	32.911
S10	92.956	35.215	93.653	34.494	93.321	34.481	93.139	34.691	...	...
S11	95.291	33.942	94.673	32.414	93.885	32.754	94.047	33.112	...	...
S12	100.341	39.523	101.012	39.172	100.846	39.262	100.653	39.138	...	...
S13	102.411	39.041	103.112	39.095	102.672	39.028	103.308	39.557	...	...
S14	102.398	41.102	103.200	40.767	102.878	40.827	102.773	41.093	...	...
S15	104.668	38.086	103.582	36.180	101.866	37.035	101.840	37.827	...	...
S16	97.778	39.131	98.522	38.486	98.292	38.490	98.333	38.553	98.377	38.690
S17	96.113	39.150	95.511	37.346	95.373	37.391	95.534	37.368	95.727	37.682
S18	109.994	45.097	110.747	45.643	110.199	45.710	110.472	45.736	...	...
S19	125.071	57.531	124.397	55.507	122.596	56.099	123.017	56.051	...	...
S20	121.860	57.814	122.010	56.614	121.852	56.644	121.743	57.061	121.644	57.562

Table D.10: Same as Table D.7 but at 1500 K.

System	MC-HO		MST-(U)		MS-T(C)		E2D-NS		Exp.	
	S^{o}_{m}	$C_{p,m}$	S^{o}_{m}	$C_{p,m}$	S^{o}_{m}	$C_{p,m}$	S^{o}_{m}	$C_{p,m}$	S^{o}_{m}	$C_{p,m}$
S1	115.387	34.236	115.835	33.813	115.676	33.775	116.558	34.237	...	...
S2	118.420	37.426	117.211	35.710	116.756	35.826	116.791	36.400	...	...
S3	116.236	37.879	115.451	36.054	115.191	36.213	115.514	36.322	...	...
S4	112.088	40.876	111.355	39.208	111.288	39.224	111.176	39.250	111.695	39.677
S5	125.286	44.380	126.022	43.745	125.712	43.696	126.058	44.255	124.928	42.017
S6	122.865	49.301	123.679	49.786	123.210	49.614	124.738	50.659	...	...
S7	133.835	47.931	133.794	46.321	133.550	46.373	133.723	46.466	...	...
S8	126.771	46.694	123.971	44.847	123.284	45.038	123.607	45.329	...	...
S9	127.232	46.604	126.100	44.732	125.894	44.774	126.054	44.814	...	...
S10	124.409	46.814	124.101	45.084	123.816	45.178	123.817	45.401	...	...
S11	126.189	46.491	124.185	44.482	123.641	44.759	123.966	44.866	...	...
S12	135.874	52.788	135.758	51.211	135.625	51.234	135.778	51.892	...	...
S13	137.460	52.168	137.829	51.203	137.361	51.218	138.272	51.410	...	...
S14	138.288	52.616	138.298	51.064	138.036	51.125	138.245	51.526	...	...
S15	139.421	52.216	136.770	50.045	135.572	50.571	136.181	51.246	...	...
S16	134.348	55.914	134.176	54.309	133.969	54.343	134.021	54.330	134.314	54.711
S17	132.683	55.918	130.621	53.936	130.520	53.983	130.674	53.981	131.171	54.369
S18	149.823	58.488	150.314	57.328	149.796	57.357	150.521	58.159	...	...
S19	177.285	77.952	174.929	75.642	173.536	76.113	173.913	76.065	...	...
S20	174.182	78.008	173.145	76.201	173.015	76.242	173.088	76.346	173.513	77.020

Table D.11: Same as Table D.7 but at 2500 K.

System	MC-HO		MST-(U)		MS-T(C)		E2D-NS		Exp.	
	$S^{\mathrm{o}}_{\mathrm{m}}$	$C_{\mathrm{p,m}}$	$S^{\mathrm{o}}_{\mathrm{m}}$	$C_{\mathrm{p,m}}$	$S^{\mathrm{o}}_{\mathrm{m}}$	$C_{\mathrm{p,m}}$	$S^{\mathrm{o}}_{\mathrm{m}}$	$C_{\mathrm{p,m}}$	$S^{\mathrm{o}}_{\mathrm{m}}$	$C_{\mathrm{p,m}}$
S1	133.543	36.526	133.586	35.355	133.419	35.366	134.435	35.453	...	...
S2	138.518	40.919	136.371	39.063	135.993	39.151	136.224	39.380	...	...
S3	136.479	41.081	134.834	39.321	134.578	39.375	134.890	39.267	...	...
S4	134.363	45.821	132.716	43.948	132.658	43.964	132.554	43.971	133.247	44.192
S5	148.884	47.551	149.002	45.922	148.702	45.978	149.343	46.490	...	...
S6	148.081	48.954	148.546	47.540	148.091	47.643	149.960	47.880	...	...
S7	159.541	52.261	158.587	50.372	158.376	50.420	158.582	50.462	...	...
S8	152.058	51.766	148.256	49.870	147.700	50.007	148.085	50.020	...	...
S9	152.467	51.671	150.339	49.703	150.163	49.741	150.335	49.750	...	...
S10	149.705	51.734	148.448	49.781	148.212	49.878	148.290	49.970	...	...
S11	151.385	51.625	148.327	49.527	147.908	49.741	148.267	49.778	...	...
S12	164.265	57.813	163.252	55.932	163.133	55.964	163.548	56.327	...	...
S13	165.600	57.461	165.319	55.928	164.878	56.003	165.826	55.997	...	...
S14	166.564	57.602	165.684	55.748	165.458	55.796	165.815	55.990	...	...
S15	167.622	57.594	163.839	55.344	162.876	55.749	163.732	56.069	...	...
S16	164.788	62.546	163.715	60.685	163.534	60.723	163.578	60.706	164.027	60.911
S17	163.127	62.552	160.044	60.543	159.965	60.583	160.118	60.585	160.770	60.786
S18	181.157	63.635	180.885	61.916	180.396	61.974	181.441	62.413	...	...
S19	219.274	85.604	215.718	83.260	214.558	83.673	214.916	83.645	...	...
S20	216.189	85.624	214.187	83.679	214.079	83.720	214.185	83.756	...	...

Table D.12: Several one-dimensional partition functions evaluated at different temperatures for system **S1**.

T(K)	Partition functions for ϕ_1					
	q^{CT}	q^{RPG}	q^{SRPG}	q_{cl}	q^{TPG}	q^{TES}
100	3.267E-01	5.441E-01	3.446E-01	4.453E-01	3.631E-01	3.649E-01
150	5.566E-01	9.607E-01	6.084E-01	6.697E-01	6.104E-01	6.122E-01
200	7.771E-01	1.362E+00	8.623E-01	8.951E-01	8.493E-01	8.511E-01
250	9.925E-01	1.754E+00	1.111E+00	1.122E+00	1.084E+00	1.086E+00
300	1.205E+00	2.142E+00	1.357E+00	1.349E+00	1.318E+00	1.319E+00
400	1.626E+00	2.916E+00	1.847E+00	1.807E+00	1.783E+00	1.785E+00
500	2.044E+00	3.691E+00	2.338E+00	2.270E+00	2.251E+00	2.253E+00
700	2.881E+00	5.267E+00	3.342E+00	3.219E+00	3.205E+00	3.207E+00
1000	4.189E+00	7.721E+00	4.956E+00	4.757E+00	4.746E+00	4.749E+00
1500	6.716E+00	1.207E+01	8.080E+00	7.779E+00	7.772E+00	7.775E+00
2000	9.825E+00	1.660E+01	1.169E+01	1.133E+01	1.133E+01	1.133E+01
2500	1.348E+01	2.115E+01	1.559E+01	1.520E+01	1.520E+01	1.520E+01

Table D.13: Several one-dimensional partition functions evaluated at different temperatures for system **S1**.

T(K)	Partition functions for ϕ_2					
	q^{CT}	q^{RPG}	q^{SRPG}	q_{cl}	q^{TPG}	q^{TES}
100	8.249E-03	2.358E-02	1.202E-02	1.151E-01	1.194E-02	1.522E-02
150	4.228E-02	1.042E-01	5.487E-02	1.793E-01	5.484E-02	6.364E-02
200	9.925E-02	2.210E-01	1.220E-01	2.519E-01	1.225E-01	1.356E-01
250	1.709E-01	3.515E-01	2.039E-01	3.329E-01	2.056E-01	2.215E-01
300	2.517E-01	4.852E-01	2.950E-01	4.211E-01	2.987E-01	3.163E-01
400	4.289E-01	7.508E-01	4.941E-01	6.147E-01	5.040E-01	5.231E-01
500	6.176E-01	1.011E+00	7.070E-01	8.249E-01	7.252E-01	7.447E-01
700	1.011E+00	1.521E+00	1.158E+00	1.278E+00	1.196E+00	1.215E+00
1000	1.618E+00	2.287E+00	1.876E+00	2.013E+00	1.948E+00	1.967E+00
1500	2.644E+00	3.613E+00	3.166E+00	3.339E+00	3.291E+00	3.309E+00
2000	3.675E+00	4.999E+00	4.537E+00	4.744E+00	4.705E+00	4.723E+00
2500	4.703E+00	6.411E+00	5.944E+00	6.178E+00	6.145E+00	6.162E+00

Table D.14: Several partition function ratios evaluated at different temperatures for system **S1**. It also includes the two-dimensional partition function $Q_{\mathrm{tor}}^{\mathrm{2D-NS}}$.

T(K)	$F^{\mathrm{HO-NM}}$	$F^{\mathrm{TPG(C)}}$	$F^{\mathrm{MC-TPG(C)}}$	F^{TES}	$F^{\mathrm{2D-NS}}$	$Q_{\mathrm{tor}}^{\mathrm{2D-NS}}$
100.0	0.062	0.095	0.095	0.108	0.109	5.863E-03
150.0	0.235	0.298	0.299	0.325	0.325	4.147E-02
200.0	0.415	0.481	0.484	0.512	0.512	1.261E-01
250.0	0.556	0.615	0.619	0.644	0.644	2.722E-01
300.0	0.658	0.708	0.712	0.735	0.734	4.907E-01
400.0	0.785	0.819	0.823	0.841	0.840	1.188E+00
500.0	0.855	0.879	0.882	0.896	0.895	2.296E+00
700.0	0.922	0.936	0.938	0.947	0.947	5.960E+00
1000.0	0.961	0.968	0.969	0.975	0.975	1.560E+01
1500.0	0.983	0.985	0.986	0.990	1.000	4.443E+01
2000.0	0.991	0.992	0.992	0.995	1.000	8.887E+01
2500.0	0.994	0.995	0.995	0.997	1.000	1.483E+02

Table D.15: Several rovibrational partition functions evaluated at different temperatures for system **S1**.

T(K)	Multidimensional partition functions				
	$\tilde{Q}_{\mathrm{rv}}^{\mathrm{1W-H}}$	$\tilde{Q}_{\mathrm{rv}}^{\mathrm{MC-H}}$	$\tilde{Q}_{\mathrm{rv}}^{\mathrm{MS-T(U)}}$	$\tilde{Q}_{\mathrm{rv}}^{\mathrm{MS-T(C)}}$	$\tilde{Q}_{\mathrm{rv}}^{\mathrm{EHR}}$
100.0	1.400E+04	1.463E+04	1.475E+04	1.392E+04	1.482E+04
150.0	3.143E+04	3.511E+04	3.560E+04	3.345E+04	3.557E+04
200.0	6.229E+04	7.662E+04	7.828E+04	7.317E+04	7.791E+04
250.0	1.162E+05	1.586E+05	1.636E+05	1.522E+05	1.630E+05
300.0	2.095E+05	3.163E+05	3.299E+05	3.059E+05	3.305E+05
400.0	6.374E+05	1.152E+06	1.233E+06	1.139E+06	1.256E+06
500.0	1.823E+06	3.812E+06	4.188E+06	3.866E+06	4.352E+06
700.0	1.286E+07	3.328E+07	3.820E+07	3.528E+07	4.124E+07
1000.0	1.751E+08	5.564E+08	6.644E+08	6.148E+08	7.551E+08
1500.0	6.886E+09	2.699E+10	3.304E+10	3.059E+10	4.068E+10
2000.0	1.442E+11	6.494E+11	7.912E+11	7.314E+11	1.020E+12
2500.0	1.917E+12	9.554E+12	1.137E+13	1.050E+13	1.516E+13

Table D.16: Several one-dimensional partition functions evaluated at different temperatures for system **S2**.

T(K)	Partition functions for ϕ_1					
	q^{CT}	q^{RPG}	q^{SRPG}	q_{cl}	q^{TPG}	q^{TES}
100	1.725E-01	3.519E-01	1.410E-01	2.796E-01	1.675E-01	1.741E-01
150	3.493E-01	7.598E-01	3.085E-01	4.254E-01	3.348E-01	3.430E-01
200	5.688E-01	1.167E+00	4.909E-01	5.896E-01	5.139E-01	5.238E-01
250	8.601E-01	1.566E+00	6.937E-01	7.824E-01	7.158E-01	7.279E-01
300	1.237E+00	1.959E+00	9.210E-01	1.008E+00	9.471E-01	9.612E-01
400	2.240E+00	2.738E+00	1.448E+00	1.552E+00	1.499E+00	1.516E+00
500	3.528E+00	3.524E+00	2.058E+00	2.201E+00	2.152E+00	2.172E+00
700	6.662E+00	5.141E+00	3.448E+00	3.718E+00	3.675E+00	3.697E+00
1000	1.173E+01	7.683E+00	5.766E+00	6.293E+00	6.258E+00	6.280E+00
1500	1.907E+01	1.203E+01	9.785E+00	1.080E+01	1.077E+01	1.079E+01
2000	2.485E+01	1.626E+01	1.368E+01	1.518E+01	1.516E+01	1.518E+01
2500	2.959E+01	2.025E+01	1.733E+01	1.930E+01	1.928E+01	1.929E+01

Table D.17: Several one-dimensional partition functions evaluated at different temperatures for system **S2**.

T(K)	Partition functions for ϕ_2					
	q^{CT}	q^{RPG}	q^{SRPG}	q_{cl}	q^{TPG}	q^{TES}
100	6.107E-01	2.366E-01	4.063E-01	9.022E-01	6.928E-01	7.746E-01
150	1.050E+00	5.136E-01	8.647E-01	1.353E+00	1.199E+00	1.265E+00
200	1.468E+00	7.940E-01	1.290E+00	1.772E+00	1.654E+00	1.706E+00
250	1.870E+00	1.073E+00	1.672E+00	2.163E+00	2.070E+00	2.111E+00
300	2.260E+00	1.353E+00	2.022E+00	2.533E+00	2.457E+00	2.490E+00
400	3.009E+00	1.923E+00	2.654E+00	3.223E+00	3.168E+00	3.191E+00
500	3.721E+00	2.505E+00	3.229E+00	3.865E+00	3.823E+00	3.839E+00
700	5.045E+00	3.679E+00	4.287E+00	5.050E+00	5.021E+00	5.032E+00
1000	6.825E+00	5.387E+00	5.754E+00	6.659E+00	6.640E+00	6.647E+00
1500	9.377E+00	7.968E+00	8.004E+00	9.034E+00	9.023E+00	9.027E+00
2000	1.156E+01	1.023E+01	1.005E+01	1.113E+01	1.112E+01	1.112E+01
2500	1.349E+01	1.223E+01	1.193E+01	1.301E+01	1.300E+01	1.300E+01

Table D.18: Several ratios evaluated at different temperatures for system **S2**. It also includes the two-dimensional partition function $Q_{\mathrm{tor}}^{\mathrm{2D-NS}}$.

T(K)	$F^{\mathrm{HO-NM}}$	$F^{\mathrm{TPG(C)}}$	$F^{\mathrm{MC-TPG(C)}}$	F^{TES}	$F^{\mathrm{2D-NS}}$	$Q_{\mathrm{tor}}^{\mathrm{2D-NS}}$
100.0	0.477	0.487	0.487	0.535	0.563	1.495E-01
150.0	0.711	0.717	0.719	0.754	0.773	4.711E-01
200.0	0.827	0.827	0.830	0.855	0.867	9.694E-01
250.0	0.888	0.885	0.889	0.908	0.915	1.676E+00
300.0	0.922	0.918	0.923	0.937	0.942	2.627E+00
400.0	0.958	0.953	0.957	0.967	0.969	5.357E+00
500.0	0.974	0.970	0.973	0.980	0.981	9.271E+00
700.0	0.987	0.984	0.986	0.991	1.000	2.096E+01
1000.0	0.994	0.992	0.993	0.996	1.000	4.714E+01
1500.0	0.997	0.997	0.997	0.999	1.000	1.114E+02
2000.0	0.998	0.998	0.998	0.999	1.000	1.952E+02
2500.0	0.999	0.999	0.999	1.000	1.000	2.929E+02

Table D.19: Several rovibrational partition functions evaluated at different temperatures for system **S2**.

T(K)	Multidimensional partition functions				
	$\tilde{Q}_{\mathrm{rv}}^{\mathrm{1W-H}}$	$\tilde{Q}_{\mathrm{rv}}^{\mathrm{MC-H}}$	$\tilde{Q}_{\mathrm{rv}}^{\mathrm{MS-T(U)}}$	$\tilde{Q}_{\mathrm{rv}}^{\mathrm{MS-T(C)}}$	$\tilde{Q}_{\mathrm{rv}}^{\mathrm{EHR}}$
100.0	1.469E+04	1.472E+04	1.556E+04	1.388E+04	1.323E+04
150.0	3.389E+04	3.530E+04	3.883E+04	3.449E+04	3.337E+04
200.0	6.949E+04	7.880E+04	9.037E+04	7.928E+04	7.465E+04
250.0	1.336E+05	1.696E+05	2.019E+05	1.741E+05	1.569E+05
300.0	2.468E+05	3.536E+05	4.334E+05	3.668E+05	3.161E+05
400.0	7.868E+05	1.404E+06	1.777E+06	1.459E+06	1.170E+06
500.0	2.366E+06	5.036E+06	6.393E+06	5.141E+06	3.948E+06
700.0	1.876E+07	5.093E+07	6.210E+07	4.893E+07	3.694E+07
1000.0	3.108E+08	1.044E+09	1.147E+09	8.973E+08	6.915E+08
1500.0	1.716E+10	6.917E+10	6.308E+10	4.969E+10	4.114E+10
2000.0	5.009E+11	2.224E+12	1.713E+12	1.364E+12	1.201E+12
2500.0	9.107E+12	4.292E+13	2.849E+13	2.295E+13	2.117E+13

Table D.20: Several one-dimensional partition functions evaluated at different temperatures for system **S3**.

T(K)	Partition functions for ϕ_1					
	q^{CT}	q^{RPG}	q^{SRPG}	q_{cl}	q^{TPG}	q^{TES}
100	2.555E-01	5.966E-01	2.585E-01	2.698E-01	1.575E-01	1.673E-01
150	4.550E-01	1.038E+00	4.500E-01	4.098E-01	3.184E-01	3.304E-01
200	6.464E-01	1.466E+00	6.356E-01	5.537E-01	4.790E-01	4.917E-01
250	8.340E-01	1.887E+00	8.201E-01	7.029E-01	6.400E-01	6.532E-01
300	1.023E+00	2.308E+00	1.008E+00	8.600E-01	8.055E-01	8.190E-01
400	1.419E+00	3.155E+00	1.415E+00	1.212E+00	1.168E+00	1.182E+00
500	1.863E+00	4.021E+00	1.885E+00	1.633E+00	1.595E+00	1.611E+00
700	2.929E+00	5.825E+00	3.070E+00	2.720E+00	2.687E+00	2.705E+00
1000	4.951E+00	8.668E+00	5.380E+00	4.864E+00	4.835E+00	4.855E+00
1500	9.085E+00	1.349E+01	9.982E+00	9.135E+00	9.111E+00	9.130E+00
2000	1.364E+01	1.812E+01	1.480E+01	1.359E+01	1.357E+01	1.359E+01
2500	1.822E+01	2.246E+01	1.949E+01	1.792E+01	1.790E+01	1.791E+01

Table D.21: Several one-dimensional partition functions evaluated at different temperatures for system **S3**.

T(K)	Partition functions for ϕ_2					
	q^{CT}	q^{RPG}	q^{SRPG}	q_{cl}	q^{TPG}	q^{TES}
100	5.956E-02	9.014E-02	6.811E-02	2.458E-01	1.318E-01	1.361E-01
150	1.558E-01	2.589E-01	1.956E-01	3.706E-01	2.760E-01	2.816E-01
200	2.590E-01	4.498E-01	3.399E-01	4.967E-01	4.192E-01	4.252E-01
250	3.608E-01	6.427E-01	4.856E-01	6.243E-01	5.593E-01	5.657E-01
300	4.601E-01	8.336E-01	6.299E-01	7.535E-01	6.978E-01	7.043E-01
400	6.533E-01	1.211E+00	9.154E-01	1.018E+00	9.745E-01	9.813E-01
500	8.440E-01	1.587E+00	1.203E+00	1.292E+00	1.257E+00	1.264E+00
700	1.237E+00	2.356E+00	1.807E+00	1.882E+00	1.856E+00	1.863E+00
1000	1.902E+00	3.554E+00	2.802E+00	2.870E+00	2.850E+00	2.858E+00
1500	3.253E+00	5.578E+00	4.607E+00	4.674E+00	4.659E+00	4.667E+00
2000	4.838E+00	7.527E+00	6.436E+00	6.508E+00	6.496E+00	6.504E+00
2500	6.544E+00	9.357E+00	8.202E+00	8.280E+00	8.271E+00	8.278E+00

Table D.22: Several ratios evaluated at different temperatures for system **S3**. It also includes the two-dimensional partition function $Q_{\mathrm{tor}}^{\mathrm{2D-NS}}$.

T(K)	$F^{\mathrm{HO-NM}}$	$F^{\mathrm{TPG(C)}}$	$F^{\mathrm{MC-TPG(C)}}$	F^{TES}	$F^{\mathrm{2D-NS}}$	$Q_{\mathrm{tor}}^{\mathrm{2D-NS}}$
100.0	0.245	0.229	0.229	0.343	0.187	1.140E-02
150.0	0.507	0.489	0.489	0.613	0.444	6.178E-02
200.0	0.673	0.659	0.659	0.760	0.627	1.580E-01
250.0	0.774	0.762	0.763	0.842	0.745	3.004E-01
300.0	0.837	0.826	0.829	0.890	0.821	4.948E-01
400.0	0.909	0.897	0.904	0.941	0.907	1.099E+00
500.0	0.945	0.932	0.942	0.964	0.949	2.136E+00
700.0	0.976	0.965	0.974	0.985	0.982	6.226E+00
1000.0	0.990	0.983	0.989	0.994	1.000	1.928E+01
1500.0	0.996	0.992	0.996	0.998	1.000	6.042E+01
2000.0	0.998	0.996	0.998	0.999	1.000	1.223E+02
2500.0	0.999	0.997	0.999	1.000	1.000	1.995E+02

Table D.23: Several rovibrational partition functions evaluated at different temperatures for system **S3**.

T(K)	Multidimensional partition functions				
	$\tilde{Q}_{\mathrm{rv}}^{\mathrm{1W-H}}$	$\tilde{Q}_{\mathrm{rv}}^{\mathrm{MC-H}}$	$\tilde{Q}_{\mathrm{rv}}^{\mathrm{MS-T(U)}}$	$\tilde{Q}_{\mathrm{rv}}^{\mathrm{MS-T(C)}}$	$\tilde{Q}_{\mathrm{rv}}^{\mathrm{EHR}}$
100.0	7.063E+03	7.187E+03	7.283E+03	6.139E+03	7.627E+03
150.0	1.547E+04	1.566E+04	1.598E+04	1.355E+04	1.722E+04
200.0	3.002E+04	3.033E+04	3.119E+04	2.664E+04	3.409E+04
250.0	5.461E+04	5.550E+04	5.763E+04	4.968E+04	6.340E+04
300.0	9.560E+04	9.895E+04	1.042E+05	9.072E+04	1.148E+05
400.0	2.744E+05	3.105E+05	3.404E+05	3.021E+05	3.706E+05
500.0	7.487E+05	9.867E+05	1.132E+06	1.016E+06	1.202E+06
700.0	5.048E+06	9.629E+06	1.158E+07	1.044E+07	1.177E+07
1000.0	7.076E+07	2.155E+08	2.513E+08	2.255E+08	2.524E+08
1500.0	3.350E+09	1.643E+10	1.680E+10	1.499E+10	1.694E+10
2000.0	9.023E+10	5.789E+11	5.163E+11	4.591E+11	5.248E+11
2500.0	1.565E+12	1.189E+13	9.356E+12	8.306E+12	9.549E+12

Table D.24: Several one-dimensional partition functions evaluated at different temperatures for system **S4**.

T(K)	Partition functions for ϕ_1					
	q^{CT}	q^{RPG}	q^{SRPG}	q_{cl}	q^{TPG}	q^{TES}
100	3.515E-01	3.781E-01	2.679E-01	5.179E-01	2.614E-01	3.255E-01
150	7.618E-01	8.356E-01	6.590E-01	9.038E-01	6.532E-01	7.461E-01
200	1.184E+00	1.314E+00	1.098E+00	1.321E+00	1.095E+00	1.200E+00
250	1.601E+00	1.792E+00	1.550E+00	1.751E+00	1.551E+00	1.659E+00
300	2.007E+00	2.259E+00	2.001E+00	2.183E+00	2.005E+00	2.111E+00
400	2.784E+00	3.147E+00	2.872E+00	3.023E+00	2.881E+00	2.978E+00
500	3.516E+00	3.969E+00	3.689E+00	3.817E+00	3.701E+00	3.786E+00
700	4.856E+00	5.434E+00	5.157E+00	5.253E+00	5.171E+00	5.237E+00
1000	6.616E+00	7.291E+00	7.030E+00	7.098E+00	7.043E+00	7.091E+00
1500	9.082E+00	9.808E+00	9.575E+00	9.618E+00	9.585E+00	9.615E+00
2000	1.116E+01	1.188E+01	1.167E+01	1.170E+01	1.168E+01	1.170E+01
2500	1.297E+01	1.368E+01	1.349E+01	1.351E+01	1.350E+01	1.351E+01

Table D.25: Several one-dimensional partition functions evaluated at different temperatures for system **S4**.

T(K)	Partition functions for ϕ_2					
	q^{CT}	q^{RPG}	q^{SRPG}	q_{cl}	q^{TPG}	q^{TES}
100	1.318E-01	1.591E-01	1.605E-01	2.736E-01	1.617E-01	1.710E-01
150	2.740E-01	3.194E-01	3.220E-01	4.151E-01	3.245E-01	3.358E-01
200	4.135E-01	4.782E-01	4.822E-01	5.603E-01	4.864E-01	4.984E-01
250	5.484E-01	6.359E-01	6.412E-01	7.094E-01	6.474E-01	6.599E-01
300	6.799E-01	7.944E-01	8.011E-01	8.627E-01	8.094E-01	8.222E-01
400	9.366E-01	1.118E+00	1.127E+00	1.181E+00	1.139E+00	1.153E+00
500	1.188E+00	1.450E+00	1.462E+00	1.512E+00	1.477E+00	1.491E+00
700	1.680E+00	2.124E+00	2.141E+00	2.185E+00	2.159E+00	2.172E+00
1000	2.397E+00	3.110E+00	3.136E+00	3.171E+00	3.152E+00	3.164E+00
1500	3.536E+00	4.608E+00	4.647E+00	4.667E+00	4.655E+00	4.664E+00
2000	4.606E+00	5.926E+00	5.975E+00	5.982E+00	5.973E+00	5.980E+00
2500	5.611E+00	7.097E+00	7.156E+00	7.150E+00	7.143E+00	7.149E+00

Table D.26: Several ratios evaluated at different temperatures for system **S4**. It also includes the two-dimensional partition function $Q_{\mathrm{tor}}^{\mathrm{2D-NS}}$.

T(K)	$F^{\mathrm{HO-NM}}$	$F^{\mathrm{TPG(C)}}$	$F^{\mathrm{MC-TPG(C)}}$	F^{TES}	$F^{\mathrm{2D-NS}}$	$Q_{\mathrm{tor}}^{\mathrm{2D-NS}}$
100.0	0.328	0.326	0.310	0.393	0.368	5.299E-02
150.0	0.591	0.590	0.573	0.668	0.640	2.400E-01
200.0	0.738	0.738	0.725	0.808	0.785	5.738E-01
250.0	0.822	0.822	0.812	0.881	0.862	1.049E+00
300.0	0.872	0.872	0.864	0.922	0.907	1.661E+00
400.0	0.925	0.925	0.921	0.961	0.951	3.274E+00
500.0	0.951	0.951	0.948	0.978	0.970	5.370E+00
700.0	0.975	0.975	0.973	0.991	1.000	1.097E+01
1000.0	0.988	0.988	0.987	0.997	1.000	2.152E+01
1500.0	0.994	0.994	0.994	0.999	1.000	4.315E+01
2000.0	0.997	0.997	0.997	1.000	1.000	6.760E+01
2500.0	0.998	0.998	0.998	1.000	1.000	9.361E+01

Table D.27: Several rovibrational partition functions evaluated at different temperatures for system **S4**.

T(K)	Multidimensional partition functions				
	$\tilde{Q}_{\mathrm{rv}}^{\mathrm{1W-H}}$	$\tilde{Q}_{\mathrm{rv}}^{\mathrm{MC-H}}$	$\tilde{Q}_{\mathrm{rv}}^{\mathrm{MS-T(U)}}$	$\tilde{Q}_{\mathrm{rv}}^{\mathrm{MS-T(C)}}$	$\tilde{Q}_{\mathrm{rv}}^{\mathrm{EHR}}$
100.0	3.287E+03	6.616E+03	7.130E+03	6.863E+03	6.813E+03
150.0	6.986E+03	1.578E+04	1.782E+04	1.716E+04	1.683E+04
200.0	1.317E+04	3.161E+04	3.714E+04	3.576E+04	3.476E+04
250.0	2.330E+04	5.798E+04	7.024E+04	6.760E+04	6.529E+04
300.0	3.966E+04	1.012E+05	1.253E+05	1.205E+05	1.159E+05
400.0	1.082E+05	2.848E+05	3.620E+05	3.479E+05	3.326E+05
500.0	2.842E+05	7.630E+05	9.792E+05	9.407E+05	8.960E+05
700.0	1.856E+06	5.100E+06	6.469E+06	6.213E+06	5.976E+06
1000.0	2.693E+07	7.537E+07	9.019E+07	8.669E+07	8.262E+07
1500.0	1.522E+09	4.320E+09	4.525E+09	4.357E+09	4.140E+09
2000.0	5.201E+10	1.487E+11	1.358E+11	1.310E+11	1.244E+11
2500.0	1.163E+12	3.338E+12	2.682E+12	2.592E+12	2.462E+12

Table D.28: Several one-dimensional partition functions evaluated at different temperatures for system **S5**.

T(K)	Partition functions for ϕ_1					
	q^{CT}	q^{RPG}	q^{SRPG}	q_{cl}	q^{TPG}	q^{TES}
100	6.739E-01	8.624E-01	5.561E-01	7.703E-01	6.846E-01	6.893E-01
150	1.208E+00	1.418E+00	1.018E+00	1.304E+00	1.237E+00	1.242E+00
200	1.769E+00	1.958E+00	1.504E+00	1.874E+00	1.819E+00	1.824E+00
250	2.344E+00	2.494E+00	2.005E+00	2.463E+00	2.416E+00	2.420E+00
300	2.926E+00	3.031E+00	2.515E+00	3.063E+00	3.022E+00	3.026E+00
400	4.101E+00	4.112E+00	3.562E+00	4.286E+00	4.254E+00	4.257E+00
500	5.286E+00	5.215E+00	4.642E+00	5.532E+00	5.505E+00	5.509E+00
700	7.659E+00	7.505E+00	6.900E+00	8.086E+00	8.066E+00	8.070E+00
1000	1.120E+01	1.113E+01	1.050E+01	1.202E+01	1.201E+01	1.201E+01
1500	1.694E+01	1.741E+01	1.673E+01	1.861E+01	1.860E+01	1.861E+01
2000	2.244E+01	2.357E+01	2.286E+01	2.495E+01	2.494E+01	2.494E+01
2500	2.767E+01	2.944E+01	2.870E+01	3.090E+01	3.089E+01	3.090E+01

Table D.29: Several one-dimensional partition functions evaluated at different temperatures for system **S5**.

T(K)	Partition functions for ϕ_2					
	q^{CT}	q^{RPG}	q^{SRPG}	q_{cl}	q^{TPG}	q^{TES}
100	9.898E-03	2.102E-02	1.144E-02	1.127E-01	1.162E-02	1.386E-02
150	4.619E-02	9.648E-02	5.253E-02	1.706E-01	5.199E-02	5.793E-02
200	1.005E-01	2.084E-01	1.135E-01	2.290E-01	1.111E-01	1.196E-01
250	1.619E-01	3.347E-01	1.822E-01	2.879E-01	1.775E-01	1.874E-01
300	2.251E-01	4.649E-01	2.531E-01	3.472E-01	2.460E-01	2.565E-01
400	3.504E-01	7.239E-01	3.943E-01	4.670E-01	3.826E-01	3.933E-01
500	4.728E-01	9.775E-01	5.331E-01	5.889E-01	5.175E-01	5.279E-01
700	7.162E-01	1.474E+00	8.115E-01	8.441E-01	7.896E-01	7.997E-01
1000	1.106E+00	2.217E+00	1.262E+00	1.277E+00	1.235E+00	1.246E+00
1500	1.871E+00	3.498E+00	2.160E+00	2.172E+00	2.141E+00	2.153E+00
2000	2.775E+00	4.838E+00	3.235E+00	3.262E+00	3.235E+00	3.248E+00
2500	3.782E+00	6.211E+00	4.426E+00	4.475E+00	4.452E+00	4.465E+00

Table D.30: Several ratios evaluated at different temperatures for system **S5**. It also includes the two-dimensional partition function $Q_{\mathrm{tor}}^{\mathrm{2D-NS}}$.

T(K)	$F^{\mathrm{HO-NM}}$	$F^{\mathrm{TPG(C)}}$	$F^{\mathrm{MC-TPG(C)}}$	F^{TES}	$F^{\mathrm{2D-NS}}$	$Q_{\mathrm{tor}}^{\mathrm{2D-NS}}$
100.0	0.088	0.100	0.106	0.110	0.113	1.023E-02
150.0	0.286	0.303	0.318	0.323	0.330	7.621E-02
200.0	0.470	0.485	0.502	0.508	0.515	2.289E-01
250.0	0.605	0.618	0.633	0.640	0.646	4.727E-01
300.0	0.700	0.710	0.723	0.730	0.735	8.051E-01
400.0	0.814	0.821	0.830	0.837	0.839	1.727E+00
500.0	0.876	0.880	0.887	0.893	0.894	2.990E+00
700.0	0.934	0.936	0.940	0.945	0.946	6.623E+00
1000.0	0.968	0.968	0.971	0.975	0.975	1.541E+01
1500.0	0.986	0.986	0.987	0.991	1.000	4.198E+01
2000.0	0.993	0.992	0.993	0.996	1.000	8.475E+01
2500.0	0.995	0.995	0.996	0.998	1.000	1.440E+02

Table D.31: Several rovibrational partition functions evaluated at different temperatures for system **S5**.

T(K)	Multidimensional partition functions				
	$\tilde{Q}_{\mathrm{rv}}^{\mathrm{1W-H}}$	$\tilde{Q}_{\mathrm{rv}}^{\mathrm{MC-H}}$	$\tilde{Q}_{\mathrm{rv}}^{\mathrm{MS-T(U)}}$	$\tilde{Q}_{\mathrm{rv}}^{\mathrm{MS-T(C)}}$	$\tilde{Q}_{\mathrm{rv}}^{\mathrm{EHR}}$
100.0	1.749E+04	2.208E+04	2.238E+04	2.037E+04	2.310E+04
150.0	4.163E+04	5.917E+04	6.041E+04	5.479E+04	6.178E+04
200.0	8.731E+04	1.334E+05	1.372E+05	1.242E+05	1.392E+05
250.0	1.727E+05	2.768E+05	2.870E+05	2.595E+05	2.898E+05
300.0	3.317E+05	5.501E+05	5.752E+05	5.198E+05	5.785E+05
400.0	1.168E+06	2.031E+06	2.162E+06	1.953E+06	2.165E+06
500.0	3.963E+06	7.110E+06	7.728E+06	6.979E+06	7.719E+06
700.0	4.103E+07	7.745E+07	8.805E+07	7.942E+07	8.773E+07
1000.0	1.025E+09	2.103E+09	2.553E+09	2.289E+09	2.536E+09
1500.0	1.062E+11	2.569E+11	3.336E+11	2.954E+11	3.359E+11
2000.0	5.332E+12	1.504E+13	1.972E+13	1.732E+13	2.015E+13
2500.0	1.548E+14	4.950E+14	6.324E+14	5.529E+14	6.621E+14

Table D.32: Several one-dimensional partition functions evaluated at different temperatures for system **S6**.

T(K)	Partition functions for ϕ_1					
	q^{CT}	q^{RPG}	q^{SRPG}	q_{cl}	q^{TPG}	q^{TES}
100	1.447E-01	3.100E-01	1.671E-01	3.251E-01	2.256E-01	2.270E-01
150	2.937E-01	6.194E-01	3.338E-01	4.892E-01	4.132E-01	4.147E-01
200	4.388E-01	9.206E-01	4.961E-01	6.535E-01	5.936E-01	5.950E-01
250	5.792E-01	1.213E+00	6.535E-01	8.182E-01	7.690E-01	7.703E-01
300	7.163E-01	1.499E+00	8.078E-01	9.830E-01	9.414E-01	9.427E-01
400	9.844E-01	2.062E+00	1.111E+00	1.313E+00	1.282E+00	1.283E+00
500	1.248E+00	2.619E+00	1.411E+00	1.645E+00	1.619E+00	1.620E+00
700	1.771E+00	3.732E+00	2.012E+00	2.311E+00	2.293E+00	2.294E+00
1000	2.568E+00	5.417E+00	2.940E+00	3.339E+00	3.326E+00	3.327E+00
1500	4.037E+00	8.310E+00	4.668E+00	5.234E+00	5.225E+00	5.226E+00
2000	5.775E+00	1.134E+01	6.734E+00	7.459E+00	7.452E+00	7.453E+00
2500	7.793E+00	1.450E+01	9.143E+00	1.001E+01	1.000E+01	1.000E+01

Table D.33: Several one-dimensional partition functions evaluated at different temperatures for system **S6**.

T(K)	Partition functions for ϕ_2					
	q^{CT}	q^{RPG}	q^{SRPG}	q_{cl}	q^{TPG}	q^{TES}
100	1.540E-03	1.104E-02	6.503E-03	9.067E-02	3.827E-03	5.473E-03
150	1.334E-02	6.268E-02	3.691E-02	1.375E-01	2.484E-02	3.109E-02
200	3.931E-02	1.500E-01	8.835E-02	1.850E-01	6.370E-02	7.450E-02
250	7.542E-02	2.553E-01	1.504E-01	2.330E-01	1.130E-01	1.269E-01
300	1.170E-01	3.675E-01	2.164E-01	2.816E-01	1.672E-01	1.830E-01
400	2.062E-01	5.950E-01	3.504E-01	3.800E-01	2.801E-01	2.972E-01
500	2.961E-01	8.187E-01	4.821E-01	4.801E-01	3.933E-01	4.104E-01
700	4.705E-01	1.254E+00	7.386E-01	6.844E-01	6.170E-01	6.331E-01
1000	7.221E-01	1.894E+00	1.117E+00	1.003E+00	9.525E-01	9.671E-01
1500	1.145E+00	2.971E+00	1.774E+00	1.586E+00	1.550E+00	1.563E+00
2000	1.610E+00	4.087E+00	2.510E+00	2.272E+00	2.243E+00	2.257E+00
2500	2.140E+00	5.245E+00	3.343E+00	3.074E+00	3.049E+00	3.063E+00

Table D.34: Several ratios evaluated at different temperatures for system **S6**. It also includes the two-dimensional partition function $Q_{\mathrm{tor}}^{\mathrm{2D-NS}}$.

T(K)	$F^{\mathrm{HO-NM}}$	$F^{\mathrm{TPG(C)}}$	$F^{\mathrm{MC-TPG(C)}}$	F^{TES}	$F^{\mathrm{2D-NS}}$	$Q_{\mathrm{tor}}^{\mathrm{2D-NS}}$
100.0	0.011	0.049	0.049	0.042	0.051	1.676E-03
150.0	0.088	0.206	0.206	0.192	0.211	1.580E-02
200.0	0.218	0.381	0.381	0.367	0.388	5.184E-02
250.0	0.354	0.524	0.524	0.513	0.531	1.113E-01
300.0	0.471	0.630	0.630	0.623	0.638	1.929E-01
400.0	0.642	0.765	0.765	0.764	0.772	4.177E-01
500.0	0.748	0.840	0.840	0.842	0.847	7.199E-01
700.0	0.860	0.914	0.914	0.918	0.919	1.555E+00
1000.0	0.930	0.957	0.957	0.961	0.961	3.488E+00
1500.0	0.973	0.980	0.982	0.984	1.000	9.911E+00
2000.0	0.988	0.989	0.991	0.992	1.000	2.294E+01
2500.0	0.993	0.993	0.995	0.996	1.000	4.551E+01

Table D.35: Several rovibrational partition functions evaluated at different temperatures for system **S6**.

T(K)	Multidimensional partition functions				
	$\tilde{Q}_{\mathrm{rv}}^{\mathrm{1W-H}}$	$\tilde{Q}_{\mathrm{rv}}^{\mathrm{MC-H}}$	$\tilde{Q}_{\mathrm{rv}}^{\mathrm{MS-T(U)}}$	$\tilde{Q}_{\mathrm{rv}}^{\mathrm{MS-T(C)}}$	$\tilde{Q}_{\mathrm{rv}}^{\mathrm{EHR}}$
100.0	1.345E+04	1.315E+04	1.320E+04	1.133E+04	1.356E+04
150.0	2.836E+04	2.794E+04	2.808E+04	2.412E+04	2.978E+04
200.0	5.429E+04	5.369E+04	5.406E+04	4.645E+04	5.881E+04
250.0	9.946E+04	9.857E+04	9.944E+04	8.549E+04	1.106E+05
300.0	1.781E+05	1.768E+05	1.786E+05	1.537E+05	2.031E+05
400.0	5.539E+05	5.508E+05	5.586E+05	4.812E+05	6.607E+05
500.0	1.689E+06	1.682E+06	1.713E+06	1.477E+06	2.099E+06
700.0	1.487E+07	1.493E+07	1.533E+07	1.325E+07	1.994E+07
1000.0	3.184E+08	3.429E+08	3.612E+08	3.117E+08	4.999E+08
1500.0	2.895E+10	4.395E+10	5.052E+10	4.273E+10	7.555E+10
2000.0	1.365E+12	3.203E+12	3.935E+12	3.268E+12	6.191E+12
2500.0	3.828E+13	1.299E+14	1.627E+14	1.338E+14	2.686E+14

Table D.36: Several one-dimensional partition functions evaluated at different temperatures for system **S7**.

T(K)	Partition functions for ϕ_1					
	q^{CT}	q^{RPG}	q^{SRPG}	q_{cl}	q^{TPG}	q^{TES}
100	6.848E-02	4.909E-02	2.618E-02	1.933E-01	7.472E-02	7.900E-02
150	1.716E-01	1.960E-01	1.045E-01	2.915E-01	1.839E-01	1.903E-01
200	2.803E-01	3.970E-01	2.118E-01	3.910E-01	2.988E-01	3.065E-01
250	3.876E-01	6.168E-01	3.295E-01	4.925E-01	4.134E-01	4.218E-01
300	4.944E-01	8.417E-01	4.512E-01	5.976E-01	5.285E-01	5.378E-01
400	7.171E-01	1.294E+00	7.037E-01	8.256E-01	7.699E-01	7.812E-01
500	9.683E-01	1.750E+00	9.732E-01	1.086E+00	1.038E+00	1.052E+00
700	1.596E+00	2.677E+00	1.571E+00	1.710E+00	1.671E+00	1.688E+00
1000	2.855E+00	4.080E+00	2.575E+00	2.831E+00	2.799E+00	2.818E+00
1500	5.459E+00	6.331E+00	4.321E+00	4.868E+00	4.844E+00	4.862E+00
2000	8.124E+00	8.398E+00	5.997E+00	6.866E+00	6.847E+00	6.863E+00
2500	1.054E+01	1.028E+01	7.553E+00	8.740E+00	8.724E+00	8.737E+00

Table D.37: Several one-dimensional partition functions evaluated at different temperatures for system **S7**.

T(K)	Partition functions for ϕ_2					
	q^{CT}	q^{RPG}	q^{SRPG}	q_{cl}	q^{TPG}	q^{TES}
100	5.827E-01	1.538E+00	5.322E-01	6.778E-01	6.183E-01	6.213E-01
150	9.522E-01	2.496E+00	8.900E-01	1.052E+00	1.009E+00	1.012E+00
200	1.377E+00	3.450E+00	1.308E+00	1.494E+00	1.460E+00	1.464E+00
250	1.878E+00	4.419E+00	1.811E+00	2.024E+00	1.994E+00	1.999E+00
300	2.455E+00	5.412E+00	2.402E+00	2.642E+00	2.614E+00	2.620E+00
400	3.801E+00	7.467E+00	3.823E+00	4.100E+00	4.076E+00	4.083E+00
500	5.344E+00	9.589E+00	5.489E+00	5.778E+00	5.757E+00	5.765E+00
700	8.793E+00	1.388E+01	9.237E+00	9.480E+00	9.462E+00	9.471E+00
1000	1.435E+01	2.009E+01	1.519E+01	1.524E+01	1.523E+01	1.524E+01
1500	2.349E+01	2.941E+01	2.476E+01	2.434E+01	2.433E+01	2.434E+01
2000	3.183E+01	3.753E+01	3.342E+01	3.250E+01	3.249E+01	3.250E+01
2500	3.935E+01	4.472E+01	4.122E+01	3.981E+01	3.980E+01	3.981E+01

Table D.38: Several ratios evaluated at different temperatures for system **S7**. It also includes the two-dimensional partition function $Q_{\mathrm{tor}}^{\mathrm{2D-NS}}$.

T(K)	$F^{\mathrm{HO-NM}}$	$F^{\mathrm{TPG(C)}}$	$F^{\mathrm{MC-TPG(C)}}$	F^{TES}	$F^{\mathrm{2D-NS}}$	$Q_{\mathrm{tor}}^{\mathrm{2D-NS}}$
100.0	0.299	0.338	0.300	0.375	0.329	7.542E-02
150.0	0.550	0.592	0.549	0.629	0.584	3.475E-01
200.0	0.703	0.737	0.702	0.768	0.734	8.651E-01
250.0	0.794	0.819	0.793	0.846	0.821	1.660E+00
300.0	0.850	0.870	0.850	0.892	0.874	2.764E+00
400.0	0.912	0.924	0.912	0.942	0.931	6.035E+00
500.0	0.943	0.950	0.943	0.966	0.959	1.091E+01
700.0	0.971	0.974	0.971	0.986	0.982	2.603E+01
1000.0	0.986	0.987	0.986	0.995	1.000	6.296E+01
1500.0	0.994	0.994	0.994	0.999	1.000	1.554E+02
2000.0	0.997	0.997	0.997	0.999	1.000	2.769E+02
2500.0	0.998	0.998	0.998	1.000	1.000	4.177E+02

Table D.39: Several rovibrational partition functions evaluated at different temperatures for system **S7**.

T(K)	Multidimensional partition functions				
	$\tilde{Q}_{\mathrm{rv}}^{\mathrm{1W-H}}$	$\tilde{Q}_{\mathrm{rv}}^{\mathrm{MC-H}}$	$\tilde{Q}_{\mathrm{rv}}^{\mathrm{MS-T(U)}}$	$\tilde{Q}_{\mathrm{rv}}^{\mathrm{MS-T(C)}}$	$\tilde{Q}_{\mathrm{rv}}^{\mathrm{EHR}}$
100.0	2.112E+04	2.890E+04	2.986E+04	2.879E+04	2.891E+04
150.0	5.345E+04	8.744E+04	9.186E+04	8.827E+04	9.140E+04
200.0	1.206E+05	2.244E+05	2.401E+05	2.303E+05	2.420E+05
250.0	2.583E+05	5.312E+05	5.802E+05	5.556E+05	5.886E+05
300.0	5.372E+05	1.201E+06	1.341E+06	1.281E+06	1.364E+06
400.0	2.214E+06	5.664E+06	6.625E+06	6.274E+06	6.715E+06
500.0	8.734E+06	2.490E+07	3.038E+07	2.849E+07	3.054E+07
700.0	1.205E+08	4.057E+08	5.248E+08	4.838E+08	5.186E+08
1000.0	4.461E+09	1.787E+10	2.365E+10	2.148E+10	2.320E+10
1500.0	8.206E+11	3.926E+12	4.920E+12	4.426E+12	4.785E+12
2000.0	6.737E+13	3.585E+14	4.085E+14	3.669E+14	3.984E+14
2500.0	3.001E+15	1.714E+16	1.761E+16	1.583E+16	1.727E+16

Table D.40: Several one-dimensional partition functions evaluated at different temperatures for system **S8**.

T(K)	Partition functions for ϕ_1					
	q^{CT}	q^{RPG}	q^{SRPG}	q_{cl}	q^{TPG}	q^{TES}
100	1.824E-01	3.852E-01	1.690E-01	3.002E-01	1.919E-01	2.021E-01
150	3.503E-01	8.114E-01	3.563E-01	4.560E-01	3.704E-01	3.805E-01
200	5.206E-01	1.234E+00	5.437E-01	6.148E-01	5.457E-01	5.550E-01
250	7.162E-01	1.647E+00	7.325E-01	7.800E-01	7.223E-01	7.310E-01
300	9.687E-01	2.054E+00	9.297E-01	9.567E-01	9.067E-01	9.154E-01
400	1.747E+00	2.863E+00	1.372E+00	1.361E+00	1.320E+00	1.330E+00
500	2.979E+00	3.678E+00	1.900E+00	1.846E+00	1.810E+00	1.821E+00
700	6.771E+00	5.357E+00	3.223E+00	3.053E+00	3.023E+00	3.036E+00
1000	1.391E+01	8.000E+00	5.734E+00	5.307E+00	5.281E+00	5.296E+00
1500	2.330E+01	1.253E+01	1.061E+01	9.602E+00	9.582E+00	9.596E+00
2000	2.960E+01	1.694E+01	1.566E+01	1.399E+01	1.398E+01	1.399E+01
2500	3.443E+01	2.112E+01	2.055E+01	1.822E+01	1.821E+01	1.822E+01

Table D.41: Several one-dimensional partition functions evaluated at different temperatures for system **S8**.

T(K)	Partition functions for ϕ_2					
	q^{CT}	q^{RPG}	q^{SRPG}	q_{cl}	q^{TPG}	q^{TES}
100	1.563E-01	1.695E-01	1.709E-01	2.937E-01	1.817E-01	1.970E-01
150	3.110E-01	3.345E-01	3.373E-01	4.485E-01	3.585E-01	3.745E-01
200	4.611E-01	4.972E-01	5.013E-01	6.062E-01	5.331E-01	5.483E-01
250	6.062E-01	6.583E-01	6.638E-01	7.668E-01	7.058E-01	7.201E-01
300	7.480E-01	8.201E-01	8.269E-01	9.305E-01	8.782E-01	8.920E-01
400	1.025E+00	1.150E+00	1.159E+00	1.267E+00	1.226E+00	1.240E+00
500	1.297E+00	1.489E+00	1.501E+00	1.614E+00	1.580E+00	1.593E+00
700	1.830E+00	2.182E+00	2.201E+00	2.319E+00	2.294E+00	2.307E+00
1000	2.606E+00	3.210E+00	3.237E+00	3.356E+00	3.338E+00	3.349E+00
1500	3.839E+00	4.793E+00	4.833E+00	4.940E+00	4.929E+00	4.937E+00
2000	4.995E+00	6.197E+00	6.249E+00	6.341E+00	6.332E+00	6.339E+00
2500	6.079E+00	7.451E+00	7.513E+00	7.589E+00	7.583E+00	7.588E+00

Table D.42: Several ratios evaluated at different temperatures for system **S8**. It also includes the two-dimensional partition function $Q_{\mathrm{tor}}^{\mathrm{2D-NS}}$.

T(K)	$F^{\mathrm{HO-NM}}$	$F^{\mathrm{TPG(C)}}$	$F^{\mathrm{MC-TPG(C)}}$	F^{TES}	$F^{\mathrm{2D-NS}}$	$Q_{\mathrm{tor}}^{\mathrm{2D-NS}}$
100.0	0.372	0.383	0.383	0.451	0.412	3.283E-02
150.0	0.630	0.639	0.640	0.697	0.671	1.225E-01
200.0	0.772	0.774	0.778	0.817	0.804	2.677E-01
250.0	0.855	0.847	0.859	0.880	0.876	4.748E-01
300.0	0.906	0.891	0.909	0.917	0.918	7.604E-01
400.0	0.958	0.937	0.959	0.956	0.961	1.658E+00
500.0	0.978	0.959	0.979	0.974	0.980	3.138E+00
700.0	0.992	0.979	0.992	0.989	1.000	8.380E+00
1000.0	0.997	0.990	0.997	0.996	1.000	2.224E+01
1500.0	0.999	0.995	0.999	0.999	1.000	5.976E+01
2000.0	0.999	0.997	0.999	0.999	1.000	1.105E+02
2500.0	1.000	0.998	1.000	1.000	1.000	1.700E+02

Table D.43: Several rovibrational partition functions evaluated at different temperatures for system **S8**.

T(K)	Multidimensional partition functions				
	$\tilde{Q}_{\mathrm{rv}}^{\mathrm{1W-H}}$	$\tilde{Q}_{\mathrm{rv}}^{\mathrm{MC-H}}$	$\tilde{Q}_{\mathrm{rv}}^{\mathrm{MS-T(U)}}$	$\tilde{Q}_{\mathrm{rv}}^{\mathrm{MS-T(C)}}$	$\tilde{Q}_{\mathrm{rv}}^{\mathrm{EHR}}$
100.0	7.234E+03	7.321E+03	7.442E+03	7.186E+03	7.428E+03
150.0	1.595E+04	1.617E+04	1.661E+04	1.604E+04	1.667E+04
200.0	3.163E+04	3.322E+04	3.475E+04	3.308E+04	3.408E+04
250.0	5.948E+04	6.866E+04	7.377E+04	6.747E+04	6.737E+04
300.0	1.086E+05	1.460E+05	1.604E+05	1.387E+05	1.320E+05
400.0	3.475E+05	6.838E+05	7.483E+05	5.839E+05	5.058E+05
500.0	1.085E+06	3.062E+06	3.174E+06	2.325E+06	1.908E+06
700.0	1.009E+07	4.830E+07	4.284E+07	2.982E+07	2.433E+07
1000.0	2.419E+08	1.839E+09	1.298E+09	8.923E+08	7.664E+08
1500.0	2.820E+10	3.166E+11	1.643E+11	1.147E+11	1.080E+11
2000.0	1.759E+12	2.419E+13	9.908E+12	7.061E+12	7.058E+12
2500.0	6.541E+13	1.019E+15	3.442E+14	2.499E+14	2.598E+14

Table D.44: Several one-dimensional partition functions evaluated at different temperatures for system **S9**.

T(K)	Partition functions for ϕ_1					
	q^{CT}	q^{RPG}	q^{SRPG}	q_{cl}	q^{TPG}	q^{TES}
100	7.839E-01	7.972E-01	6.761E-01	7.377E-01	4.787E-01	5.739E-01
150	1.312E+00	1.425E+00	1.185E+00	1.145E+00	9.369E-01	1.025E+00
200	1.836E+00	2.038E+00	1.699E+00	1.576E+00	1.405E+00	1.484E+00
250	2.374E+00	2.648E+00	2.238E+00	2.038E+00	1.892E+00	1.964E+00
300	2.934E+00	3.265E+00	2.811E+00	2.535E+00	2.408E+00	2.475E+00
400	4.123E+00	4.530E+00	4.068E+00	3.635E+00	3.530E+00	3.591E+00
500	5.391E+00	5.837E+00	5.447E+00	4.845E+00	4.755E+00	4.812E+00
700	8.066E+00	8.519E+00	8.406E+00	7.445E+00	7.374E+00	7.425E+00
1000	1.214E+01	1.250E+01	1.293E+01	1.142E+01	1.137E+01	1.141E+01
1500	1.850E+01	1.864E+01	1.999E+01	1.763E+01	1.760E+01	1.763E+01
2000	2.415E+01	2.410E+01	2.627E+01	2.316E+01	2.314E+01	2.316E+01
2500	2.917E+01	2.897E+01	3.189E+01	2.810E+01	2.808E+01	2.810E+01

Table D.45: Several one-dimensional partition functions evaluated at different temperatures for system **S9**.

T(K)	Partition functions for ϕ_2					
	q^{CT}	q^{RPG}	q^{SRPG}	q_{cl}	q^{TPG}	q^{TES}
100	2.394E-01	2.569E-01	2.019E-01	5.020E-01	2.500E-01	2.913E-01
150	5.448E-01	6.218E-01	5.240E-01	8.207E-01	5.892E-01	6.530E-01
200	8.760E-01	1.015E+00	9.019E-01	1.184E+00	9.773E-01	1.054E+00
250	1.218E+00	1.416E+00	1.304E+00	1.572E+00	1.388E+00	1.470E+00
300	1.564E+00	1.818E+00	1.714E+00	1.971E+00	1.807E+00	1.890E+00
400	2.259E+00	2.613E+00	2.529E+00	2.770E+00	2.637E+00	2.716E+00
500	2.943E+00	3.381E+00	3.313E+00	3.543E+00	3.433E+00	3.505E+00
700	4.249E+00	4.810E+00	4.759E+00	4.975E+00	4.895E+00	4.954E+00
1000	6.032E+00	6.691E+00	6.651E+00	6.853E+00	6.799E+00	6.843E+00
1500	8.589E+00	9.307E+00	9.265E+00	9.456E+00	9.423E+00	9.451E+00
2000	1.077E+01	1.149E+01	1.144E+01	1.162E+01	1.160E+01	1.162E+01
2500	1.267E+01	1.338E+01	1.333E+01	1.351E+01	1.349E+01	1.351E+01

Table D.46: Several ratios evaluated at different temperatures for system **S9**. It also includes the two-dimensional partition function $Q_{\mathrm{tor}}^{\mathrm{2D-NS}}$.

T(K)	$F^{\mathrm{HO-NM}}$	$F^{\mathrm{TPG(C)}}$	$F^{\mathrm{MC-TPG(C)}}$	F^{TES}	$F^{\mathrm{2D-NS}}$	$Q_{\mathrm{tor}}^{\mathrm{2D-NS}}$
100.0	0.384	0.355	0.362	0.451	0.424	1.753E-01
150.0	0.640	0.613	0.620	0.712	0.686	6.891E-01
200.0	0.777	0.754	0.763	0.838	0.821	1.603E+00
250.0	0.852	0.833	0.842	0.901	0.892	2.986E+00
300.0	0.897	0.880	0.889	0.936	0.931	4.909E+00
400.0	0.943	0.930	0.938	0.969	0.968	1.053E+01
500.0	0.964	0.955	0.961	0.983	0.983	1.858E+01
700.0	0.982	0.977	0.981	0.993	1.000	4.163E+01
1000.0	0.992	0.988	0.991	0.997	1.000	8.871E+01
1500.0	0.996	0.995	0.996	0.999	1.000	1.889E+02
2000.0	0.998	0.997	0.998	1.000	1.000	3.043E+02
2500.0	0.999	0.998	0.999	1.000	1.000	4.279E+02

Table D.47: Several rovibrational partition functions evaluated at different temperatures for system **S9**.

T(K)	Multidimensional partition functions				
	$\tilde{Q}_{\mathrm{rv}}^{\mathrm{1W-H}}$	$\tilde{Q}_{\mathrm{rv}}^{\mathrm{MC-H}}$	$\tilde{Q}_{\mathrm{rv}}^{\mathrm{MS-T(U)}}$	$\tilde{Q}_{\mathrm{rv}}^{\mathrm{MS-T(C)}}$	$\tilde{Q}_{\mathrm{rv}}^{\mathrm{EHR}}$
100.0	1.695E+04	3.119E+04	3.294E+04	2.978E+04	2.860E+04
150.0	3.900E+04	8.060E+04	8.842E+04	8.016E+04	7.898E+04
200.0	8.032E+04	1.828E+05	2.090E+05	1.896E+05	1.887E+05
250.0	1.562E+05	3.884E+05	4.613E+05	4.177E+05	4.180E+05
300.0	2.941E+05	7.933E+05	9.722E+05	8.777E+05	8.821E+05
400.0	9.955E+05	3.087E+06	3.936E+06	3.531E+06	3.575E+06
500.0	3.271E+06	1.133E+07	1.463E+07	1.307E+07	1.332E+07
700.0	3.308E+07	1.341E+08	1.691E+08	1.505E+08	1.560E+08
1000.0	8.655E+08	4.047E+09	4.659E+09	4.149E+09	4.333E+09
1500.0	1.093E+11	5.799E+11	5.570E+11	4.983E+11	5.265E+11
2000.0	7.091E+12	4.030E+13	3.262E+13	2.934E+13	3.124E+13
2500.0	2.694E+14	1.598E+15	1.110E+15	1.004E+15	1.074E+15

Table D.48: Several one-dimensional partition functions evaluated at different temperatures for system **S10**.

T(K)	Partition functions for ϕ_1					
	q^{CT}	q^{RPG}	q^{SRPG}	q_{cl}	q^{TPG}	q^{TES}
100	4.753E-02	9.923E-02	4.907E-02	1.667E-01	4.936E-02	5.271E-02
150	1.335E-01	2.768E-01	1.370E-01	2.515E-01	1.379E-01	1.436E-01
200	2.307E-01	4.749E-01	2.361E-01	3.388E-01	2.378E-01	2.451E-01
250	3.321E-01	6.743E-01	3.389E-01	4.311E-01	3.419E-01	3.506E-01
300	4.386E-01	8.718E-01	4.458E-01	5.308E-01	4.509E-01	4.611E-01
400	6.730E-01	1.263E+00	6.783E-01	7.582E-01	6.908E-01	7.041E-01
500	9.404E-01	1.657E+00	9.421E-01	1.025E+00	9.655E-01	9.815E-01
700	1.566E+00	2.463E+00	1.562E+00	1.662E+00	1.612E+00	1.632E+00
1000	2.664E+00	3.713E+00	2.654E+00	2.782E+00	2.741E+00	2.763E+00
1500	4.685E+00	5.789E+00	4.627E+00	4.789E+00	4.757E+00	4.779E+00
2000	6.714E+00	7.750E+00	6.570E+00	6.749E+00	6.723E+00	6.743E+00
2500	8.639E+00	9.566E+00	8.399E+00	8.587E+00	8.567E+00	8.583E+00

Table D.49: Several one-dimensional partition functions evaluated at different temperatures for system **S10**.

T(K)	Partition functions for ϕ_2					
	q^{CT}	q^{RPG}	q^{SRPG}	q_{cl}	q^{TPG}	q^{TES}
100	2.942E-01	2.719E-01	2.719E-01	3.949E-01	3.022E-01	3.122E-01
150	5.101E-01	4.893E-01	4.893E-01	6.021E-01	5.327E-01	5.439E-01
200	7.165E-01	7.069E-01	7.069E-01	8.168E-01	7.619E-01	7.739E-01
250	9.169E-01	9.282E-01	9.282E-01	1.039E+00	9.931E-01	1.006E+00
300	1.113E+00	1.153E+00	1.153E+00	1.265E+00	1.227E+00	1.239E+00
400	1.497E+00	1.610E+00	1.610E+00	1.725E+00	1.695E+00	1.708E+00
500	1.869E+00	2.063E+00	2.063E+00	2.181E+00	2.156E+00	2.169E+00
700	2.583E+00	2.932E+00	2.932E+00	3.050E+00	3.032E+00	3.043E+00
1000	3.582E+00	4.111E+00	4.111E+00	4.225E+00	4.213E+00	4.222E+00
1500	5.075E+00	5.785E+00	5.785E+00	5.891E+00	5.883E+00	5.889E+00
2000	6.396E+00	7.197E+00	7.197E+00	7.295E+00	7.290E+00	7.294E+00
2500	7.583E+00	8.429E+00	8.429E+00	8.520E+00	8.516E+00	8.519E+00

Table D.50: Several ratios evaluated at different temperatures for system **S10**. It also includes the two-dimensional partition function $Q_{\mathrm{tor}}^{\mathrm{2D-NS}}$.

T(K)	$F^{\mathrm{HO-NM}}$	$F^{\mathrm{TPG(C)}}$	$F^{\mathrm{MC-TPG(C)}}$	F^{TES}	$F^{\mathrm{2D-NS}}$	$Q_{\mathrm{tor}}^{\mathrm{2D-NS}}$
100.0	0.222	0.227	0.227	0.250	0.248	1.629E-02
150.0	0.480	0.486	0.486	0.516	0.513	7.734E-02
200.0	0.652	0.655	0.656	0.686	0.682	1.875E-01
250.0	0.758	0.759	0.761	0.788	0.784	3.477E-01
300.0	0.826	0.824	0.828	0.851	0.848	5.619E-01
400.0	0.901	0.895	0.901	0.919	0.917	1.174E+00
500.0	0.938	0.931	0.938	0.952	0.950	2.066E+00
700.0	0.971	0.964	0.970	0.980	0.979	4.786E+00
1000.0	0.987	0.982	0.986	0.992	1.000	1.132E+01
1500.0	0.995	0.992	0.994	0.998	1.000	2.726E+01
2000.0	0.997	0.996	0.997	0.999	1.000	4.782E+01
2500.0	0.998	0.997	0.998	0.999	1.000	7.138E+01

Table D.51: Several rovibrational partition functions evaluated at different temperatures for system **S10**.

T(K)	Multidimensional partition functions				
	$\tilde{Q}_{\mathrm{rv}}^{\mathrm{1W-H}}$	$\tilde{Q}_{\mathrm{rv}}^{\mathrm{MC-H}}$	$\tilde{Q}_{\mathrm{rv}}^{\mathrm{MS-T(U)}}$	$\tilde{Q}_{\mathrm{rv}}^{\mathrm{MS-T(C)}}$	$\tilde{Q}_{\mathrm{rv}}^{\mathrm{EHR}}$
100.0	8.447E+03	8.422E+03	8.694E+03	8.361E+03	8.561E+03
150.0	1.840E+04	1.839E+04	1.933E+04	1.860E+04	1.909E+04
200.0	3.623E+04	3.651E+04	3.918E+04	3.767E+04	3.874E+04
250.0	6.865E+04	7.040E+04	7.741E+04	7.421E+04	7.622E+04
300.0	1.280E+05	1.348E+05	1.522E+05	1.452E+05	1.483E+05
400.0	4.362E+05	4.936E+05	5.884E+05	5.528E+05	5.547E+05
500.0	1.464E+06	1.797E+06	2.240E+06	2.072E+06	2.040E+06
700.0	1.552E+07	2.213E+07	2.895E+07	2.613E+07	2.512E+07
1000.0	4.279E+08	7.214E+08	9.412E+08	8.338E+08	8.017E+08
1500.0	5.680E+10	1.133E+11	1.353E+11	1.186E+11	1.147E+11
2000.0	3.786E+12	8.329E+12	8.847E+12	7.748E+12	7.588E+12
2500.0	1.463E+14	3.426E+14	3.235E+14	2.838E+14	2.812E+14

Table D.52: Several one-dimensional partition functions evaluated at different temperatures for system **S11**.

T(K)	Partition functions for ϕ_1					
	q^{CT}	q^{RPG}	q^{SRPG}	q_{cl}	q^{TPG}	q^{TES}
100	1.069E-01	1.774E-01	8.761E-02	2.112E-01	8.069E-02	9.362E-02
150	2.759E-01	4.169E-01	2.275E-01	3.610E-01	2.264E-01	2.515E-01
200	4.797E-01	6.657E-01	3.979E-01	5.405E-01	4.117E-01	4.444E-01
250	7.037E-01	9.134E-01	5.882E-01	7.414E-01	6.208E-01	6.579E-01
300	9.409E-01	1.161E+00	7.936E-01	9.582E-01	8.460E-01	8.854E-01
400	1.439E+00	1.661E+00	1.240E+00	1.426E+00	1.329E+00	1.370E+00
500	1.954E+00	2.171E+00	1.720E+00	1.925E+00	1.839E+00	1.881E+00
700	2.997E+00	3.211E+00	2.733E+00	2.962E+00	2.894E+00	2.934E+00
1000	4.520E+00	4.747E+00	4.266E+00	4.511E+00	4.460E+00	4.495E+00
1500	6.853E+00	7.113E+00	6.652E+00	6.901E+00	6.866E+00	6.893E+00
2000	8.928E+00	9.213E+00	8.777E+00	9.019E+00	8.993E+00	9.015E+00
2500	1.079E+01	1.109E+01	1.067E+01	1.091E+01	1.089E+01	1.091E+01

Table D.53: Several one-dimensional partition functions evaluated at different temperatures for system **S11**.

T(K)	Partition functions for ϕ_2					
	q^{CT}	q^{RPG}	q^{SRPG}	q_{cl}	q^{TPG}	q^{TES}
100	1.249E+00	1.039E+00	1.039E+00	1.198E+00	1.169E+00	1.180E+00
150	1.748E+00	1.562E+00	1.562E+00	1.702E+00	1.684E+00	1.694E+00
200	2.176E+00	2.011E+00	2.011E+00	2.138E+00	2.125E+00	2.134E+00
250	2.554E+00	2.407E+00	2.407E+00	2.523E+00	2.513E+00	2.521E+00
300	2.895E+00	2.762E+00	2.762E+00	2.870E+00	2.862E+00	2.868E+00
400	3.497E+00	3.383E+00	3.383E+00	3.479E+00	3.473E+00	3.478E+00
500	4.021E+00	3.922E+00	3.922E+00	4.008E+00	4.004E+00	4.007E+00
700	4.920E+00	4.838E+00	4.838E+00	4.912E+00	4.910E+00	4.912E+00
1000	6.036E+00	5.970E+00	5.970E+00	6.032E+00	6.031E+00	6.032E+00
1500	7.549E+00	7.496E+00	7.496E+00	7.548E+00	7.547E+00	7.548E+00
2000	8.810E+00	8.766E+00	8.766E+00	8.810E+00	8.810E+00	8.810E+00
2500	9.914E+00	9.875E+00	9.875E+00	9.915E+00	9.915E+00	9.915E+00

Table D.54: Several ratios evaluated at different temperatures for system **S11**. It also includes the two-dimensional partition function $Q_{\mathrm{tor}}^{\mathrm{2D-NS}}$.

T(K)	$F^{\mathrm{HO-NM}}$	$F^{\mathrm{TPG(C)}}$	$F^{\mathrm{MC-TPG(C)}}$	F^{TES}	$F^{\mathrm{2D-NS}}$	$Q_{\mathrm{tor}}^{\mathrm{2D-NS}}$
100.0	0.447	0.349	0.360	0.437	0.387	8.908E-02
150.0	0.689	0.599	0.620	0.693	0.648	3.457E-01
200.0	0.811	0.741	0.764	0.820	0.788	7.697E-01
250.0	0.876	0.822	0.843	0.886	0.865	1.350E+00
300.0	0.913	0.872	0.890	0.923	0.908	2.080E+00
400.0	0.951	0.925	0.938	0.960	0.953	3.960E+00
500.0	0.969	0.951	0.960	0.977	0.973	6.362E+00
700.0	0.984	0.975	0.980	0.990	1.000	1.265E+01
1000.0	0.992	0.987	0.990	0.996	1.000	2.436E+01
1500.0	0.997	0.994	0.996	0.999	1.000	4.812E+01
2000.0	0.998	0.997	0.998	1.000	1.000	7.484E+01
2500.0	0.999	0.998	0.999	1.000	1.000	1.032E+02

Table D.55: Several rovibrational partition functions evaluated at different temperatures for system **S11**.

T(K)	Multidimensional partition functions				
	$\tilde{Q}_{\mathrm{rv}}^{\mathrm{1W-H}}$	$\tilde{Q}_{\mathrm{rv}}^{\mathrm{MC-H}}$	$\tilde{Q}_{\mathrm{rv}}^{\mathrm{MS-T(U)}}$	$\tilde{Q}_{\mathrm{rv}}^{\mathrm{MS-T(C)}}$	$\tilde{Q}_{\mathrm{rv}}^{\mathrm{EHR}}$
100.0	1.665E+04	1.758E+04	2.076E+04	1.388E+04	1.521E+04
150.0	4.566E+04	5.191E+04	6.215E+04	4.020E+04	4.260E+04
200.0	1.049E+05	1.270E+05	1.518E+05	9.646E+04	1.002E+05
250.0	2.201E+05	2.809E+05	3.336E+05	2.098E+05	2.155E+05
300.0	4.390E+05	5.848E+05	6.887E+05	4.305E+05	4.389E+05
400.0	1.613E+06	2.292E+06	2.634E+06	1.638E+06	1.664E+06
500.0	5.599E+06	8.332E+06	9.252E+06	5.768E+06	5.882E+06
700.0	6.053E+07	9.570E+07	9.743E+07	6.162E+07	6.462E+07
1000.0	1.667E+09	2.774E+09	2.441E+09	1.588E+09	1.697E+09
1500.0	2.186E+11	3.801E+11	2.654E+11	1.802E+11	1.982E+11
2000.0	1.444E+13	2.569E+13	1.468E+13	1.030E+13	1.155E+13
2500.0	5.544E+14	1.000E+15	4.807E+14	3.464E+14	3.936E+14

Table D.56: Several one-dimensional partition functions evaluated at different temperatures for system **S12**.

T(K)	Partition functions for ϕ_1					
	q^{CT}	q^{RPG}	q^{SRPG}	q_{cl}	q^{TPG}	q^{TES}
100	2.985E-01	5.962E-01	2.882E-01	4.518E-01	3.710E-01	3.717E-01
150	5.164E-01	1.036E+00	5.006E-01	6.786E-01	6.206E-01	6.214E-01
200	7.254E-01	1.459E+00	7.055E-01	9.064E-01	8.615E-01	8.624E-01
250	9.307E-01	1.875E+00	9.078E-01	1.136E+00	1.100E+00	1.101E+00
300	1.137E+00	2.288E+00	1.112E+00	1.370E+00	1.340E+00	1.341E+00
400	1.564E+00	3.112E+00	1.536E+00	1.862E+00	1.839E+00	1.840E+00
500	2.030E+00	3.942E+00	1.999E+00	2.400E+00	2.380E+00	2.382E+00
700	3.104E+00	5.639E+00	3.077E+00	3.640E+00	3.625E+00	3.627E+00
1000	5.044E+00	8.306E+00	5.081E+00	5.890E+00	5.878E+00	5.881E+00
1500	8.879E+00	1.302E+01	9.180E+00	1.032E+01	1.031E+01	1.031E+01
2000	1.311E+01	1.786E+01	1.374E+01	1.510E+01	1.509E+01	1.510E+01
2500	1.750E+01	2.262E+01	1.841E+01	1.990E+01	1.990E+01	1.990E+01

Table D.57: Several one-dimensional partition functions evaluated at different temperatures for system **S12**.

T(K)	Partition functions for ϕ_2					
	q^{CT}	q^{RPG}	q^{SRPG}	q_{cl}	q^{TPG}	q^{TES}
100	3.981E-01	4.326E-01	4.326E-01	5.205E-01	4.400E-01	4.577E-01
150	6.573E-01	7.389E-01	7.389E-01	8.100E-01	7.507E-01	7.703E-01
200	9.053E-01	1.051E+00	1.051E+00	1.113E+00	1.066E+00	1.086E+00
250	1.146E+00	1.363E+00	1.363E+00	1.419E+00	1.381E+00	1.400E+00
300	1.381E+00	1.670E+00	1.670E+00	1.722E+00	1.689E+00	1.708E+00
400	1.835E+00	2.257E+00	2.257E+00	2.303E+00	2.279E+00	2.295E+00
500	2.270E+00	2.803E+00	2.803E+00	2.845E+00	2.825E+00	2.840E+00
700	3.087E+00	3.780E+00	3.780E+00	3.816E+00	3.803E+00	3.813E+00
1000	4.194E+00	5.023E+00	5.023E+00	5.054E+00	5.045E+00	5.052E+00
1500	5.795E+00	6.714E+00	6.714E+00	6.739E+00	6.734E+00	6.738E+00
2000	7.175E+00	8.112E+00	8.112E+00	8.133E+00	8.130E+00	8.133E+00
2500	8.395E+00	9.324E+00	9.324E+00	9.343E+00	9.341E+00	9.343E+00

Table D.58: Several ratios evaluated at different temperatures for system **S12**. It also includes the two-dimensional partition function $Q_{\mathrm{tor}}^{\mathrm{2D-NS}}$.

T(K)	$F^{\mathrm{HO-NM}}$	$F^{\mathrm{TPG(C)}}$	$F^{\mathrm{MC-TPG(C)}}$	F^{TES}	$F^{\mathrm{2D-NS}}$	$Q_{\mathrm{tor}}^{\mathrm{2D-NS}}$
100.0	0.644	0.698	0.698	0.723	0.720	1.669E-01
150.0	0.818	0.849	0.849	0.871	0.869	4.706E-01
200.0	0.892	0.912	0.912	0.929	0.928	9.211E-01
250.0	0.930	0.942	0.942	0.956	0.955	1.515E+00
300.0	0.950	0.960	0.960	0.970	0.970	2.251E+00
400.0	0.972	0.977	0.977	0.984	0.984	4.148E+00
500.0	0.982	0.985	0.985	0.991	1.000	6.705E+00
700.0	0.991	0.992	0.993	0.996	1.000	1.364E+01
1000.0	0.996	0.996	0.996	0.998	1.000	2.927E+01
1500.0	0.998	0.998	0.998	0.999	1.000	6.871E+01
2000.0	0.999	0.999	0.999	1.000	1.000	1.220E+02
2500.0	0.999	0.999	0.999	1.000	1.000	1.857E+02

Table D.59: Several rovibrational partition functions evaluated at different temperatures for system **S12**.

T(K)	Multidimensional partition functions				
	$\tilde{Q}_{\mathrm{rv}}^{\mathrm{1W-H}}$	$\tilde{Q}_{\mathrm{rv}}^{\mathrm{MC-H}}$	$\tilde{Q}_{\mathrm{rv}}^{\mathrm{MS-T(U)}}$	$\tilde{Q}_{\mathrm{rv}}^{\mathrm{MS-T(C)}}$	$\tilde{Q}_{\mathrm{rv}}^{\mathrm{EHR}}$
100.0	1.944E+04	1.978E+04	2.044E+04	1.786E+04	2.147E+04
150.0	5.243E+04	5.303E+04	5.591E+04	4.885E+04	6.126E+04
200.0	1.267E+05	1.279E+05	1.379E+05	1.205E+05	1.548E+05
250.0	2.879E+05	2.907E+05	3.212E+05	2.808E+05	3.634E+05
300.0	6.292E+05	6.379E+05	7.219E+05	6.315E+05	8.143E+05
400.0	2.808E+06	2.906E+06	3.432E+06	3.011E+06	3.778E+06
500.0	1.185E+07	1.270E+07	1.552E+07	1.367E+07	1.667E+07
700.0	1.860E+08	2.185E+08	2.788E+08	2.480E+08	2.800E+08
1000.0	8.530E+09	1.149E+10	1.483E+10	1.335E+10	1.417E+10
1500.0	2.326E+12	3.713E+12	4.517E+12	4.116E+12	4.303E+12
2000.0	2.827E+14	5.041E+14	5.577E+14	5.117E+14	5.459E+14
2500.0	1.819E+16	3.497E+16	3.493E+16	3.221E+16	3.523E+16

Table D.60: Several one-dimensional partition functions evaluated at different temperatures for system **S13**.

T(K)	Partition functions for ϕ_1					
	q^{CT}	q^{RPG}	q^{SRPG}	q_{cl}	q^{TPG}	q^{TES}
100	6.498E-01	1.102E+00	5.003E-01	6.693E-01	6.020E-01	6.041E-01
150	1.115E+00	1.860E+00	9.399E-01	1.125E+00	1.073E+00	1.073E+00
200	1.655E+00	2.600E+00	1.463E+00	1.679E+00	1.635E+00	1.634E+00
250	2.252E+00	3.339E+00	2.059E+00	2.311E+00	2.271E+00	2.271E+00
300	2.892E+00	4.086E+00	2.714E+00	3.002E+00	2.967E+00	2.967E+00
400	4.255E+00	5.618E+00	4.165E+00	4.519E+00	4.488E+00	4.491E+00
500	5.686E+00	7.206E+00	5.750E+00	6.156E+00	6.129E+00	6.133E+00
700	8.639E+00	1.050E+01	9.129E+00	9.607E+00	9.586E+00	9.592E+00
1000	1.310E+01	1.550E+01	1.430E+01	1.483E+01	1.481E+01	1.482E+01
1500	2.024E+01	2.341E+01	2.242E+01	2.299E+01	2.298E+01	2.298E+01
2000	2.687E+01	3.055E+01	2.971E+01	3.028E+01	3.027E+01	3.028E+01
2500	3.298E+01	3.699E+01	3.625E+01	3.681E+01	3.681E+01	3.681E+01

Table D.61: Several one-dimensional partition functions evaluated at different temperatures for system **S13**.

T(K)	Partition functions for ϕ_2					
	q^{CT}	q^{RPG}	q^{SRPG}	q_{cl}	q^{TPG}	q^{TES}
100	1.527E-01	1.516E-01	8.316E-02	2.280E-01	8.884E-02	9.978E-02
150	3.648E-01	3.726E-01	2.306E-01	3.939E-01	2.494E-01	2.706E-01
200	6.057E-01	6.060E-01	4.098E-01	5.826E-01	4.464E-01	4.731E-01
250	8.601E-01	8.384E-01	6.050E-01	7.860E-01	6.607E-01	6.901E-01
300	1.122E+00	1.070E+00	8.105E-01	9.996E-01	8.851E-01	9.158E-01
400	1.656E+00	1.535E+00	1.245E+00	1.450E+00	1.353E+00	1.385E+00
500	2.194E+00	2.009E+00	1.704E+00	1.922E+00	1.839E+00	1.871E+00
700	3.257E+00	2.980E+00	2.666E+00	2.903E+00	2.838E+00	2.870E+00
1000	4.777E+00	4.439E+00	4.132E+00	4.380E+00	4.331E+00	4.360E+00
1500	7.075E+00	6.730E+00	6.451E+00	6.692E+00	6.659E+00	6.682E+00
2000	9.110E+00	8.794E+00	8.544E+00	8.768E+00	8.743E+00	8.762E+00
2500	1.094E+01	1.065E+01	1.043E+01	1.063E+01	1.061E+01	1.063E+01

Table D.62: Several ratios evaluated at different temperatures for system **S13**. It also includes the two-dimensional partition function $Q_{\mathrm{tor}}^{\mathrm{2D-NS}}$.

T(K)	$F^{\mathrm{HO-NM}}$	$F^{\mathrm{TPG(C)}}$	$F^{\mathrm{MC-TPG(C)}}$	F^{TES}	$F^{\mathrm{2D-NS}}$	$Q_{\mathrm{tor}}^{\mathrm{2D-NS}}$
100.0	0.485	0.335	0.353	0.395	0.366	5.267E-02
150.0	0.703	0.590	0.606	0.655	0.620	2.412E-01
200.0	0.806	0.735	0.744	0.790	0.756	6.089E-01
250.0	0.863	0.818	0.822	0.863	0.834	1.181E+00
300.0	0.897	0.869	0.870	0.905	0.881	1.978E+00
400.0	0.937	0.923	0.922	0.949	0.932	4.328E+00
500.0	0.958	0.950	0.949	0.970	0.958	7.801E+00
700.0	0.977	0.974	0.973	0.987	0.981	1.852E+01
1000.0	0.989	0.987	0.987	0.995	1.000	4.492E+01
1500.0	0.995	0.994	0.994	0.998	1.000	1.131E+02
2000.0	0.997	0.997	0.997	0.999	1.000	2.059E+02
2500.0	0.998	0.998	0.998	1.000	1.000	3.166E+02

Table D.63: Several rovibrational partition functions evaluated at different temperatures for system **S13**.

T(K)	Multidimensional partition functions				
	$\tilde{Q}_{\mathrm{rv}}^{\mathrm{1W-H}}$	$\tilde{Q}_{\mathrm{rv}}^{\mathrm{MC-H}}$	$\tilde{Q}_{\mathrm{rv}}^{\mathrm{MS-T(U)}}$	$\tilde{Q}_{\mathrm{rv}}^{\mathrm{MS-T(C)}}$	$\tilde{Q}_{\mathrm{rv}}^{\mathrm{EHR}}$
100.0	2.114E+04	2.668E+04	2.745E+04	2.193E+04	2.628E+04
150.0	5.760E+04	8.368E+04	8.753E+04	7.011E+04	8.303E+04
200.0	1.383E+05	2.259E+05	2.405E+05	1.931E+05	2.268E+05
250.0	3.111E+05	5.581E+05	6.055E+05	4.874E+05	5.693E+05
300.0	6.754E+05	1.306E+06	1.444E+06	1.165E+06	1.357E+06
400.0	3.015E+06	6.510E+06	7.472E+06	6.043E+06	7.056E+06
500.0	1.290E+07	3.015E+07	3.574E+07	2.892E+07	3.412E+07
700.0	2.116E+08	5.504E+08	6.849E+08	5.536E+08	6.741E+08
1000.0	1.029E+10	2.951E+10	3.813E+10	3.069E+10	3.962E+10
1500.0	2.953E+12	9.276E+12	1.200E+13	9.603E+12	1.315E+13
2000.0	3.657E+14	1.210E+15	1.505E+15	1.202E+15	1.712E+15
2500.0	2.366E+16	8.091E+16	9.516E+16	7.599E+16	1.110E+17

Table D.64: Several one-dimensional partition functions evaluated at different temperatures for system **S14**.

T(K)	Partition functions for ϕ_1					
	q^{CT}	q^{RPG}	q^{SRPG}	q_{cl}	q^{TPG}	q^{TES}
100	4.064E-01	6.809E-01	2.951E-01	5.135E-01	4.401E-01	4.410E-01
150	6.701E-01	1.249E+00	5.413E-01	7.714E-01	7.194E-01	7.203E-01
200	9.254E-01	1.797E+00	7.802E-01	1.031E+00	9.911E-01	9.919E-01
250	1.181E+00	2.334E+00	1.019E+00	1.296E+00	1.264E+00	1.265E+00
300	1.445E+00	2.866E+00	1.265E+00	1.573E+00	1.546E+00	1.547E+00
400	2.026E+00	3.929E+00	1.811E+00	2.185E+00	2.163E+00	2.165E+00
500	2.711E+00	5.003E+00	2.451E+00	2.896E+00	2.878E+00	2.880E+00
700	4.425E+00	7.218E+00	4.036E+00	4.623E+00	4.608E+00	4.611E+00
1000	7.739E+00	1.072E+01	7.020E+00	7.795E+00	7.782E+00	7.787E+00
1500	1.445E+01	1.680E+01	1.281E+01	1.381E+01	1.380E+01	1.380E+01
2000	2.163E+01	2.284E+01	1.884E+01	1.996E+01	1.995E+01	1.996E+01
2500	2.859E+01	2.863E+01	2.471E+01	2.590E+01	2.589E+01	2.590E+01

Table D.65: Several one-dimensional partition functions evaluated at different temperatures for system **S14**.

T(K)	Partition functions for ϕ_2					
	q^{CT}	q^{RPG}	q^{SRPG}	q_{cl}	q^{TPG}	q^{TES}
100	7.020E-02	5.464E-02	2.673E-02	1.951E-01	7.667E-02	8.030E-02
150	1.758E-01	2.108E-01	1.040E-01	2.951E-01	1.877E-01	1.934E-01
200	2.927E-01	4.203E-01	2.118E-01	4.011E-01	3.081E-01	3.156E-01
250	4.204E-01	6.475E-01	3.376E-01	5.180E-01	4.362E-01	4.457E-01
300	5.628E-01	8.796E-01	4.780E-01	6.488E-01	5.751E-01	5.867E-01
400	8.992E-01	1.347E+00	7.993E-01	9.545E-01	8.913E-01	9.069E-01
500	1.302E+00	1.819E+00	1.169E+00	1.313E+00	1.256E+00	1.275E+00
700	2.263E+00	2.778E+00	2.009E+00	2.139E+00	2.091E+00	2.113E+00
1000	3.910E+00	4.218E+00	3.385E+00	3.498E+00	3.460E+00	3.483E+00
1500	6.664E+00	6.498E+00	5.668E+00	5.757E+00	5.728E+00	5.749E+00
2000	9.115E+00	8.568E+00	7.779E+00	7.845E+00	7.823E+00	7.840E+00
2500	1.125E+01	1.044E+01	9.698E+00	9.745E+00	9.728E+00	9.742E+00

Table D.66: Several ratios evaluated at different temperatures for system **S14**. It also includes the two-dimensional partition function $Q_{\mathrm{tor}}^{\mathrm{2D-NS}}$.

T(K)	$F^{\mathrm{HO-NM}}$	$F^{\mathrm{TPG(C)}}$	$F^{\mathrm{MC-TPG(C)}}$	F^{TES}	$F^{\mathrm{2D-NS}}$	$Q_{\mathrm{tor}}^{\mathrm{2D-NS}}$
100.0	0.314	0.350	0.350	0.353	0.353	3.521E-02
150.0	0.574	0.605	0.606	0.612	0.612	1.383E-01
200.0	0.726	0.747	0.750	0.757	0.757	3.108E-01
250.0	0.815	0.828	0.832	0.840	0.839	5.599E-01
300.0	0.869	0.876	0.881	0.889	0.888	9.022E-01
400.0	0.927	0.928	0.933	0.941	0.940	1.953E+00
500.0	0.955	0.953	0.958	0.966	0.964	3.650E+00
700.0	0.978	0.976	0.979	0.986	0.984	9.657E+00
1000.0	0.989	0.988	0.990	0.995	1.000	2.701E+01
1500.0	0.995	0.995	0.995	0.998	1.000	7.900E+01
2000.0	0.997	0.997	0.997	0.999	1.000	1.564E+02
2500.0	0.998	0.998	0.998	1.000	1.000	2.533E+02

Table D.67: Several rovibrational partition functions evaluated at different temperatures for system **S14**.

T(K)	Multidimensional partition functions				
	$\tilde{Q}_{\mathrm{rv}}^{\mathrm{1W-H}}$	$\tilde{Q}_{\mathrm{rv}}^{\mathrm{MC-H}}$	$\tilde{Q}_{\mathrm{rv}}^{\mathrm{MS-T(U)}}$	$\tilde{Q}_{\mathrm{rv}}^{\mathrm{MS-T(C)}}$	$\tilde{Q}_{\mathrm{rv}}^{\mathrm{EHR}}$
100.0	1.746E+04	1.717E+04	1.758E+04	1.640E+04	1.755E+04
150.0	4.150E+04	4.130E+04	4.286E+04	4.000E+04	4.304E+04
200.0	9.028E+04	9.213E+04	9.713E+04	9.052E+04	9.786E+04
250.0	1.902E+05	2.032E+05	2.182E+05	2.026E+05	2.193E+05
300.0	3.957E+05	4.511E+05	4.955E+05	4.574E+05	4.934E+05
400.0	1.693E+06	2.278E+06	2.627E+06	2.392E+06	2.537E+06
500.0	7.150E+06	1.151E+07	1.390E+07	1.249E+07	1.298E+07
700.0	1.177E+08	2.614E+08	3.363E+08	2.974E+08	3.001E+08
1000.0	5.839E+09	1.835E+10	2.428E+10	2.128E+10	2.143E+10
1500.0	1.721E+12	7.617E+12	9.603E+12	8.410E+12	8.631E+12
2000.0	2.166E+14	1.166E+15	1.344E+15	1.181E+15	1.246E+15
2500.0	1.416E+16	8.642E+16	9.024E+16	7.962E+16	8.596E+16

Table D.68: Several one-dimensional partition functions evaluated at different temperatures for system **S15**.

T(K)	Partition functions for ϕ_1					
	q^{CT}	q^{RPG}	q^{SRPG}	q_{cl}	q^{TPG}	q^{TES}
100	5.598E-01	7.574E-01	3.696E-01	5.438E-01	4.708E-01	4.735E-01
150	1.155E+00	1.267E+00	6.406E-01	8.670E-01	8.124E-01	8.164E-01
200	2.087E+00	1.762E+00	9.369E-01	1.250E+00	1.204E+00	1.209E+00
250	3.340E+00	2.250E+00	1.262E+00	1.684E+00	1.644E+00	1.650E+00
300	4.850E+00	2.738E+00	1.613E+00	2.157E+00	2.122E+00	2.128E+00
400	8.312E+00	3.720E+00	2.380E+00	3.187E+00	3.157E+00	3.163E+00
500	1.185E+01	4.719E+00	3.216E+00	4.287E+00	4.262E+00	4.267E+00
700	1.807E+01	6.787E+00	5.044E+00	6.613E+00	6.593E+00	6.598E+00
1000	2.516E+01	1.006E+01	8.066E+00	1.026E+01	1.024E+01	1.025E+01
1500	3.373E+01	1.575E+01	1.344E+01	1.638E+01	1.637E+01	1.637E+01
2000	4.037E+01	2.138E+01	1.881E+01	2.227E+01	2.226E+01	2.226E+01
2500	4.598E+01	2.676E+01	2.397E+01	2.780E+01	2.779E+01	2.779E+01

Table D.69: Several one-dimensional partition functions evaluated at different temperatures for system **S15**.

T(K)	Partition functions for ϕ_2					
	q^{CT}	q^{RPG}	q^{SRPG}	q_{cl}	q^{TPG}	q^{TES}
100	3.577E-01	4.195E-01	4.195E-01	4.974E-01	4.147E-01	4.320E-01
150	6.001E-01	7.189E-01	7.189E-01	7.745E-01	7.132E-01	7.329E-01
200	8.320E-01	1.024E+00	1.024E+00	1.066E+00	1.018E+00	1.038E+00
250	1.057E+00	1.330E+00	1.330E+00	1.363E+00	1.323E+00	1.343E+00
300	1.277E+00	1.631E+00	1.631E+00	1.658E+00	1.624E+00	1.644E+00
400	1.705E+00	2.208E+00	2.208E+00	2.228E+00	2.201E+00	2.219E+00
500	2.117E+00	2.746E+00	2.746E+00	2.760E+00	2.740E+00	2.755E+00
700	2.895E+00	3.710E+00	3.710E+00	3.719E+00	3.704E+00	3.716E+00
1000	3.963E+00	4.940E+00	4.940E+00	4.944E+00	4.934E+00	4.942E+00
1500	5.523E+00	6.613E+00	6.613E+00	6.614E+00	6.608E+00	6.613E+00
2000	6.879E+00	7.997E+00	7.997E+00	7.996E+00	7.993E+00	7.996E+00
2500	8.084E+00	9.197E+00	9.197E+00	9.196E+00	9.193E+00	9.196E+00

Table D.70: Several ratios evaluated at different temperatures for system **S15**. It also includes the two-dimensional partition function $Q_{\mathrm{tor}}^{\mathrm{2D-NS}}$.

T(K)	$F^{\mathrm{HO-NM}}$	$F^{\mathrm{TPG(C)}}$	$F^{\mathrm{MC-TPG(C)}}$	F^{TES}	$F^{\mathrm{2D-NS}}$	$Q_{\mathrm{tor}}^{\mathrm{2D-NS}}$
100.0	0.733	0.710	0.717	0.756	0.753	2.055E-01
150.0	0.884	0.856	0.871	0.891	0.892	6.286E-01
200.0	0.939	0.916	0.930	0.942	0.944	1.357E+00
250.0	0.963	0.945	0.957	0.965	0.967	2.420E+00
300.0	0.975	0.962	0.971	0.977	0.978	3.819E+00
400.0	0.987	0.978	0.985	0.989	1.000	7.659E+00
500.0	0.992	0.986	0.990	0.993	1.000	1.259E+01
700.0	0.996	0.993	0.995	0.997	1.000	2.559E+01
1000.0	0.998	0.996	0.998	0.999	1.000	5.186E+01
1500.0	0.999	0.998	0.999	1.000	1.000	1.098E+02
2000.0	1.000	0.999	0.999	1.000	1.000	1.803E+02
2500.0	1.000	0.999	1.000	1.000	1.000	2.591E+02

Table D.71: Several rovibrational partition functions evaluated at different temperatures for system **S15**.

T(K)	Multidimensional partition functions				
	$\tilde{Q}_{\mathrm{rv}}^{\mathrm{1W-H}}$	$\tilde{Q}_{\mathrm{rv}}^{\mathrm{MC-H}}$	$\tilde{Q}_{\mathrm{rv}}^{\mathrm{MS-T(U)}}$	$\tilde{Q}_{\mathrm{rv}}^{\mathrm{MS-T(C)}}$	$\tilde{Q}_{\mathrm{rv}}^{\mathrm{EHR}}$
100.0	2.277E+04	2.571E+04	2.731E+04	2.143E+04	2.540E+04
150.0	6.578E+04	1.011E+05	1.157E+05	7.142E+04	8.562E+04
200.0	1.670E+05	3.534E+05	4.275E+05	2.141E+05	2.507E+05
250.0	3.922E+05	1.072E+06	1.326E+06	5.807E+05	6.559E+05
300.0	8.751E+05	2.907E+06	3.594E+06	1.452E+06	1.584E+06
400.0	3.982E+06	1.728E+07	2.051E+07	7.705E+06	8.046E+06
500.0	1.687E+07	8.687E+07	9.676E+07	3.567E+07	3.592E+07
700.0	2.633E+08	1.662E+09	1.601E+09	6.009E+08	5.918E+08
1000.0	1.190E+10	8.796E+10	6.881E+10	2.736E+10	2.760E+10
1500.0	3.188E+12	2.675E+13	1.558E+13	6.766E+12	7.359E+12
2000.0	3.833E+14	3.432E+15	1.573E+15	7.304E+14	8.498E+14
2500.0	2.448E+16	2.280E+17	8.552E+16	4.184E+16	5.130E+16

Table D.72: Several one-dimensional partition functions evaluated at different temperatures for system **S16**.

T(K)	Partition functions for ϕ_1					
	q^{CT}	q^{RPG}	q^{SRPG}	q_{cl}	q^{TPG}	q^{TES}
100	1.162E+00	1.146E+00	1.100E+00	1.201E+00	9.750E-01	1.030E+00
150	2.042E+00	1.939E+00	1.971E+00	1.968E+00	1.790E+00	1.843E+00
200	2.915E+00	2.731E+00	2.870E+00	2.769E+00	2.624E+00	2.674E+00
250	3.780E+00	3.539E+00	3.801E+00	3.600E+00	3.478E+00	3.526E+00
300	4.636E+00	4.367E+00	4.760E+00	4.456E+00	4.350E+00	4.397E+00
400	6.316E+00	6.064E+00	6.732E+00	6.210E+00	6.127E+00	6.170E+00
500	7.949E+00	7.781E+00	8.723E+00	7.974E+00	7.906E+00	7.946E+00
700	1.106E+01	1.114E+01	1.260E+01	1.140E+01	1.135E+01	1.138E+01
1000	1.536E+01	1.580E+01	1.795E+01	1.610E+01	1.607E+01	1.610E+01
1500	2.167E+01	2.253E+01	2.563E+01	2.286E+01	2.284E+01	2.286E+01
2000	2.716E+01	2.826E+01	3.216E+01	2.859E+01	2.858E+01	2.859E+01
2500	3.204E+01	3.329E+01	3.787E+01	3.361E+01	3.359E+01	3.361E+01

Table D.73: Several one-dimensional partition functions evaluated at different temperatures for system **S16**.

T(K)	Partition functions for ϕ_2					
	q^{CT}	q^{RPG}	q^{SRPG}	q_{cl}	q^{TPG}	q^{TES}
100	1.493E-01	1.497E-01	1.509E-01	2.715E-01	1.598E-01	1.675E-01
150	3.005E-01	3.043E-01	3.068E-01	4.110E-01	3.206E-01	3.299E-01
200	4.475E-01	4.573E-01	4.611E-01	5.531E-01	4.796E-01	4.894E-01
250	5.898E-01	6.081E-01	6.132E-01	6.982E-01	6.367E-01	6.467E-01
300	7.286E-01	7.587E-01	7.650E-01	8.463E-01	7.936E-01	8.038E-01
400	9.999E-01	1.064E+00	1.073E+00	1.152E+00	1.111E+00	1.122E+00
500	1.266E+00	1.378E+00	1.389E+00	1.469E+00	1.435E+00	1.446E+00
700	1.788E+00	2.024E+00	2.041E+00	2.124E+00	2.099E+00	2.109E+00
1000	2.549E+00	2.999E+00	3.024E+00	3.106E+00	3.088E+00	3.098E+00
1500	3.761E+00	4.532E+00	4.569E+00	4.644E+00	4.631E+00	4.640E+00
2000	4.900E+00	5.913E+00	5.962E+00	6.024E+00	6.015E+00	6.021E+00
2500	5.970E+00	7.156E+00	7.216E+00	7.264E+00	7.257E+00	7.263E+00

Table D.74: Several ratios evaluated at different temperatures for system **S16**. It also includes the two-dimensional partition function $Q_{\mathrm{tor}}^{\mathrm{2D-NS}}$.

T(K)	$F^{\mathrm{HO-NM}}$	$F^{\mathrm{TPG(C)}}$	$F^{\mathrm{MC-TPG(C)}}$	F^{TES}	$F^{\mathrm{2D-NS}}$	$Q_{\mathrm{tor}}^{\mathrm{2D-NS}}$
100.0	0.559	0.462	0.550	0.529	0.575	2.234E-01
150.0	0.765	0.699	0.759	0.752	0.781	7.587E-01
200.0	0.859	0.814	0.855	0.855	0.873	1.612E+00
250.0	0.907	0.876	0.904	0.907	0.920	2.795E+00
300.0	0.934	0.912	0.932	0.937	0.946	4.324E+00
400.0	0.962	0.949	0.961	0.967	0.972	8.464E+00
500.0	0.976	0.967	0.975	0.981	0.984	1.405E+01
700.0	0.988	0.983	0.987	0.992	1.000	2.941E+01
1000.0	0.994	0.992	0.994	0.997	1.000	6.014E+01
1500.0	0.997	0.996	0.997	0.999	1.000	1.254E+02
2000.0	0.998	0.998	0.998	1.000	1.000	2.007E+02
2500.0	0.999	0.999	0.999	1.000	1.000	2.818E+02

Table D.75: Several rovibrational partition functions evaluated at different temperatures for system **S16**.

T(K)	Multidimensional partition functions				
	$\tilde{Q}_{\mathrm{rv}}^{\mathrm{1W-H}}$	$\tilde{Q}_{\mathrm{rv}}^{\mathrm{MC-H}}$	$\tilde{Q}_{\mathrm{rv}}^{\mathrm{MS-T(U)}}$	$\tilde{Q}_{\mathrm{rv}}^{\mathrm{MS-T(C)}}$	$\tilde{Q}_{\mathrm{rv}}^{\mathrm{EHR}}$
100.0	1.014E+04	3.809E+04	3.972E+04	2.864E+04	2.927E+04
150.0	2.380E+04	9.138E+04	9.775E+04	7.585E+04	7.852E+04
200.0	5.037E+04	1.983E+05	2.184E+05	1.758E+05	1.828E+05
250.0	1.012E+05	4.065E+05	4.622E+05	3.803E+05	3.960E+05
300.0	1.981E+05	8.083E+05	9.483E+05	7.918E+05	8.240E+05
400.0	7.372E+05	3.075E+06	3.817E+06	3.243E+06	3.369E+06
500.0	2.725E+06	1.153E+07	1.493E+07	1.281E+07	1.329E+07
700.0	3.671E+07	1.580E+08	2.135E+08	1.853E+08	1.932E+08
1000.0	1.583E+09	6.903E+09	9.297E+09	8.142E+09	8.451E+09
1500.0	4.789E+11	2.110E+12	2.618E+12	2.315E+12	2.397E+12
2000.0	7.145E+13	3.164E+14	3.520E+14	3.135E+14	3.240E+14
2500.0	5.818E+15	2.584E+16	2.573E+16	2.306E+16	2.380E+16

Table D.76: Several one-dimensional partition functions evaluated at different temperatures for system **S17**.

T(K)	Partition functions for ϕ_1					
	q^{CT}	q^{RPG}	q^{SRPG}	q_{cl}	q^{TPG}	q^{TES}
100	5.083E-01	5.165E-01	5.165E-01	5.811E-01	5.051E-01	5.267E-01
150	8.121E-01	8.712E-01	8.712E-01	9.123E-01	8.564E-01	8.800E-01
200	1.101E+00	1.225E+00	1.225E+00	1.252E+00	1.208E+00	1.231E+00
250	1.380E+00	1.569E+00	1.569E+00	1.587E+00	1.551E+00	1.573E+00
300	1.648E+00	1.898E+00	1.898E+00	1.910E+00	1.879E+00	1.899E+00
400	2.158E+00	2.509E+00	2.509E+00	2.513E+00	2.490E+00	2.507E+00
500	2.636E+00	3.063E+00	3.063E+00	3.061E+00	3.044E+00	3.058E+00
700	3.509E+00	4.031E+00	4.031E+00	4.025E+00	4.013E+00	4.023E+00
1000	4.655E+00	5.242E+00	5.242E+00	5.233E+00	5.226E+00	5.232E+00
1500	6.263E+00	6.875E+00	6.875E+00	6.865E+00	6.860E+00	6.864E+00
2000	7.619E+00	8.222E+00	8.222E+00	8.212E+00	8.209E+00	8.212E+00
2500	8.807E+00	9.391E+00	9.391E+00	9.381E+00	9.379E+00	9.381E+00

Table D.77: Several one-dimensional partition functions evaluated at different temperatures for system **S17**.

T(K)	Partition functions for ϕ_2					
	q^{CT}	q^{RPG}	q^{SRPG}	q_{cl}	q^{TPG}	q^{TES}
100	5.083E-01	5.165E-01	5.165E-01	5.811E-01	5.051E-01	5.267E-01
150	8.121E-01	8.712E-01	8.712E-01	9.123E-01	8.564E-01	8.800E-01
200	1.101E+00	1.225E+00	1.225E+00	1.252E+00	1.208E+00	1.231E+00
250	1.380E+00	1.569E+00	1.569E+00	1.587E+00	1.551E+00	1.573E+00
300	1.648E+00	1.898E+00	1.898E+00	1.910E+00	1.879E+00	1.899E+00
400	2.158E+00	2.509E+00	2.509E+00	2.513E+00	2.490E+00	2.507E+00
500	2.636E+00	3.063E+00	3.063E+00	3.061E+00	3.044E+00	3.058E+00
700	3.509E+00	4.031E+00	4.031E+00	4.025E+00	4.013E+00	4.023E+00
1000	4.655E+00	5.242E+00	5.242E+00	5.233E+00	5.226E+00	5.232E+00
1500	6.263E+00	6.875E+00	6.875E+00	6.865E+00	6.860E+00	6.864E+00
2000	7.619E+00	8.222E+00	8.222E+00	8.212E+00	8.209E+00	8.212E+00
2500	8.807E+00	9.391E+00	9.391E+00	9.381E+00	9.379E+00	9.381E+00

Table D.78: Several ratios evaluated at different temperatures for system **S17**. It also includes the two-dimensional partition function $Q_{\mathrm{tor}}^{\mathrm{2D-NS}}$.

T(K)	$F^{\mathrm{HO-NM}}$	$F^{\mathrm{TPG(C)}}$	$F^{\mathrm{MC-TPG(C)}}$	F^{TES}	$F^{\mathrm{2D-NS}}$	$Q_{\mathrm{tor}}^{\mathrm{2D-NS}}$
100.0	0.764	0.755	0.755	0.821	0.819	2.731E-01
150.0	0.886	0.881	0.881	0.930	0.931	7.708E-01
200.0	0.934	0.931	0.931	0.967	0.968	1.521E+00
250.0	0.957	0.955	0.955	0.982	0.983	2.492E+00
300.0	0.970	0.969	0.969	0.989	1.000	3.682E+00
400.0	0.983	0.982	0.982	0.995	1.000	6.394E+00
500.0	0.989	0.989	0.989	0.998	1.000	9.496E+00
700.0	0.994	0.994	0.994	0.999	1.000	1.640E+01
1000.0	0.997	0.997	0.997	1.000	1.000	2.769E+01
1500.0	0.999	0.999	0.999	1.000	1.000	4.756E+01
2000.0	0.999	0.999	0.999	1.000	1.000	6.798E+01
2500.0	1.000	1.000	1.000	1.000	1.000	8.864E+01

Table D.79: Several rovibrational partition functions evaluated at different temperatures for system **S17**.

T(K)	Multidimensional partition functions				
	$\tilde{Q}_{\mathrm{rv}}^{\mathrm{1W-H}}$	$\tilde{Q}_{\mathrm{rv}}^{\mathrm{MC-H}}$	$\tilde{Q}_{\mathrm{rv}}^{\mathrm{MS-T(U)}}$	$\tilde{Q}_{\mathrm{rv}}^{\mathrm{MS-T(C)}}$	$\tilde{Q}_{\mathrm{rv}}^{\mathrm{EHR}}$
100.0	6.596E+03	6.567E+03	7.566E+03	6.950E+03	7.935E+03
150.0	1.866E+04	1.861E+04	2.330E+04	2.140E+04	2.523E+04
200.0	4.559E+04	4.550E+04	6.032E+04	5.536E+04	6.585E+04
250.0	1.023E+05	1.022E+05	1.395E+05	1.280E+05	1.521E+05
300.0	2.185E+05	2.182E+05	3.007E+05	2.759E+05	3.295E+05
400.0	9.215E+05	9.205E+05	1.244E+06	1.142E+06	1.339E+06
500.0	3.703E+06	3.700E+06	4.773E+06	4.390E+06	5.079E+06
700.0	5.519E+07	5.515E+07	6.314E+07	5.825E+07	6.624E+07
1000.0	2.571E+09	2.570E+09	2.447E+09	2.268E+09	2.543E+09
1500.0	8.261E+11	8.258E+11	6.020E+11	5.618E+11	6.228E+11
2000.0	1.270E+14	1.270E+14	7.442E+13	6.983E+13	7.698E+13
2500.0	1.053E+16	1.053E+16	5.147E+15	4.850E+15	5.329E+15

Table D.80: Several one-dimensional partition functions evaluated at different temperatures for system **S18**.

T(K)	Partition functions for ϕ_1					
	q^{CT}	q^{RPG}	q^{SRPG}	q_{cl}	q^{TPG}	q^{TES}
100	2.444E-01	6.985E-01	3.143E-01	5.264E-01	4.545E-01	4.553E-01
150	4.392E-01	1.274E+00	5.734E-01	7.907E-01	7.400E-01	7.407E-01
200	6.266E-01	1.830E+00	8.244E-01	1.057E+00	1.018E+00	1.019E+00
250	8.121E-01	2.375E+00	1.074E+00	1.328E+00	1.296E+00	1.297E+00
300	1.003E+00	2.914E+00	1.328E+00	1.610E+00	1.584E+00	1.585E+00
400	1.424E+00	3.992E+00	1.875E+00	2.230E+00	2.209E+00	2.211E+00
500	1.925E+00	5.082E+00	2.496E+00	2.946E+00	2.928E+00	2.930E+00
700	3.201E+00	7.331E+00	3.981E+00	4.675E+00	4.661E+00	4.664E+00
1000	5.720E+00	1.088E+01	6.707E+00	7.851E+00	7.840E+00	7.844E+00
1500	1.096E+01	1.706E+01	1.194E+01	1.389E+01	1.388E+01	1.389E+01
2000	1.685E+01	2.319E+01	1.736E+01	2.010E+01	2.009E+01	2.010E+01
2500	2.289E+01	2.907E+01	2.265E+01	2.610E+01	2.610E+01	2.610E+01

Table D.81: Several one-dimensional partition functions evaluated at different temperatures for system **S18**.

T(K)	Partition functions for ϕ_2					
	q^{CT}	q^{RPG}	q^{SRPG}	q_{cl}	q^{TPG}	q^{TES}
100	1.372E-01	6.591E-01	3.223E-01	4.983E-01	4.231E-01	4.240E-01
150	2.841E-01	1.125E+00	5.528E-01	7.534E-01	6.997E-01	7.006E-01
200	4.341E-01	1.575E+00	7.840E-01	1.024E+00	9.823E-01	9.835E-01
250	5.898E-01	2.017E+00	1.025E+00	1.319E+00	1.284E+00	1.285E+00
300	7.538E-01	2.456E+00	1.281E+00	1.640E+00	1.610E+00	1.611E+00
400	1.109E+00	3.333E+00	1.837E+00	2.356E+00	2.331E+00	2.333E+00
500	1.497E+00	4.216E+00	2.449E+00	3.154E+00	3.133E+00	3.135E+00
700	2.344E+00	6.019E+00	3.806E+00	4.929E+00	4.912E+00	4.914E+00
1000	3.719E+00	8.843E+00	6.098E+00	7.880E+00	7.866E+00	7.869E+00
1500	6.143E+00	1.384E+01	1.037E+01	1.319E+01	1.318E+01	1.318E+01
2000	8.641E+00	1.901E+01	1.488E+01	1.863E+01	1.862E+01	1.862E+01
2500	1.117E+01	2.415E+01	1.942E+01	2.397E+01	2.397E+01	2.397E+01

Table D.82: Several ratios evaluated at different temperatures for system **S18**. It also includes the two-dimensional partition function $Q_{\mathrm{tor}}^{\mathrm{2D-NS}}$.

T(K)	$F^{\mathrm{HO-NM}}$	$F^{\mathrm{TPG(C)}}$	$F^{\mathrm{MC-TPG(C)}}$	F^{TES}	$F^{\mathrm{2D-NS}}$	$Q_{\mathrm{tor}}^{\mathrm{2D-NS}}$
100.0	0.394	0.646	0.646	0.736	0.656	1.462E-01
150.0	0.648	0.818	0.819	0.871	0.825	4.170E-01
200.0	0.781	0.892	0.892	0.926	0.896	8.202E-01
250.0	0.854	0.929	0.930	0.952	0.932	1.371E+00
300.0	0.897	0.950	0.951	0.967	0.952	2.094E+00
400.0	0.943	0.972	0.972	0.982	0.973	4.174E+00
500.0	0.964	0.982	0.982	0.989	0.983	7.319E+00
700.0	0.983	0.991	0.991	0.995	1.000	1.799E+01
1000.0	0.992	0.995	0.996	0.998	1.000	4.749E+01
1500.0	0.997	0.998	0.998	0.999	1.000	1.401E+02
2000.0	0.998	0.999	0.999	1.000	1.000	2.869E+02
2500.0	0.999	0.999	0.999	1.000	1.000	4.808E+02

Table D.83: Several rovibrational partition functions evaluated at different temperatures for system **S18**.

T(K)	Multidimensional partition functions				
	$\tilde{Q}_{\mathrm{rv}}^{\mathrm{1W-H}}$	$\tilde{Q}_{\mathrm{rv}}^{\mathrm{MC-H}}$	$\tilde{Q}_{\mathrm{rv}}^{\mathrm{MS-T(U)}}$	$\tilde{Q}_{\mathrm{rv}}^{\mathrm{MS-T(C)}}$	$\tilde{Q}_{\mathrm{rv}}^{\mathrm{EHR}}$
100.0	3.982E+04	3.926E+04	3.977E+04	2.720E+04	3.749E+04
150.0	1.288E+05	1.284E+05	1.309E+05	8.966E+04	1.223E+05
200.0	3.676E+05	3.736E+05	3.839E+05	2.637E+05	3.582E+05
250.0	9.708E+05	1.019E+06	1.056E+06	7.287E+05	9.876E+05
300.0	2.439E+06	2.673E+06	2.794E+06	1.940E+06	2.623E+06
400.0	1.408E+07	1.721E+07	1.840E+07	1.294E+07	1.732E+07
500.0	7.541E+07	1.044E+08	1.149E+08	8.168E+07	1.077E+08
700.0	1.835E+09	3.248E+09	3.816E+09	2.758E+09	3.547E+09
1000.0	1.495E+11	3.567E+11	4.507E+11	3.312E+11	4.142E+11
1500.0	8.920E+13	2.938E+14	3.834E+14	2.863E+14	3.657E+14
2000.0	2.031E+16	8.125E+16	1.028E+17	7.752E+16	1.035E+17
2500.0	2.201E+18	1.000E+19	1.194E+19	9.078E+18	1.265E+19

Table D.84: Several one-dimensional partition functions evaluated at different temperatures for system **S19**.

T(K)	Partition functions for ϕ_1					
	q^{CT}	q^{RPG}	q^{SRPG}	q_{cl}	q^{TPG}	q^{TES}
100	2.458E+00	8.868E-01	1.093E+00	1.769E+00	1.539E+00	1.651E+00
150	3.694E+00	1.463E+00	1.826E+00	2.652E+00	2.491E+00	2.567E+00
200	4.868E+00	2.032E+00	2.569E+00	3.513E+00	3.390E+00	3.448E+00
250	5.985E+00	2.609E+00	3.323E+00	4.355E+00	4.257E+00	4.303E+00
300	7.047E+00	3.197E+00	4.080E+00	5.178E+00	5.096E+00	5.135E+00
400	9.025E+00	4.414E+00	5.584E+00	6.764E+00	6.704E+00	6.733E+00
500	1.083E+01	5.672E+00	7.050E+00	8.273E+00	8.226E+00	8.250E+00
700	1.406E+01	8.228E+00	9.837E+00	1.109E+01	1.105E+01	1.107E+01
1000	1.817E+01	1.195E+01	1.366E+01	1.488E+01	1.486E+01	1.487E+01
1500	2.382E+01	1.759E+01	1.924E+01	2.037E+01	2.036E+01	2.037E+01
2000	2.854E+01	2.252E+01	2.407E+01	2.511E+01	2.510E+01	2.511E+01
2500	3.265E+01	2.689E+01	2.836E+01	2.931E+01	2.930E+01	2.929E+01

Table D.85: Several one-dimensional partition functions evaluated at different temperatures for system **S19**.

T(K)	Partition functions for ϕ_2					
	q^{CT}	q^{RPG}	q^{SRPG}	q_{cl}	q^{TPG}	q^{TES}
100	2.034E-01	3.033E-01	2.201E-01	3.528E-01	8.668E-02	1.702E-01
150	4.718E-01	7.030E-01	5.233E-01	5.881E-01	2.915E-01	4.354E-01
200	7.678E-01	1.128E+00	8.675E-01	8.741E-01	5.767E-01	7.547E-01
250	1.082E+00	1.559E+00	1.237E+00	1.201E+00	9.136E-01	1.108E+00
300	1.409E+00	1.989E+00	1.623E+00	1.555E+00	1.282E+00	1.481E+00
400	2.092E+00	2.832E+00	2.408E+00	2.299E+00	2.059E+00	2.252E+00
500	2.790E+00	3.636E+00	3.182E+00	3.050E+00	2.841E+00	3.017E+00
700	4.163E+00	5.111E+00	4.637E+00	4.483E+00	4.322E+00	4.465E+00
1000	6.064E+00	7.030E+00	6.561E+00	6.401E+00	6.287E+00	6.392E+00
1500	8.778E+00	9.674E+00	9.234E+00	9.082E+00	9.009E+00	9.078E+00
2000	1.106E+01	1.187E+01	1.146E+01	1.132E+01	1.127E+01	1.132E+01
2500	1.303E+01	1.378E+01	1.339E+01	1.326E+01	1.322E+01	1.326E+01

Table D.86: Several ratios evaluated at different temperatures for system **S19**. It also includes the two-dimensional partition function $Q_{\mathrm{tor}}^{\mathrm{2D-NS}}$.

T(K)	$F^{\mathrm{HO-NM}}$	$F^{\mathrm{TPG(C)}}$	$F^{\mathrm{MC-TPG(C)}}$	F^{TES}	$F^{\mathrm{2D-NS}}$	$Q_{\mathrm{tor}}^{\mathrm{2D-NS}}$
100.0	0.468	0.439	0.443	0.450	0.498	3.009E-01
150.0	0.727	0.675	0.688	0.717	0.741	1.103E+00
200.0	0.851	0.796	0.813	0.847	0.858	2.523E+00
250.0	0.910	0.862	0.879	0.911	0.917	4.634E+00
300.0	0.941	0.901	0.917	0.945	0.948	7.463E+00
400.0	0.970	0.943	0.955	0.975	0.976	1.520E+01
500.0	0.982	0.963	0.972	0.986	1.000	2.571E+01
700.0	0.991	0.981	0.986	0.995	1.000	5.165E+01
1000.0	0.996	0.991	0.993	0.998	1.000	9.987E+01
1500.0	0.998	0.996	0.997	0.999	1.000	1.934E+02
2000.0	0.999	0.998	0.998	1.000	1.000	2.949E+02
2500.0	0.999	0.998	0.999	0.999	1.000	4.004E+02

Table D.87: Several rovibrational partition functions evaluated at different temperatures for system **S19**.

T(K)	Multidimensional partition functions				
	$\tilde{Q}_{\mathrm{rv}}^{\mathrm{1W-H}}$	$\tilde{Q}_{\mathrm{rv}}^{\mathrm{MC-H}}$	$\tilde{Q}_{\mathrm{rv}}^{\mathrm{MS-T(U)}}$	$\tilde{Q}_{\mathrm{rv}}^{\mathrm{MS-T(C)}}$	$\tilde{Q}_{\mathrm{rv}}^{\mathrm{EHR}}$
100.0	2.511E+05	2.651E+05	2.824E+05	2.155E+05	2.718E+05
150.0	8.208E+05	1.056E+06	1.198E+06	7.977E+05	9.972E+05
200.0	2.394E+06	3.767E+06	4.548E+06	2.628E+06	3.277E+06
250.0	6.678E+06	1.246E+07	1.570E+07	8.123E+06	1.015E+07
300.0	1.837E+07	3.933E+07	5.065E+07	2.422E+07	3.037E+07
400.0	1.396E+08	3.656E+08	4.700E+08	2.051E+08	2.586E+08
500.0	1.081E+09	3.247E+09	4.026E+09	1.683E+09	2.156E+09
700.0	6.381E+10	2.275E+11	2.516E+11	1.028E+11	1.305E+11
1000.0	2.171E+13	8.896E+13	8.113E+13	3.361E+13	4.230E+13
1500.0	1.229E+17	5.648E+17	3.841E+17	1.666E+17	2.075E+17
2000.0	2.018E+20	9.850E+20	5.238E+20	2.375E+20	2.936E+20
2500.0	1.232E+23	6.239E+23	2.696E+23	1.270E+23	1.562E+23

Table D.88: Several one-dimensional partition functions evaluated at different temperatures for system **S20**.

T(K)	Partition functions for ϕ_1					
	q^{CT}	q^{RPG}	q^{SRPG}	q_{cl}	q^{TPG}	q^{TES}
100	9.775E-02	1.831E-01	1.000E-01	2.246E-01	8.903E-02	1.012E-01
150	2.577E-01	4.264E-01	2.608E-01	3.837E-01	2.452E-01	2.673E-01
200	4.459E-01	6.781E-01	4.526E-01	5.673E-01	4.370E-01	4.650E-01
250	6.466E-01	9.284E-01	6.616E-01	7.683E-01	6.482E-01	6.797E-01
300	8.538E-01	1.178E+00	8.829E-01	9.829E-01	8.724E-01	9.061E-01
400	1.278E+00	1.684E+00	1.354E+00	1.444E+00	1.349E+00	1.385E+00
500	1.708E+00	2.200E+00	1.853E+00	1.935E+00	1.853E+00	1.890E+00
700	2.572E+00	3.252E+00	2.894E+00	2.966E+00	2.900E+00	2.937E+00
1000	3.849E+00	4.809E+00	4.459E+00	4.518E+00	4.469E+00	4.502E+00
1500	5.878E+00	7.212E+00	6.890E+00	6.932E+00	6.898E+00	6.924E+00
2000	7.763E+00	9.347E+00	9.053E+00	9.082E+00	9.057E+00	9.077E+00
2500	9.510E+00	1.125E+01	1.099E+01	1.100E+01	1.098E+01	1.100E+01

Table D.89: Several one-dimensional partition functions evaluated at different temperatures for system **S20**.

T(K)	Partition functions for ϕ_2					
	q^{CT}	q^{RPG}	q^{SRPG}	q_{cl}	q^{TPG}	q^{TES}
100	7.095E-01	4.995E-01	5.036E-01	5.949E-01	5.243E-01	5.384E-01
150	1.090E+00	8.439E-01	8.510E-01	9.227E-01	8.716E-01	8.885E-01
200	1.446E+00	1.191E+00	1.201E+00	1.259E+00	1.219E+00	1.237E+00
250	1.781E+00	1.531E+00	1.544E+00	1.593E+00	1.560E+00	1.577E+00
300	2.097E+00	1.860E+00	1.875E+00	1.916E+00	1.889E+00	1.905E+00
400	2.683E+00	2.476E+00	2.496E+00	2.524E+00	2.504E+00	2.517E+00
500	3.215E+00	3.037E+00	3.063E+00	3.080E+00	3.064E+00	3.076E+00
700	4.158E+00	4.026E+00	4.060E+00	4.062E+00	4.051E+00	4.060E+00
1000	5.357E+00	5.269E+00	5.313E+00	5.298E+00	5.291E+00	5.297E+00
1500	6.997E+00	6.948E+00	7.006E+00	6.971E+00	6.967E+00	6.970E+00
2000	8.363E+00	8.334E+00	8.403E+00	8.353E+00	8.350E+00	8.353E+00
2500	9.554E+00	9.536E+00	9.615E+00	9.553E+00	9.551E+00	9.553E+00

Table D.90: Several ratios evaluated at different temperatures for system **S20**. It also includes the two-dimensional partition function $Q_{\mathrm{tor}}^{\mathrm{2D-NS}}$.

T(K)	$F^{\mathrm{HO-NM}}$	$F^{\mathrm{TPG(C)}}$	$F^{\mathrm{MC-TPG(C)}}$	F^{TES}	$F^{\mathrm{2D-NS}}$	$Q_{\mathrm{tor}}^{\mathrm{2D-NS}}$
100.0	0.394	0.373	0.377	0.408	0.412	5.445E-02
150.0	0.643	0.625	0.630	0.671	0.672	2.283E-01
200.0	0.775	0.761	0.767	0.805	0.805	5.413E-01
250.0	0.848	0.838	0.843	0.876	0.876	9.982E-01
300.0	0.892	0.883	0.888	0.917	0.917	1.601E+00
400.0	0.937	0.932	0.935	0.957	0.958	3.244E+00
500.0	0.959	0.956	0.958	0.975	0.976	5.449E+00
700.0	0.979	0.977	0.978	0.990	1.000	1.146E+01
1000.0	0.990	0.989	0.989	0.996	1.000	2.316E+01
1500.0	0.995	0.995	0.995	0.999	1.000	4.742E+01
2000.0	0.997	0.997	0.997	0.999	1.000	7.496E+01
2500.0	0.998	0.998	0.998	1.000	1.000	1.043E+02

Table D.91: Several rovibrational partition functions evaluated at different temperatures for system **S20**.

T(K)	Multidimensional partition functions				
	$\tilde{Q}_{\mathrm{rv}}^{\mathrm{1W-H}}$	$\tilde{Q}_{\mathrm{rv}}^{\mathrm{MC-H}}$	$\tilde{Q}_{\mathrm{rv}}^{\mathrm{MS-T(U)}}$	$\tilde{Q}_{\mathrm{rv}}^{\mathrm{MS-T(C)}}$	$\tilde{Q}_{\mathrm{rv}}^{\mathrm{EHR}}$
100.0	8.357E+04	8.949E+04	9.938E+04	9.173E+04	8.339E+04
150.0	2.640E+05	3.032E+05	3.542E+05	3.269E+05	2.825E+05
200.0	7.778E+05	9.451E+05	1.145E+06	1.056E+06	8.908E+05
250.0	2.243E+06	2.846E+06	3.539E+06	3.262E+06	2.721E+06
300.0	6.443E+06	8.455E+06	1.072E+07	9.870E+06	8.201E+06
400.0	5.369E+07	7.392E+07	9.565E+07	8.802E+07	7.344E+07
500.0	4.516E+08	6.421E+08	8.334E+08	7.668E+08	6.473E+08
700.0	3.021E+10	4.470E+10	5.636E+10	5.188E+10	4.555E+10
1000.0	1.155E+13	1.765E+13	2.044E+13	1.885E+13	1.711E+13
1500.0	7.263E+16	1.139E+17	1.115E+17	1.033E+17	9.766E+16
2000.0	1.263E+20	2.008E+20	1.675E+20	1.557E+20	1.511E+20
2500.0	7.993E+22	1.281E+23	9.254E+22	8.629E+22	8.517E+22